Identification of tryparedoxin peroxidase as a chalcone target in Leishmania

OLIVEIRA, DOUGLAS,ESCRIVANI,DE

Identification of tryparedoxin peroxidase as a chalcone target in *Leishmania*

Douglas Escrivani de Oliveira

A thesis submitted in partial fulfilment of the requirements
for the degree of Doctor of Philosophy in Science

Department of Chemistry
Durham University
United Kingdom

2019

Identification of tryparedoxin peroxidase as a chalcone target in *Leishmania*

Douglas Escrivani de Oliveira

A thesis submitted in partial fulfilment of the requirements
for the degree of Doctor of Philosophy in Science

Instituto de Biofísica Carlos Chagas Filho
Universidade Federal do Rio de Janeiro
Brazil

2019

DOUGLAS ESCRIVANI DE OLIVEIRA

Identification of tryparedoxin peroxidase as a chalcone target in *Leishmania*

A thesis in international joint supervision submitted in partial fulfilment of the requirements for the degree of Doctor of Philosophy in Science (Federal University of Rio de Janeiro, Brazil) and Doctor of Philosophy in Chemical Biology (Durham University, United Kingdom).

Supervisor in Brazil: Profª Bartira Rossi Bergmann

Supervisors in United Kingdom: Prof Patrick G. Steel

Dr Paul W. Denny

Rio de Janeiro

2019

"IDENTIFICATION OF TRYPAREDOXIN PEROXIDASE AS A CHALCONE TARGET IN LEISHMANIA"

DOUGLAS ESCRIVANI DE OLIVEIRA

TESE DE DOUTORADO SUBMETIDA À UNIVERSIDADE FEDERAL DO RIO DE JANEIRO VISANDO A OBTENÇÃO DO GRAU DE DOUTOR EM CIÊNCIAS.

APROVADA POR:

RIO DE JANEIRO, 04 DE ABRIL DE 2019.

DRA. SILVANA ALLODI (DOUTOR – UFRJ)
COORDENADORA DO CURSO DE PÓS-GRADUAÇÃO EM CIÊNCIAS BIOLÓGICAS (BIOFÍSICA)

DRA. BARTIRA ROSSI BERGMANN (DOUTOR – UFRJ) – ORIENTADOR

DR. PATRICK GILES STEEL (DOUTOR – DURHAM/UK) – ORIENTADOR

DRA. JULIANY COLA FERNANDES RODRIGUES (DOUTOR – UFRJ) - REVISOR

DRA. ANA PAULA CABRAL DE ARAUJO LIMA (DOUTOR - UFRJ)

DRA. SILVIA RENI BORTOLIN ULIANA (DOUTOR - USP)

DR. STEVEN COBB (DOUTOR - DURHAM UNIVERSITY)

Oliveira, Douglas Escrivani de.

Identification of tryparedoxin peroxidase as a chalcone target in Leishmania. / Douglas Escrivani de Oliveira. – Rio de Janeiro: Federal University of Rio de Janeiro, Carlos Chagas Filho Institute of Biophysics; Durham: Durham University, Department of Chemistry, 2019.

201 p.: il.; 31 cm.

Advisors: Bartira Rossi Bergmann (Federal University of Rio de Janeiro), Patrick G. Steel (Durham University) and Paul W. Denny (Durham University).

Thesis (post doctoral degree) -- UFRJ, Carlos Chagas Filho Institute of Biophysics; Durham University, Department of Chemistry, 2019.

References: p.174 -192.

1. Leishmaniasis -therapy. 2. Chalcones - pharmacology. 3. Molecular Targeted Therapy. 4. Peroxidases -chemistry. 5. Philosophy in Science (UFRJ)- Thesis. 6. Philosophy in Chemical Biology (Durham University).- Thesis. I. Bergmann, Bartira Rossi. II. Steel, Patrick G. III. Denny, Paul W. IV. Federal University of Rio de Janeiro. V. Durham University, VI. Title.

ABSTRACT

ESCRIVANI, Douglas Oliveira. **Identification of tryparedoxin peroxidase as chalcone target in *Leishmania.*** Rio de Janeiro, 2018. Thesis (PhD in Sciences) Instituto de Biofísica Carlos Chagas Filho, Universidade Federal do Rio de Janeiro, Brazil); (PhD in Chemical Biology), Chemistry Department, Durham University, United Kingdom.

Leishmaniasis is a group of vector-borne neglected diseases caused by intracellular protozoan parasites of the *Leishmania* genus. Without an approved vaccine, current chemotherapy is based on drugs producing severe toxic side effects, and susceptible to resistance. To help the discovery of safer and more effective drugs, this work proposed to identify the parasite molecular target of chalcones, a promising new class of antileishmanial. The nitro chalcone ((2E)-3-(3-nitrophenyl)-1-(2,4,6-trimethoxyphenyl)prop-2-en-1-one; compound **11**) was employed as a model molecule for its high selective activity against *Leishmania amazonensis* (IC_{50}= 0.34µM) and other parasite species. A NAT22 analogue containing an alkyne group ((2E)-1-[4-(hex-5-yn-1-yloxy)-2,6-dimethoxyphenyl]-3-(3-nitrophenyl)prop-2-en-1-one; **19**), and a trifunctional probe accommodating biotin, rhodamine and an azide group (**20**) for chemical linkage to **19** were synthesized for protein target identification by Activity Based Protein Profiling (ABPP) approach. To validate the ABPP method, it was demonstrated that **19** retained anti-promastigote activity (IC_{50}= 0.29 µM). Moreover, **19** was shown to permeate live promastigotes and bind to compartmentalized intracellular sites, as revealed by conjugation with the fluorescent probe (**20**). After SDS-PAGE, a single 22 kDa protein band was labelled by the probe. These were identified by mass spectrometry, and subsequently confirmed by Western blot, as the cytosolic tryparedoxin peroxidase (cTXNPx), a critical parasite detoxifying enzyme. Biophysical and molecular docking studies using recombinant cTXNPx, with chalcone **19** and a dihydrochalcone analogue (**18**) support a model in which chalcone **11** inhibits cTXNPx by covalent interaction of Cys52 with the α,β-unsaturated ketone. Lack of parasite survival after gene deletion using CRISPR-Cas9 approach suggested the essentiality of the identified enzyme. Overall, these results demonstrate that ABPP methods can be used for new drug target discovery in *Leishmania*, enabling the identification of cTXNPx as an important *Leishmania* drug target, providing detailed insight into the mechanism of action.

Keywords: leishmaniasis, treatment, chalcone, mechanism of action, drug target, ABPP, chemical proteomic approach.

RESUMO

ESCRIVANI, Douglas Oliveira. **Identificação da enzima triparedoxina peroxidase como um alvo de chalconas em *Leishmania***. Rio de Janeiro, 2018. Tese (Doutorado em ciências) Instituto de Biofísica Carlos Chagas Filho, Universidade Federal do Rio de Janeiro, Brasil); (Doutorado em Química biológica), Departamento de Química, Durham University, Reino Unido.

A leishmaniose é um grupo de doenças negligenciadas causadas por protozoários intracelulares do gênero *Leishmania*. Sem nenhuma vacina aprovada, a quimioterapia atual baseia-se em medicamentos que possuem efeitos colaterais severos e são suscetíveis à resistência. Com o objetivo de auxiliar na descoberta de fármacos mais seguros e eficazes, este trabalho visou identificar o alvo molecular de chalconas, uma classe promissora de novos antileishmaniais. A nitrochalcona ((2E)-3-(3-nitrofenil)-1-(2,4,6-trimetoxifenil)prop-2-en-1-ona; composto **11**) foi escolhida como molécula modelo para o trabalho, devido à sua alta atividade contra *Leishmania amazonensis* (IC_{50} = 0,34µM) e outras espécies do parasito. Um análogo do composto **11**, contendo um grupo alcino ((2E) -1- [4- (hex-5-in-1-iloxi)-2,6-dimetoxifenil]-3-(3-nitrofenil)prop-2-en-1-ona, **19**), e uma sonda trifuncional contendo biotina, rodamina e um grupamento azida (**20**) foram sintetizados para possibilitar a ligação química com **19** e permitir a identificação dos alvos moleculares pela técnica de Activity Based Protein Profiling (ABPP). Para validar o método de ABPP, foi demonstrado que a modificação em **19** manteve a atividade anti-promastigota da molécula (IC_{50} = 0,29 µM). Além disso, **19** foi capaz de permear a membrana de promastigotas e ligar-se em compartimentos intracelulares específicos, após a conjugação com a sonda fluorescente (**20**). Por SDS-PAGE, a sonda foi capaz de marcar uma única banda de proteína com 22 kDa. As análises por espectrometria de massas e western blot levaram a identificação do alvo, a triparedoxina peroxidase citoplasmática (cTXNPx), uma enzima crítica para detoxificação do parasito. Estudos biofísicos de interação utilizando cTXNPx recombinante e a chalcona **11** ou uma di-hidrochalcona (**18**) e de modelagem molecular, embasaram nosso modelo onde a chalcona **11** inibe cTXNPx através de uma ligação irreversível com a Cys52 de forma dependente da cetona α, β-insaturada na molécula. Além disso, utilizando a técnica de CRISPR-Cas9, para a deleção gênica da enzima, foi possível comprovar a essencialidade da enzima identificada para a sobrevivência do parasito. Em linhas gerais, os resultados demonstram que o método de ABPP pode ser aplicado para a descoberta de novos alvos moleculares em *Leishmania*, o que permitiu a identificação da cTXNPx como um importante alvo de fármacos anti-*Leishmania*, fornecendo informações detalhadas sobre o mecanismo de ação.

Palavras-chave: leishmaniose, tratamento, chalcona, mecanismo de ação, alvo de medicamentos, ABPP, abordagem química e proteômica.

CONTENTS

TABLE LIST

SCHEME LIST

FIGURE LIST

ABBREVIATIONS

ABPP	Activity based protein profiling
AFU	Arbitrary fluorescence units
AmB	Amphotericin B
ANOVA	Analysis of variants
BMDM	Bone Marrow Derived Macrophage
Boc	*tert*-Butyloxycarbonyl
BP	Band pass
Cas9	CRISPR associated protein 9
CC_{50}	Half maximal cytotoxic concentration
$CDCl_3$	Chloroform
CH8	3-nitro-2'-hydro-4',6'-dimethoxychalcone
CL	Cutaneous leishmaniasis
CRISPR	Clustered Regularly Interspaced Short Palindromic Repeats
cTXNPx	Cytosolic tryparedoxin peroxidase
CuAAC	Copper(I)-catalyzed azide-alkyne cycloaddition
Da	Dalton
DCL	Disseminated cutaneous leishmaniasis
DCM	Dichloromethane
DMC	2',6'-dihydroxy-4'-methoxychalcone
DMF	*N*,*N'*-Dimethylformamide
DMSO	Dimethyl sulphoxide
DNA	Deoxyribonucleic acid
DNDi	Drugs for Neglected Disease initiative

dNTPs	Deoxynucleotides
DTT	Dithiothreitol
ESI	Electrospray ionisation
EtOAc	Ethyl acetate
FDA	Food and Drug Administration
Fmoc	9-Fluorenylmethyl carbamate
FPLC	Fast protein liquid chromatography
FT-IR	Fourier-transform infrared spectroscopy
H_2DCFDA	2',7'-dichlorodihydrofluorescein diacetate
HIFCS	Heat-inactivated fetal bovin serum
HPLC	High performance liquid chromatography
HTS	High throughput screening
IAA	Iodoacetamide
IC_{50}	Half maximal inhibitory concentration
IEF	Isoelectric focussing
LB	Luria-Bertani broth
LDH	Lactate dehydrogenase
LPG	Lipophosphoglycan
m/z	Mass to charge ratio
MALDI	Matrix assisted laser desorption ionisation mass spectrometry
MeCN	Acetonitrile
MeOH	Methanol
ML	Mucosal leishmaniasis
MoA	Mechanism of action
mTXNPx	Mitochondrial tryparedoxin peroxidase

MW	Molecular weight
NAT22	3-nitro-2’,4’,6’-trimethoxychalcone
NMR	Nuclear magnetic resonance
NO	Nitric oxide
ORF	Open reading frame
PBS	Phosphate buffered saline
PCR	Polymerase chain reaction
Q-Tof	Quadrupole time of flight
RNA	Ribonucleic acid
ROS	Reactive oxygen species
RT	Room temperature
RT-PCR	Real-time polymerase chain reaction
Sb^{3+}	Trivalent antimonial
Sb^{5+}	Pentavalent antimonials
SDS	Sodium dodecyl sulfate
sgRNA	single guide ribonucleic acid
SI	Selectivity Index
$T(SH_2)$	Trypanothione
THF	*Tetrahydrofuran*
TLC	Thin layer chromatography
TR	Trypanothione reductase
TSA	Protein thermal shift assay
TXN	Tryparedoxin
UTR	Untranslated region
UV-Vis	Ultraviolet-visible

Abbreviations

VL	Visceral leishmaniasis
WHO	World Health Organization
ΔTm	Melting temperature variation

DECLARATION

The scientific work described in this thesis was carried out in the Department of Chemistry, Durham University, United Kingdom and Instituto de Biofísica Carlos Chagas Filho, Universidade Federal do Rio de Janeiro, Brazil between March 2015 and March 2019. This work has not been previously submitted for a degree at this or any other institution.

STATEMENT OF COPYRIGHT

ACKNOWLEDGEMENTS

First and foremost, I would like to thank my supervisors Prof Bartira Rossi Bergmann, Prof Patrick G. Steel and Dr Paul W. Denny, for the guidance, encouragement and advice he has provided throughout my studies. Individually, I would like to warmly thank Prof Bartira for her advices, support and cooperation during all my academic life, her brilliant insights have very often times been crucial to the completion of a thesis. Patrick Steel with his splendid capacity for teaching and patience was essential on my PhD, providing me sharp knowledge of chemistry and guidance to work in completely different field. Thank you Paul, for open the doors of your lab for me and provide deep knowledge in parasitology, cellular and molecular biology. Secondly, I would like to thank all collaborators who enriched my thesis, in special Dr Marjolly Brigido and Prof Lina Zingali, from Medical Biochemistry Institute (IBqM), Dr Ehmke Pohl and Dr Stefanie Freitag-Pohl, from Durham University and Prof Bárbara Abrahim-Vieira and Prof Alessandra de Souza from Molecular Modelling Lab at UFRJ.

During my journey in search of my PhD, I was honoured by having and meeting fantastic people who gave me assistance to overcome all obstacles on this journey. I have many special people to thank for supporting me over the past four years. First of all, my best friend, partner in crime and wife Beatriz, who accepts to embark on all my adventures without fear and has been a constant source of assistance and love. My friends from Immunopharmacology Lab, Ana, Ariane, Arielly, Felipe, Izabella, Maria Paula, Milene, Natália, Vânia and Wallace, for all their support inside and outside the lab, you have brought lightness and happiness into my life in the tensest moments. Also, all the members of the Patrick and Paul's Lab for providing a great environment to learn and grow. In addition, a special thanks to Bex Charlton for her huge help to finish my thesis.

Finally, I would like to thank my friends and family. Especially my mother, Rosilane, for always believing in my potential and being an example of integrity, strength and humility.

Dedication

Dedicado às minhas amadas

esposa e mãe, Beatriz e Rosilane

1. INTRODUCTION

1.1 Leishmaniasis

Leishmaniasis is a vector borne group of diseases caused by protozoan parasites of the *Leishmania* genus. It is classified by WHO as one of the most important neglected tropical disease, because it affects regions with high poverty and consequently has low priority on international public healthcare efforts, leading to insufficient prevention and non-efficient treatment options[1].

Leishmaniasis can present itself as, Visceral Leishmaniasis (VL) and Cutaneous Leishmaniasis (CL), which is divided in sub-groups. Reports estimate that Leishmaniasis is endemic in around 100 countries spread around the globe, with approximately 1 billion people at risk of infection. Additionally, there are 700,00 to 1 million new cases a year with 20,000 to 30,000 deaths annually [2; 3; 4; 5] (Figure 1).

The clinical forms of disease appear according to the parasite species and the host's immunological status[6]. The most serious form is visceral leishmaniasis (VL, Figure 2A), also known as kala-azar or black-fever, which is fatal in more than 95% of untreated cases[6]. This illness is caused by *Leishmania donovani* and *L. infantum* (*syn L. chagasi*) species that affect internal organs, such as the liver, the spleen and bone marrow, leading to fever, weight loss, weakness, lymphadenopathy, hepatomegaly, splenomegaly and anaemia[6]. VL is highly endemic in seven countries, Brazil, India, South Sudan, Sudan, Ethiopia, Kenya and Somalia, and these represent approximately 90% of cases globally (Figure 1)[3] . VL in rare cases could evolve to a dermal manifestation called Post-kala-

azar dermal leishmaniasis (PKDL, Figure 2B), which is characterized by a skin rash on face and can persist for months[4]. VL emerged as an opportunistic disease associated with immunologically vulnerable patients, so HIV infection increases risk to develop VL and increase the Leishmaniasis incidence in areas with incidence of HIV, such as in Brazil[7].

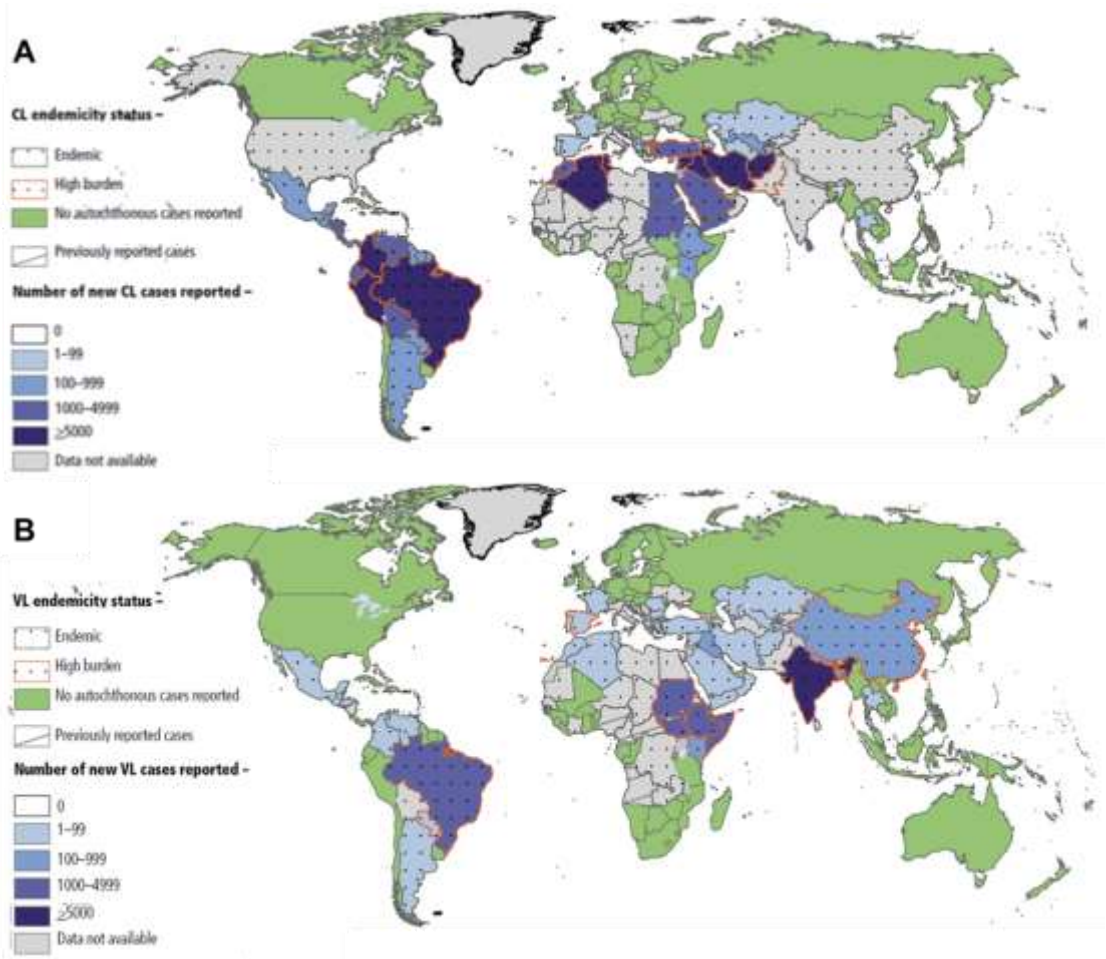

Figure 1. Global distribution of new cases of Leishmaniasis in 2015. **A**- CL worldwide endemicity. **B**- VL worldwide endemicity. Figure adapted from the World Health Organisation (WHO), Weekly epidemiological record[3].

The most prevalent form of the disease is cutaneous leishmaniasis (CL, Figure 2C) and its variations, which are characterized by localized, painless and

self-healing skin lesions, mainly ulcers, on exposed parts of the body, leading to permanent scarring and serious disability. Species which commonly cause CL are *L. major, L. mexicana, L. amazonensis, L. braziliensis* in the New World*, L. tropica, L. aethiopica, L. panamanensis and L. infantum* in the Old World [8]. CL is widely distributed among the endemic regions, about 90% of cases are reported in 12 countries. Risks factors including patient's immunological status, *Leishmania* specie, poor nutrition, age, size, number and locations of CL lesions could lead to two severe secondary CL clinical manifestations, mucosal Leishmaniasis (ML, Figure 2D), diffuse Leishmaniasis (DL, Figure 2E) and disseminated cutaneous Leishmaniasis (DCL, Figure 2F). In ML, highly inflammatory lesions appear on mucosal of upper digestive and respiratory tracts and without treatment it can progress to disfiguring lesions with extensive destruction of affected tissues[8]. In DCL, a high number of pleomorphic lesions appear in anatomical regions different to the initial localized skin lesion. Both ML and DCL are more prevalent in South America and they are caused mainly by *L. braziliensis* for ML and *L. amazonensis* for DCL and DL[9].

Figure 2. Clinical manifestations of Leishmaniasis. **A**- Visceral leishmaniasis (VL). **B**- Post-kala-azar dermal leishmaniasis (PKDL). **C-** Cutaneous leishmaniasis (CL)[6]. **D-** Mucosal leishmaniasis (ML)[10]. **E-** Diffuse leishmaniasis (DL)[11]. **F**- Disseminated cutaneous leishmaniasis (DCL)[12].

Brazil occupies a notable position in the disease epidemiological scenario. Among all endemic countries, Brazil is uniquely a nation classified as a high-burden country for both CL and VL (Figure 1) with CL caused by *L. braziliensis, L. guyanensis* and *L. amazonensis* and VL by *L. infantum (syn L. chagasi).* Moreover, cases of ML and DCL have been reported in Northern regions in Brazil meaning that all forms of leishmaniasis are found in the country[10]. Official reports indicate that there are approximately 30,000 and 4,000 annual cases of CL and VL, respectively with a lethality rate of 8.5% for VL[2; 13].

Notwithstanding leishmaniasis economic and social impact, there is no approved vaccine against *Leishmania* infection in humans[14]. Current disease control is based on a limited number of old drugs with many drawbacks, such as high toxicity, invasive and painful routes and cases of resistance. These drugs are described in detail in Section 1.3 (Table 1).

1.2 The parasite *Leishmania*

Protozoans of the *Leishmania* genus are unicellular eukaryotic cells with a digenetic life cycle, with distinct life stages and two hosts, vertebrate and invertebrate. *Leishmania* parasites have peculiar structures and organelles, such as kinetoplast, subpellicular microtubules, glycosomes and megasomes, which distinguish them to other microorganisms (Figure 3A and B)[15].

The parasite has two main life stages named promastigotes and amastigotes. Promastigote forms are found inside of invertebrate host, they are extracellular, elongated and have motility due to a single long flagellum (Figure 3A). In contrast, amastigotes, are necessarily intracellular and found inside of the parasitophorous vacuole of host macrophages, where they assume a round shape with reduced motility (Figure 3B)[16].

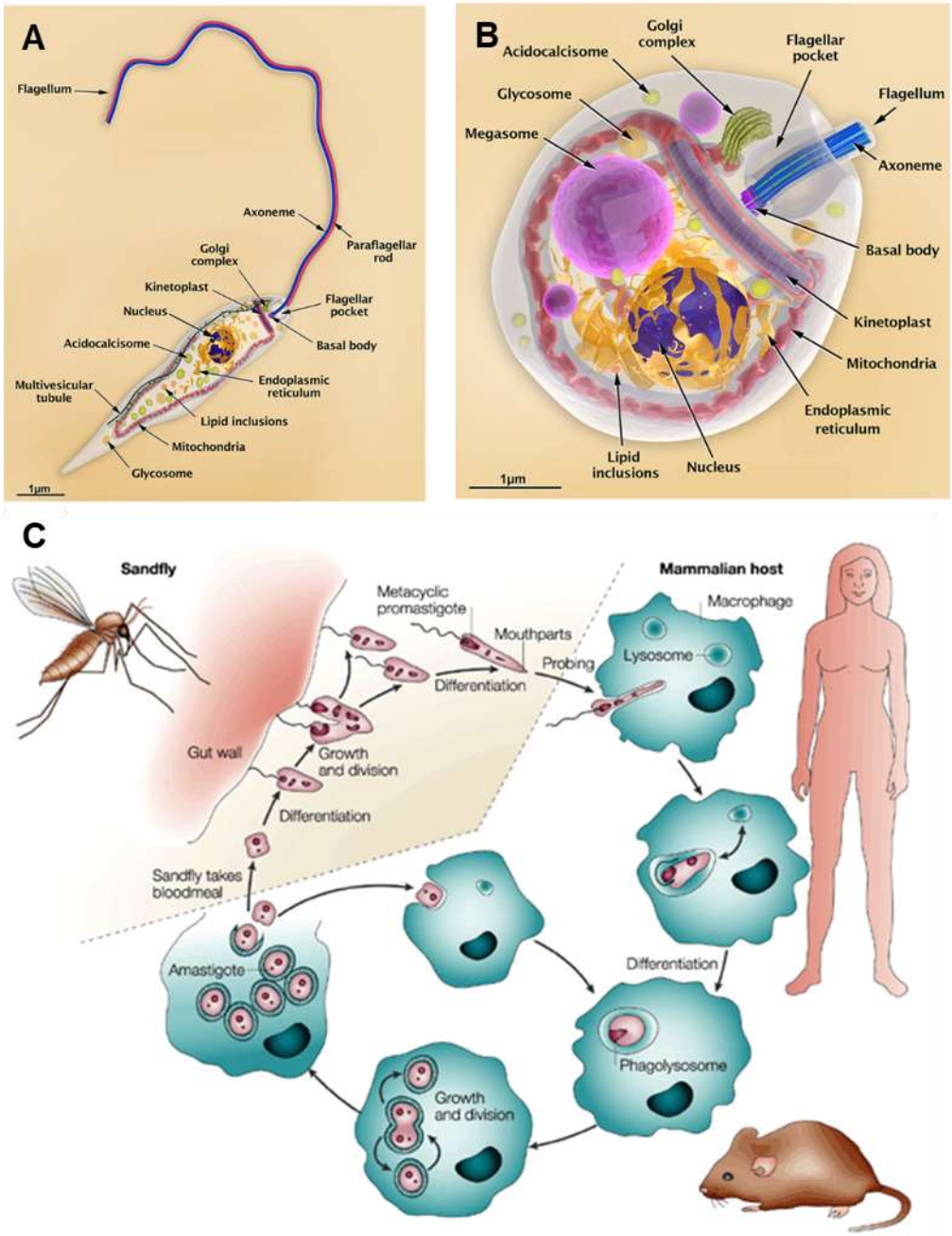

Figure 3. *Leishmania* spp. developmental stages and life cycle. **A**- *Leishmania* promastigote form. **B**- Amastigote form. **C-** Parasite life cycle including vertebrate and invertebrate hosts. Images were adapted from Teixeira et al[16]. and Sacks et al[17].

The parasite's life cycle may start with the phlebotomine sandfly bite. During the blood meal, the insect vector inoculates promastigote forms on a mammalian host skin, the parasite is quickly endocytosed by phagocytic cells, e.g. macrophages, neutrophils and dendritic cells[18]. Once inside of the cell,

promastigotes begin to differentiate into the amastigote form within the phagosome compartment, later called parasitophorous vacuole. Phagocytes have several mechanisms to kill extracellular parasites during the phagolysosome maturation, such as production of reactive species of oxygen (ROS) and nitrogen oxide (NO), although *Leishmania* promastigotes carry surface molecules, such as lipopolysaccharide (LPS), GP63, which downregulate host microbicide mechanism[19]. The capacity to modulate cell host and detoxify oxidative species are essential for promastigotes to have a chance to become amastigotes and continue the life cycle[19].

Once transformed, amastigotes proliferate inside the parasitophorous vacuole. A large amount of parasite causes cell lysis, releasing amastigotes to extracellular compartment extending the infection to adjacent cells. Clinical symptoms of leishmaniasis are related to the presence of intracellular amastigotes on target tissues, skin and mucosa for CL and spleen, liver, lymph nodes and bone marrow for VL. During a blood meal from an infected vertebrate host, a new sandfly may ingest a macrophage containing intracellular amastigotes. These undergo differentiation into the promastigote form in the insect's intestinal tract and further multiply in the midgut. When nutrients start to become insufficient, promastigotes cease to replicate and migrate to the proboscis as a metacyclic form and can then infect a new mammalian host[16; 19] (Figure 3C).

1.3 Current treatments for Leishmaniasis

During the last decades, pentavalent antimonials (Sb^{5+}) were the first-line drugs. They were developed during the 1920s and in some countries are still used as the basis of anti-leishmanial chemotherapy. Meglumine antimoniate (**1**) (Glucantime) and sodium stibogluconate (**2)** (Pentostam) are the available formulations of the pentavalent antimonials (Figure 4). Both drugs need to be administrated by daily parenteral infections for 20 to 30 days. This long treatment regimen leads to tissue drug accumulation causing severe side effects, like myalgia, pancreatitis, pancytopenia, hepatic and cardiotoxicity[20]. Prolonged antimonial exposure can also give rise to the selection of Sb^{5+} resistant parasite strains[14]. To reduce systemic side effects in CL treatment, the WHO has endorsed intralesional infiltrations of 1–3 mL of pentavalent antimonial solution, every 5–7 days for two to five times[5]. Whilst this intralesional approach reduces antimonial toxicity, the local injections are painful, they may cause systemic toxicity, and cannot be applied for ML and MCL[14]. The WHO has recently recommended the antimonials as a second-line drugs for the treatment of VL or in association with drugs such as miltefosine (**6**) and amphotericin B (**3**)[5; 21; 22].

The mechanism of action of antimonials is not well understood. Some reports attribute the antileishmanial activity to the inhibition of enzymes related to DNA synthesis[23] and redox balance, such as trypanothione reductase[24].

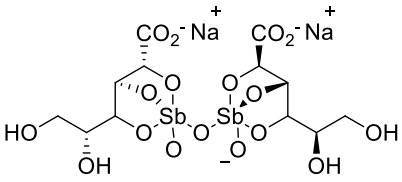

Sodium stibogluconate **1**

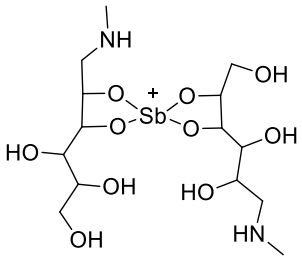

Meglumine antimoniate **2**

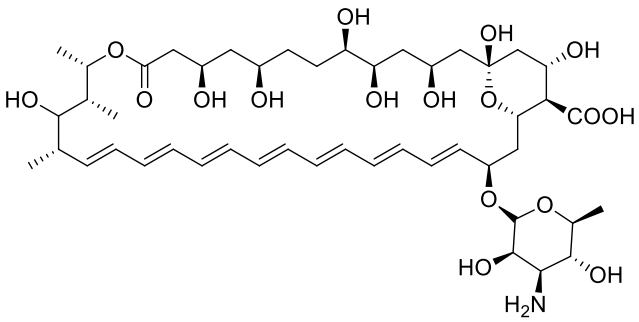

Amphotericin B **3**

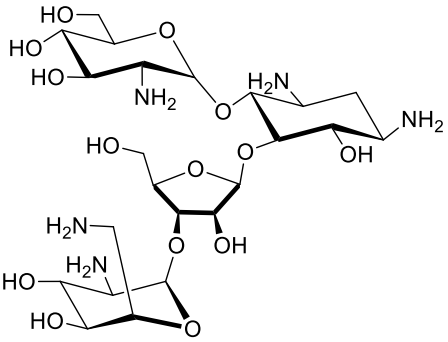

Paramomycin **4**

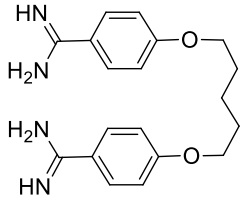

Pentamidine **5**

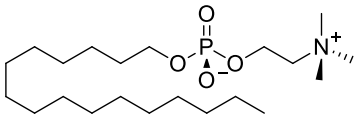

Miltefosine **6**

Figure 4. Chemical structures of the current treatments for leishmaniasis.

The second-line of antileishmanial chemotherapy is composed by parenteral drugs such as amphotericin B (**3**), paramomycin (4) or pentamidine (**5**) (Figure 4).

Amphotericin B (AmB, **7**) is a polyenic antibiotic used for systemic fungal infections and recommended mainly for VL and ML. The drug mode of action is related to its capacity to induce oxidative stress and binds to ergosterol in the parasite membrane leading to membrane perturbation and cell death[25; 26]. The

drug has severe adverse side-effects such as nephrotoxicity, myocarditis, hypokalaemia among others. Due to its poor bioavailability by oral route, administration of AmB consists of slow intravenous infusion for 4 to 6 h, requiring patient hospitalization[14; 22]. A formulation of AmB (**3**) B encapsulated on liposomes, AmBisome (L-AmB), was proposed to reduce the side effects of free drug and L-AmB indeed displayed good efficacy; although, its high cost limits its use in several endemic regions[22].

Paramomycin (**1**) is an aminoglycoside-aminocyclitol antibiotic, employed for VL treatment as a parenteral formulation and by topical and oral route for CL treatment. The drug acts by altering macromolecule biosynthesis and causing membrane alterations in promastigotes. Through parenteral route, the drug showed variable efficacy against VL. Whilst topical formulations of paramomycin display good effectiveness against old world species but efficacy is lower with new world species [22; 27]. The most common side-effects are pain at injection site, reversible toxicity and increase of hepatic transaminases[27].

Pentamidine (**5**) is a diamidine drug with efficacy comparable to the antimonials. Its mode of action is uncertain but it has been proposed an interaction between compound and kinetoplast DNA leading to its condensation and disruption [28]. The drug also accumulates at mitochondrion, changing the mitochondrial membrane potential (δψm)[28]. Several adverse reactions have been linked to this treatment including pain at the injection site, vomiting, headache, hypotension, syncope, nephrotoxicity, diabetes, transient hyperglycaemia and hypoglycaemia[27]. Similar to the antimonials, cases of resistance to pentamidine are rising, compromising its use in some endemic areas[29].

The third-line treatment is an oral drug named miltefosine (**10**) a hexadecylphosphocholine developed to treat breast cancer. It was repositioned to treat VL in south Asia. However, clinical studies in patients infected with species predominant in Americas revealed variable efficacy among the new world *Leishmania* species[30] meaning its clinical use is not approved in Brazil. The mode of action is still controversial, with effects being attributed to modulation of sterol and phospholipid biosynthesis[31], induction of apoptosis-like death[32] and intracellular calcium imbalance and cell signalling[33]. The drug therapeutic regimen is 2.5 mg/kg daily for 28 days. As miltefosine has a long elimination half-life, around 152 h, its body accumulation may increase toxic effects, such as gastrointestinal complications and teratogenicity, which hinders its use in women of childbearing age[27].

Table 1. Current anti-leishmanial drugs, administration routes, treatment duration, disadvantages and their related toxicity[5; 34].

Drugs	Administration route	Treatment duration	Disadvantages	Toxicity
Pentavalent Antimonials- **1, 2**	IM, IV or IL	28-30 days	Quality control; length of treatment; painful injection; toxicity; resistance in India	Severe cardiotoxicity, pancreatitis, nephrotoxicity, hepatotoxicity
Amphotericin B- **3**	IV	15-20 days	Need for slow intravenous infusion; dose-limiting nephrotoxicity; heat instability	Severe nephrotoxicity, infusion-related reactions, hypokalaemia, high fever
Liposomal amphotericin B	IV	Single dose	Price; need for slow intravenous infusion; heat stability (needs to be stored below 25◦C)	Mild rigors and chills during infusion Mild nephrotoxicity (infrequent and mild)
Paramomycin- **4**	IM or topic	17-21 days	Efficacy varies between and within regions; potential for resistance	Severe nephrotoxicity, ototoxicity, hepatotoxicity
Pentamidine- **5**	IM	4 days	Efficacy varies between Leishmania species	High rate of hyperglycaemia, as a result of pancreatic damage; hypotension, tachycardia, and electrocardiographic changes
Miltefosine- **6**	Oral	28 days	Price; possibly teratogenic; potential for resistance (half-life); poor patient compliance	Vomiting and diarrhoea, nephrotoxicity, hepatotoxicity, teratogenicity

In summary, all available treatments currently approved for Leishmaniasis have several disadvantages (Table 1), which reduce their effectiveness and limit control of a disease that impacts millions of people around the world. Faced with of all these problems mentioned above, the development of new therapies is extremely urgent and necessary.

1.4 Chalcones to treat Leishmaniasis

Due to all issues related to current treatments, the Drugs for Neglected Disease initiative (DNDi) has promoted the search for safe, effective, non-invasive and affordable molecules and formulations to replace the current chemotherapies[35]. In this context, several classes of natural molecules have been studied and, among these, chalcones have been reported as promising anti-Leishmanial candidates[36].

In nature, chalcones are small molecules, commonly found as flavonoid biosynthesis precursors that can also be easily synthesized in the laboratory[37]. Chalcones (**7**) have a core structure composed by two aromatic rings A and B linked by a three carbon α,β-unsaturated carbonyl system (Figure 5A)[38]. Many biological activities are associated with this class of molecules including, amongst others anti-inflammatory[39], neuroprotective, anticancer[40], antimicrobial[41], antiviral[42], antibacterial and antimalarial activities[37; 43], demonstrating the pharmacological potential of chalcones[37].

Chalcones have been widely studied for their antileishmanial activity against several species causing both VL and CL, with promising outcomes. The first study reporting activity of a chalcone against *Leishmania*, were performed

with a natural chalcone extracted from *Glycyrrhiza glabra,* licochalcone A (**8**) (Figure 5B)[44]. Today, approximately 330 natural or synthetic chalcones have been reported with antileishmanial activity, both *in vitro* and *in vivo*[45].

In a previous study, our research group demonstrated the antileishmanial efficacy of a natural chalcone, 2',6'-dihydroxy-4'-methoxychalcone (**9**) (DMC-Figure 5C) extracted from *Piper aduncum*[46]. This work showed good activity and selectivity of DMC *in vitro* against *L*. *amazonensis* parasites (IC_{50}= 1.8 µM and 88.8 µM for *L. amazonensis* promastigotes and intracellular amastigotes, respectively and CC_{50}= 370 µM for macrophages). Aiming to elucidate DMC's mechanism of action, our research group demonstrated that chalcone could partially interfere with ergosterol biosynthesis. However, this inhibition appears to be a secondary rather than the primary anti-parasitic mechanism [47].

Further work improved the activity of DMC (**9**) through the modification of substituents on ring A and B with, 3-nitro-2'-hydro-4',6'-dimethoxychalcone (**10**) (CH8 Figure 5D) showing both high activity *in vitro* (IC_{50}= 0.7 µM and 15.8 µM for *L. amazonensis* promastigotes and intracellular amastigotes, respectively) and lower host cell cytotoxicity (S.I. > 143) than DMC (**9**)[48]. CH8 (**10**) was also tested against other *Leishmania* species with *L. infantum, L. braziliensis, L. major* and *L. donovani* showing similar susceptibility and activity against *Trypanosoma cruzi*[49].

In an *in vivo* murine model, CH8 (**10**) afforded an effective and safe treatment for CL and VL by the oral route[50]. Moreover, local subcutaneous injections with CH8 (**10**) either in the free form[48] or loaded in slow-release

systems[51; 52] effectively reduced parasite load and lesion size in murine CL infections.

A

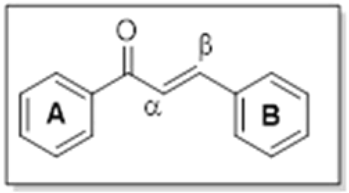

Chalcone backbone **7**

B

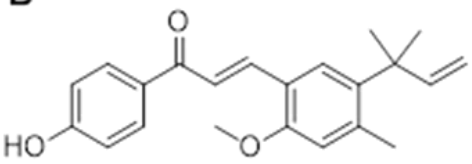

Licochalcone A **8**

C

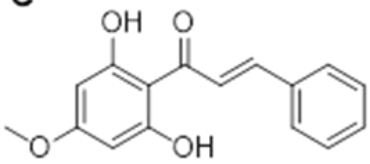

Chalcone DMC **9**

D

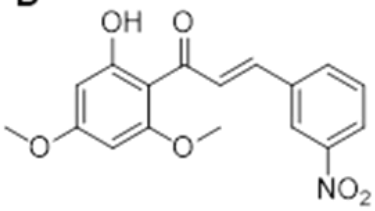

Chalcone CH8 **10**

E

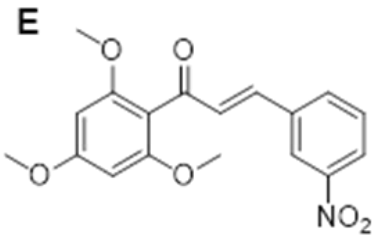

Chalcone NAT22 **11**

F

Chalcones IC_{50} [µM]	**10**	**11**
Promastigotes	0.70 ± 0.08	0.34 ± 0.07
Amastigotes	1.10 ± 0.06	0.32 ± 0.07
Purification yield	18%	89%

Figure 5. Chalcones for leishmaniasis treatment. **A-** General structure of chalcones. **B-** Licochalcone A[44]. **C-** Chalcone DMC[46]. **D-** Chalcone CH8[48]. **E-** Chalcone NAT22[53]. **F-** Antileishmanial activity *in vitro of* chalcone analogues **10** and **11**.

Despite these promissing results, the mechanism of action and molecular targets of CH8 (**10**) remain to be elucidated and this became the primary goal of this thesis. One barrier to the pharmaceutical development of CH8 derivatives was a difficult synthetic process. In work to simplify and improve the synthesis further derivatives were prepared [53]. Among them, the best analogue was a 3-nitro-2',4',6'-trimethoxychalcone (NAT22, **11**) (Figure 5E), which had similar activity to CH8 (**10**) against promastigotes and amastigotes *in vitro* (Figure 5F), a higher selectivity index and more efficient synthesis (89% yield, as compared with 18 % for CH8 (**10**))[53].

Reflecting these benefits NAT22 was selected as the lead structure for further chemical modifications and probe synthesis to establish a mode of action and validate the molecular target.

1.5 Drug discovery efforts on Leishmaniasis

With the urgent necessity for new targets or inhibitors for the chemotherapy of leishmaniasis, many research groups and pharmaceutical companies are aiming to discover new compounds to suppress essential pathways for the parasite or identify and validate new molecular targets. A candidate drug needs to be able to kill the parasite intracellular stage, acting selectively on parasite pathways or targets without affecting the mammalian cell host[35] However, the development of innovative medicines is extremely hard for leishmaniasis due to the complex disease life-cycle and intracellular location of the parasite and also because it is an eukaryotic cell. New drugs not only have to be active but also need to cross multiple membranes to engage and kill the

amastigote form within the parasitophorous vacuole. Moreover, the disease is caused by different parasite species, with distinct gene expression, leading to complex physiopathology and affecting different organs, so drugs need to be effective against the most prevalent, and ideally all, species and have appropriate bioavailability to reach infected organs[54].

Drug discovery for leishmaniasis follows two main approaches: phenotypic screening or whole-cell/-organism screening and target-based screening (Figure 6)[54].

1.5.1 Phenotypic screening

Phenotypic screening (Figure 6) is an approach to identify compounds with a particular biological outcome in cell-based assays or animal models[55]. They are considered excellent tools to measure activity of molecules on whole-cell system instead of isolated targets. This kind of approach was used to identify most of new FDA-approved compounds for several pathologies[55]. In this case, compounds library is tested against parasites without considering specific molecular targets or a pathway and promising compounds are selected based on their ability to kill the parasite. As compounds can inhibit more than one target or pathway, a difficulty of phenotypic screening is the target deconvolution.

The principal advantage of phenotypic assays is the possibility to show an unbiased direct effect of a compound on the parasite. This potentially gives an indication of host cell toxicity and other compound properties, such as cell permeability, solubility and stability[56]. A second benefit which arises from this approach is the possibility to discover molecules, with synergistic

polypharmacology, which can modulate more than one pathway or analyze secondary consequences related to inhibition of a specific route, as observed for miltefosine which has distinct mechanisms of action in *Leishmania* parasites [56; 57].

As *Leishmania* parasite has an heteroxenous life cycle, more than one developmental stage can be screened although the stage chosen for screening can impact on the assay analysis[56]. Sometimes, drugs that showed activity against promastigotes are not able to kill the amastigote forms[58]. For reasons of simplicity, most screening campaigns have been done using promastigote or axenic amastigote stage due to the availability of biochemical screening kits to measure parasite killing. However, they are not the parasite form that cause the disease. Ideally, drug candidates should be tested against intracellular amastigotes and the most efficient way to assess it is the direct counting intracellular parasites on macrophages. However, this approach offers lower throughput[59]. To prevent this kind of bias and save time, researchers are doing high throughput screenings (HTS) with promastigotes and axenic amastigotes and performing anti-intracellular amastigote assay with the most promising candidates[59]. Luckily, new High-Throughput Screening assays for intracellular amastigotes have been reported demonstrating excellent applicability on drug discovery[60].

HTS methodology with advantages and disadvantages enabled many research groups to find antileishmanial hit compounds among extensive libraries of natural or synthetic molecules[59; 61; 62].

1.5.2 Target based screening

This approach screens compounds against well-defined and validated parasite targets, which usually are proteins related with a specific pathway. Target based screening is extensively employed by pharmaceutical companies as a tool to find hit compounds[54].

This methodology benefits from testing molecules against targets which are essential for parasite survival, allowing discovery of potent compounds with high selectivity and cellular activity (Figure 6). Additionally, the discovery of inhibitors for specific targets allows for the possibility of drug combination to improve its efficacy and decrease related side effects[63]. On the other hand, in *Leishmania* there are a restricted number of validated molecular targets and target-based screens that do not consider the whole parasite physiology. For example, in live parasites some compensatory mechanisms could be induced when a specific pathway is inhibited by a compound, decreasing its druggability[54]. Some potential therapeutic targets or specific pathways have been proposed and they will be discussed in detail below.

It is widely debated which screening approach delivers the best result, however, both approaches have been utilized for the discovery of hit compounds to treat Leishmaniasis. In addition, they allow drug repurposing of molecules employed for distinct diseases, an approach widely used today that bypass steps in developing a new drug and delivering it to the market[64].

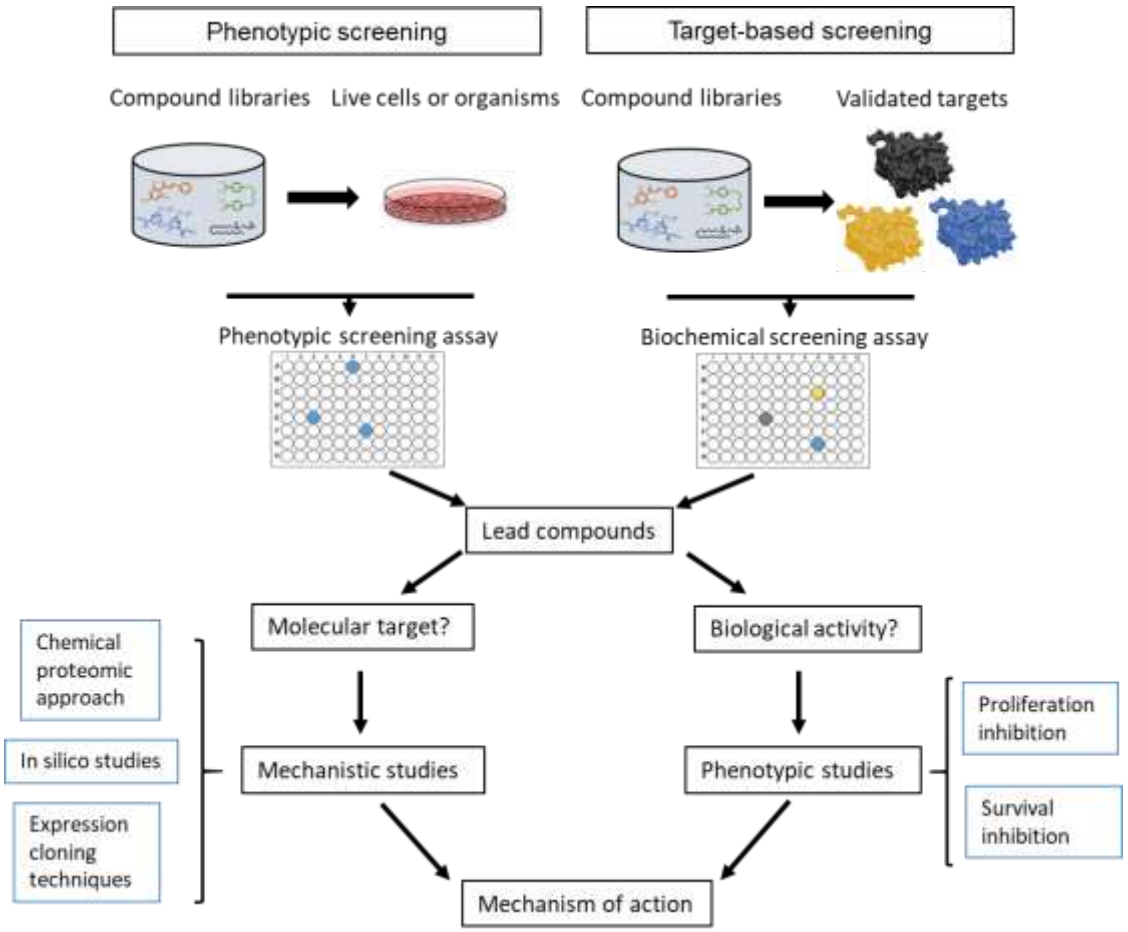

Figure 6. Drug discovery by phenotypic and target-based screenings.

1.6 Known *Leishmania* drug targets

The knowledge of the drug target of a compound is extremely relevant; it enables prediction of side effects and allows drug association between compounds with synergic effects. This leads to improvements in treatment efficacy, reduction in therapeutic dose and increase in chance for drug approval which saves time, money and patients life[65]. This section will describe some of most promising therapeutic targets or pathways of *Leishmania* which have been explored for drug screening.

1.6.1 Lipids biosynthesis pathway

Sterols are essential components of cell membranes related to regulation of biological processes and maintenance of cell membrane structure. Mammalian cells have cholesterol, as their major membrane sterol, whereas trypanosomatids synthesize ergosterol and others 24-methyl sterols rather than cholesterol, which are absent in mammals. Thus, this pathway represents an excellent way to kill the parasite with less adverse effect to host cell[66].

Many enzymes play essential roles in this route including: farnesyl diphosphate synthase, acetoacetyl-CoA thiolase, HMG-CoA synthase, HMG-CoA reductase, squalene synthase, squalene oxidase, $\Delta^{24,25}$sterol methyltransferase and sterol 14 alpha-demethylase. All enzymes involved in sterol biosynthesis can be considered as drug targets and many of their potent inhibitors have generated positive results in literature[67].

Other essential membrane components are sphingolipids, such as ceramides and sphingomyelins, their importance relates to membrane function and integrity maintenance. Unlike, mammalian cells that transfer phosphorylcholine from phosphatidylcholine (PC) to ceramide to give sphingomyelin, trypanosomatids synthesize inositol phosphorylceramide (IPC) by inositol phosphorylceramide synthase (IPCS). Recently, IPCS was validated as a drug target, and using a plate-based assay for IPCS, some good hit inhibitors could be identified, showing the applicability of this new target[68; 69; 70].

1.6.2 Folate metabolism

Folates are essential vitamins that work as cofactors for important biochemical reactions related to amino acid metabolism and nucleotide biosynthesis. Once this pathway was discovered in trypanosomatids and its essentiality for parasite growth was described, enzymes involved in all steps have been studied as drug targets[71]. The enzymes dihydrofolate reductase (DHFR) and thymidylate synthase (TS), responsible for converting dihydrofolate to tetrahydrofolate, are found as separate proteins in most of organisms, whereas in *Leishmania* they are one bifunctional protein. Several compounds, such as 2,4-diaminopyridimine (Figure 7, **12**) derivatives[72], were screened against DHFR-TS, but these inhibitors are not selective to *Leishmania* enzymes, due to activity of another enzyme which can reduce folate when DHFR are blocked, pteridine reductase (PTR1)[73].

PTR1 enable *Leishmania* parasites to produce folate intermediates in a distinct manner, as an alternative and compensatory pathway when DHFR is inhibited. Efforts to discover potent inhibitors are in progress, for instance, a combination of inhibitors for both DHFR-TS and PTR1 could represent a promising way to kill parasites[74].

1.6.3 Protein kinases

Proteins kinases, including cyclin dependent kinases (CDKs), mitogen-activated protein kinases (MAPKs) and glycogen synthase kinase-3 (GSK-3), are known as essential for cell division, cell differentiation, cell proliferation and signal transduction. The essentiality of these proteins for parasites and their differences

to host cells makes them attractive targets in obtain selective inhibitors[75]. Indeed, several published papers describe the applicability of these proteins as drug targets, some validated kinases include: CDKs as CRK3[76], CRK6 and CRK12[77], MAPKs like MPK4[78] and GSK-3[79].

1.6.4 Peptidases

The next group of promising targets include the proteolytic enzymes or proteases, which are able to break peptide bonds and are necessary for parasite physiology. There are a total of 154 peptidases in the *Leishmania* genome grouped according to their catalytic mechanism: aspartic proteases, serine proteases, cysteine proteases, metalloproteases and threonine proteases[80]. The most studied peptidase is the metalloprotease, GP63, which can be found in the promastigote glycocalyx and is essential for parasite infection and downregulation of phagocytic cells[81]. Other examples of proteases can be found as drug targets, such as CPA, CPB and CPC cysteine protease families[82], the serine protease known as oligopeptidase B[83], among others. Additionally, earlier studies pointed out proteasomes as potential drug targets, they are essential for the parasite and can be selectively inhibited by small molecules[84].

1.6.5 Polyamine biosynthesis

Polyamines are organic polycations synthesized from amino acids as L-arginine, which play an essential role in parasite survival and infectivity. Enzymes engaged in this pathway include: arginase (ARG), ornithine decarboxylase (ODC), spermidine synthase (SpdS) and trypanothione synthase (TS). In this

pathway, L-arginine is converted, after some enzymatic steps, to spermidine, which is a precursor of trypanothione ($T(SH)_2$); this is an essential molecule for parasite resistance in oxidative environments such as phagocyte infection, differentiation to amastigotes and proliferation[85]. Arginase and ornithine decarboxylase are the most studied polyamine enzymes, both were validated as drug target[85] and had inhibitors available in literature and on the market, for example, 2(S)-amino-6-boronohexanoic acid (**13**) (ABH)[86] and eflornithine (**14**) (DFMO) [87] for ARG and ODC, respectively. Polyamine pathway is directly related to trypanothione metabolism.

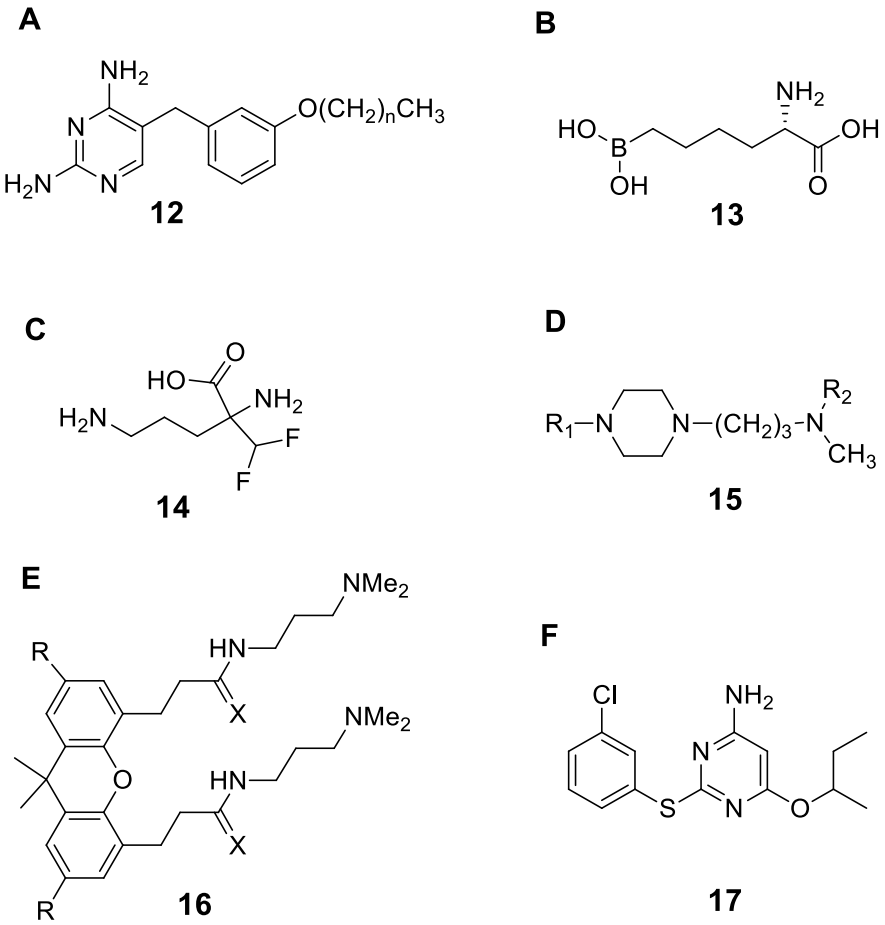

Figure 7. Inhibitors for essential parasite drug targets. **A**- 2,4-diaminopyridimine, **12**[72]. **B-**2(S)-amino-6-boronohexanoic acid, **13**[86]. **C-** Eflornithine,**14**[87]. **D-** Piperazine derivatives, **15**[88]. **E-** 9, 9-dimethylxanthene derivatives, **16**[89]. **F-** Diaryl sulfide derivative,**17**[90].

1.6.6 Redox metabolism

Leishmania parasites, during their life cycle, are exposed to oxidizing species of oxygen, such as superoxide anion (O_2^-), peroxide (O_2^{-2}), hydroxyl radical ($^{\bullet}OH$) and hydrogen peroxide (H_2O_2)[91]. Superoxide anion can react with nitric oxide and generates peroxynitrite ($ONOO^-$), a strong oxidizing and nitrating agent considered essential for parasite killing by phagocytic cells[92]. In addition, hydrogen peroxide may be converted to hydroxyl radicals in the presence of a transition metal such as iron (Fe^{2+}). This radical is a non-specific oxidant, which can cause damage to lipids, proteins and nucleic acids, resulting in cell death without antioxidant balance[93].

Trypanosomatids lack genes related to thiol redox balance in mammalian cells, such as glutathione (GSH)/glutathione reductase and catalase[94]. In contrast, redox metabolism in trypanosomatids is based on a dithiol trypanothione ($T(SH_2)$), composed by conjugation of two molecules of glutathione (GSH) with spermidine, N1,N8-bis(l-γ-glutamyl-l-hemicystinylglycyl)[95]. Reactive oxygen species (ROS) are reduced by $T(SH_2)$ generating trypanothione disulfite (TS_2), and $T(SH_2)$ returns to its reduced state by trypanothione reductase (TR) which uses NADPH as an electron donor (Figure 8A)[96].

Some TR inhibitors were investigate as drug candidates, for example trivalent antimony (Sb^{+3})[97], lunarine[98], piperazines derivatives (**15**)[88], 9, 9-

dimethylxanthene derivatives (**16**)[89], diaryl sulfide derivatives (**17**)[90] (Figure 7) and others.

The capacity of $T(SH_2)$ to detoxify H_2O_2 species in trypanosomatids is dependent of two proteins, tryparedoxin (TXN) and tryparedoxin peroxidase (TXNPx). Continuing the detoxifying cascade, $T(SH_2)$ reduces TXN rather than NADPH flavoprotein, and then TXNPx accepts an electron from TXN and reduces H_2O_2[99] (Figure 8).

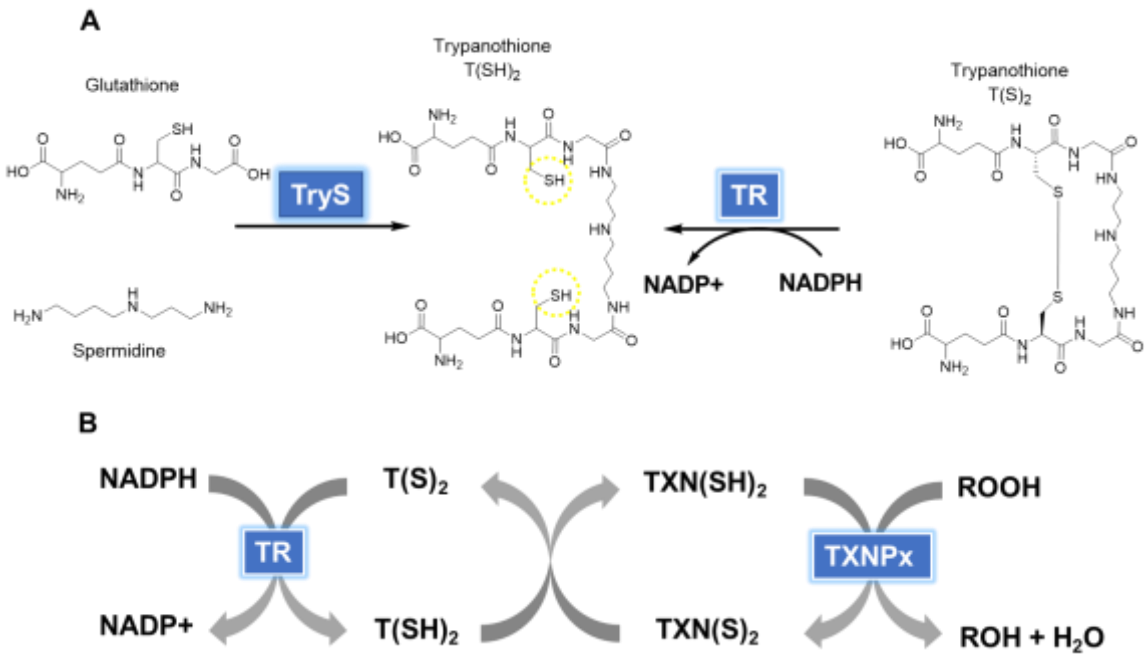

Figure 8. Parasite redox balance based on trypanothione. **A-** Trypanothione synthesis. **B-** Representative illustration of all proteins related to trypanothione based redox balance.

TXNPx belongs to a well-conserved 2-cysteine peroxiredoxins family that detoxify H_2O_2, $ONOO^-$ and contribute for DNA biosynthesis[100; 101]. *Leishmania* encodes two isoforms of TXNPx, one mitochondrial (mTXNPx) and other cytosolic (cTXNPx), responsible for metabolizing endogenous and exogenous peroxides, respectively[99; 102]. Despite their cell compartmentalization, only

cTXNPx was described as essential to parasite survival in *Trypanosome brucei*[103].

In general, TXNPx is related to the survival and virulence of trypanosomatids. In *Leishmania*, overexpression of TXNPx in *L.donovani* and *L.amazonensis* improves protection against oxidative stress from macrophages and increases parasite infectivity[100; 104]. Higher expression levels of TXNPx were found in *Leishmania* isolate strains resistant to drugs including arsenite[105], amphotericin B(**3**) [26; 106] and antimonials (**1, 2**)[97; 107]. To date, only two inhibitors to cTXNPx were reported, *in silico* by high throughput docking[108].

1.6.7 Other molecular targets

Many other relevant targets or specific pathways were described and their inhibition resulted in promising outcomes. Examples of validated targets are calcium channels and aquaporin[109; 110], metacaspases[111], topoisomerase II[112], enzymes related to glycolysis, including hexokinase and phosphofructokinases[113], purine salvage pathway[114], among others that can be found in literature.

As discussed more in Section 1.7, many antileishmanial targets have been identified and validated but this recognition of essential proteins is not enough to describe the mechanism of action (MoA), as can be observed for most antileishmanial drugs whose MoA still unknown. Drugs like antimonials, pentamidine and miltefosine lack a well-defined MoA. This paradigm turned the focus of researchers towards the identification and development of methodologies to determine the biological target of hit compounds from the

phenotypic screens. Thus, the next section will address techniques commonly employed for target deconvolution, emphasizing ABPP approach that will be used in this work.

1.7 Methods for target deconvolution

The knowledge on genomic, proteomic fields and computational methods enable the emergence of powerful techniques to elucidate mechanism of action of drugs. They can be categorized into three main approaches: expression cloning techniques and protein microarray, *in silico* screenings, and chemical proteomic based approach[115; 116].

In expression cloning techniques, a library of complementary DNA (cDNA) is inserted into cloning vectors to express a library of proteins, then the capacity of hit compounds to interact with target proteins allows the detection and purification of only binding proteins. Examples of this methodology are phage display[117], mRNA display[118], ribosomal display[119] and yeast three-hybrid screen[120].

Protein microarray involves the expression of several proteins from a specific proteome and spotting them on a microarray plate. These proteins on a microarray chip are then incubated with hit compounds and measurements of the binding strength will determine possible drug targets[121].

In silico screenings make use of computational resources and virtual drug to protein databases to predict targets of active compounds from their structural similarities with known target drugs[122; 123]. This procedure could reduce cost and time in drug development.

Chemical proteomic-based approaches are the most popular methodologies employed in drug target discovery. There are many methods that can be categorized as chemical proteomic-based, although affinity chromatography[115], photoaffinity labeling (PAL)[124], cellular thermal shift assay (CETSA)[125] and activity-based protein profile (ABPP) are the most studied methods. ABPP methodology will be explain in details on next section

1.7.1 Activity-Based protein profiling for drug target

ABPP is a recent methodology that combines chemistry and proteomics to comprehensively elucidate molecular targets of small molecules[126]. The ABPP approach is based on utilization of an active site and directed covalent probe (Figure 9). Generally, these probes are composed of three fundamental elements: (i) a reactive site which reacts covalently with the active site of proteins or with small molecules linked to proteins, for example bio-orthogonal groups, including azide and acetylenes; (ii) a linker region, to extend the distance between reactive group and tag group to avoid steric hindrance; (iii) a reporter tag for identification and purification of binding proteins; fluorophores such as rhodamine, fluorescein and Cy3 are commonly employed as a tag group for protein identification as well as biotin for protein purification[127] (Figure 9A).

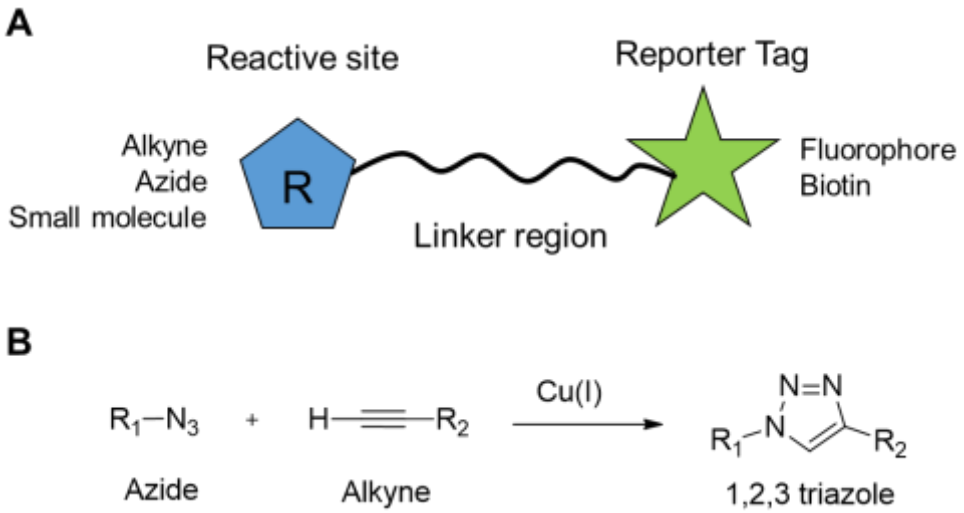

Figure 9. ABPP essential tools. **A**- Three main features of ABPP probes, a reactive site, linker region and a reporter Tag. **B**- Scheme of copper (I)-catalyzed azide-alkyne cycloaddition (CuAAC), click chemistry.

ABPP workflow usually starts when the probe is incubated with proteins, tissue, living cells or animals for minutes to hours to allow target binding. The size of the probe or chemical moiety sometimes hinders its cellular uptake and therefore decreases its activity and on-target effect. To circumvent, this issue small molecules, such as drug candidates, can be modified by the addition of a bio-orthogonal handle to further conjugation with the probe. A widely used bio-orthogonal reaction is the copper(I)-catalyzed azide-alkyne cycloaddition (CuAAC) which generates a 1,4-disubstituted 1,2,3-triazole[128] (Figure 9B).

Following target protein binding and the CuAAC, all proteins are exposed by cell lysis, and the target could be identified through two distinct approaches: (i) using biotin tags, target proteins linked to the chemical probe can be purified using streptavidin coated beads or affinity columns; and (ii) fluorescent tags which are useful to visualize protein targets. The next step is to perform gel electrophoresis to separate all proteins followed by target visualization using

fluorescence scanning. The last step is the target identification by mass spectrometry, western blot and computational approaches[129] (Figure 9).

ABPP approach was successfully used for the identification of targets and description of the mechanism of action of many compounds. Lin et al., identified 197 proteins targets for curcumin, a natural product with anti-cancer properties, helping them to describe the curcumin mechanism of action in colon cancer cell line[130]. Several proteins of *Plasmodium falciparum* were identified as targets for artemisinin, a potent anti-malarial drug, improving the current knowledge about how this natural product can kill the parasite[131]. ABPP was also employed to elucidate cellular targets of β-lactam in bacteria[132] and to determine new molecular targets for drugs available in the market, including orlistat[133], aspirin[134] and omeprazole[135].

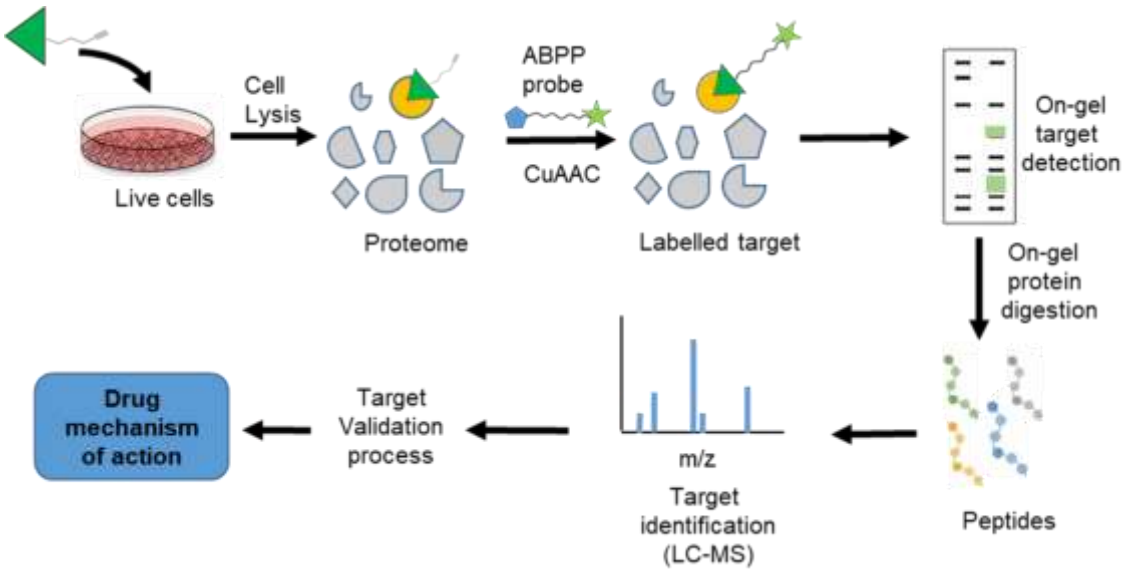

Figure 10. Activity-based protein profiling workflow.

2. MAIN OBJECTIVE

In light of the excellent potential of chalcones as a novel antileishmanial drug, in this thesis we sought to use the active NAT22 as a model chalcone to identify and characterize its target(s) in *Leishmania* employing the Activity Based Protein Profiling (ABPP) approach.

2.1 SPECIFIC OBJECTIVES

1- Synthesize active ligand-containing NAT22 analogues and fluorescent / biotinylated probes for ABPP.

2- Identify and isolate parasite proteins ligands to chalcone.

3- Analyse the interaction between the identified protein targets and NAT22.

4- Validate NAT22 mechanism of action based on target protein function.

5- Validate discovered drug targets for *Leishmania* survival.

3. MATERIALS AND METHODS

3.1 General chemical experimental details

3.1.1 IUPAC nomenclature

The IUPAC names and atom numbering were obtained using ChemDraw Ultra (v15.0) CambridgeSoft.

3.1.2 Solvents and reagents

All chemicals were purchased from commercial suppliers and used without further purification. All used solvents THF, DCM, MeCN, EtOAc, MeOH, DMF and $CDCl_3$ were obtained dry and stored under argon.

3.1.3 Reactional conditions

All reactions were performed in round-bottom flasks, with stirring, under argon atmosphere unless otherwise stated. Reactions under microwave irradiation conditions were performed using monomodal EmrysTM Optimizer from Personal Chemistry, in sealed microwave process vials under argon atmosphere. The reaction progress was followed by thin layer chromatography (TLC) using Merck aluminium precoated plates (silica gel 60 Å F254). Compounds visualization were taken by UV radiation (λ_{max} = 254 nm and 365 nm) followed by staining with the appropriate reagent and heating. Purification were conducted by flash chromatography using CombiFlash EZ Prep system with RediSep normal-phase silica flash columns (Teledyne Isco).

3.1.4 Spectroscopic analysis

Infrared: IR spectra were documented using a Perkin-Elmer Spectrum 1000 FT-IR Spectrometer with a ATR module, and absorption maxima ν_{max} were reported as wavenumbers (cm^{-1}).

Nuclear magnetic resonance: ^{1}H and ^{13}C NMR spectra were acquired on Varian VNMRS 700 (^{1}H at 700 MHz, ^{13}C at 176 MHz) or Varian VNMRS 600 (^{1}H at 600 MHz, ^{13}C at 151 MHz), $CDCl_3$ was used as solvent and the chemical shifts (δ_H or δ_C) reported in parts per million (ppm), number of protons, multiplicity (s, singlet; d, doublet; t, triplet; m, multiplet), coupling constants (J) and assignment. The assignment was performed with COSY, HSQC, HMBC and NOESY experiments.

Mass spectrometry: Low resolution mass spectra (LRMS) were recorded via electrospray ionisation (ESI), using a Waters TQD spectrometer equipped with an Acquity UPLC or by matrix-assisted laser desorption/ionization (MALDI) Autoflex II ToF/ToF (Bruker). High resolution mass spectra (HRMS) were obtained using Waters LCT Premier XE by Durham University Mass Spectroscopy service. Mass to charge ratios (m/z) are reported in Daltons with the corresponding fragment ion.

3.1.5 Analogues and probe synthesis

3-(3'-nitrophenyl)-1-(2",4",6"-trimethoxyphenyl)propan-1-one (**18**)

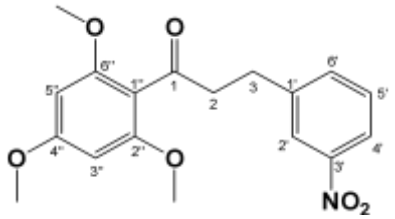

18

A solution of 1-(2,4,6-trimethoxyphenyl)ethanone (210 mg, 1.0 mmol) in anhydrous THF (3 mL) at 0 ºC was treated with LiHMDS solution in anhydrous THF (1.2 mL of a 1M solution in THF, 1.2 mmol). The reaction mixture was then stirred for 1h at 0°C. Benzyl bromide (281 mg, 1.3 mmol) in THF (2 mL) was added as a solution and the resulting mixture was stirred at RT overnight (o/n). Saturated ammonium chloride solution (2 mL) was added to quench the reaction followed by DCM (20 mL). The aqueous phase was washed with DCM (3 x 10 mL) and combined organic phase was dried over $MgSO_4$ and solvent removed *in vacuo.* The compound was purified by reverse phase chromatography (5 to 100% MeCN in H_2O) to afford product **18** (60 mg, 0.17 mmol, 17%). ν_{max}. (ATR) 1696 (C=O), 1525, 1347 (N=O), cm^{-1}; δ_H (700 MHz, $CDCl_3$) 8.07 (1H, m, 2'-*H*), 8.03 (1H, m, 4'-*H*), 7.58 (1H, m, 6'-*H*), 7.42 (1H, m, 5'-*H*), 6.08 (2H, s, 3",5"-*H*), 3.81 (3H, s, 4"-OC*H*$_3$), 3.74 (6H, s, 2",6"-OC*H*$_3$), 3.13 – 3.12 (4H, m, 2-*H*$_2$, 3-*H*$_2$); δ_c (176 MHz, $CDCl_3$) 202.5 (*C*-1), 162.6 (*C*-4"), 158.4 (*C*-2", 6"), 148.4 (*C*-3'), 143.7 (*C*-1'), 135.2 (*C*-6'), 129.2 (*C*-2'), 123.3 (*C*-5'), 121.2 (*C*-4'), 113.1 (*C*-1"), 90.8 (*C*-3",5"), 55.9 (2", 6"-O*C*H$_3$), 55.6 (4"-O*C*H$_3$), 45.3 (*C*-2), 29.6 (*C*-3); m/z (LCMS,

ESI$^+$) 346 (MH+); Accurate mass: (ES$^+$) Found MH+, 346.1298: $C_{18}H_{20}NO_6$ requires *M*, 345.1291.

1-(2,6-dimethoxy-4-(4,4,5,5-tetramethyl-1,3,2-dioxaborolan-2-yl)phenyl) ethanone (**19a**)

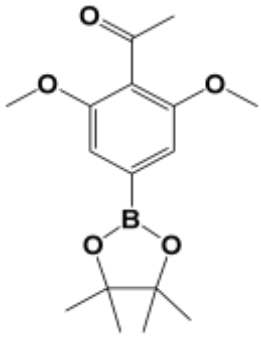

19a

2,6-dimethoxyacetophenone (0.18 g, 1.0 mmol) was dissolved in dry THF (1 mL), and added to a mixture of B_2pin_2 (0.25 g, 1.0 mmol, 1.0 equiv), $[Ir(OMe)(cod)]_2$ (9.9 mg, 1.5 mol %), and 4,4′- di-tert-butyl-2,2′-dipyridine (8.0 mg, 3 mol %) in THF (1 mL) in a sealed microwave vessel under nitrogen. The reaction was then heated in a microwave reactor at 80°C for 40 min. Then the reaction mixture was filtered through silica gel and the solid residue washed with DCM (2 x 5 mL). The combined filtrate was then concentrated under reduced pressure to afford the title boronate ester (**19a**) which was used directly in the next step with no further purification (0.11 g), TLC confirmed the formation of **19a**.

2,6-dimethoxy-4-hydroxy-acetophenone **(19b)**

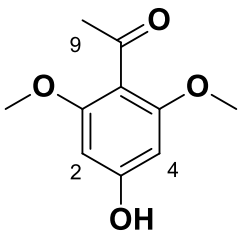

19b

The crude intermediate (**19a)** (0.11 g, 0.36 mmol) was dissolved in acetone (1 mL) in a round flask and oxone (0.24 g, 0.39 mmol) in water (1 mL) was added and the reaction was stirred for 20 min at RT, then sodium bisulfite (0.04 g, 0.39 mmol) was added to quench the reaction. After acetone evaporation, the mixture was extracted with DCM (3 x 5 mL) and the combined organics concentrated under vacuum. The crude product was dissolved in EtOAc (15 mL) and extracted by acid-base extraction (NaOH 1M and HCl 3M). The crude product was purified by flash column chromatography (EtOAc/hexane = 1:1) to afford the title phenol **19b** (0.04 g, 61%). δ_H (400 MHz, $CDCl_3$) 6.08 (2H, s, 2,4-*H*), 3.89 (6H, s, OC*H*$_3$), 2.48 (3H, s, C*H*$_3$). All data was in accordance with the literature[136].

5-Hexyn-1-bromide **(19c)**[137]

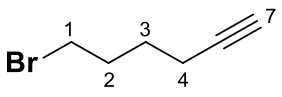

19c

5-Hexyn-1-ol (2.45 g, 25 mmol) was dissolved in DCM (50 mL) and added to mixture of CBr_4 (12.43 g, 37.5 mmol) and PPh_3 (9.83 g, 37.5 mmol). The reaction was stirred for 1.5 h, at RT, then a small amount of silica gel was added

and the solvent evaporated under vacuum. The silica residue was washed with hexane (3 x 5 mL) and the combined filtrate concentrated *in vacuo*. After evaporation, purification of the crude residue by distillation using a Kugelrohr Distillation Apparatus afforded the title bromide **19c** (1.21 g, 30%) as a colourless oil (bp 167.0 ± 23.0 °C at 760 mmHg). δ_H (400 MHz, $CDCl_3$) 3.46 (2H, t, J = 6.6 Hz, 1-*H*$_2$), 2.27 (2H, td, J = 7.0, 2.7 Hz, 4-*H*$_2$), 2.08 – 1.96 (3H, m, 2-*H*$_2$,6-*H*), 1.77 – 1.65 (2H, m, 3-*H*$_2$). All data was in accordance with the literature[138].

2,6-dimethoxy-4-(hex-5'-yn-1'-yloxy)acetophenone **19d**

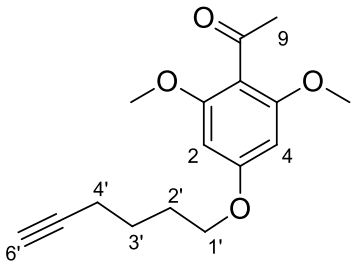

19d

4-hydroxy-2,6-dimethoxyacetophenone (**19b**) (1.00 g, 5.10 mmol) and 5-bromohexyne (**3c**) (1.63 g, 10.20 mmol) was dissolved in DMF (10 mL), then $CsCO_3$ (3.32 g, 10.20 mmol) and Bu_4NI (0.19 g, 0.51 mmol) was added. The reaction was stirred overnight at 60°C, and the mixture was then washed with water (2 x 10 mL) and the product extracted with DCM (2 x 10 mL). The organic layer was washed with water (2 x 10 mL), Brine (1 x 10 mL) and dried over $MgSO_4$. The product was concentrated under vacuum and purified by flash column chromatography (hexane/EtOAc = 8:2) to afford the title acetophenone (**19d**) (0.32 g, 23%). δ_H (400 MHz, $CDCl_3$) 6.09 (2H, s, 2,4-*H*), 4.00 (2H, t, J = 6.2 Hz, 1'-*H*$_2$), 3.78 (6H, s, OC*H*$_3$), 2.45 (3H, s, 9-C*H*$_3$), 2.29 – 2.19 (2H, m, 4'-*H*$_2$), 2.04 – 1.93 (3H, m, 2'-*H*$_2$, 6'-*H*), 1.78 – 1.62 (2H, m, 3'-*H*$_2$).

1-(4'-(hex-5"-yn-1"-yloxy)-2',6'-dimethoxyphenyl)-3-(3"'-nitrophenyl)prop-2-en-1-one (**19**)

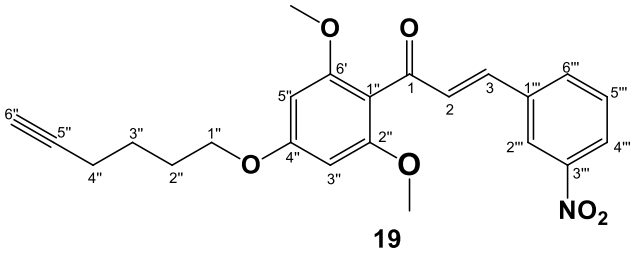

19

A mixture of the acetophenone (**19d**) (74 mg, 0.27 mmol), 3-nitrobenzaldehyde (40 mg, 0.27 mmol) and $Ba(OH)_2.8H_2O$ (21 mg, 0.07 mmol) in MeOH (5 mL) was stirred overnight at 40°C. After solvent evaporation, the product was extracted with EtOAc (3 x 10 mL) and the combined extracts washed with HCl - 1M (2 x 10mL), dried over $MgSO_4$ and concentrated under vacuum. The crude product was a yellow oil that was purified by flash column chromatography (hexane/EtOAc = 4:1), to afford the desired chalcone **19** (40 mg, 54%). ν_{max}. (ATR) 3291 (C≡C-H), 2939 (C-H Alkane), 1653 (C=O) cm^{-1}; δ_H (599 MHz, $CDCl_3$) 8.34 (1H, m, 2"'-*H*), 8.20 (1H, m, 4"'-*H*), 7.83 (1H, m 6"'-*H*), 7.55 (1H, m, 5"'-*H*), 7.43 (1H, d, J= 16.0 Hz, 3-*H*), 7.06 (1H, d, J= 16.0 Hz, 2-*H*), 6.16 (2H, s, 2',4'-*H*), 4.05 (2H, t J= 6.3 Hz, 1"-H_2), 3.78 (6H, s, OC$\underline{H}_3$), 2.30 (2H, m, 4"-H_2), 2.03 – 1.85 (3H, m, 2"-H_2,6"-*H*), 1.79 (2H, m, 3"-H_2). δc (151 MHz, $CDCl_3$) 193.1 (*C*-1), 162.4 (*C*-4'), 159.3 (*C*-2',6'), 148.8 (*C*-3"'), 140.2 (*C*-2), 137.1 (*C*-1"'), 133.9 (*C*-6"'), 131.6 (*C*-3), 123.0 (*C*-5"'), 124.4 (*C*-4"'), 122.8 (*C*-2"'), 111.5 (*C*-1'), 91.4 (*C*-4', 5'), 84.1 (*C*-5''), 68.9 (*C*-6''), 67.7 (*C*-1''), 56.1 (*C*-2', 5'-O*C*H_3), 28.3 (*C*-2''), 25.1 (*C*-3''), 18.3 (*C*-4''); m/z (LCMS, ESI+) 410.95 (MH^+); Accurate mass: (ES^+) Found MH^+, 410.1585: $C_{23}H_{24}NO_6$ requires *M*, 409.1525.

(9H-fluoren-9-yl)methyl tert-butyl (6-(2,5-dioxopyrrolidin-1-yl)-6-oxohexane-1,5-diyl)dicarbamate (**20a**)

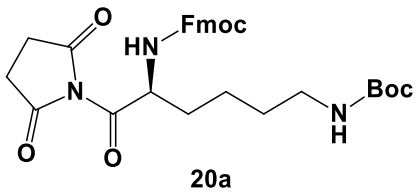

20a

The carboxylic acid, Fmoc-Lys(Boc)OH (0.24 g, 0.5 mmol) was solubilized in DMF (12 mL) and 1-(3-dimethylaminopropyl)-3-ethylcarbodiimide hydrochloride (0.13 g, 0.70 mmol) and N-hydroxysuccinimide (NHS) (0.132 g, 1.15 mmol) were added. The reaction was stirred for 24 h at 25 °C, and then quenched with saturated $NaHCO_{3(aq)}$ (10 mL). The product was extracted with EtOAc (3 x 10 mL) and washed with water (2 x 10 mL) and saturated $NaCl_{(aq)}$ (15 mL). The organic layer was dried over $MgSO_4$, and concentrated under vacuum to provide the desired activated ester **20a** (56 mg, 20%), LC-MS (*m/z* ESI+) = 566.194 (MH^+) $C_{30}H_{35}N_3O_8$ requires *M*, 565,242. The data was in accordance with the literature[139].

(9H-fluoren-9-yl)methyl tert-butyl(6-oxo-6-((5-(5-(2-oxohexahydro-1H-thieno[3,4-d]imidazol-4-yl)pentanamido)pentyl)amino)hexane-1,5-diyl) dicarbamate (**20b**)

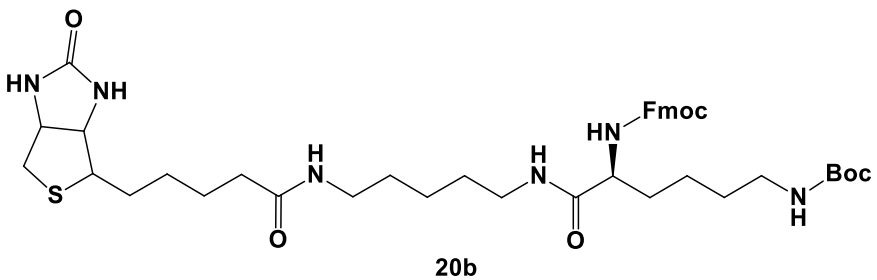

20b

The resulting NHS ester (56.5 mg, 0.1 mmol) was dissolved in MeOH (3 mL) and stirred for 2 h at 25°C with 5-(biotinamido)-pentylamine (13.2 mg, 0.04 mmol). The solvent was evaporated and the remaining residue was washed with EtOAc (2 X 6 mL), solubilized in chloroform and the solvent was evaporated to afford the desired amide **20b** (54.20 mg, 70%) confirmed by LC-MS (m/z ESI+) = 779.914 ($M2H^+$), $C_{41}H_{58}N_6O_7S$ requires *M*, 778.408. All data was in accordance with the literature[139].

(9H-fluoren-9-yl)methyl(6-amino-1-oxo-1-((5-(5-(2-oxohexahydro-1H-thieno[3,4-d]imidazol-4-yl)pentanamido)pentyl)amino)hexan-2-yl)carbamate (**20c**)

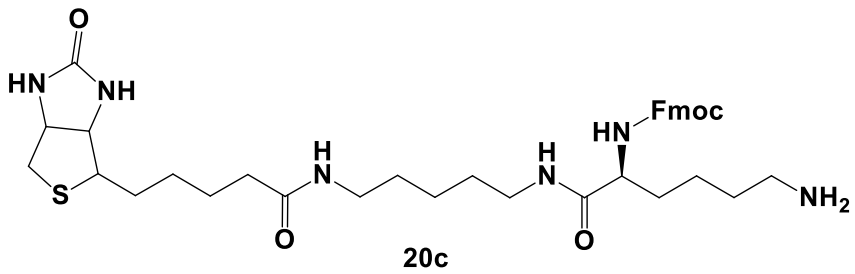

20c

The biotinylated carbamate **20b** (150 mg, 0.20 mmol) was dissolved in 4 M HCl/dioxane (8 mL) and stirred for 2h at RT. The solvent was evaporated to afford the deprotected amine **20c** (80 mg, 60%) and carried forward without further purification or analysis.

(9H-fluoren-9-yl)methyl(6-(6-azidohexanamido)-1-oxo-1-((5-(5-(2-oxohexahydro-1H-thieno[3,4-d]imidazol-4-yl)pentanamido)pentyl)amino)hexan-2-yl)carbamate (**20d**)

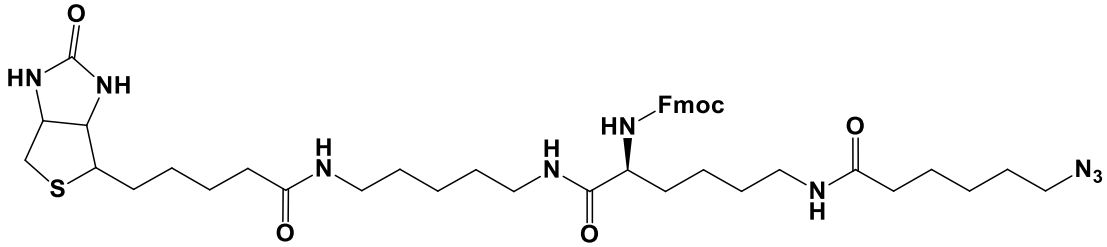

20d

A solution of the deprotected amine **4c** (80 mg, 0.12 mmol) in MeOH (2 mL) was added to NHS-6-azido hexanoic acid (120 mg, 0.48 mmol) and $NaHCO_3$ (20 mg, 0.24 mmol) in MeOH (8 mL) and stirred for 6h at RT. The reaction was then filtered and the solvent was removed under vacuum. The intermediate product was purified by flash column chromatography (chloroform/MeOH = 9:1) to afford the desired product **20d** (21 mg, 21%, crude product).

2-amino-6-(6-azidohexanamido)-N-(5-(5-(2-oxohexahydro-1H-thieno[3,4-d]imidazol-4-yl)pentanamido)pentyl)hexanamide (**20e**)

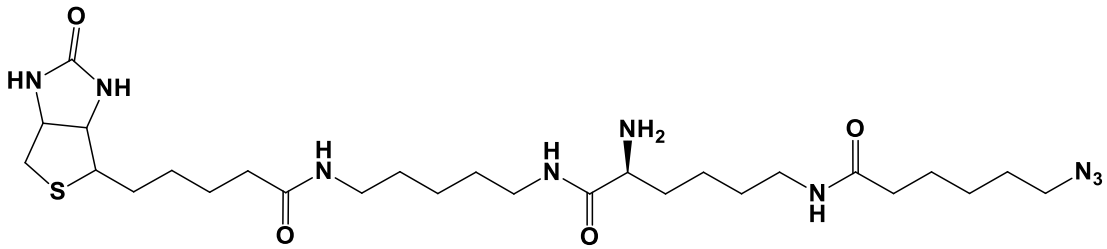

20e

Morpholine (0.58 g, 6.7 mmol) was added to a solution of the Fmoc amine **20d** (54.2 mg, 0.07 mmol) in DMF (5 mL) and stirred for 3 h at RT. DMF was then removed under vacuum and the product washed with EtOAc (2 x 2 mL) and concentrated under reduced pressure. The crude product was purified by flash

column chromatography (chloroform/MeOH = 9:1) to afford the desired product **20e** (21.0 mg, 42% crude).

5-((6-(6-azidohexanamido)-1-oxo-1-((5-(5-(2-oxohexahydro-1H-thieno[3,4-d] imidazol-4-yl)pentanamido)pentyl)amino)hexan-2-yl)carbamoyl)-2-(6-(dimethylamino)-3-(dimethyliminio)-3H-xanthen-9-yl)benzoate (**20**)

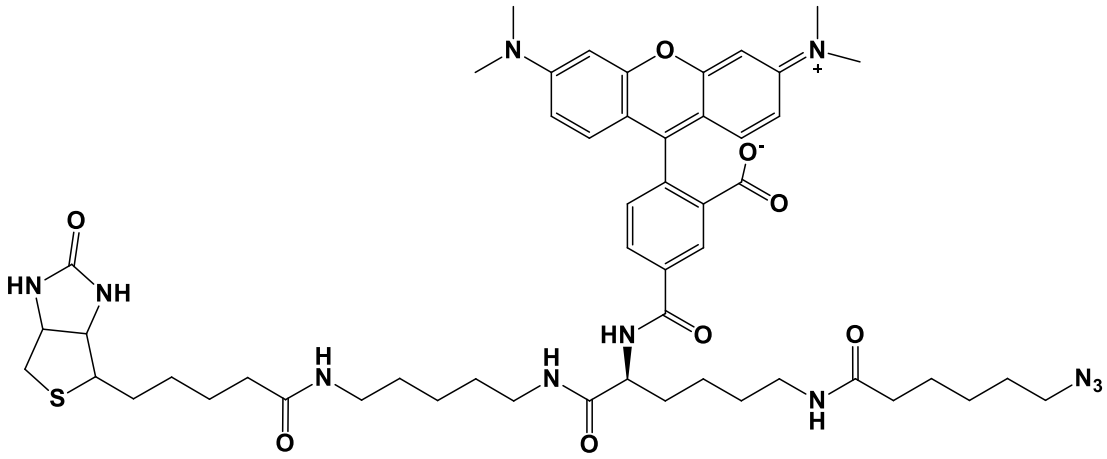

20

The deprotected intermediate **20e** (16.70 mg, 0.03 mmol) and 5-(and-6)-carboxytetramethylrhodamine, succinimidyl ester (15 mg, 0.03 mmol) was solubilized in DMF (1 mL). Triethylamine (28.30 mg, 0.28 mmol) was then added and the reaction stirred for 3 h, at RT under argon atmosphere. The solvent was removed under reduced pressure and the crude product purified by high performance liquid chromatography (HPLC) to afford desired product **20** (8.5 mg, 30%). MALDI-ToF m/z: 1008.5 (MH^+), 1031.5 (MNa^+); 1052.6 ($M2Na^+$). Accurate mass: Found (MH^+), 1008.5143: $C_{52}H_{70}N_{11}O_8S$ requires M, 1008.5129.

3.2 Biological experimental details

3.2.1 Parasites

L. amazonensis (MHOM/BR/75/Josefa), *L. infantum* (MHOM/MA67ITMAP263), *L. braziliensis* (MHOM/BR/75/M2903), *L. major* (MHOM/IL/81/Friedlin), *L. donovani* (MHOM/ET/67/HU3/LV9) and *L. mexicana* (MNYC/BZ/62/M379) were maintained as promastigotes at 26°C in M199 medium (CultiLab, Campinas, SP, Brazil) supplemented with 10% heat-inactivated fetal bovin serum (HIFCS) (CultiLab), 0.2% hemin (Sigma-Aldrich Co., St Louis, MO, USA), 100µg/mL streptomycin and 100 IU/mL penicillin (Sigma-Aldrich Co.). Parasites were used in the stationary phase of culture.

3.2.2 Animals and ethics statement

BALB/c mice used in the experiments were maintained under controlled temperature, filtered air and water, autoclaved bedding, and commercial food at our animal facilities at Federal University of Rio de Janeiro.

The animal protocols for this study were approved by the Federal University of Rio de Janeiro institutional Animal Care and Use Committee under the number 030/17. The research was conducted in compliance with the principles stated in the *Guide for the Care and Use of Laboratory Animals* (NIH)[140].

3.2.3 Anti-promastigote activity

Promastigotes of *L. amazonensis* (5 x 10^5/mL), *L. braziliensis* (2 x 10^6/mL) and *L. infantum* (2 x 10^6/mL), *L. major* (2 x 10^6/mL), *L. donovani* (2 x 10^6/mL) and

L. mexicana (5 x 10^5/mL), were incubated with different compound concentrations in M199 medium in 96-well plates (Corning) for 72h at 26ºC. Parasite viability was then assessed fluorimetrically (Spectramax M5, Molecular Devices) using alamarBlue (ThermoFisher scientific) according to manufacturer's protocol at 555/585nm (band pass-BP excitation/emission wavelength). The concentration required to reduce cell viability by 50% (IC_{50}-values) were calculated using non-linear regression analysis and GraphPad Prism 6.0 software.

3.2.4 ROS production by promastigotes

L. amazonensis promastigotes (1 x 10^6/mL) cultured in M199 medium supplemented with 5% HIFCS in 24 well-plates (Corning), were incubated with different drug concentrations (0.35, 0.7 and 1.4 µM) for 48h at 26ºC. Cells were then harvested and adjusted to (2 x 10^6/mL) in PBS, transferred to black 96 well plates (Corning) and incubated with a free oxygen radical sensor, H_2DCFDA (20 µM), for 30 min at RT. ROS production was assessed by fluorimetry at 485 / 528 nm BP (ex / em) using the Spectramax M5. Results were expressed as Arbitrary Fluorescence Units (AFU).

3.2.5 Promastigote lysate

L. amazonensis promastigotes were grown to a density of 6×10^7 parasites/mL. Cultures were then incubated at 26°C for 4 h with compound **19** (1 or 5 µM). Subsequently, cells were harvested (800 × *g*, 15 min, 4°C), washed twice with cold PBS and lysed by sonication (Branson) (4x 12 seconds, 15% on dutycycle-10, on ice) in lysis buffer (1% sodium deoxycholate, 0.5% SDS, 50 mM Tris (pH 7.4), 150 mM NaCl and EDTA-free protease inhibitor Sigma-Fast

(Sigma-Aldrich)). The resulting lysates were centrifuged (13,000 × *g*, 15 min, 4°C) to remove insoluble material. Protein concentration in each sample was quantified by BCA method (Sigma-Aldrich) according to manufactures' protocol.

3.2.6 Bone Marrow Derived Macrophages (BMDM)

BMDM were differentiated from bone marrow of BALB/c mice as described previously[141]. Briefly, bone marrow was extracted from femurs and tibias of euthanized mice and maintained in RPMI medium (Cultilab) supplemented with 10% HIFCS and 20 % of transfected L-cell conditioned media as source of MCSF (macrophage colony-stimulating factor) at 37° C / 5 % CO_2 for 7 days. After that, plates were washed with warm PBS to remove non-adherent cells, the adherent BMDM were gently scraped off and maintained in RPMI supplemented with 10% HIFCS without L-cell conditioned media until use for no longer than two days.

3.2.7 Anti-amastigote activity

BMDM (2×10^5) were seeded and cultured on circular glass coverslips in 24-well plate for 24 h at 37° C / 5 % CO_2. The monolayers were then infected with 10^6 *L. amazonensis* promastigotes for 4 h at 34°C / 5% CO_2. After removal of free parasites by washing with PBS, the culture was incubated for 24h at 37°C / 5% CO_2, before the addition of drugs in different concentrations for 48h at 37°C / CO_2. Cells were stained using the Panotic kit (Newprov, Brazil) according to manufacturer's instructions. For each coverslip, about 200 macrophages were examined using Nikon Eclipse Ti at 1000 x magnification to count the number of amastigotes per macrophage. The IC_{50} values were determined as described above in Section 3.2.3.

3.2.8 Intracellular amastigotes and macrophages lysates

BMDM (2.5 x 10^6 / well) were cultured in 6 well-plates (Corning). After 24 h incubation at 37 ºC, cells were infected as described for anti-amastigote assay in Section 3.2.6. After 72 h of infection, intracellular amastigotes were purified as described previously[142]. In short, infected macrophages were washed twice with PBS and incubated with RPMI supplemented with 0.008% SDS for 1 min at room temperature, any remaining cells were scraped from the plate. Macrophage disintegration confirmed by microscopy (Nikon Eclipse E200-LED) with 400× magnification. RPMI medium supplemented with 10% HIFCS (complete medium) was added and the milieu centrifuged for 8 min at 2400 × g, RT. The supernatant was discarded and pellet resuspended in complete medium and re-centrifuged for 8 min at 75 × g. The supernatant containing the amastigotes was retained. This process was repeated three times and the pooled supernatants centrifuged for 8 min at 2400 × g giving a pellet enriched with amastigotes that was resuspended in complete medium. Presence of amastigotes was confirmed by optical microscopy.

For amastigote tagging, all resulting purified amastigotes were incubated with compound **19** (5 µM) for 5 h at 26ºC and the lysate prepared as described above for promastigote forms in Section 3.2.5.

For macrophage tagging, uninfected macrophages (2.5 x 10^6 / well) were incubated with same amount of compound **19** for 5 h at 37ºC and the cell lysate prepared as above.

3.2.9 Cytotoxicity

BMDM (1 x 10^5) were plated into 96-well culture plates and maintained for 24 h at 37 °C / 5% CO_2. Cells were then incubated with different drug concentrations (0.137 to 100 µM) for 48 h. The release of the cytosolic enzyme lactate dehydrogenase (LDH) was measured using a colorimetric kit (Doles, Brazil), according to the manufacturer's protocol adapted for 96-well plates. Optical density readings were at 492nm using Spectramax M5 (Molecular devices, USA). Results were expressed as percentage of specific release of LDH:

% Specific LDH release = (Treatment-medium) / (Triton-medium) x 100

Positive controls were macrophages incubated with 2% Triton x100 (Sigma–Aldrich, Brazil). CC_{50} values were calculated using non-linear regression analysis as for IC_{50} values in Section 3.2.3. The selectivity index (SI) for each compound was calculated as the ratio between cytotoxicity (CC_{50}) and anti-amastigote activity (IC_{50}).

3.2.10 Confocal microscopy

L. amazonensis promastigotes were incubated with or without compound **19** (5 µM) for 5 h at 26 ºC. Parasites were then washed with PBS and fixed with 4% of paraformaldehyde in PBS (pH 7.4). Fixed parasites were then submitted to cycloaddition reaction (click reaction) with **20** (5 µM) for 1 h, at RT, in the presence of $CuSO_4$ (1 mM), sodium ascorbate (2 mM) and Tris((1-hydroxy-propyl-1H-1,2,3-triazol-4-yl)methyl)amine – THPTA (2 mM). Following incubation with Hoechst 33342 for 15 min for nucleus and kinetoplast labelling, cells were

washed with PBS, plated onto a microscope slide pre-treated with poly-L-lysine (Sigma-Aldrich) and mounted with ProLong Antifade Mounting Medium (ThermoFisher, P7481). The fluorescence of molecule **20** and Hoechst were acquired using a Leica TCS-SPE confocal microscope at 63x (ACS APO 63x 1.30 oil objective) on Hoechst (350 / 461 nm) and TAMRA (555 / 580 nm) wavelengths. Differential interference contrast (DIC) microscopy was used to capture light images. Images were analysed using Adobe Photoshop CC software (version 14.2.1).

3.2.11 Competition assay

L. amazonensis promastigotes (6×10^7/mL) were incubated with compound **11** at different concentrations (1.0, 3.0, 9.0, 27.0 µM) for 4 h at 26ºC in M199 medium. Cells were then washed twice with PBS and incubated with compound **19** (1 µM) for additional 4 h in M199 medium at 26ºC. Subsequently, parasites were washed with PBS and the promastigote lysates obtained as described above in Section 3.2.5.

3.2.12 Copper(I)-catalyzed alkyne-azide cycloaddition (CuAAC) labelling

Proteins of promastigotes, intracellular amastigotes and macrophage lysates obtained in Sections 3.2.5 and 3.2.7 were precipitated with acetone (4 volumes at −20°C for 1 h) and resuspended in PBS. Protein concentration was then assayed using Bicinchoninic Acid Kit (Sigma Aldrich, BCA1) according to manufacturer's protocol. Protein concentration was adjusted to 1 mg/mL and a mixture of click reagents (5 µM (compound **20**), 1 mM $CuSO_4$, 2 mM THPTA and

Sodium Ascorbate 1 mM) were added and cycloaddition reaction was carried out for 1 hr at room temperature, then quenched by addition of 4x Laemmli sample loading buffer (8% SDS, 40% glycerol, 200mM Tris-HCl and 0.4% Bromophenol Blue) with 50 mM of Dithiothreitol – DTT (Bio-Rad).

3.2.13 SDS-PAGE

Protein samples obtained in Section 3.2.12 were mixed with sample loading buffer, heated for 5 min at 95 °C and centrifuged for 1 min at 13,000 x g. Protein concentration was adjusted to 30 to 50 µg and 30 µL-samples were loaded on 8 to 12% polyacrylamide-SDS gels. Samples were electrophoresed at 200 V for 1 hour in a MiniProtean system (BioRad) containing 1x Tris-Glycine electrophoresis buffer (25 mM Tris-base, 190 mM Glycine, 0.1% SDS (v/v) pH 8.3). Protein prestained ladders (BioRad) were loaded onto gels as a molecular weight standard. At the end of each run, gel images were taken to detect fluorescent bands using a Gel Doc XR imager (Bio-Rad) with the Oriole filter (270 / 604 nm BP). Gels were then stained with Comassie Brilliant Blue G-250 (Bio-Rad) to detect all protein bands. All gel images were analysed and edited using Image Lab software (Bio-Rad).

3.2.14 Western Blot analysis

Proteins in CuAAC labelled gel bands from Section 3.2.13 were transferred from gels to PVDF membrane (Immun-Blot, Bio-Rad) using a wet transfer system (Mini-PROTEAN, Bio-Rad) containing 1x transfer buffer (25 mM Tris-base, 190 mM Glycine, 20 % Methanol), at 100V for 1 hour. Following blocking step (5 % BSA in TBST), membranes were incubated with polyclonal

mouse anti-cytosolic TXNPx antibody (1:4000) (kindly donated by Prof Angela Cruz, Faculdade de Medicina de Ribeirão Preto - USP, Brazil) overnight at 4°C in blocking solution. After two washing steps with TBST, membranes were then incubated with secondary antibody (anti-Mouse IgG-HRP, Thermo Fisher, 1:5000) for 1h in blocking solution. Chemiluminescence detection was carried out using Clarity Max Western ECL (Bio-Rad) according to the manufacturer's instructions on an ImageQuant LAS 4000 Imager (GE Healthcare).

3.2.15 Two-dimensional gel electrophoresis

This part of work was performed in collaboration with Dr Marjolly Caruso Brígido and Professor Russolina Zingali from Medical Biochemistry Institute (IBqM) at UFRJ.

Protein samples (1mg/mL) from *L. amazonensis* promastigotes treated with **19** and linked to **20** as in 3.2.12 were processed using a Ettan 2D Clean-Up kit (GE Healthcare) to remove salt excess, according to manufacturer's procedure. Protein lysates (500 µg) were primarily separated in the first dimension by IEF (Isoelectric focussing) on 7 cm pH 3-10 (Immobiline® Dry Strip, GE Healthcare), using the IEF unit Ettan IPGphor II (Amersham Biosciences, GE Healthcare). IEF process was done at 20°C, 50 mA, 60 V, using the overnight programme detailed in Table 2. Once completed, strips were equilibrated by 20-min incubation in 10 mL of equilibration buffer (6 M urea, 30% glycerol, 2% SDS and 75 mM Tris pH 8.8) with 10 mg/mL of dithiothreitol (DTT). This was followed by a second 20-minute incubation in 10 mL equilibration buffer with 12.5 mg/mL of iodoacetamide (IAA). Strips were placed on to a 10 % 1.5 mm polyacrylamide gels and SDS-PAGE was run in the second dimension at 121 V for 1.5 h. For all

2-D experiments, two gels with same samples were run in parallel (Gel 1 and Gel 2). The fluorescence of both gels was scanned using the Gel Doc XR imager (Bio-Rad). Proteins from Gel 1 were stained using Comassie Brilliant Blue G-250 and scanned again. Gel 2 proteins were transferred from gels to PVDF membrane as described above, incubated with polyclonal mouse anti-cytosolic TXNPx antibody (1:4000) and IRDye® 800CW Goat anti-Mouse IgG (1:20000) (LI-COR) as a secondary antibody. The gel fluorescence was scanned using LI-COR Odyssey® Infrared Imaging System.

Table 2. IEF running programme.

Steps	**Voltage**	**Volt hours**
Rehydration step	60 V	12:00 h
Focussing step & hold	100 V	100 V / h
Focussing step & hold	200 V	200 V / h
Focussing step & hold	500 V	500 V / h
Focussing step & hold	1000 V	1000 V / h
Focussing gradient & hold	3500 V	14000 V / h

3.2.16 Protein identification by Mass Spectrometry- UFRJ

Proteins from promastigotes treated with **19** and linked to **20** as in Section 3.2.12 were separated by SDS-PAGE (1D and 2D) and fluorescence imaged as above. Bands (1D) or spots (2D) were manually excised and incubated overnight with 25 mM NH_4HCO_3 in 50% acetonitrile to remove comassie blue stain. Protein disulfite bonds were reduced with 10 mM DTT (USB Corporation) in 25 mM

NH_4HCO_3 at 56°C for 1h, followed by cysteine alkylation by addition of 55 mM iodoacetamide in the same buffer for 45 min at RT. Digestion was achieved by adding 10 µL of trypsin (modified sequencing grade; Promega) solution (0.01 µg μL^{-1} in 25 mM NH_4HCO_3) and incubating overnight at 37°C. The peptides generated were extracted with 5% trifluoroacetic acid (TFA) dissolved in 50% acetonitrile. This solution was concentrated in a Speed-Vac system (Thermo Fisher scientific).

Each sample was then solubilized in 20 µL 0.1% formic acid and 3% acetonitrile in deionized water and the extracted peptides loaded onto a Waters Nano acquity system (Waters, Milford, MA). Peptides were desalted on-line using a Waters Symmetry C18 180 µm X 20 mm, 5 µm trap column. The sample injection volume was typically 7.5 µL, and the LC was performed by using BEH 130 C18 100 µm X 100 mm, 1.7 µm column (Waters, Milford, MA) and eluting (0.5 µL/min) with a linear gradient (10–40%) of acetonitrile containing 0.1% formic acid.

Electrospray tandem mass spectra were recorded using a Q-ToF quadrupole/orthogonal acceleration time-of-flight spectrometer (Waters, Milford, MA) interfaced to the Nano acquity system capillary chromatograph. ESI voltage was set at 3500 V, source temperature was 80 °C and cone voltage was 30 V. The instrument control and data acquisition were conducted by a MassLynx data system (Version 4.1, Waters), and experiments were performed by scanning from a mass-to-charge ratio (*m*/*z*) of 400–2000 using a scan time of 1 s, applied during the whole chromatographic process. The mass spectra corresponding to each signal from the total ion current (TIC) chromatogram were averaged, allowing for

an accurate molecular mass measurement. The exact mass was determined automatically using the Q-ToF's LockSpray™ (Waters, Milford, MA).

Data-dependent MS/MS acquisitions were performed on precursors with charge states of 2, 3 or 4 over a range of 50–2000 *m*/*z* and under a 2 *m*/*z* window. A maximum of three ions were selected for MS/MS from a single MS survey. Collision-induced dissociation (CID) MS/MS spectra were obtained using argon as the collision gas at a pressure of 40 psi, and the collision voltage was varied between 18 and 90 V depending on the mass and charge of the precursor.

All data were processed using the ProteinLynx Global server (version 2.5, Waters). The processing automatically lock mass corrected the *m*/*z* scale of both the MS and MS/MS data utilizing the lock spray reference ion.

3.2.17 Protein alignment

Peptide sequences from all *Leishmania* species used in this work were obtained in FASTA format from the UniProt website (https://www.uniprot.org). Sequences were aligned with the Clustal Omega program and the generated multiple sequence alignment were coloured by BoxShade tool (http://sourceforge.net/projects/boxshade).

3.3 DNA methods

3.3.1 Transformation into StellarTM competent Cells (*E. coli* HST08)

Stellar Competent Cells are an *E. coli* HST08 strain that provide high transformation efficiency. Fifty µL of frozen Stellar cells (Clontech) were thawed

for 30 min on ice. Then, 1.0 µL of pUC57 plasmid (200 ng; ampicillin resistant) containing the open reading frames for cTXNPx from *L. amazonensis, L. major, L. mexicana* and *L. donovani,* purchased from Genscript (Figure 21- Table 9), was added to the cells and mixed gently. The tubes were maintained on ice for 30 min prior a heat shock in a 42°C water bath for 45 seconds and 2 min in ice. After that, 450 µL of pre-warmed SOC medium was added to the cells and incubated at 37°C for 45-60 min with shaking at 200 rpm. Then, 50 µL of this culture was diluted in 50 µL of warm SOC media and spread onto a LB-agar ampicillin (100 µg/mL) plate and incubated at 37°C overnight.

From each plate 5 colonies were taken and individually cultivated in 5 mL of LB media with ampicillin overnight at 37ºC with shaking. Then, 0.5 mL of culture was diluted in 0.5 mL of sterile 50% (v/v) glycerol solution, placed in labelled cryovials and frozen at -196°C. The plasmid DNA was purified from the remaining 4.5 mL using the QIAprep Spin Miniprep Kit (QIAGEN), according to the manufacturer's instructions.

3.3.2 Polymerase chain reaction (PCR)

DNA fragments were amplified using Phusion® High-Fidelity PCR Master Mix (New England BioLabs- NEB). PCR reaction mixture was set up on ice as per manufacturer's instructions, as detailed on Table 3. The reaction was completed according to the programme detailed in Table 4 using 3Prime Thermal Cycler (Techne). All used primers are described in Table 5. Reaction products were resolved using 1.5 % agarose gel electrophoresis.

Table 3. PCR mixture composition.

PCR reaction mix	1 reaction	8 reactions
DNA template – 20 ng	1.0 µL	8.0 µL
Forward primer- 0.5 µM	2.5 µL	20.0 µL
Reverse primer- 0.5 µM	2.5 µL	20.0 µL
HiFi PCR Mix 2X	12.5 µL	100.0 µL
Water	6.25 µL	50.0 µL
DMSO	0.25 µL	2.0 µL
Total volume	25 µL	200 µL

Table 4. PCR reaction programme.

PCR reaction steps	Temperature	Time
Initial denaturation	98 ºC	1 minute
Denaturation	98 ºC	10 seconds
Annealing	62 ºC	15 seconds
Elongation	72 ºC	30 seconds
Final elongation	72 ºC	5 minutes

Table 5. Primers used for PCR amplification.

Primers used	
L.ama_Rev	5' - ATGGTCTAGAAAGCTTTATTGTTTGCTAAAATAGCCTTCAAC - 3'
L.ama_For	5' - AAGTTCTGTTTCAGGGCCCGATGAGCTGCGGTGACGC - 3'
L.maj_Rev	5' - ATGGTCTAGAAAGCTTTATTGTTTGCTAAAATAGCCTTCAACG - 3'
L.maj_For	5' - AAGTTCTGTTTCAGGGCCCATGAGCTGCGGTAACGCGA - 3'
L.mex_Rev	5' - ATGGTCTAGAAAGCTTTATTGTTTGCTAAAATAGCCTTCAATG - 3'
L.mex_For	5' - AAGTTCTGTTTCAGGGCCCGATGAGCTGCGGTGATGCGAA - 3'
L.don_Rev	5' - ATGGTCTAGAAAGCTTTATTGTTTGCTAAAATAGCCTTCAACG - 3'
L.don_For	5' - AAGTTCTGTTTCAGGGCCCGATGAGCTGCGGTGATGCGAA - 3'

3.3.3 Agarose gel electrophoresis

Five µL of 6x Gel Loading Dye Blue (NEB) was added to the DNA solution (25 µL) and loaded onto a 1.5% (v/w) agarose TAE (40 mM Tris, 20 mM acetic acid, and 1 mM EDTA) gel with 10 ng/mL ethidium bromide. Five µL of GeneRuler DNA Ladder (Thermo-Scientific) was used as standard to DNA sizes. Then, gel was run in TAE buffer for 45 min at 100 V. DNA bands were visualized by UV transilluminator and documented using Gel Doc XR imager (Bio-Rad).

3.3.4 DNA purification from agarose gel

The desired band was excised from the gel and transferred to a 1.5 mL Eppendorf tube. DNA product was extracted and purified from gel slice using NucleoSpin Gel and PCR Clean-up kit (Macherey-Nagel), according to manufacturer's instructions.

3.3.5 Restriction enzyme digestion and fusion using In-Fusion cloning Kit

The expression vector pOPINF[143] was linearized by double digestion using restriction enzymes HindIII and KpnI (NEB) according to the manufacturer's protocol. Digestion was confirmed by gel electrophoresis.

Each insert In-Fusion reaction was set up according manufacturer's protocol (In-Fusion HD, Clontech). The reaction mixture containing 2 µL of 5x in-fusion enzyme, 2 µL of linearized pOPINF, 1 µL of Insert and 5 µL of water was incubated for 15 min at 50ºC. The products were then transformed into Stellar™ competent cells and the plasmids were purified by miniprep as described above (Section 3.3.1).

Miniprep purified plasmids were submitted to gene sequencing (15 µL at 60 ng/µL) using T7 promoter and terminator at Durham University DBS GENOMICS. The resulting nucleotide sequences were translated to the protein sequence using ExPASy tool and then aligned with their respective protein sequence from Protein Data Bank (PDB) using Clustal Omega program.

3.3.6 Transformation into BL21 (DE3) competent *E. coli*

pOPINF plasmids carrying the desired open reading frames were transformed into BL21 (DE3) competent *E. coli* (NEB) as per supplier's protocol. Transformed bacteria were then spread on LB-agar ampicillin plates and clones processed as above.

3.4 Protein methods

3.4.1 Expression of recombinant proteins in *E. coli* – BL21 (DE3)

E. coli BL21(DE3) carrying open reading frames of interest in pOPINF, were used for protein expression. For each frame, a respective glycerol cell stock was thawed and grown in 50 mL of LB-ampicillin overnight under shaking at 37º C. These were used as starter cultures for 1 litre LB-ampicillin at 37º C. When an absorbance value of 0.7- 0.8 at 600 nm was reached, 1 mL of Isopropyl β-D-1-thiogalactopyranoside-IPTG (Promega) (1M) was added and protein expression allowed to proceed for 20 h at 30ºC under shaking at 180 rpm. Cells were harvested (4000 rpm, 30 min, 4ºC), and resuspended in 50 mL of lysis buffer (20 mM Tris-HCl pH 7.5, 500 mM NaCl, 30 mM imidazole and 2 mM β-mercaptoethanol) with one tablet of Sigma-Fast protease inhibitors (Sigma-Aldrich). Then, cells were disrupted by sonication (2 cycles of 10% of burst on ice for 2 min at 40 % of intensity) and lysates were centrifuged at 21,000 rpm for 30 min at 4°C. The resulting supernatants were filtered through a 0.45 µm syringe filter to eliminate solid materials.

3.4.2 His-tag fusion protein purification

HisTrap HP-1 mL column (GE healthcare) was used for each recombinant protein purification. Columns were equilibrated with distilled water (10 column volume - CV) and then with lysis buffer (10 CV). The crude supernatant was loaded on column using a peristaltic pump - Econo Pump (Bio-Rad) at 1ml/min. Recombinant cTXNPx protein was eluted from HisTrap column with increasing amounts (20%, 40%, 60%, 80%, 100%) of elution buffer (50mM Tris-HCl pH 7.5,

500 mM NaCl, 1 M imidazole and 2 mM β-mercaptoethanol) using a AKTA Pure system (GE healthcare). During all purification steps, samples were taken and process efficiency was confirmed by SDS-PAGE (Novex™ 10% Tris-Glycine Mini Gels, Invitrogen).

Purified proteins were dialyzed into 10 mM ammonium bicarbonate solution, to eliminate imidazole excess, using 3.0 mL Slide-A-Lyser dialysis cassettes - 10K MWCO (ThermoFisher), overnight at 4ºC. The protein was quantified using a NanoDrop 2000 spectrophotometer (ThermoFisher) and calculated protein extinction coefficient (http://www.biomol.net/tools-protein-extinction-coefficient.php).

3.4.3 cTXNPx Mass Spectrometry analysis

Concentration of purified protein was adjusted to 0.6 mg/mL in 10 mM ammonium bicarbonate solution, pH 7.4, and submitted to the Durham University Mass Spectroscopy service. Mass spectra data was obtained using a Waters QToF Premier and the mass to charge ratios (*m/z*) reported in Daltons with the corresponding fragment ion.

3.2.4 Protein Thermal Shift Assay (TSA)

The thermal unfolding of cTXNPx alone or in the presence of ligands was monitored by real-time PCR. Concentration of purified proteins was adjusted to 1mg/mL, then SYPRO Orange 5000X (Sigma-Aldrich), an environmentally sensitive fluorescent dye, was added to a final dye concentration of 10X. Ten µL of proteins solution and dye were transferred to a 96-well PCR plate, and 10 µL

of the Durham pH and salt screen solutions (Molecular dimensions) added. PCR plate was sealed and centrifuged at 1000rpm for 2 min. Reaction mixture was incubated in a RT-PCR machine (7500 FAST Real-Time PCR System, Applied Biosystems) and samples heated from 24 to 95°C at a rate of 1°C per minute. Fluorescence data were collected using SYPRO Orange wavelengths, 455-485 nm for excitation and 567-596 nm for emission. The melting temperature curves ΔTm were calculated using the NAMI software[144].

For protein and ligand interaction analyses, 10 µL of cTXNPx (1mg/mL) in 20 mM HEPES buffer, pH 6.9, 50 mM NaCl and 5 mM DTT were incubated with ligands at different ratios for 30 min. The proteins were then transferred into 48-well PCR plates containing 10 µL of SYPRO Orange in water, sealed and reactions incubated in an RT-PCR machine, and SYPRO Orange fluorescence measured, as above. The melting point curves were calculated by Protein Thermal Shift software 1.3 (ThermoFisher Scientific).

3.5 Interaction between cTXNPx and chalcones *in silico*

3.5.1 cTXNPx molecular modelling

In order to understand the mechanism of interaction between the chalcone and cTXNPx, as well as the influence of the enone group on this interaction we first performed molecular modelling of cTXNPx enzyme. This part of work was done in collaboration with Professors Bárbara Abrahim-Vieira and Alessandra de Souza from Molecular Modelling Lab at UFRJ.

cTXNPx from *L. amazonensis* (LaTXNPx) was chosen as a model to help understand all biological results. Only of *L. major* TXNPx 3D structure is available in the literature[145]. Due to lack of LaTXNPx elucidation, a comparative modeling with LmTXNPx was employed to generate the structure of LaTXNPx. The template search, selection, model building and quality estimation were conducted within the an updated SWISS-MODEL server[146]. 3D-LacTXNPx model was validated for its stereochemical quality and 1D-3D comparison using SAVES server (http://servicesn.mbi.ucla.edu/SAVES/).

3.5.2 Chalcone docking studies

In order to investigate the binding mode of compound **11** with LaTXNPx, we performed molecular docking studies. AutoDock 4.2 software was used running on a Windows-based PC[147]. Further, to understand the importance of chalcone moiety, we also performed docking studies with the chalcone with the α-β bond saturated (compound **18**).

First, three-dimensional structures of molecule **11** and **18** were built and optimized using Spartan'10 software (Wavefunction Inc., 2012). The structures were minimized and a conformational analysis was done using Molecular Mechanics Force Field (MMFF). Then, lowest energy conformation obtained was subjected to geometric optimization in vacuum using the semi-empirical RM1. The tridimensional structure of LaTXNPx was obtained from comparative modeling as described previously.

Docking files were prepared using AutoDockTools. The protein was treated as rigid, polar hydrogen atoms were added, nonpolar hydrogen atoms

were merged and Gasteiger charges were assigned by default. The grid box was centered near of the catalytic cysteine residue (Cys52D) on x, y and z positions (-37.85, -87.43 and 8.50, respectively) with 0.375 Å spacing and identical 60x60x60 points. Docking studies were carried out using empirical free energy function and Lamarckian Genetic Algorithm. A total of 50 independent docking runs were carried out for each molecule using program default parameters. Results of the most favourable free energies of binding in more populous clusters were selected as possible structures of resultant complexes. Docking interaction analyses were performed using Pymol software (Schrodinger, LCC, 2009).

3.6 cTXNPx - Knockout parasites

To understand the importance of the enzyme for *Leishmania* survival, CRISPR-Cas9 approach was chosen as an acceptable methodology to generate parasites lacking cTXNPx. Experiments were conducted using *Leishmania mexicana* (MNYC/BZ/62/M379) due to the availability of its entire genome in the databases, similarity with *L. amazonensis* and the availability of a well-described and well-developed methodology for generation of knockout parasites using CRISPR-Cas9[148].

The website http://tritrypdb.org/tritrypdb/ was accessed to identify gene position and number of copies on parasite's genome. Two copies of the gene were found on parasite genome at chromosome 15 (LmxM.15.1040 and LmxM.15.1160) (Figure 47).

sgRNAs were designed by CRISPR Design Tool (http://www.leishgedit.net/) using gene IDs. For each target mutation, a set of one

5’ sgRNA, 3’sgRNA, upstream forward primer and downstream reverse primer was generated, the sequence of all generated primers is depicted on Table 10. All oligonucleotides were purchased from Sigma-Aldrich.

sgRNAs for each gene were amplified by PCR using a generic primer G00 as follows: 0.2 mM dNTPs, 2 µM of primer G00, 4 µM of gene-specific sgRNA, 1.25 unit of GoTaq polymerase (Promega), were mixed in 5× GoTaq reaction buffer with $MgCl_2$ (Promega), diluted in nuclease-free water to a 25 µl total volume. PCR steps were 30 s at 98°C followed by 35 cycles of 10 s at 98°C, 30 s at 60°C, 15 s at 72°C. The presence of expected PCR product was confirmed by 2% agarose gel.

DNA cassettes containing puromycin resistance gene, as drug-selective marker, were amplified by PCR from pT plasmids, gently gifted by Eva Gluenz group. PCR reaction was carried out with 30 ng circular pT Puro plasmid, 0.2 mM dNTPs, 10 µM of Upstream forward primer, 10 µM of Downstream reverse primer, 1.25 units of GoTaq Polymerase (Promega), were mixed in 5× GoTaq reaction buffer with $MgCl_2$ (Promega), diluted in nuclease-free water to a 25 µl total volume. PCR steps were 5 min at 94°C followed by 40 cycles of 30 s at 94°C, 30 s at 65°C, 2 min 15 s at 72°C followed by a final elongation step for 7 min at 72°C. Presence of the expected PCR product was confirmed by 2% agarose gel.

Once with *L. mexicana* promastigotes expressing Cas9 and T7 RNA polymerase[148] and all PCR products in hand, the next step was to transfect *L. mexicana* promastigotes with sgRNAs and donor DNA. Tree distinct transfections were performed, one for LmxM.15.1040 gene, one for LmxM.15.1160 gene, and one for both genes. In all transfections, promastigotes of *L.mex* Cas9 T7 were

transfected with two sgRNA 5' and 3' templates to generate a double-strand break upstream and downstream of the gene, and with the repair cassettes containing the Puromycin resistance gene. For transfections, *L.mex* Cas9 T7 ($2x10^7$) were washed twice with 1× Tb-BSF, and resuspended to 100 µL. Parasites were transferred to an electroporation cuvette followed by addition of a mixture of the PCR products containing (sgRNA and donor DNA), approximately 50 µL. Then, cells were transfected by electroporation using one pulse with program X-001 in the Amaxa Nucleofector IIb (Lonza).

After electroporation, parasites were transferred to a culture flask with 5 mL of pre-warmed M199 medium supplemented with 20% of HIFCS, and allowed to recover overnight at 26ºC. Transfected parasites were selected by addition of Puromycin at 20 µg/mL (Sigma-Aldrich) to culture flask.

After one week under antibiotic pressure, the phenotypic changes on the cTXNPx knockout parasite were visualized by phase contrast microscopy using Nikon Eclipse Ti at 1000 x magnification.

3.7 Statistical analysis

Single-variance analysis (ANOVA) and *t*-test was used to compare differences between group samples followed by Dunett post-test, for comparisons of all groups to control group. For multiple comparison the used post-test was Bonferroni. All statistical analyses were performed using GraphPad Prism 6 software and differences were considered significant when $p \leq 0.05$, in a number of at least 2 independent experiments.

4. RESULTS

4.1 Chalcone analogues and probe synthesis

The biological target of chalcones in *Leishmania* has not been defined and therefore the aim of the work presented in this thesis was to employ activity based protein profiling (ABPP) approach to identify the protein target in the parasite[129]. The ABPP approach was chosen among all available methodologies to identify drug targets[116] because of the flexibility of using small molecules (tags) which allow intracellular visualization of possible targets through the attachments of fluorophores. In addition, bound proteins can be purified using affinity chromatography methods by the addition of a biotin group.

Our chemical tool for ABPP is a chalcone analogue modified with a spacer group and a terminal alkyne (compound **19**). The alkyne group will enable connection between chalcone and an azido containing ABPP tag through the copper(I)-catalysed azide alkyne cycloaddition reaction (CuAAC). This methodology was selected due to the reactional specificity of azide - alkyne cycloaddition and the possibility to perform the reaction in biological conditions, such as aqueous buffer and neutral pH[149].

Chalcone NAT22 (**11**) was chosen as a good lead structure for the probe as the previously developed synthetic route makes this hit compound easily accessible. This molecule is a tri-methoxylated nitro-chalcone which differs from CH8 chalcone only by methylation of the C-2 hydroxyl group in ring A (Section 1, Figure 5). In recent work our group showed that, by Claisen-Schmidt condensation[48], the synthesis of NAT22 **11** (Scheme 1) could be achieved in an

overall 85% yield, whereas the original chalcone, (CH8, **10**)**,** was obtained in only 18%. Importantly, compound **11** showed activity very similar to CH8 *in vitro* against promastigote and amastigote forms and *in vivo* in a murine CL model[53].

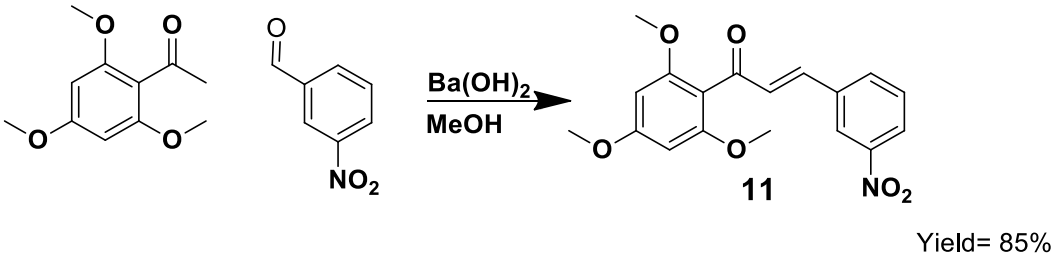

Yield= 85%

Scheme 1. Chalcone NAT22 (**11**) synthesis.

As discussed in the introduction, the fundamental tool of ABPP is an active site-directed covalent probe and it was hypothesized that the electrophilic enone would act in this regard potentially reacting with a nucleophilic residue in the active site of the target protein. Consistent with this, there are many reports in the literature that discuss the essentiality of the enone group for biological activity of chalcones[37]. In order to determine the importance of the double bond for anti-leishmanial activity in NAT22, a dihydrochalcone **18,** lacking the α,β-unsaturation was synthesized. Generation of the enolate of trimethoxyacetophenone with LiHMDS followed by addition of 3-nitrobenzylbromide afforded the dihydrochalcone **18** in 17% of yield as a pale yellow powder (Scheme 2). Although the yield was low sufficient material was obtained to be used as a control in the pharmacophore group assays described below in the Section 4.10.

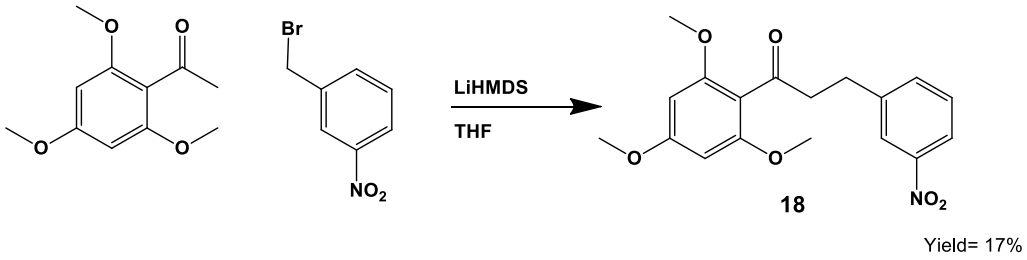

Scheme 2. Chalcone lacking enone group (**18**) synthesis.

Having synthesised the compound without the enone group, our attention turned to the remainder of the probe synthesis. The *para* -position of the A-ring was chosen for linker attachment to avoid spacer group interaction with essential groups for anti-leishmanial activity of CH8, such as the nitro group and enone linker. The synthesis started with readily available 2,6-dimethoxyacetophenone and the first objective was to selectively introduce a hydroxy group at the 4-position. To achieve this a sterically controlled C-H borylation reaction with B_2pin_2 followed by oxidation with hydrogen peroxide was developed providing the desired phenol in good yield (Scheme 3). The alkynyl spacer group was then added through reaction with 5-Hexyn-1-bromide using $CsCO_3$ and Bu_4NI in DMF. Finally, chalcone synthesis was completed by aldol condensation with 3-nitrobenzaldehyde and $Ba(OH)_2$ in MeOH. The desired compound **19** was obtained as a yellow powder with a 54% yield (Scheme 3) as evidence by ‘H NMR, with presence of peaks related to alkynyl spacer group, and mass spectrometry analysis that shows exact mass of the desired chalcone analogue (MH^+, 410.1585: $C_{23}H_{24}NO_6$).

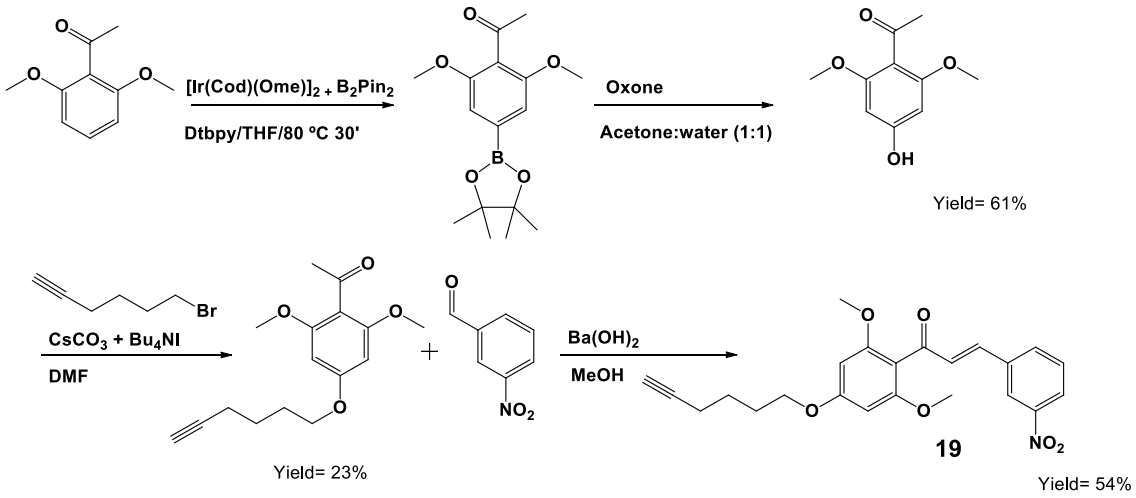

Scheme 3. Synthesis route of chalcone analogue (**19**) with an alkyne group.

With the desired probe prepared it was then necessary to prepare the ABPP purification unit. In this thesis, a strategy which utilizes a trifunctional probe (**20**)**,** containing two reporter tags, rhodamine and biotin, to enable simple target detection and purification, was chosen. Additionally, an azide group was added, as a reactive group, to foster linking with compound **19.** The trifunctional probe was synthesized based on a procedure described in the literature[139] and it is detailed in Scheme 4. Following purification by high performance liquid chromatography (HPLC) compound **20** was obtained as a pink powder with an overall yield of 30% characterised by a peak in the MALDI-ToF mass spectrum at 1008.5 *m/z* ($MH^+ = C_{52}H_{70}N_{11}O_8S$).

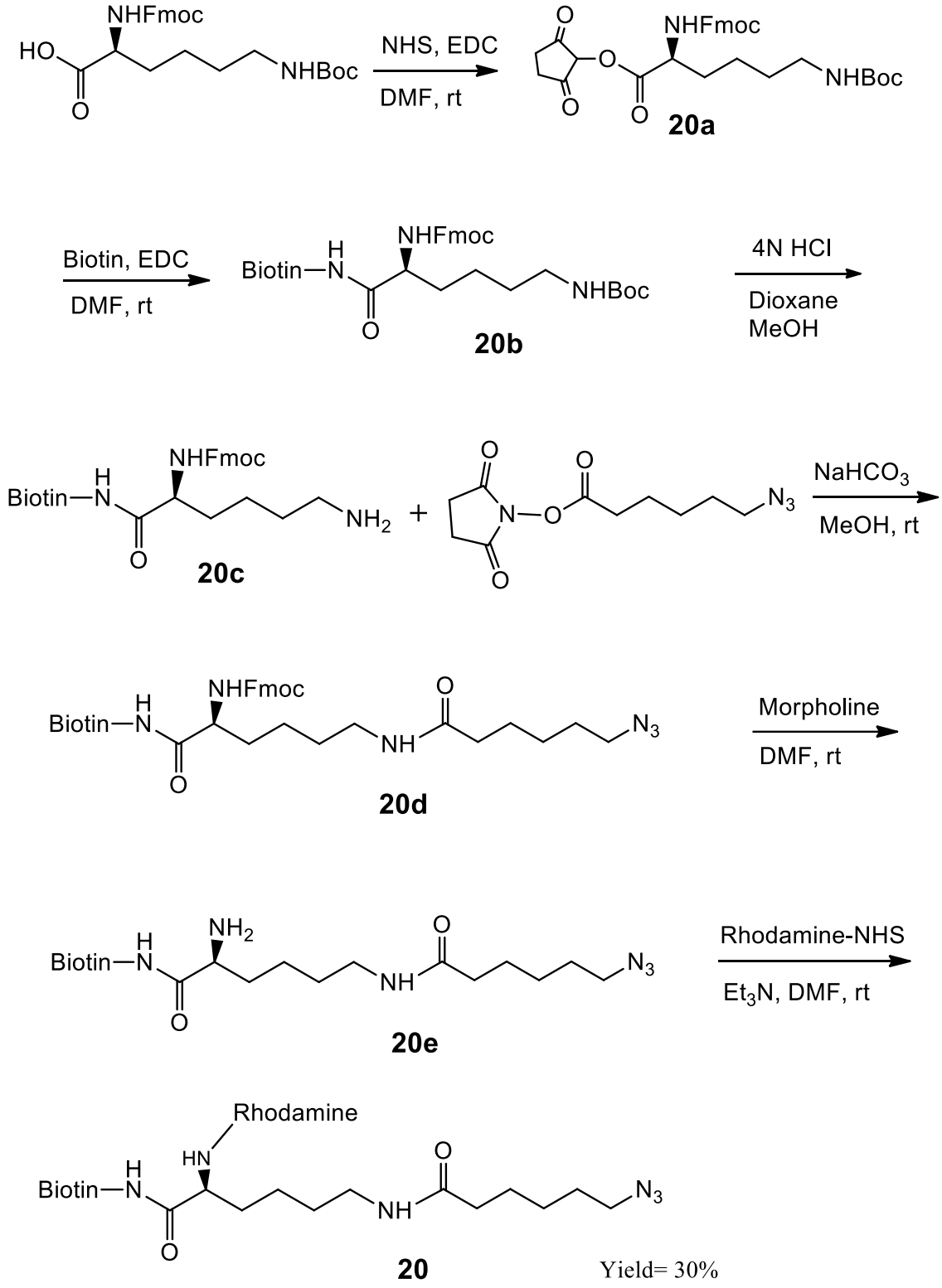

Scheme 4. Trifunctional probe (**20**) synthesis route.

In summary, the desired chalcone analogues and a trifunctional probe containing rhodamine as a fluorophore, biotin for affinity enrichment and an azide for the cycloaddition reaction were successfully synthesised[139]. Whilst some of the yields were only moderate sufficient amounts of material could be obtained. Although, further modifications to the synthetic routes could be explored to improve the yields, this was beyond the scope of this thesis.

4.2 Probe activity against *Leishmania* promastigotes

The main aim of the ABPP approach is to use a molecule based on the chalcone structure to bind to the biological target in the parasite. Then, the target visualization using ABBP tags, such as compound **20**. Followed by subsequently target protein purification and identification using affinity chromatography and fluorescence, respectively.

To validate our synthesised probes, prior to applications in ABPP, it was necessary to show that the analogue had similar activity to the original molecule which indicates that its binding to the same target. With analogues **11**, **19** and **20** in hand, our attention turned towards measuring their activity against promastigotes.

Promastigotes from different species, which cause both clinical manifestations of leishmaniasis around the world (*L. amazonensis, L. donovani, L. braziliensis, L. major and L. infantum*), were incubated with NAT22 (**11**), the analogue containing the spacer group (**19**), the trifunctional probe (**20**) and pentamindine as a positive control at different concentrations. After incubation at 26ºC for 72 h, parasite viability was assessed using the Alamar Blue method.

Figure 11A-E shows promastigote inhibition curves in the presence of each treatment. It was possible to observe a profile of similar parasite killing in all the species tested. Table 6 lists the IC_{50} values for the treatments. NAT22 (**11**), as expected, showed excellent activity against all investigated species, with an IC_{50} ranging from 0.34 to 1.25 µM (Table 6, entry 1) suggesting that this chalcone **11** has a conserved target among *Leishmania* species. Pleasingly, the addition of a spacer group did not interfere with the anti-promastigote activity with IC_{50} values for **19** being highly similar (0.29 to 1.52 µM) to compound **11** in all species (Table 6, entry 2). The trifunctional probe (**20**) does not have a reactive group and, consistent with our assumptions, had no effect against parasite *in vitro* (Table 6, entry 3). Compound **20,** even in high concentration, did not induce parasite killing in any studied species (IC_{50} > 50 µM). Pentamidine (Table 6, entry 4) was used as a control drug and its IC_{50} values varying from 0.16 to 0.92 µM.

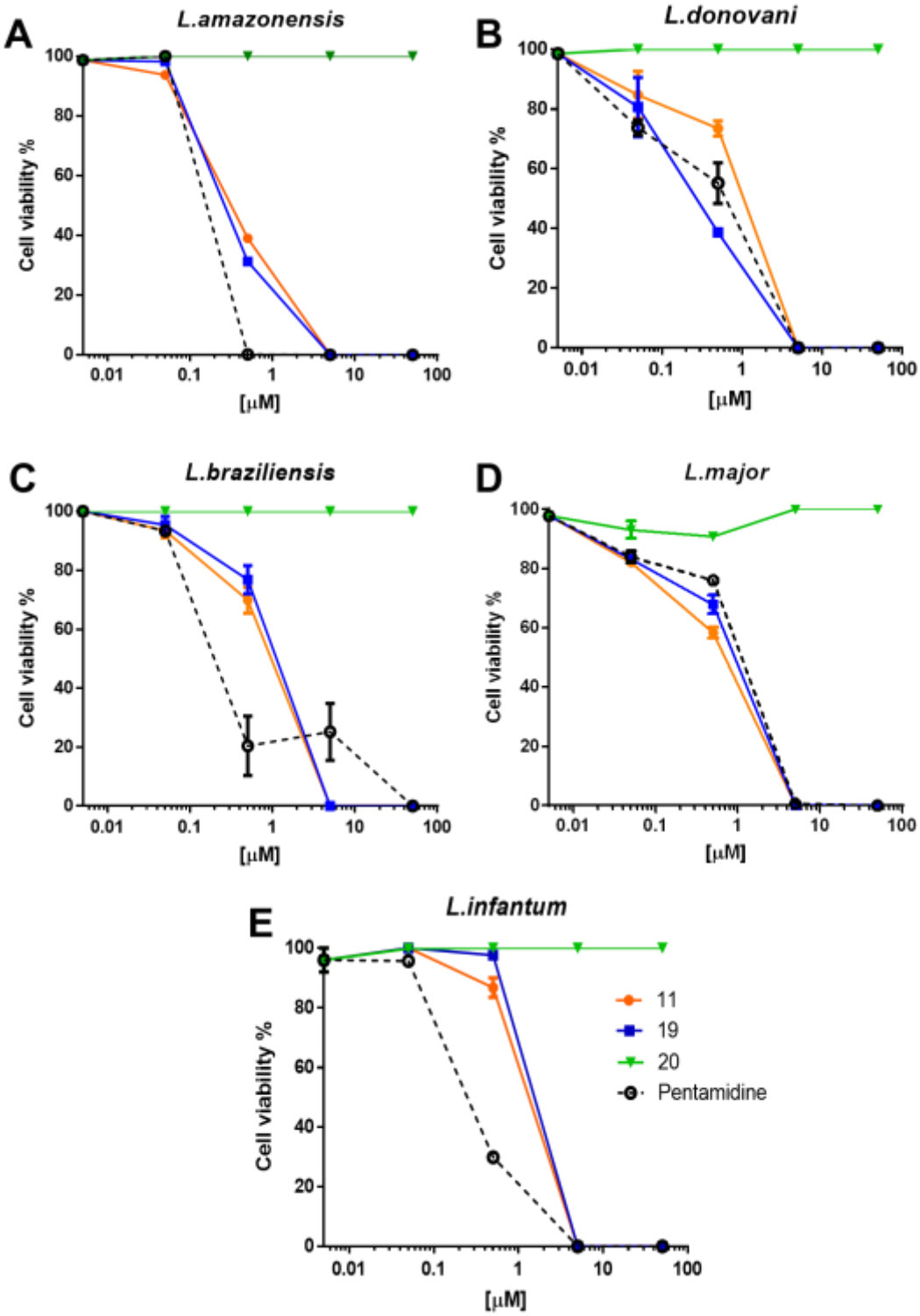

Figure 11. Inhibition of *Leishmania* promastigote growth by molecules **11**, **19** and **20**. Promastigotes of distinct *Leishmania* species were incubated with molecules **11**, **19** or **20** at different concentrations. Then, parasite viability was assessed by alamar blue method after 72 h of incubation. Pentamidine was used as a positive control. **A**- *L. amazonensis*. **B**- *L. donovani.* **C**- *L. braziliensis*. **D**- *L. major*. **E**- *L. infantum*. Means ± SD (n=3).

Table 6. Anti-promastigote activity of molecules **11**, **19** and **20**. Calculated IC_{50} values for all tested *Leishmania* species.

Entry	IC_{50} values - µM				
	L. amazonensis	*L. donovani*	*L. braziliensis*	*L. major*	*L. infantum*
1 (Compound **11**)	0.34 ± 0.07	0.76 ± 0.12	0.82 ± 0.08	0.54 ± 0.06	1.25 ± 0.11
2 (Compound **19**)	0.29 ± 0.07	0.26 ± 0.08	0.99 ± 0.09	0.73 ± 0.08	1.52 ± 0.15
3 (Compound **20**)	> 50	> 50	> 50	> 50	> 50
4 (Pentamidine)	0.16 ± 0.15	0.44 ± 0.09	0.23 ± 0.13	0.92 ± 0.09	0.29 ± 0.07

This data validated the suitability of compound **19** to bind to targets resulting in parasite death, similar to the original chalcone **11,** whereas compound **20** does not kill the parasite, working only as a probe to identify chalcone targets.

No further experiments, such as amastigote activity and host cell toxicity, were carried out with compounds **19** and **20**. Unlike the original chalcone **11**, compound **19** and **20** have been proposed to be used only as a probe for target identification. Therefore, at this point, the most important information to be extracted is whether the probe is able to permeate parasite's membrane and reach intracellular targets, killing *Leishmania* as the original chalcone.

4.3 Parasite intracellular CuAAC tagging

The anti-promastigote activity of compound **19** established its ability to permeate through the promastigote membrane and bind to possible targets inside

the parasite. Therefore, the next step was to investigate whether or not this analogue could be tagged by a trifunctional probe using CuAAC.

As discussed in Section 1.7.1, this reaction involves a bioorthogonal cycloaddition reaction between azide and alkyne groups and it is catalysed by Cu(I). $CuSO_4$ was chosen as a convenient Cu(II) source that can be reduced to Cu(I) by addition of sodium ascorbate. One limitation of the CuAAC reaction is related to the toxic effects caused by copper intracellular accumulation and low solubility of cuprous ions (Cu^+) in aqueous media. This was circumvented by the use of a low concentration of $CuSO_4$ (1 mM $CuSO_4$ as the highest concentration) and the addition of THPTA (Tris(3-hydroxypropyltriazolylmethyl)amine) to enhance the efficiency of the bioorthogonal reaction and improve reaction biocompatibility[149; 150].

Following incubation of *L. amazonensis* promastigotes with compound **19** (5 µM) at 26ºC for 5 h, cells were washed and then fixed using a solution of 4% paraformaldehyde in PBS. The parasites were then submitted to the CuAAC reaction with trifunctional probe **20** (5 µM) $CuSO_4$ (1 mM), Sodium ascorbate (2 mM) and THPTA (2 mM) for 1 h, at RT. To evaluate probe cell uptake and the intracellular location of any tagging event within the parasite, cells were visualized using confocal microscopy with Hoechst 33342 used for stain nucleus and kinetoplast (Figure 12). The red fluorescence related to **20** could be seen inside the parasite cytoplasm (Figure 12- Panel 2C) indicating that both **19** and **20** can be internalized by promastigotes after 5 h of incubation. Importantly, the fluorescence signal observed for molecule **20** is not ascribed to a nonspecific binding, since low signal could be detected on parasites not incubated with **19**

(Figure 12- 1C) and submitted to click reaction with **20**. Even after 5 h in the presence of **19**, the parasite morphology seems normal (Figure 12- 2A) with elongated cell body, long flagellum, intact nucleus and kinetoplast. The fluorescence pictures on Figure 12, also suggested molecule **19** is widely dispersed in the parasite cytoplasm, kinetoplast and mitochondrion but not in the nucleus.

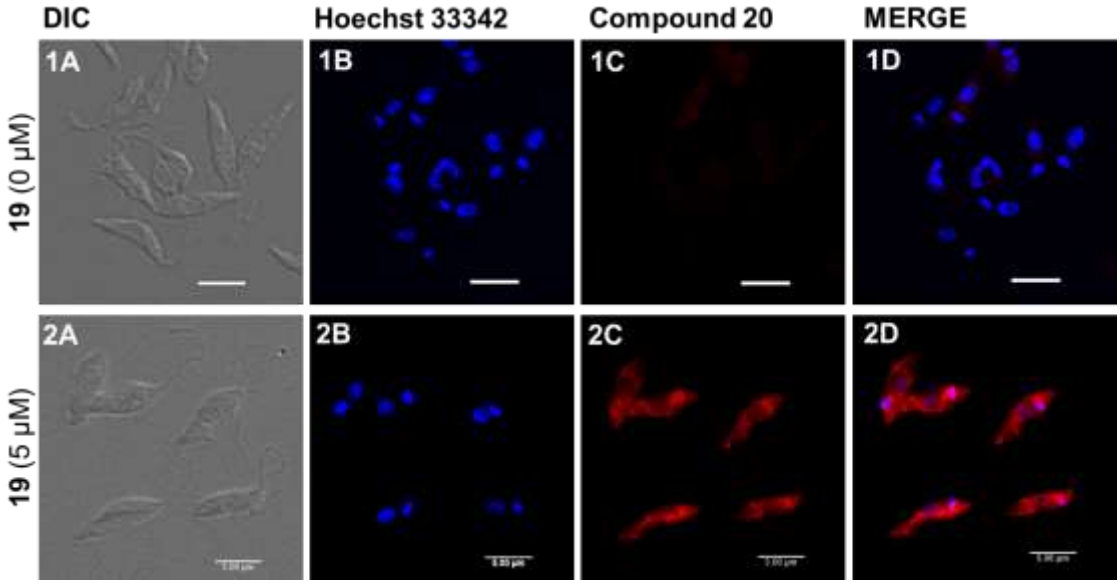

Figure 12. Promastigote intracellular probe tagging. *L. amazonensis* promastigotes treated with compound **19** (0 and 5 µM) for 5 h were submitted to CuAAC with **20** (5 µM) for 1 h at RT. Hoechst 33342 were used as nuclear acid stain. DIC images, fluorescence of molecule **20** and Hoechst at parasites were acquired by confocal microscopy. DIC-Differential Interference Contrast microscopy – grey. Hoechst- blue fluorescence. Compound **20** - red fluorescence. Representative images of three independent experiments. Bar- 5 µm. Panels 1A-D- 0 µM **18** and 2A-D 5µM **18**.

4.4 Parasite intracellular target identification

After confirmation of intracellular availability of compounds **19** and **20** by confocal microscopy, the next step was to identify the parasite protein(s) that interact with chalcone analogue **19**. This involved the use of live *L. amazonensis* promastigotes, which were incubated with compound **19** (0 µM and 5 µM) and

then lysed by sonication, to expose all proteins from the parasite proteome. These proteins were submitted to CuAAC cycloaddition reactions with compound **20** (5 µM), $CuSO_4$ (1 mM), sodium ascorbate (2 mM) and THPTA (2 mM) at RT for 1 h. Following the conjugation reaction, the resulting proteins were then analysed by 8% SDS-PAGE (Figure 13) and the fluorescence of **20** was detected using Gel Doc XR imager followed by protein staining with comassie brilliant blue G-250.

To verify specificity binding of **19**, the same controls were run on each gel: a control lane only with protein (L1), a second with proteins from parasites treated with compound **19** (L2), a third lane with proteins from parasites pre-treated with compound **19** and linked to probe **20** by CuAAC (L3) and a lane with protein without chalcone **19** but submitted to CuAAC with probe **20** (L4)**.** These studies showed that the parasite protein profile was not modified by incubation with chalcone **19** or by the cycloaddition reaction. The comassie blue stain image showed that it was possible to view similar proteins bands in all conditions.

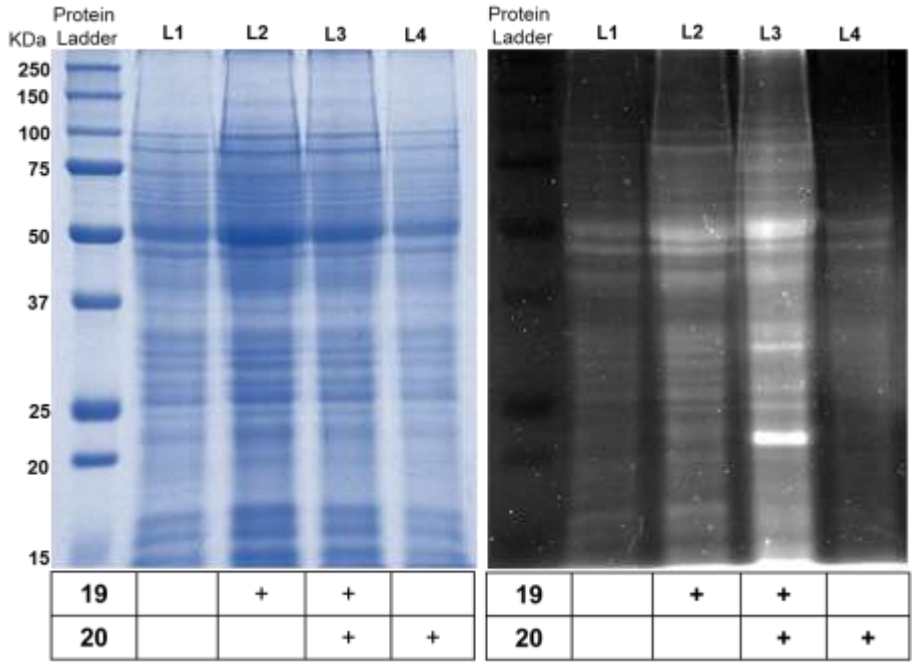

Figure 13. Chalcone probe binding on parasite proteins by SDS-PAGE. Proteins from *L. amazonensis* promastigotes pre-treated with **19** (0 and 5 µM) for 5 h were reacted with probe **20** (5 µM) for 1 h at RT. Proteins were analysed by 8% SDS-PAGE, left hand image shows proteins stained with comassie blue; Right hand image showed fluorescence signal detected by Gel Doc imager. L1- untreated parasites, L2- parasites treated with compound **19**, L3- parasites treated with chalcone **19** and linked to probe **20**, L4- untreated parasites linked to probe **20**.

From the fluorescence analysis in Figure 13 (right), some bands could be attributed to auto-fluorescence and these are shown in the lane with untreated proteins (L1). This auto-fluorescence signal can be also observed in proteins pre-treated with chalcone **19** (L2), discarding a possible interference of chalcone on detected fluorescence signal. The trifunctional probe **20** alone did not bind specifically to parasite proteins, as no strong fluorescent bands were visualized in L4. Importantly, following incubation with chalcone **19** and CuAAC with probe **20** (Lane 3) two bands were strongly labelled by probe, one band at about 22 kDa and another around 35 kDa. This labelling indicates the presence of probable chalcone targets in the parasite proteome.

Attempts to purify protein targets using the biotin moiety of the probe **20** to bind to streptavidin beads were not successful with, no specific protein bands being detected using this approach. This could be related to a number of factors including the forcing condition required to cleave bound protein form the beads leading to probe and protein degradation, such as high temperatures, pH 4.0 and highly reducing conditions. Additionally, the quantity of protein in the parasite, as low expression rates would need large quantities of protein to be detected by SDS-PAGE gel analysis.

4.5 Drug target confirmation by competition assay

Having successfully identified a putative chalcone binding protein it was then necessary to validate whether the observed binding of chalcone **19** is to a specific target site or a non-specific binding event. A competition assay between the original chalcone (**11**) and analogue (**19**) was chosen as a way to eliminate promiscuous ABPP probe labelling[151]. For this task, *L. amazonensis* promastigotes were incubated with increasing amounts of compound **11** (1, 3, 9 and 27 µM) for 4 h, cells were then washed and incubated with compound **19** at a fixed concentration of 1 µM. Parasites were disrupted by sonication, followed by a click reaction with probe **20** and analysis by SDS-PAGE as before (Figure 14).

From this it can be seen that the combination of probe **20** and chalcone **19** was able to bind in a strong manner to proteins at 22 kDa and 35 kDa (L3). Nevertheless, this binding was substantially affected when parasites were pre-incubated with different concentrations of chalcone **11** (L4-7). The band around

35 kDa was barely affected by chalcone **11** incubation, but the fluorescence signal corresponding to the band at ~22 kDa was abolished by prior incubation with **11** (Figure 13 A and B). This suggests that NAT22 (**11**) blocked the binding site of analogue **19** in the 22 kDa protein, which therefore represent a potential target protein and that the labelling of the 35 kDa protein is a non-specific binding effect that can be ignored. This data, led us to investigate proteins within the band at ~22 kDa as the chalcone target.

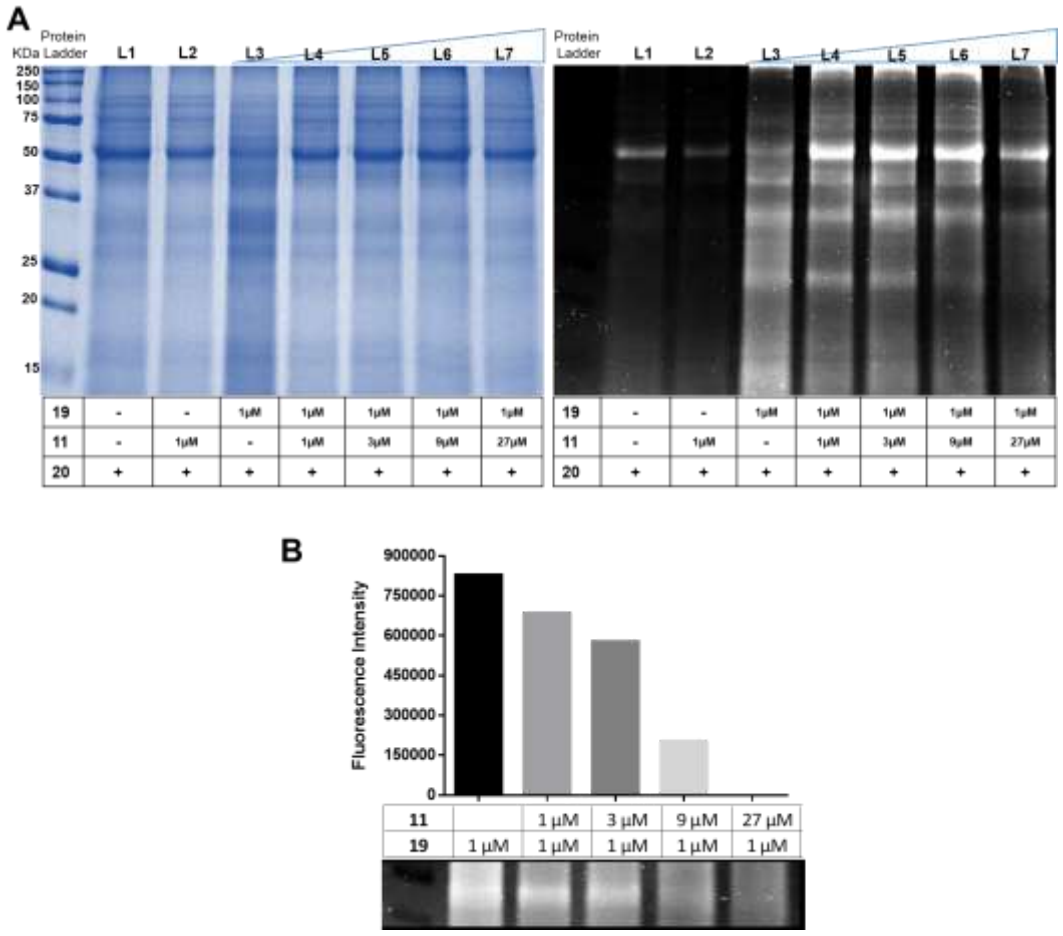

Figure 14. Target competition between compounds **11** and **19**. *L. amazonensis* promastigotes were treated with **11**, and cells were washed and incubated with **19** (1 µM). Proteins from all conditions were submitted to CuAAC with **20** (1 µM) for 1h at RT. Proteins were analysed by SDS-PAGE 10%, fluorescence signal of **20** were detected by Gel Doc imager and gel stained with comassie blue G. **A**- Representative SDS-PAGE images of proteins from all conditions. **B**- Fluorescence intensity quantification of the band at 22 kDa. L1- untreated parasites. L2- parasites

treated with **11** (1 µM). L3- parasites treated with **19** (1 µM). L4 to L7- parasites treated with **11** (1, 3, 9 and 27 µM, respectively) and **19** (1 µM). Representative image of two independent experiments.

4.6 Chalcone target identification by mass spectrometry

With attention focused on target identification in only one gel band at ~22 kDa, protein samples from promastigotes treated with chalcone analogue **19** and linked to probe **20** were separated by 8% SDS-PAGE (Figure 15). The region corresponding to the fluorescent band at ~22 kDa was excised from the comassie blue stained gel, and proteins on this gel fragment were digested by trypsin. The peptides resulting from the digestion process were submitted to mass spectrometry (Q-Tof – Waters). The identification of possible proteins in this band generated nine protein candidates as listed in Table 7.

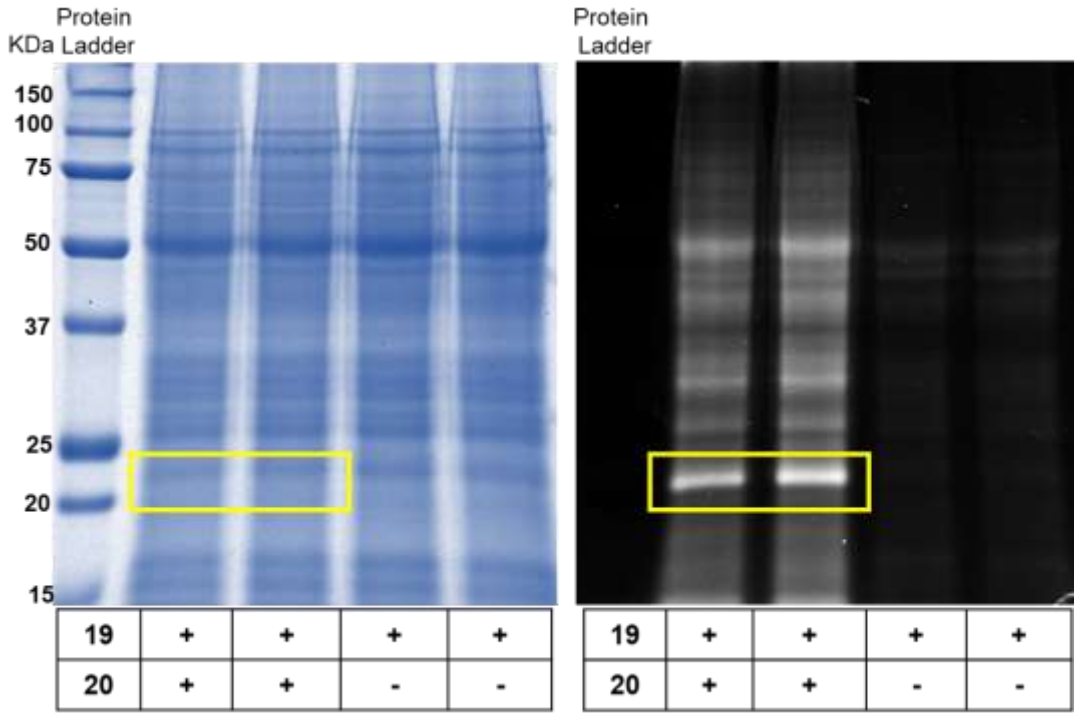

Figure 15. Representative 8% SDS-PAGE of proteins from *L. amazonensis* promastigotes were treated with compound **19** and linked to **20** by CuAAC. Yellow rectangles show the bands excised from the gel and submitted to mass spectrometry identification.

Table 7. Protein candidates identified from peptides on the band at 22 kDa by mass spectrometry (Q-ToF).

Protein number	NCBI Entries	Description	Mass	Peptide sequence
1	ABC40566.1	alpha-tubulin [*Leishmania tarentolae*]	50542	LIGQVVSSLTASLR
2	XP_003871568.1	40S ribosomal protein S7 [*Leishmania mexicana* MHOM/GT/2001/U1103]	23836	TSTAVFENILSDMIYPSDVVGR
3	XP_003873257.1	putative 60S ribosomal protein L18 [*Leishmania mexicana* MHOM/GT/2001/U1103]	22207	TAPIAVVVGDVLDDVR
4	JAS02769.1	alpha tubulin, partial [*Triatoma infestans*]	43617	LIGQVVSSITASLR
5	XP_002613005.1	hypothetical protein BRAFLDRAFT_58199 [*Branchiostoma floridae*]	50939	IIGQVVSSITASLR
6	XP_018332011.1	PREDICTED: tubulin alpha-2 chain-like [*Agrilus planipennis*]	56709	LLGQVVSSITASLR
7	JAQ08148.1	60S ribosomal protein L11, partial [*Lygus hesperus*]	12939	VLEQLCEQTPVLSR
8	AGG11660.1	hypothetical protein, partial [*Leptomonas pyrrhocoris*]	36242	ELEQIASEALEAAR
9	AAX47428.1	cytosolic tryparedoxin peroxidase [*Leishmania amazonensis*]	22344	AYGVLAEAQGVAYR

Based on the observed molecular weight (~22,000 Da), three identified candidates described for *Leishmania* species were considered promising (NCBI entries: XP_003871568.1, XP_003873257.1 and AAX47428.1). We chose cytosolic tryparedoxin peroxidase (AAX47428.1) as a target because XP_003871568.1 and XP_003873257.1 are proteins related to protein synthesis

and in theory are located in the cytoplasm. However, according to confocal microscopy results (Figure 12), the target can be found in the cytoplasm and mitochondria, and two isoforms of tryparedoxin peroxidase can be found in the parasite, one in the cytoplasm and the other in the mitochondrion. Furthermore, the peptide identified by mass spectrometry (AYGVLAEAQGVAYR) align 100% with the protein sequence of cytosolic tryparedoxin peroxidase from *L. amazonensis* (Figure 16A), *L. donovani* and *L. mexicana*.

Cytosolic tryparedoxin peroxidase (cTXNPx) is a very well characterized protein, with a high level of similarity between *Leishmania* species. Analysis using the CLUSTAL Omega tool with the protein sequence from cTXNPx from different species of *Leishmania* revealed a similarity of 75% when comparing all species together (*L. amazonensis. L. donovani, L. mexicana, L. infantum, L. major* and *L. braziliensis*) (Figure 16B). Individual alignments showed higher similarities, cTXNPx of *L. amazonensis* is 100% similar to *L. donovani*, 95% to *L. mexicana*, 90% to *L. infantum*, 88% to *L. major* and 80% to *L. braziliensis*. Despite discrepancy among species, cysteine residue 52, the enzyme active site, is 100% conserved in all aligned species. The chalcone activity against distinct *Leishmania* species may be explained by the higher cTXNPx similarity among species and protein sequence differences in each species of *Leishmania* may explain the IC_{50} variations observed in Table 6.

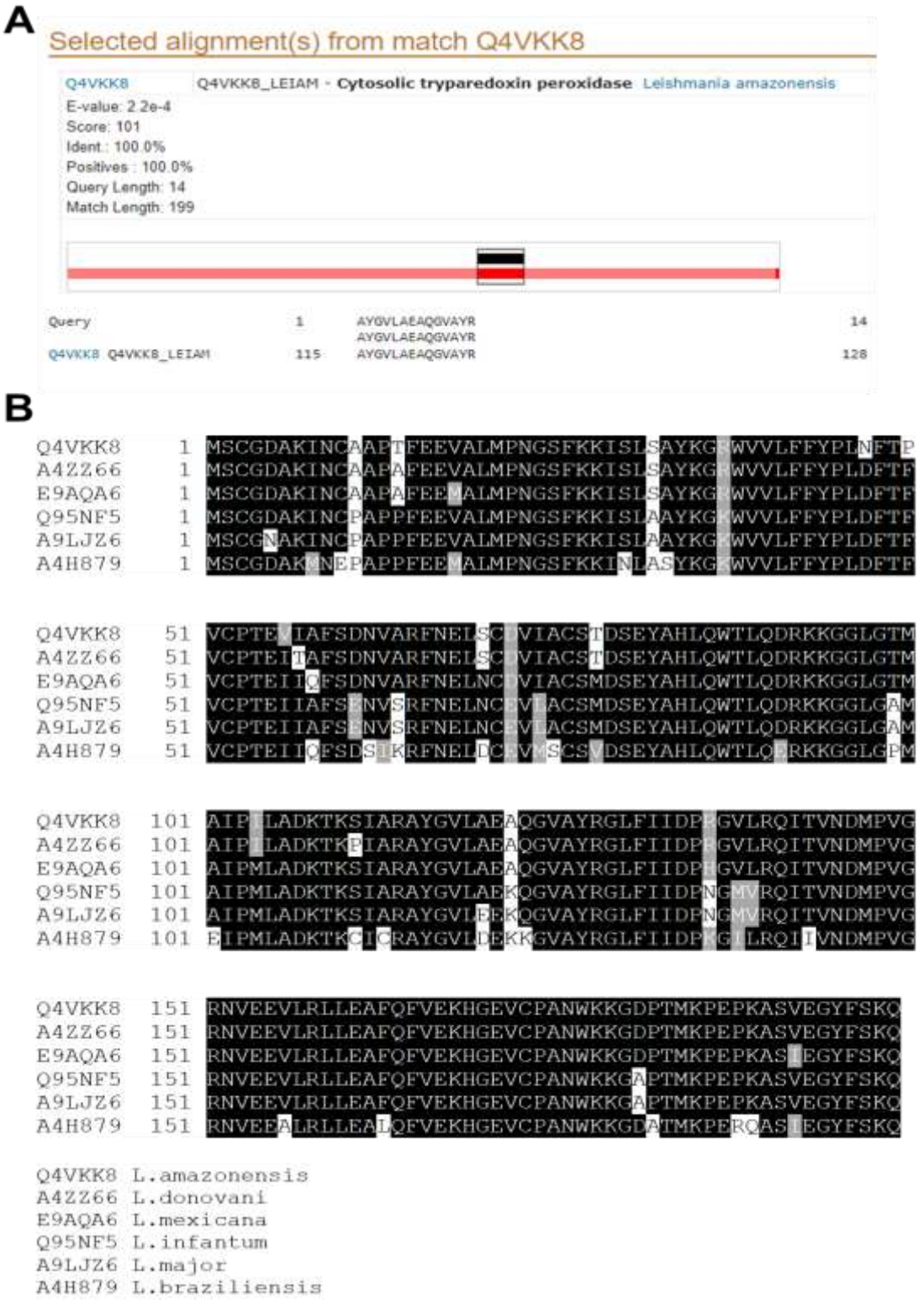

Figure 16. Protein sequence alignments. **A**- Alignment between the peptide obtained from the band at 22 kDa and the protein cytosolic tryparedoxin peroxidase [*Leishmania amazonensis*]. **B**- ClustalOmega alignment of protein sequence of cytosolic tryparedoxin peroxidase from different *Leishmania* species.

4.7 Confirmation of cTXNPx as a chalcone target

In order to confirm cTXNPx as a chalcone target, immunoblotting with an antibody against cTXNPx was performed. Proteins from lysate of live promastigotes treated with chalcone **19** (5 µM) alone or linked with probe **20** (5 µM) were analysed by 10% SDS-PAGE. After fluorescence detection, proteins were stained using comassie blue or transferred to PVDF membrane. The PVDF membrane was then incubated with polyclonal mouse anti-cytosolic TXNPx antibody (donated by Prof Angela Cruz, USP, Brazil), followed by anti-Mouse IgG-HRP, as secondary antibody, and the presence of cTXNPx evaluated by western blot (Figure 17). Fluorescence imaging (Figure 17B) showed that parasite incubation with chalcone **19** and subsequent reaction with probe **20** could bind specifically to proteins of 22 kDa, as discussed above. Confirming the hypothesis, chemiluminescence results (Figure 17C) exhibited an antibody band specifically for cTXNPx at 22 kDa and this band is at exactly the same position as the fluorescent band seen in the gel from the chalcone analogue. Structural studies[101] showed that cTXNPx can be found in a decameric form, composed by five homodimers, the dimeric form is the enzyme active conformation, whose active site is formed by the interaction between Cys52 of one subunit and Cys173 of the other monomer[108], it was interesting that no interaction could be observed for the band correlating to the cTXNPx dimer (~44 kDa) (Figure 17C). The evidence from this experiment suggest that the interaction between chalcone and cTXNPx is preferentially in the enzyme monomeric form. However, this does not exclude the possibility of an interaction with the decameric or dimeric form

culminating with the destabilization of the quaternary structure of the protein and consequently enzyme inhibition.

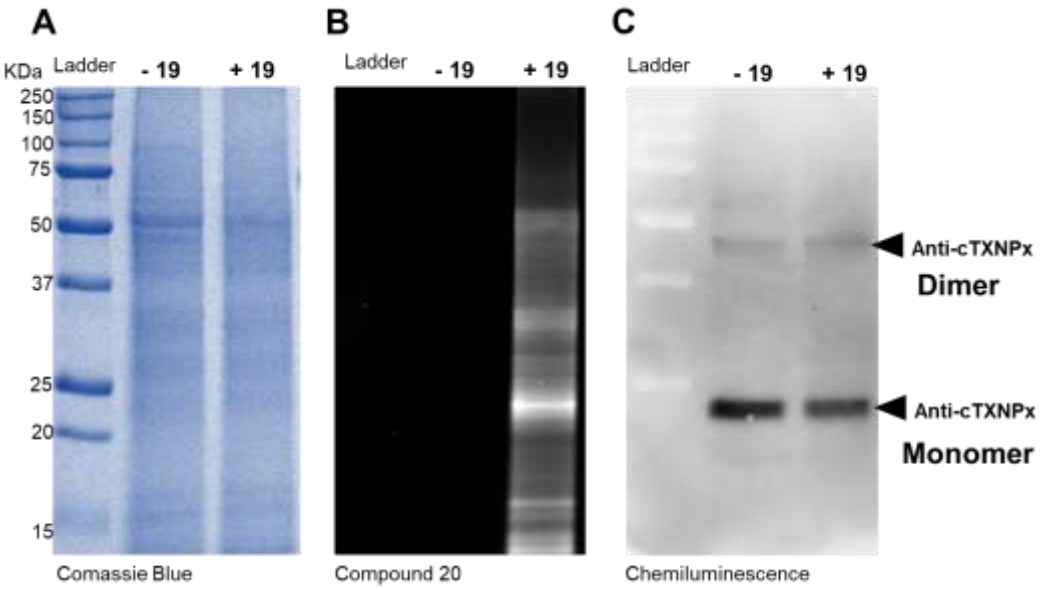

Figure 17. Confirmation of cTXNPx as a chalcone target by immunoblotting. Proteins from *L. amazonensis* promastigotes treated or not with **19** and linked to **20**, were submitted to 10% SDS PAGE. **A-** Proteins stained with Comassie Blue. **B-** Gel Fluorescence signal taken using GelDoc X imager. **C-** Detection of cTXNPx on PVDF membrane by western blot using a polyclonal antibody anti-cTXNPx.

Unidimensional polyacrylamide gels commonly generate false positive results due to their low efficiency in differentiating between proteins, which are separated only by molecular size[152]. To increase the resolution of our analysis and corroborate the hypothesis that cTXNPx was the target of NAT22, the soluble protein fraction of promastigote lysate treated with chalcone **19** and linked to probe **20** was assessed by two-dimensional electrophoresis. The fluorescence of compound **20** on the gels was documented and the presence of cTXNPx was detected by western blot analysis with anti-cTXNPx antibody (Figure 18). Monitoring by fluorescence revealed a series of bands concentrated around 22 kDa (Figure 18B) whilst imaging by western blot (Figure 18C), enabled the

detection of four distinct spots at the same molecular weight (~22 kDa) but with different pI. This in accordance to findings in the literature[153] describing the presence of 4 isoforms of the enzyme in different pIs, which can represent a differential enzyme functionality at distinct pH environment. Significantly, these spots are at same position as the fluorescence signal observed on the SDS-PAGE for the protein chalcone conjugate, confirming that the chalcone probe was specifically labelling TXNPx.

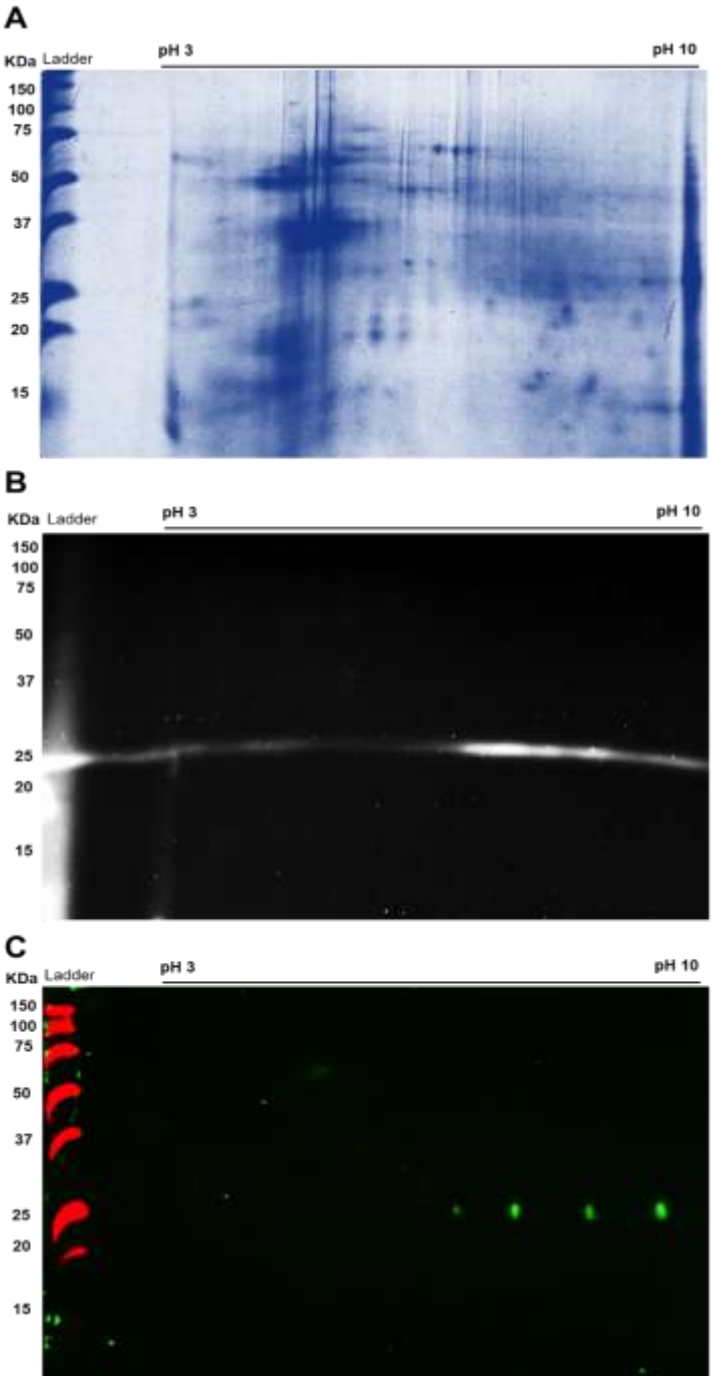

Figure 18. Confirmation of cTXNPx as a chalcone target by 2D electrophoresis. 500 µg of proteins from parasites treated with chalcone **19** and linked to probe **20** were loaded using in-gel rehydration into 7cm pH 4-7 IPG strips. Proteins were resolved in the first dimension using isoelectric focusing and the second dimension using 10% mini-format SDS-PAGE gels. Resolved proteins were visualised for their fluorescence and transferred to PVDF membrane. Polyclonal antibody anti-cTXNPx was used to detected cTXNPx on membrane by Immunoblotting. **A**- Comassie blue staining image. **B**- Compound **20** fluorescence image. **C**- cTXNPx labelling by western blot. Representative image of three independent experiments.

Aiming to obtain further proof for this labelling, several spots from the 2D-gel (Figure 19) were excised, digested with trypsin and analysed by mass spectrometry, as described for 1D analysis. The region where fluorescence can be observed from probe **20** was used to choose spots D1 to D11, spot D8 was chosen due to an antibody signal viewed on the western blot image. Protein identification based on peptides from each spot digestion are listed in Table 8. It was found that spots near the fluorescence area (D3, D4, D5 and D7) of compound **20** were cytosolic tryparedoxin peroxidase from *L. amazonensis and* non-relevant proteins or no identification was obtained from the other spots.

Together these findings provided strong evidence that the enzyme cytosolic tryparedoxin peroxidase is a molecular target of chalcone NAT22 (**11**). Significantly, TXNPx activity has been described for both parasite forms, promastigote and amastigote, and it is extremely essential for parasite redox balance and contribute for DNA biosynthesis[100; 145].

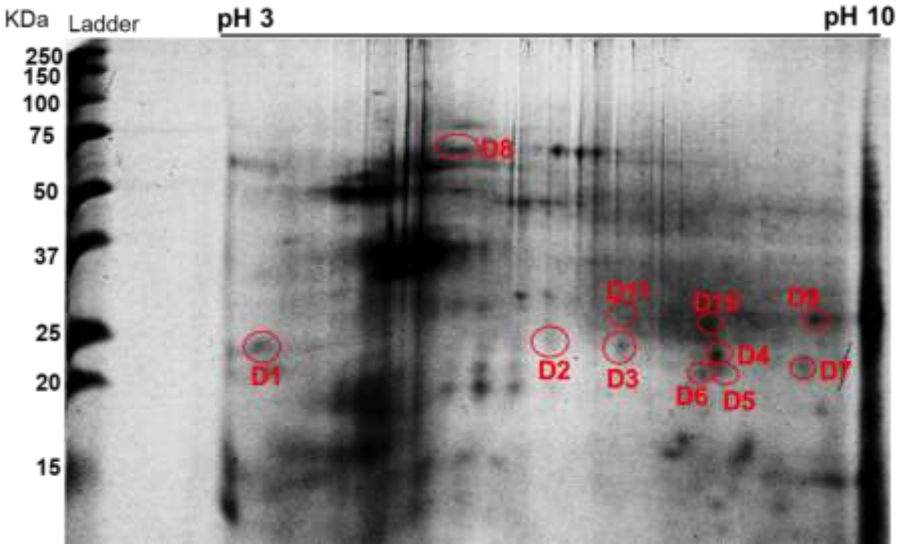

Figure 19. Schematic 2D-gel image of the spots used for protein identification. 2D-gel of proteins from *L. amazonensis* promastigotes treated with chalcone **19** and linked to **20** by CuAAC. Red circles show all spots excised from the gel and submitted to mass spectrometry (Q-ToF) identification.

Table 8. Proteins identified by mass spectrometry on each 2D-gel spot.

Spots	Protein Description
D1	No identification
D2	No identification
D3	cytosolic Tryparedoxin peroxidase [*Leishmania amazonensis*]
D4	cytosolic Tryparedoxin peroxidase [*Leishmania amazonensis*]
D5	cytosolic Tryparedoxin peroxidase [*Leishmania amazonensis*]
D6	putative iron superoxide dismutase [*Leishmania mexicana*]
D7	cytosolic Tryparedoxin peroxidase [*Leishmania amazonensis*]
D8	Heat shock protein 83 90-kDa heat-shock protein, partial [*Halichondria sp*. AR-2003] molecular chaperone HtpG [*Desulfotomaculum gibsoniae*]
D9	No identification
D10	No identification
D11	ATP-dependent RNA helicase, putative [*Trypanosoma cruzi*]

4.8 Chalcone target specificity for parasite

Having identified cTXNPx as the molecular target of NAT22 (**11**) within promastigotes, the next question was whether this remained the case in the more clinically relevant amastigote form. Moreover, whilst NAT22 (**11**) did not show significant cytotoxicity it was also of interest to determine whether any host cells proteins would interact with this compound.

To verify if amastigote cTXNPx remained susceptible to the chalcone and whether chalcone has different targets in parasite and host cell, soluble proteins

from promastigotes, purified intracellular amastigotes and macrophages treated with **19** and linked to **20**, in the same way as described above, were analysed by SDS-PAGE and western blot (Figure 20). Analysis by fluorescence (Figure 20A) show comparatively similar fluorescent bands in both promastigotes and amastigotes samples (P2 and A2), especially the band related to cTXNPx, suggesting that the chalcone exhibits similar binding in both parasite stages. P1, A1 and M1 are samples from promastigotes, amastigotes and macrophages non incubated with compound **19**. For macrophages (M2), the most prominent bands are located at high molecular weight proteins, around 37 to 50 kDa, indicating possible chalcone targets on macrophages. Whilst some of these bands ~50 kDa could be observed at amastigotes samples, these probably arise through macrophage contamination during amastigote purification process.

Immunoblotting of cTXNPx (Figure 20B) further confirms chalcone target specificity for the parasites, with only proteins in the parasites samples, both promastigotes and amastigotes being detected. However, no signal was observed in macrophages samples. These findings are in accordance with literature reports, which describe the presence of TXNPx only in trypanosomatids[154]. The most similar protein found in humans is peroxiredoxin-1 (MW= 25 KDa), although it shares poor similarity to cTXNPx (~40%)[154] .

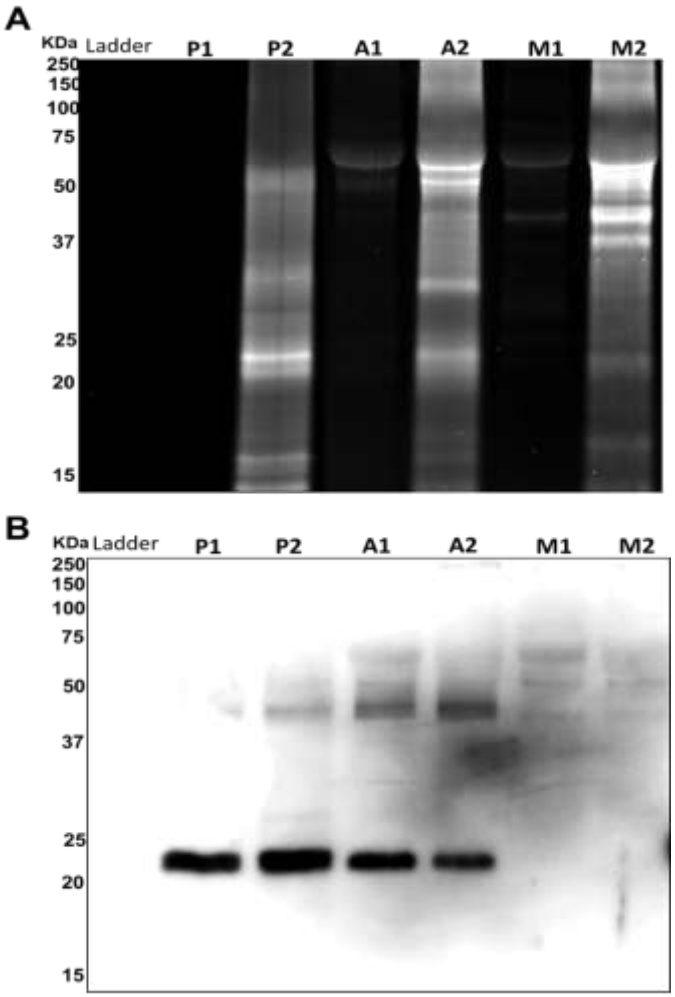

Figure 20. Chalcone target specificity for parasite. Proteins from *L. amazonensis* promastigotes, intracellular amastigotes and macrophages treated or not with **19** and linked to **20** were analysed by 10% SDS-PAGE. Proteins were visualised for their fluorescence and transferred to PVDF membrane. cTXNPx were detected on the membrane by western Blot using a polyclonal antibody anti-cTXNPx. **A**- Gel fluorescence image. **B**- cTXNPx detected by immunoblotting. P- Promastigotes proteins. A- Amastigotes proteins. M- Uninfected macrophages proteins. P1, A1 and M1- Samples non treated with **19**. P2, A2 and M2- Samples treated with **19**.

4.8.1 Summary

The use of modified chalcone probe **19** coupled with the trifunctional reagent **20** enabled the enzyme cytosolic tryparedoxin peroxidase to be identified as a target for NAT22. Moreover, western blot and 2D electrophoresis confirm

the specificity of this labelling. Consistent with this being a parasite specific enzyme little cross reactivity was observed in macrophages further emphasising the potential of chalcones for leishmaniasis chemotherapy. The results presented to date clearly demonstrate the utility of the activity-based protein profiling approach using CuAAC to enable target identification.

4.9 Expression and purification of cTXNPx

With the enzyme cytosolic tryparedoxin peroxidase confirmed as the most likely chalcone target protein, attention then turned to investigate the interaction between protein and drug. In order to do this a source of parasitic TXNPx was required and the generation of an efficient method for expression and purification of cTXNPx became the next goal.

4.9.1 Design of cTXNPx plasmids construct

We decided to employ traditional PCR cloning method to amplify and obtain the desired gene fragments[155]. The expression of cTXNPx is controlled by more than one gene on parasite genome. Here we use as selection criteria, the degree of similarity with the enzyme for *L. amazonensis* protein (AY842247.1). Using data from the GeneBank, the chosen gene sequences were *L. donovani* (XM_001681966.1, 100 % similarity), *L. mexicana* (XM_003873581.1, 95 %) and *L. major* (KC595509.1, 88 %) (Table 9, Figure 16B). For each sequence, recombinant cloning vectors (pUC57) containing open reading frames (ORFs) for cTXNPx were purchased from Genscript.

Table 9. Gene sequence used to construct the plasmids.

Leishmania gene ID	Gene sequence
AY842247.1 *Leishmania amazonensis* cytosolic tryparedoxin peroxidase	ATGTCCTGCGGTGACGCCAAGATCAACTGCGCCGCGCCGACCTTCGAGGAG GTGGCGCTCATGCCCAACGGCAGCTTCAAGAAGATCAGCCTCTCCGCCTACA AGGGCAGGTGGGTCGTGCTCTTCTTCTACCCGCTCAATTCACCCCCGTGTGC CCGACAGAAGTCATTGCGTTCTCCGACAACGTGGCTCGCTTCAACGAGCTCA GCTGCGACGTCATCGCGTGCTCCACGGACAGCGAGTACGCGCACCTGCAGT GGACGCTGCAGGACCGCAAGAAGGGCGGCCTCGGCACCATGGCGATCCCAA TACTGGCCGACAAGACCAAGTCCATCGCTCGTGCCTACGGCGTGCTGGCGG AGGCACAGGGCGTGGCCTACCGCGGTCTCTTCATCATCGACCCCCGTGGCG TCCTGCGCCAGATCACCGTCAACGACATGCCGGTGGGCCGCAACGTGGAGG AGGTTCTGCGCCTGCTGGAGGCTTTTCAGTTCGTGGAGAAGCACGGCGAGGT GTGCCCCGCCAACTGGAAGAAGGGCGACCCCACAATGAAGCCGGAACCGAA GGCATCTGTCGAGGGGTACTTCAGCAAGCAGTAA
XM_001681966.1 *Leishmania major* strain Friedlin tryparedoxin peroxidase (TRYP1)	ATGTCCTGCGGTAACGCCAAGATCAACTCTCCCGCGCCGTCCTTCGAGGAGG TGGCGCTCATGCCCAACGGCAGCTTCAAGAAGATCAGCCTCTCCTCCTACAAG GGCAAGTGGGTCGTGCTCTTCTTCTACCCGCTCGACTTTAGCTTCGTGTGCCC GACAGAGGTCATCGCGTTCTCCGACAGCGTGAGTCGCTTCAACGAGCTCAAC TGCGAGGTCCTCGCGTGCTCGATAGACAGCGAGTACGCGCACCTGCAGTGGA CGCTGCAGGACCGCAAGAAGGGCGGCCTCGGGACCATGGCGATCCCAATGC TAGCCGACAAGACCAAGAGCATCGCTCGTTCCTACGGCGTGCTGGAGGAGAG CCAGGGCGTGGCCTACCGCGGTCTCTTCATCATCGACCCCCATGGCATGCTG CGTCAGATCACCGTCAATGACATGCCGGTGGGCCGCAGCGTGGAGGAGGTTC TACGCCTGCTGGAGGCTTTTCAGTTCGTGGAGAAGCACGGCGAGGTGTGCCC CGCGAACTGGAAGAAGGGCGCCCCCACGATGAAGCCGGAACCGAATGCGTC TGTCGAGGGATACTTCAGCAAGCTCTGA
XM_003873581.1 *Leishmania mexicana* MHOM/GT/2001/U1103 tryparedoxin peroxidase	ATGTCCTGCGGTGACGCCAAGATCAACTGCGCCGCGCCGGCCTTCGAGGAGA TGGCGCTCATGCCCAACGGCAGCTTCAAGAAGATCAGCCTCTCCGCCTACAA GGGCAGGTGGGTCGTGCTCTTCTTCTACCCGTATGACTTCAGCTTCGTGTGCC CGACAGAGATCATTCAGTTCTCCGACAACGTGGCTCGCTTCAACGAGCTCAAC TGCGACGTCATCGCGTGCTCCACGGACAGCGAGTACGCGCACCTGCAGTGGA CGCTGCAGGACCGCAAGAAGGGCGGCCTCGGCACCATGGCGATCCCAATGC TGGCCGACAAGACCAAGTCCATCGCTCGTGTCTACGGCGTGCTGGCGGAGGC ACAGGGCGTGGCCTACCGCGGTCTCTTCATCATCGACCCCCATGGCGTCCTG CGCCAGATCACCGTCAACGACATGCCGGTGGGCCGCAACGTGGAGGAGGTT CTGCGCCTGCTGGAGGCTTTTCAGTTCGTGGAGAAGCACGGCGAGGTGTGCC CCGCCAACTGGAAGAAGGGCGACCCCACAATGAAGCCAGAACCGAAGGCATC TATTGAAGGGTACTTCAGCAAGCTTTGA
KC595509.1 *Leishmania donovani* cytosolic tryparedoxin peroxidase	ATGTCCTGCGGTGACGCCAAGATCAACTGCCCCGCGCCGCCCTTCGAGGAGG TGGCGCTCATGCCCAACGGCAGCTTCAAGAAGATCAGCCTCGCCGCCTACAA GGGCAAGTGGGTCGTGCTCTTCTTCTACCCGCTCGACTTCACCTTCGTGTGCC CGACAGAGATCATCGCGTTCTCCGAAAACGTGAGTCGCTTTAACGAGCTCAAC TGCGAGGTCCTCGCGTGCTCCATGGACAGCGAGTACGCGCACCTGCAGTGGA CGCTGCAGGACCGCAAGAAGGGCGGCCTCGGCGCCATGGCGATTCCAATGC TGGCCGACAAGACCAAGAGCATCGCTCGTGCCTACGGCGTGCTGGAGGAGAA ACAGGGCGTGGCCTACCGCGGTCTCTTCATCATCGACCCCAATGGCATGGTG CGCCAGATCACCGTCAACGACATGCCGGTGGGCCGCAACGTGGAGGAGGTT CTGCGCCTGCTGGAGGCTTTTCAGTTCGTGGAGAAGCACGGCGAGGTGTGCC CCGCGAACTGGAAGAAGGGCGCCCCCACGATGAAGCCGGAGCCGAAGGCGT CTGTCGAGGGGTACTTCAGTAAGCAGTAA

Each open reading frame containing 600 bp of length was cloned into pUC57 by EcoRV and according to manufacturer's certificate all constructs passed on all quality parameters, such as target sequencing alignment, DNA quality, vector sequence and absence of unexpected bands suggesting contamination. A general plasmid construct map for all genes is illustrated in Figure 21.

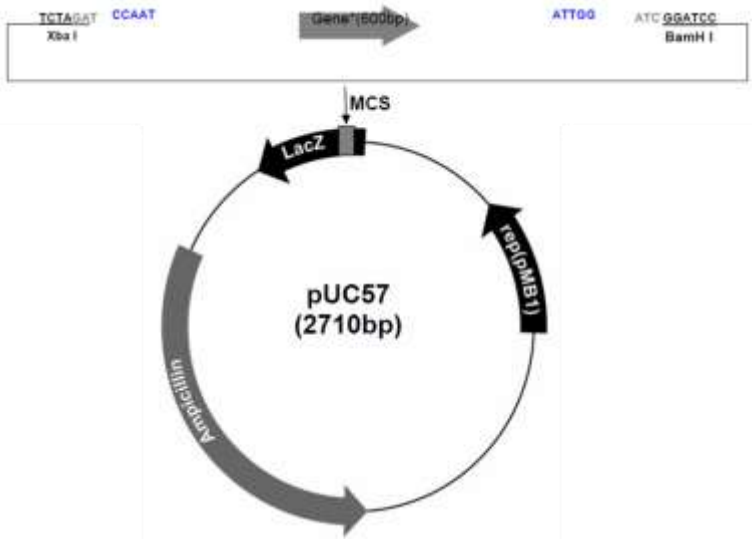

Figure 21. General plasmid construct map. The plasmid constructs were purchased from Genscript; the gene of interest were cloned at MCS position flanked by protective bases added by the company (Blue bases).

After transformation into stellar cells, ORFs sequences were amplified by PCR using primers designed for each gene sequence. Primers were created using the primer design toll from Protein production UK website (http://www.oppf.rc-harwell.ac.uk/OPPF/) and they are in Table 5 (page 75). PCR reaction was done under different annealing temperatures to find the most appropriate temperature of amplification. Then, PCR products were analysed using an agarose gel. In Figure 22, it is possible to see amplicons of each gene at approximately 600 bp related to the desired fragments; this could be observed

by UV-light, confirming fragment amplification. The annealing temperature chosen for PCR reaction was 62 ºC (Figure 22 - blue rectangles).

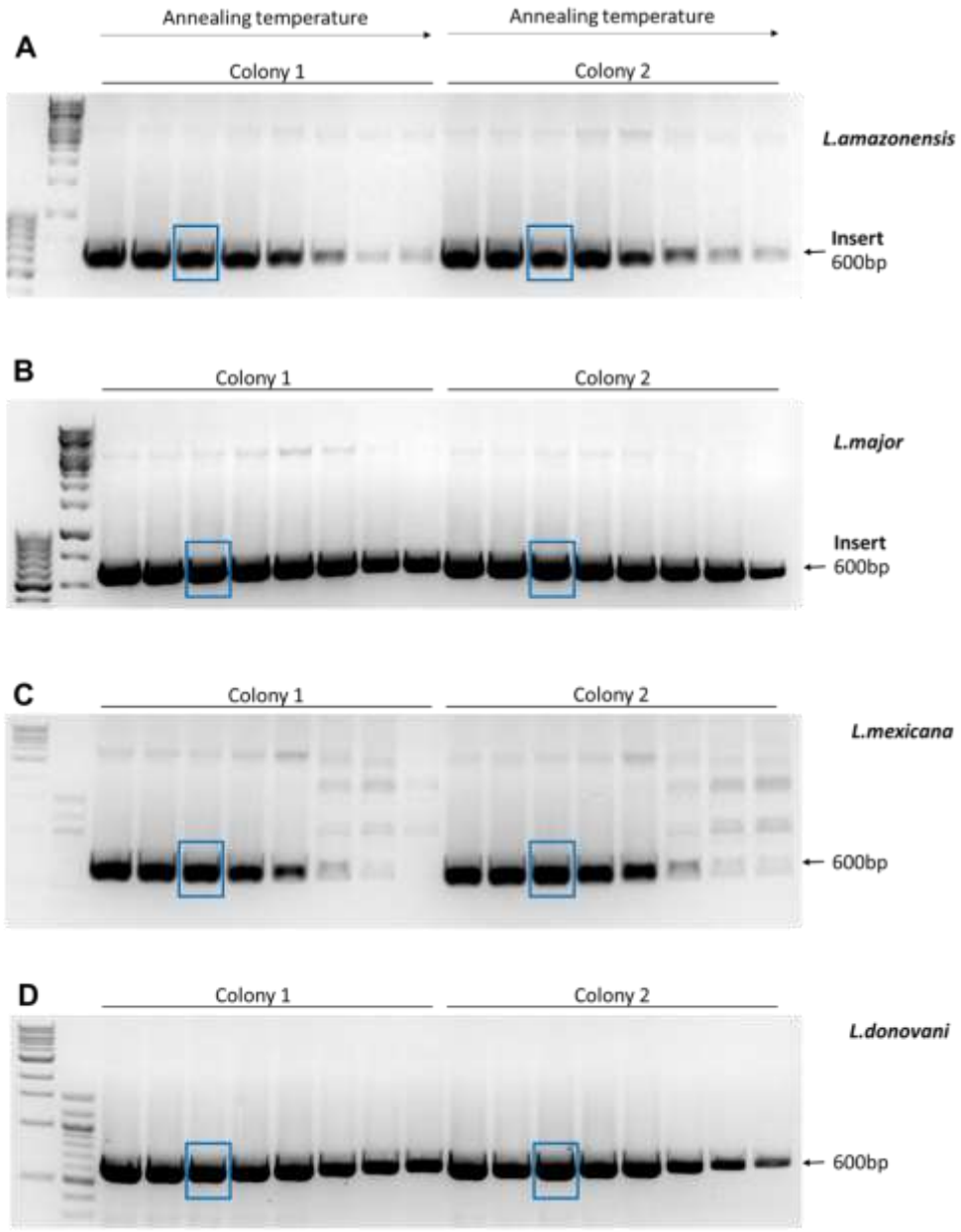

Figure 22. Agarose gels of PCR products from pUC57 plasmid. pUC57 vector plasmid were extracted from transfected stellar cells and DNA fragments of interest were amplified by PCR. PCR products were submitted to an agarose gel, and amplified fragments observed under UV-light and documented using GelDoc imager. **A**- *L. amazonensis.* **B**- *L. major.* **C**- *L. mexicana.* **D**- *L. donovani.* Blue rectangles- PCR amplification at 62 ºC of annealing temperature.

In order to facilitate subsequent protein purification, the DNA fragments from the PCR reaction were purified and successfully integrated into the pOPINF expression vector, at HindIII and KpnI positions, which introduces an N-terminal His_6-tag plus a 3C cleavage site to the recombinant protein[143] (Figure 23).

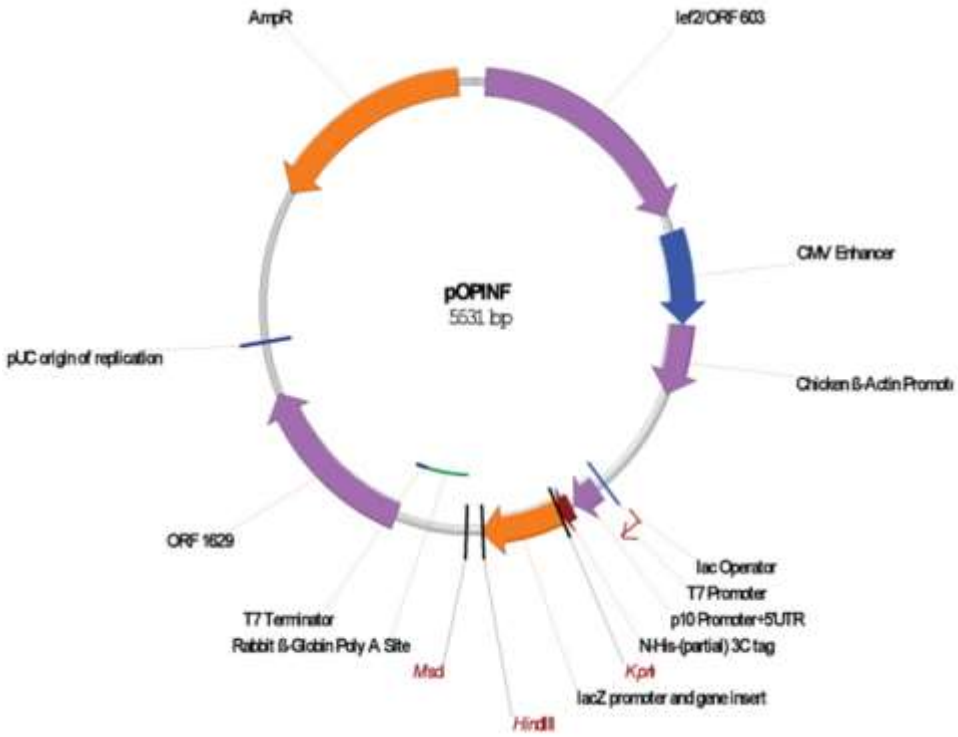

Figure 23. General pOPINF expression plasmid construct map.

4.9.2 Transformation and sequencing

Expression vectors (pOPINF) carrying ORF fragments were transfected into *E. coli* BL21(DE3) competent cells by heat shock, this strain was chosen due to its higher efficiency of recombinant protein expression. BL21 (DE3) contains a lysogen bacterium (λDE3) carrying a single T7 RNA polymerase gene controlled by lacUV5 promoter, which is maximally induced by isopropyl-p-D-thiogalactopyranoside (IPTG). T7 RNA polymerase will induce the expression of

cTXNPx recombinant genes cloned downstream of a T7 promoter pOPINF (Figure 23).

Transfection was confirmed by antibiotic selection overnight with ampicillin and DNA of 8 positive colonies were amplified by PCR using the same primers as described above (Table 5). As expected, in most of the ampicillin resistant colonies, the DNA product could be visualized at 600 bp, on agarose gels (Figure 24).

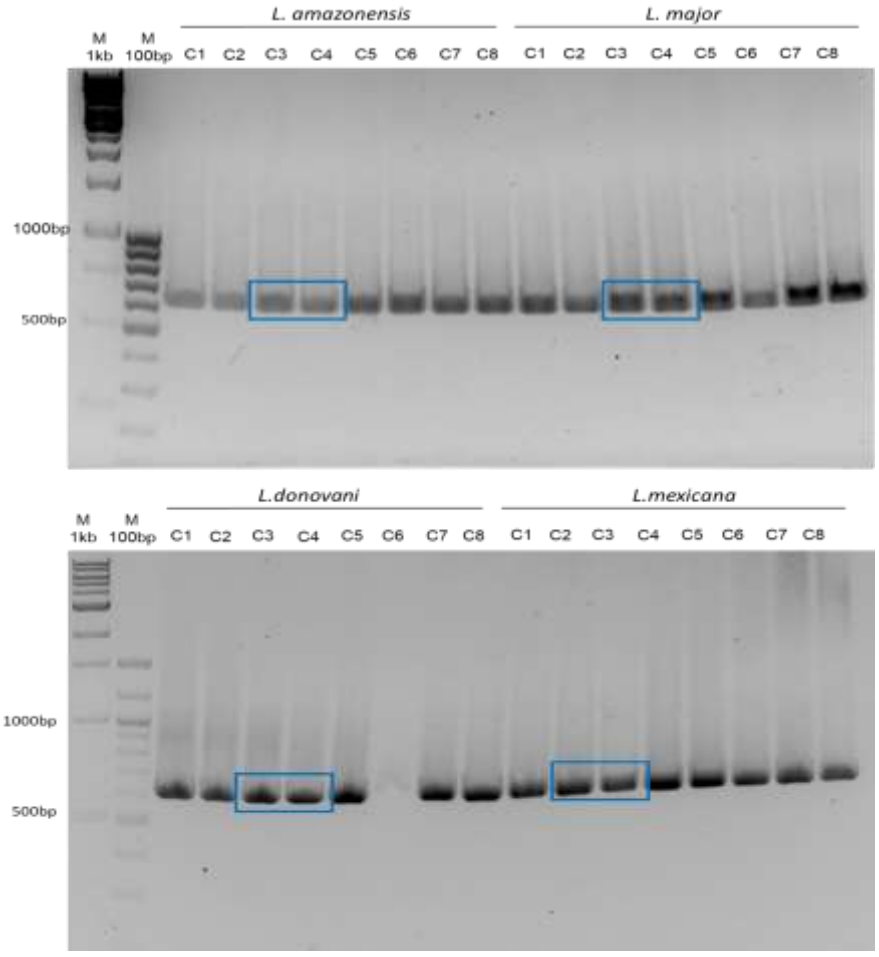

Figure 24. Agarose gels of PCR products from pOPINF plasmids. pOPINF expression vector plasmid were extracted from transfected E. coli BL21(DE3) cells and DNA fragments of interest were amplified by PCR. PCR products were submitted to an agarose gel, observed under UV-light and documented using GelDoc imager. Blue rectangles- Fragment submitted to sequencing. GeneRuler DNA Ladder was used as standard. **C1 to 8**- positive bacteria colonies.

Two PCR products of each gene were excised from the agarose gel (Figure 24 - blue rectangles), purified using miniprep purification kit (QIAGEN) and sequenced to verify the presence of desired DNA sequence. Subsequent sequencing (Figure 25) showed that the DNA sequence in pOPINF was a transcript of cTXNPx for all four species, with 100 % identity to *L. amazonensis*, *L. donovani* and *L. mexicana* and 96 % identity to *L. major*.

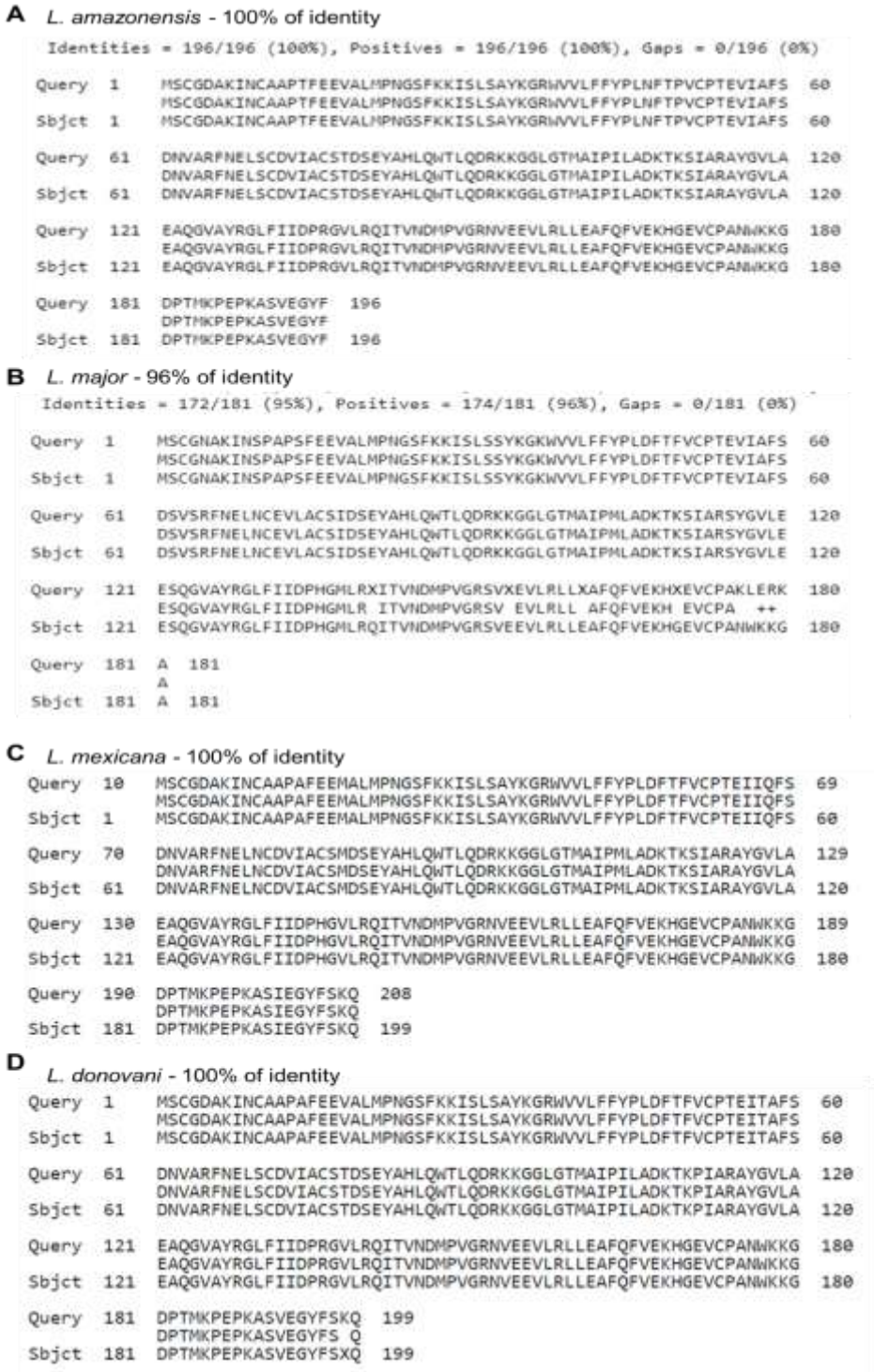

Figure 25. Protein sequence alignment. All sequences obtained by sequencing using T7 promoter and terminator were translated to protein sequence with ExPASy tool. Then, these protein sequences were aligned with its respective sequence on PDB by ClustalOmega alignment. **A**- cTXNPx of *L. amazonensis.* **B**- cTXNPx of *L. major.* **C**- cTXNPx of *L. mexicana.* **D**- cTXNPx of *L. donovani*

4.9.3 Protein overexpression and large scale purification.

With constructs successfully prepared attempts were made to induce protein expression and subsequent cTXNPx purification. Each colony of *E. coli* BL21(DE3) confirmed to be transfected with pOPINF and desired gene was grown on 50 mL of LB medium with ampicillin at 37 ºC, overnight. These cultures were used as initial inoculum for a 1 L cultures and when bacteria grew to an optical density (OD) of 0.8, protein expression was induced by addition of 1mM IPTG. Then, temperature of incubation was decreased to 30 ºC and cultures were shaken for 16 h. After that, high bacteria density was obtained as determined by spectrophotometer (OD: 2.0- 2.6).

All bacteria in each culture were lysed by sonication, using a lysis buffer containing an anti-protease cocktail. The desired cTXNPx protein was purified by affinity chromatography on Ni^{+2}-NTA columns by FPLC elution with increasing imidazole concentration (Figures 26A, 27A, 28A and 29A).

Samples were collected during all purification steps and analysed by SDS-PAGE. Figures 26B, 27B, 28B and 29B shows representative gel images of all samples of each protein. Reflecting the addition of the His_6-tag, the bands corresponding to cTXNPx was now observed at around 24 kDa. From the data shown in Figure 26, 27 and 28, it was possible to infer that after IPTG induction (AI), all *E. coli* cultures expressed more proteins in comparison to the culture before induction (BI). Lanes F1 to F5 represent the fractions from FPLC elution and they suggest all of them are composed mostly by a protein at ~24 kDa. Whilst this protocol successfully enabled the expression and purification of cTXNPx from

L. amazonensis, L. major and *L. mexicana* proteins, the orthologue from *L. donovani* was not efficiently obtained by this approach (Figure 29A) with only a low amount of protein purified by FPLC in comparison to the other proteins. Moreover, SDS-PAGE analysis of all fractions (Figure 29B) revealed that the band related to cTXNPx was not the major product isolated, probably due to a protein solubility issue, once the band at 24 KDa can be noticed on the pellet fraction (Figure 29B - Pel). Unfortunately, due to lack of time this purification was done only once, and a new L.doncTXNPx purification is required in order to circumvent this problem.

Each sample of cTXNPx was combined and the proteins dialysed with aqueous ammonium bicarbonate (10 mM), overnight, to remove excess of imidazole. This was accompanied by some protein precipitation and to provide a final solution containing only soluble proteins each sample was submitted to centrifugation to remove all precipitated material.

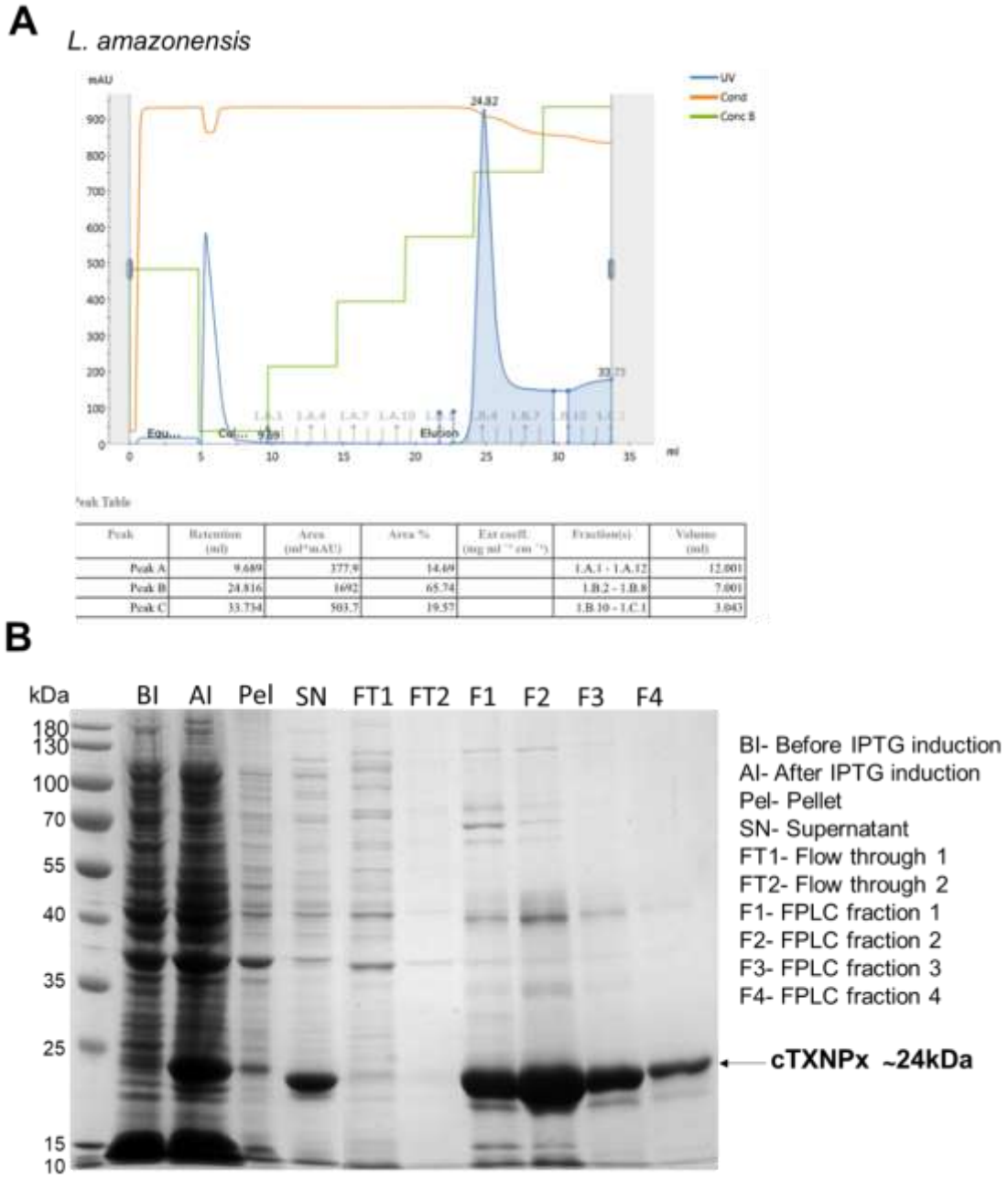

Figure 26. *L. amazonensis* cTXNPx overexpression and purification by FPLC. cTXNPx protein overexpression was induced on BL21(DE3) cells by IPTG addition. All bacteria were disrupted by sonication and desired protein was purified from the supernatant on Ni^{+2}-NTA columns by FPLC. **A**- FPLC chromatogram of *L. amazonensis* cTXNPx purification. **B**- SDS-PAGE showing samples collected during all purification steps.

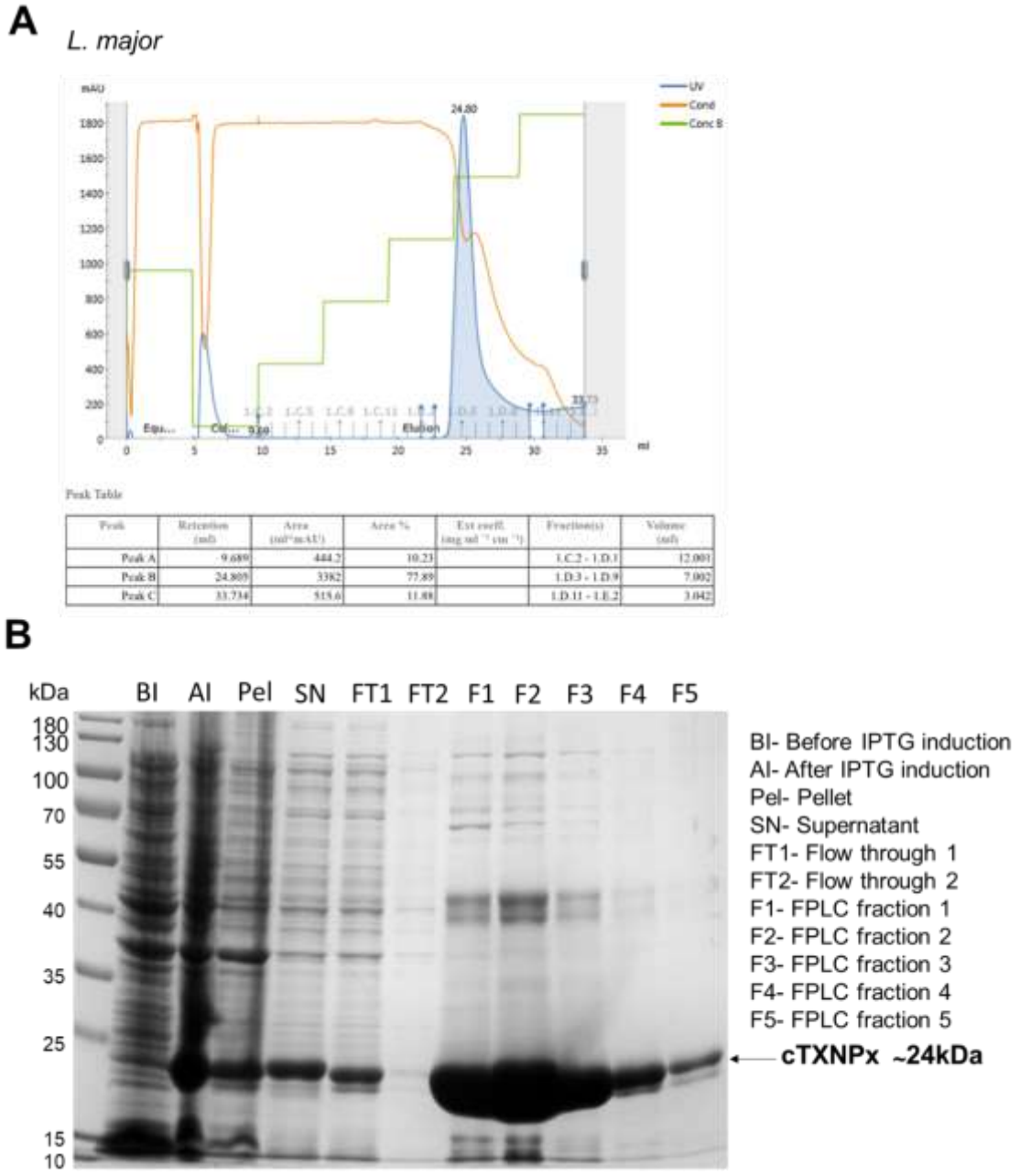

Figure 27. *L. major* cTXNPx overexpression and purification by FPLC. cTXNPx protein overexpression was induced on BL21(DE3) cells by IPTG addition. All bacteria were disrupted by sonication and desired protein was purified from culture supernatant on Ni^{+2}-NTA columns by FPLC. **A**- FPLC chromatogram of *L. major* cTXNPx purification. **B**- SDS-PAGE showing samples collected during all purification steps.

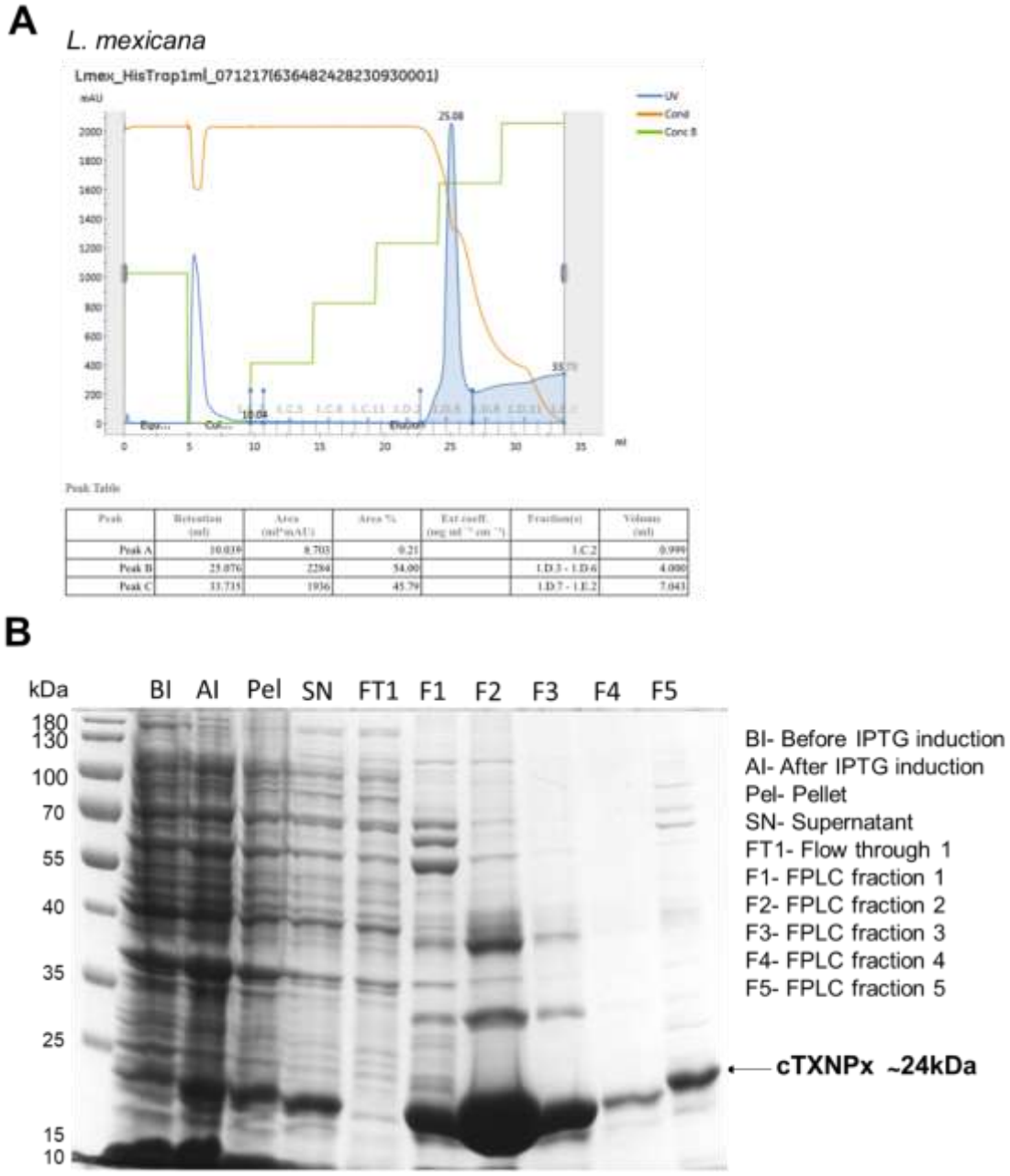

Figure 28. *L. mexicana* cTXNPx overexpression and purification by FPLC. cTXNPx protein overexpression was induced on BL21(DE3) cells by IPTG addition. All bacteria were disrupted by sonication and desired protein was purified from culture supernatant on Ni^{+2}-NTA columns by FPLC. **A**- FPLC chromatogram of *L. mexicana* cTXNPx purification. **B**- SDS-PAGE showing samples collected during all purification steps.

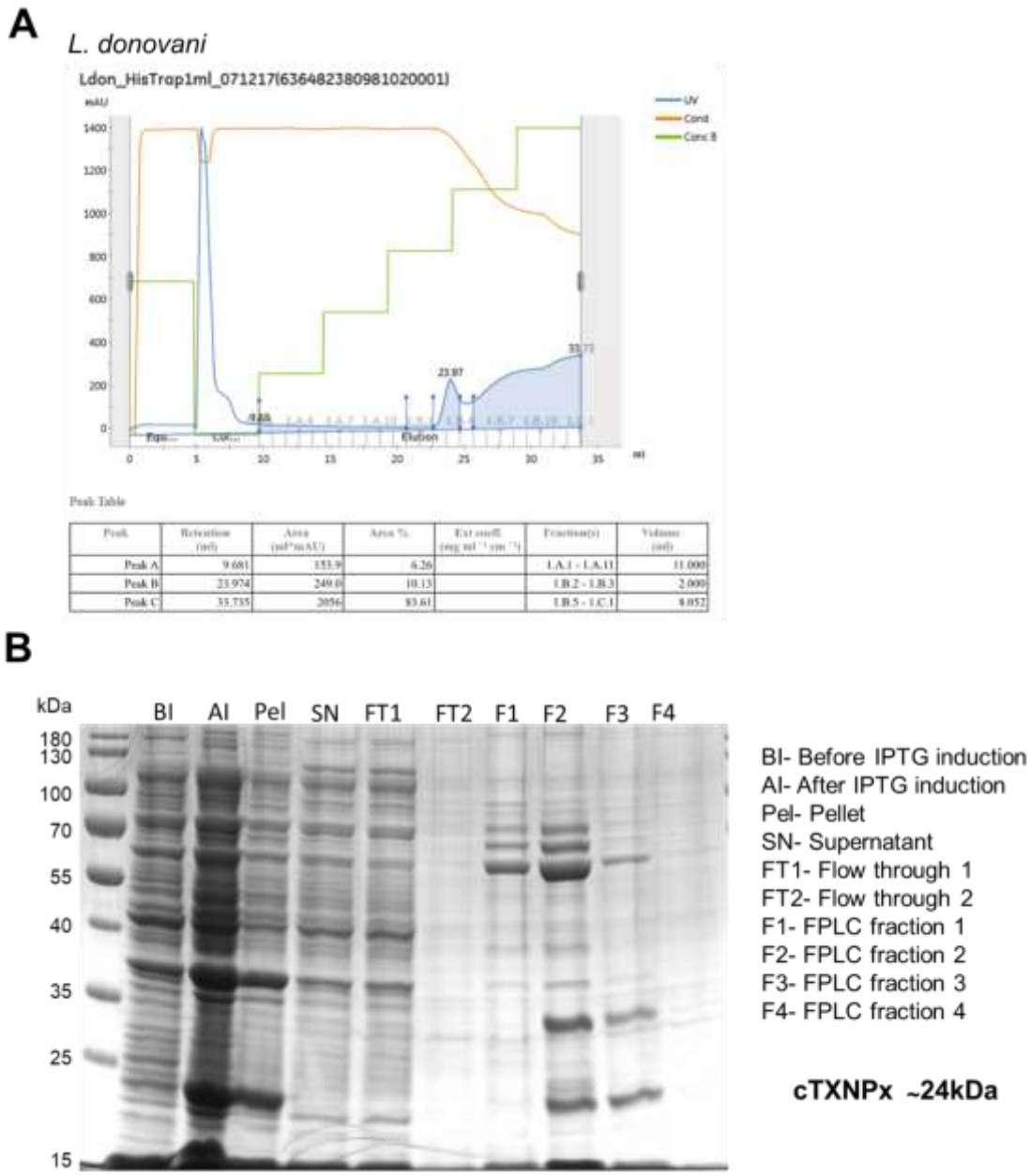

Figure 29. *L. donovani* cTXNPx overexpression and purification by FPLC. cTXNPx protein overexpression was induced on BL21(DE3) cells by IPTG addition. All bacteria were disrupted by sonication and desired protein was purified from culture supernatant on Ni^{+2}-NTA columns by FPLC. **A**- FPLC chromatogram of *L. donovani* cTXNPx purification. **B**- SDS-PAGE showing samples collected during all purification steps.

4.9.4 cTXNPx confirmation by mass spectrometry

The protein extinction coefficient calculated by an online calculator (http://www.biomol.net) from each protein sequence (Figures 30A, 31A, 32A and 33A), was used as a parameter to quantify the protein concentration for each soluble fractions using a NanoDrop spectrophotometer. With this information to hand, the proteins were then diluted to 0.6 mg/mL in ammonium bicarbonate (10 mM) and analysed by mass spectrometry (LCT premiere-Waters). For *L. amazonensis*, *L. major and L. mexicana* derived samples appropriate mass ions corresponding to loss of a Met (methionine) could be observed (Figures 30B, 31B and 32B).

In accordance with the SDS PAGE analysis for *L. donovani* derived proteins, the mass spectrum revealed no peaks attributable to the predicted mass corresponding to cTXNPx in this species (Figure 33B).

The protein mass spectrometry analysis confirmed that the desired cTXNPx for three species, *L. amazonensis*, *L. major* and *L. mexicana* could be purified using this approach.

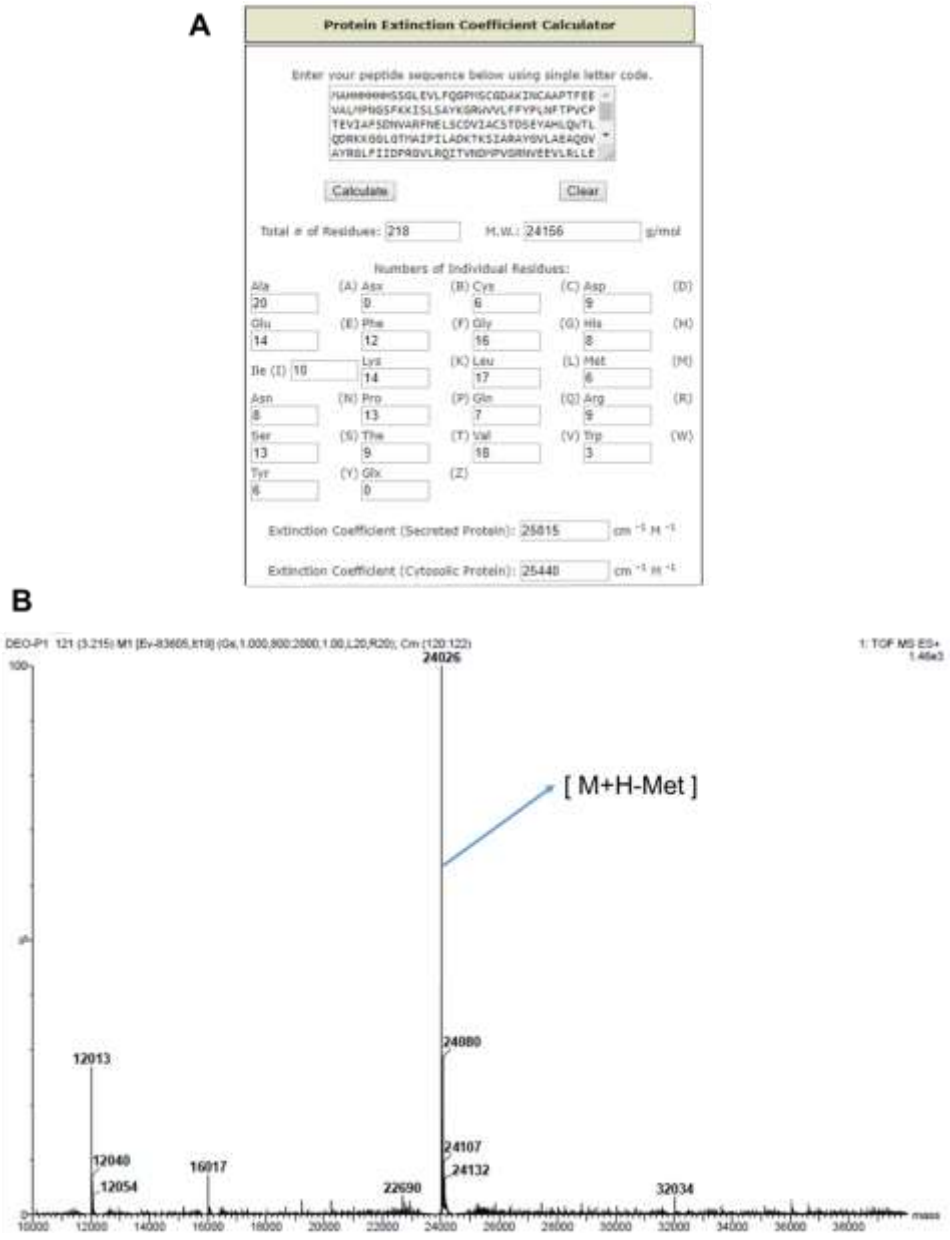

Figure 30. *L. amazonensis* cTXNPx mass spectrometry analysis. **A**- Protein mass and extinction coefficient of *L. amazonensis* cTXNPx calculated by biomol tool. **B**- *L. amazonensis* cTXNPx mass spectrum. M+H-Met requires 24026 Da.

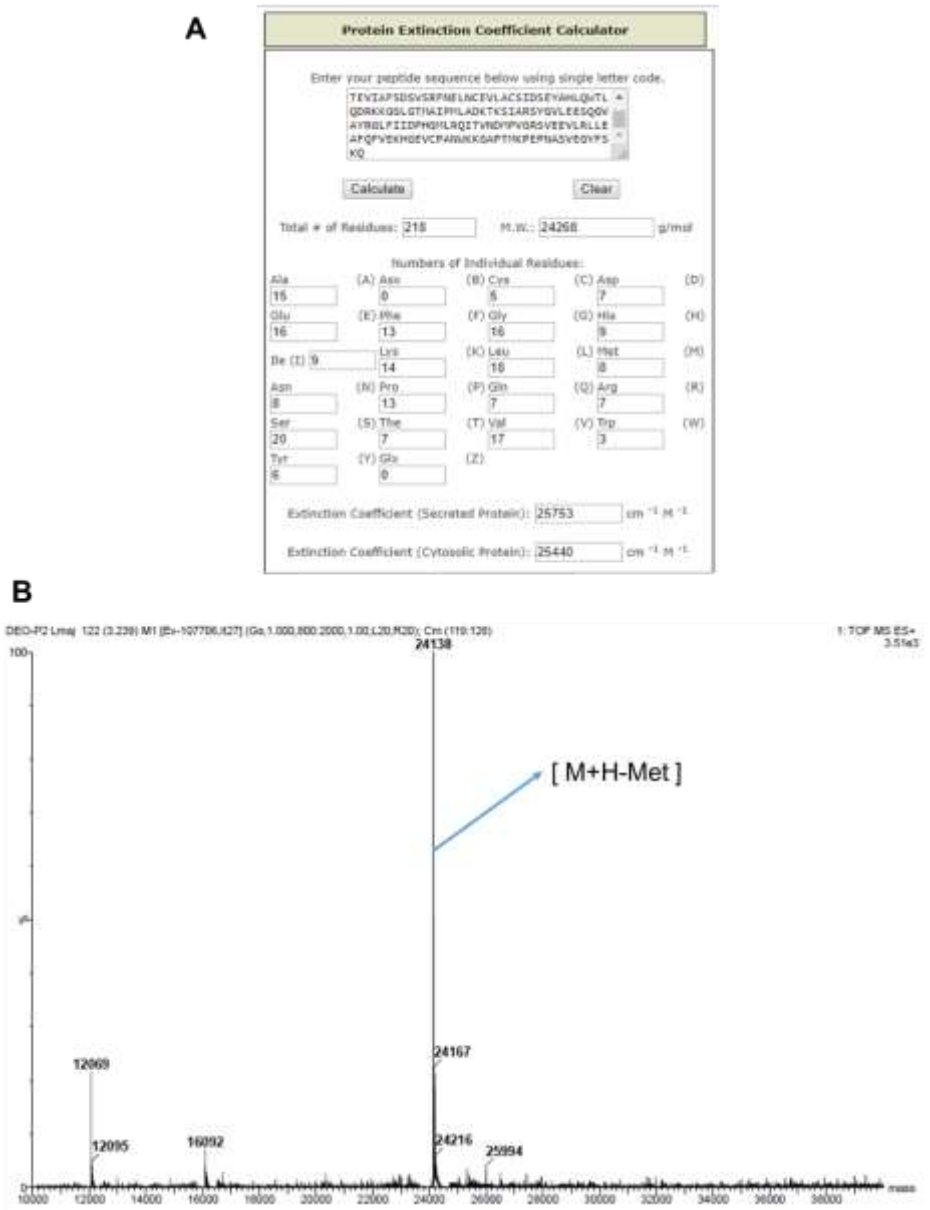

Figure 31. *L. major* cTXNPx mass spectrometry analysis. **A**- Protein mass and extinction coefficient of *L. major* cTXNPx calculated by biomol tool. **B**- *L. major* cTXNPx mass spectrum. M+H-Met requires 24138 Da.

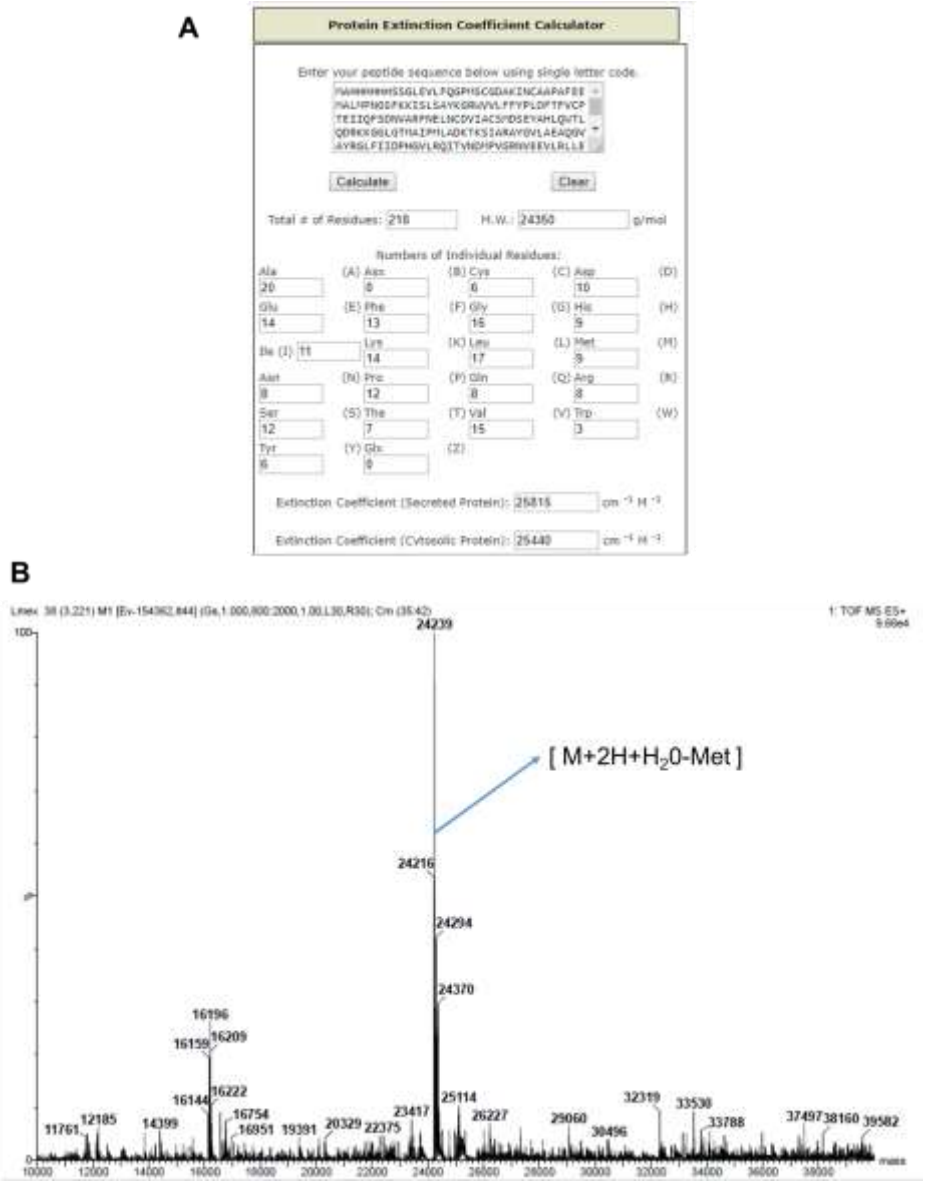

Figure 32. *L. mexicana* cTXNPx mass spectrometry analysis. **A**- Protein mass and extinction coefficient of *L. mexicana* cTXNPx calculated by biomol tool. **B**- *L. mexicana* cTXNPx mass spectrum. M+2H+H_2O-Met requires 24138 Da.

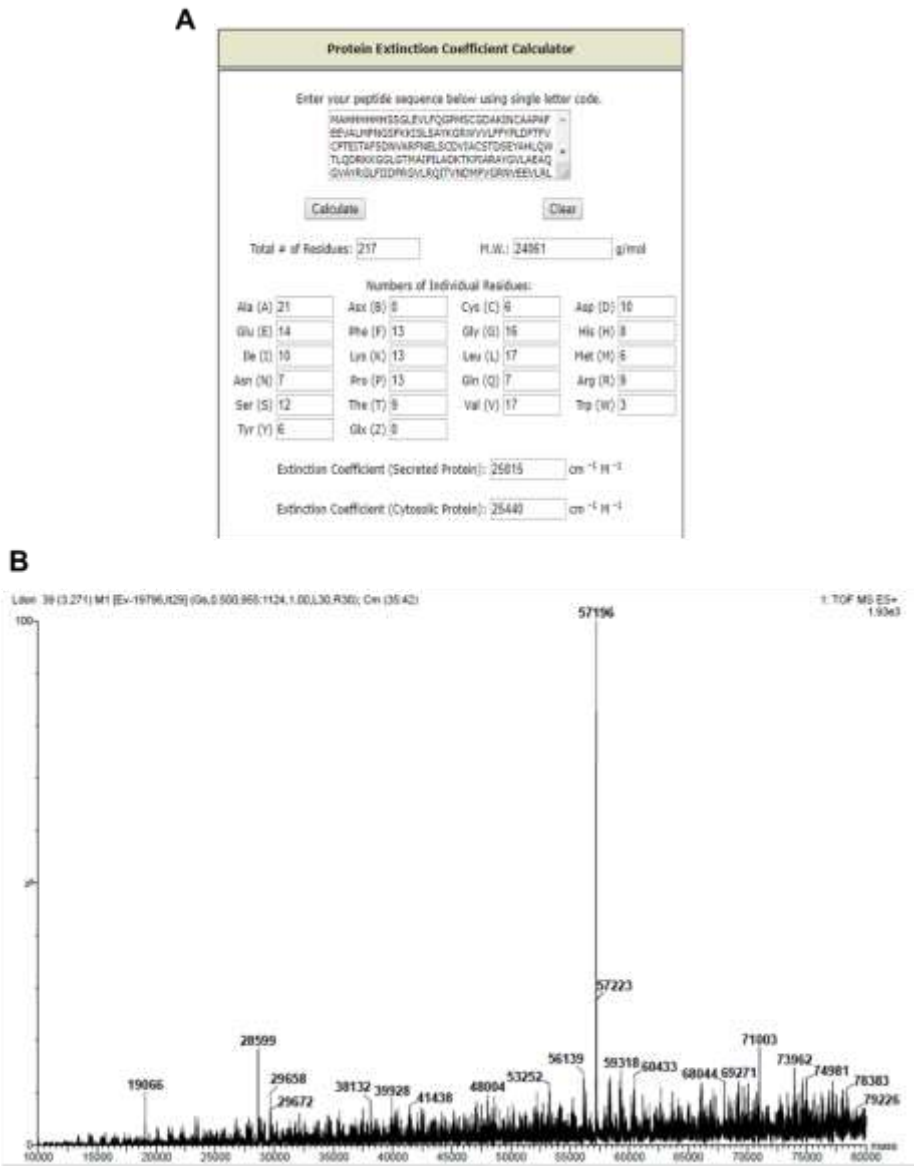

Figure 33. *L. donovani* cTXNPx mass spectrometry analysis. **A**- Protein mass and extinction coefficient of *L. donovani* cTXNPx calculated by biomol tool. **B**- *L. donovani* cTXNPx mass spectrum.

4.9.5 cTXNPx and chalcone interaction by mass spectrometry

With protein successfully purified, it was of interest to assess whether chalcone **11** is able to bind to the enzyme cTXNPx, as observed in live parasites. This confirmation was done by mass spectrometry with purified cTXNPx from *L. amazonensis* and *L. major.* Proteins were diluted to 0.6 mg/mL, in ammonium bicarbonate (10 mM), DTT (5 mM), at pH 7.2 and incubated for 30 min with compound **11** (27 µM). Then, proteins were submitted to mass spectrometry, as described before, to analyse their molecular weight.

In the absence of compound **11**, it was possible to observe only one peak corresponding to the protein molecular weight, for LaTXNPx protein mass was 24025 Da and 24138 Da for LmTXNPx, respectively (Figure 34A and C). In agreement with the earlier result using live parasites, compound **11** was found to bind strongly to the protein causing a peak shift of 343 Da which is consistent with a protein chalcone **11** conjugate (Figure 34B and D). Two small similar peak could be observed near the unbound protein, after treatment with chalcone **11** at 24368 Da [24025 + 343] for LaTXNPx whilst a similar peak could also be visualized at 24481 Da [24138 + 343] for LmTXNPx.

These mass spectrometry results helped us to confirm the interaction and it strength between protein and chalcone. Weak and middle interactions, such as ionic interactions, hydrogen bonds and hydrophobic interaction, cannot withstand the conditions used for sample analysis, which would result in the chalcone becoming unbound. The peak shift in both proteins suggest that chalcone **11** binds to cTXNPx through a covalent interaction.

A covalent interaction between chalcone and cTXNPx is in accordance with literature[37]. The active site of cTXNPx contains 2 cysteine residues (Cys52 and Cys173) that possess reactive sulfhydryl groups essential for enzymatic activity. Consistent with this, chalcone **11** contains an enone group, a Michael acceptor, which will undergo a Michael addition with the sulfhydryl on the cysteine to form a covalent bond[37].

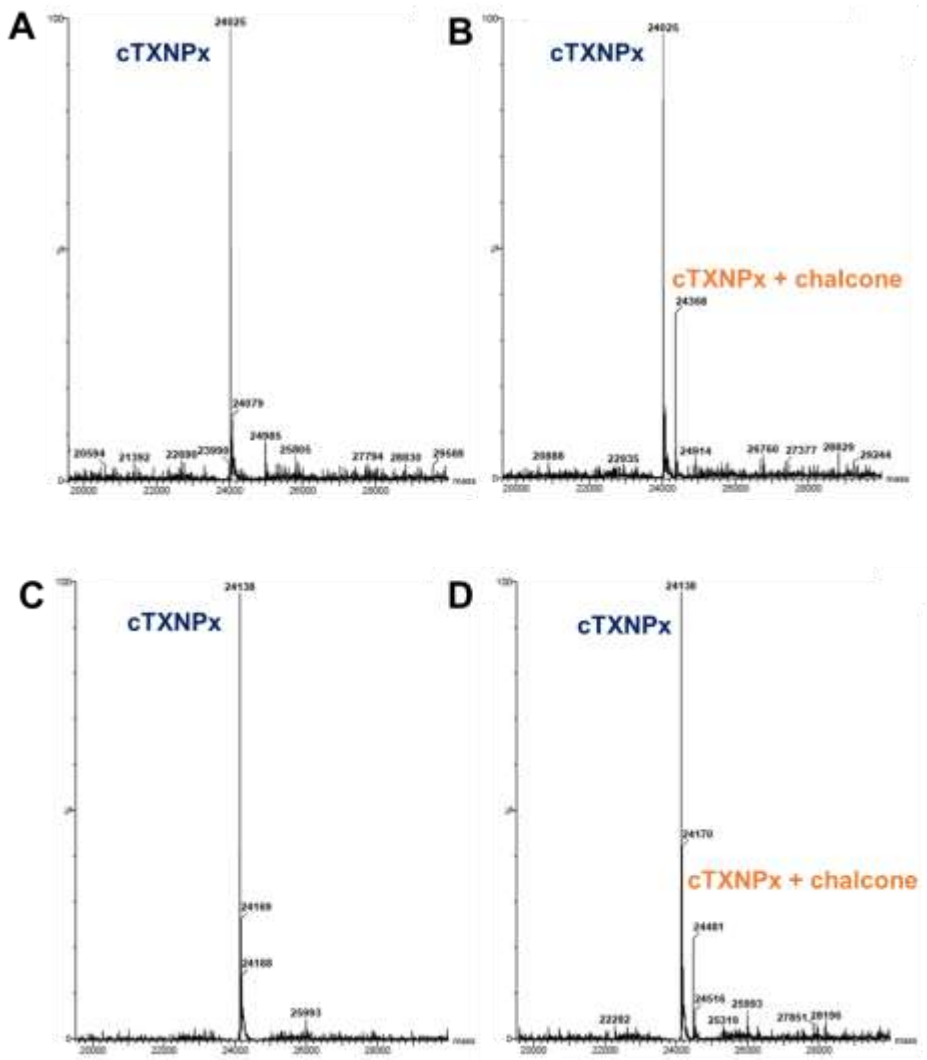

Figure 34. Mass spectrometry analysis of interaction between chalcone and cTXNPx. Purified proteins (0.6 mg/ mL) were incubated or not with compound 1 (1:1) for 30 min and their molecular weight analysed by Mass Spectrometry. **A**- cTXNPx of *L. amazonensis* molecular weight [M-Met requires 24025 Da]. **B**- cTXNPx of *L. amazonensis* with **11** [M-Met+343 requires 24368 Da]. **C**- cTXNPx of *L. major* molecular weight [M+H-Met requires 24138 Da]. **D**- cTXNPx of *L. major* with **11** [M+H-Met+343 requires 24481 Da].

4.9.6 cTXNPx and chalcone interaction by SDS-PAGE

On live promastigotes, chalcone **11** competes with chalcone **19** for protein targets, specially cTXNPx (Figure 14). In order to further assess this, a competition assay with the purified protein was carried out using *L. amazonensis* cTXNPx as a representative sample. In parallel, samples of cTXNPx (1 mg/mL-50 µM) in the presence and absence of chalcone **11** were incubated with **19** (50 µM) for 1 h at RT, followed by a cycloaddition reaction with probe **20** (50 µM), as described above. For the interaction assays the chalcone **11** was dosed at distinct ratios (protein:chalcone, 1:0.1; 1:1 and 1:10) for 1 h at RT. Then, proteins were washed, to remove excess chalcone **11**, incubated with chalcone **19** and linked to probe **20.** All samples were loaded on 10% polyacrylamide gel; fluorescent bands were imaged and proteins were stained with comassie blue (Figure 35A).

Two bands stained with comassie blue could be seen in all samples (L1 to L6), one band at ~24 kDa and another at ~48 kDa, corresponding to cTXNPx monomer and dimer, respectively. A CuAAC reaction with molecule **20** was performed on all samples and the resultant fluorescence signal was detected (Figure 35B). In accordance with previous results, the fluorescent image showed no non-specific binding of compound **20** to protein without **19** (L2) and chalcone analogue **19** was able to interact with cTXNPx monomer *in vitro* (L3, ~24 kDa). In addition, compound **19** did not bind to cTXNPx dimer, as no fluorescent bands could be viewed at ~48 kDa (L3).

As noted in previous results, incubation with **11** dramatically affected the binding of compound **19** and the subsequent fluorescent signal of molecule **20**

(Figure 35B). Significantly, the fluorescence signal of bands at 24 kDa decreased in a concentration-dependent manner. The fluorescence mean was quantified using Image Lab software and it shows a fluorescence signal decreasing to 50% when the protein was incubated with molecule **11** in at ratio 1:1; this effect was more pronounced when cTXNPx was treated with high concentrations of compound **11** (Figure 35C). This data corroborates the intracellular tagging results shown in Figure 14, confirming that chalcone **19** interacts with recombinant cTXNPx as well as with the protein in its native conformation in the parasite.

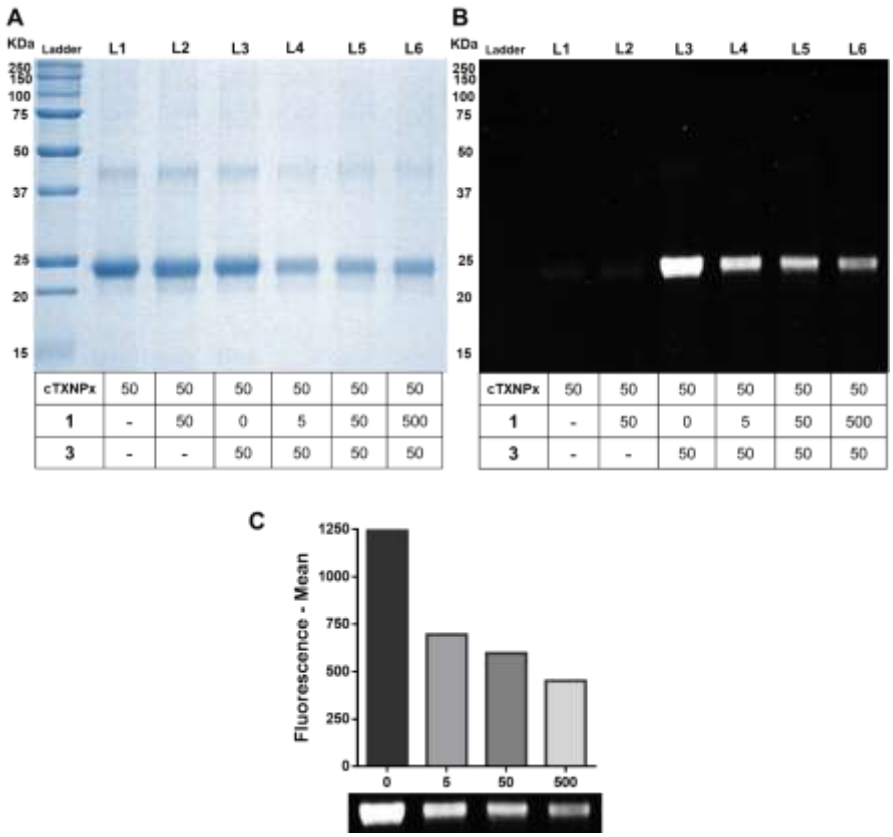

Figure 35. cTXNPx and chalcone interaction by SDS-PAGE. Purified *L. amazonensis* cTXNPx (50 µM) was incubated with **11** at different concentrations, then proteins were washed and incubated with 3 at (50 µM). All proteins were submitted to click reaction with 4 (50 µM) and all samples were analysed on 10% polyacrylamide gel. Protein fluorescence was visualised using GelDoc imager and stained with comassie blue. **A-** Comassie blue stained gel. **B**- Gel fluorescence image. **C**- Fluorescence mean quantification of band at 24 kDa. L1- untreated

protein. L2- proteins treated with **11** (50 µM). L3- proteins treated with **19** (50 µM). L4 to L6- proteins treated with **11** (5, 50 and 500 µM, respectively) and **19** (50 µM). Representative image of three independent experiments.

4.9.7 Influence of chalcone interaction on cTXNPx stability

To further explore the protein chalcone interaction, we decided to measure protein stability using a thermal shift assay (TSA)[144], an easy and straightforward method to evaluate changes in denaturation temperature of a protein (ΔTm) due to interaction with a ligand. Differential scanning fluorimetry was used to detect ligand interactions. Briefly, the protein was mixed with ligands under specific pH or salt conditions and the fluorescent dye SYPRO Orange added. Samples were then loaded into a qPCR machine and changes in fluorescence of SYPRO Orange are monitored as the temperature is slowly increased.

cTXNPx proteins from *L. amazonensis* were first tested in their initial purification buffer in a screen of 96 different pH and salt conditions from The Durham Screen- MD1-101 and MD1-102 (Molecular Dimensions)[144]. These screens contain a range of conditions, focusing on different pH and buffer conditions (pH 4.1-10.9) and numerous salt additives. Determining optimal conditions for protein stability in solution allowed perform tests with chalcone **11** (Figures 36 and 37). Results in Figures 35 and 36, provides a comparison of the melting point for distinct conditions with that found for the protein in water. The colour in each box represents this comparison, if the protein is more stable in a specific condition the box colour is blue; it is red when conditions decrease protein stability.

cTXNPx melting points under all pH conditions for *L. amazonensis* can be found in Figure 36. The tested conditions suggest that the optimum pH range to stabilise the protein is 6.6 to 7.1, similar to the protein theoretical pI (7.01, according to ProParam tool). The most suitable buffers according to Tm were bisTRIS, HEPES and MOPS (Figure 36- blue boxes).

From the screen of salt additives, melting points in Figure 37 suggest molecules that contains NH_4^+ cations, such as $(NH_4)_2SO_4$ and NH_4Cl, or $ZnCl_2$ or $NiCl_2$ or DTT (blue boxes), are good additives to improve protein stability in solution.

A cTXNPx *L. amazonensis*

	1	2	3	4	5	6	7	8	9	10	11	12
A	54.9	54.7	37.3	N/S	38.9	46.3	38.5	41.1	46.1	34.2	41.1	46.8
B	33.0	40.8	48.6	37.3	50.9	52.9	38.0	41.3	46.8	47.3	50.2	52.8
C	48.2	50.0	51.8	49.4	53.1	54.1	47.8	51.7	53.7	49.5	52.2	51.8
D	48.1	49.3	49.9	50.1	50.5	51.5	50.7	52.2	53.5	52.8	53.5	53.7
E	53.3	53.2	53.0	53.0	54.1	54.7	49.5	50.0	50.0	54.5	54.9	54.4
F	50.3	50.5	51.3	55.3	55.1	53.9	53.3	53.3	52.4	55.2	54.4	52.0
G	53.2	52.6	52.1	53.3	52.6	51.5	55.1	54.0	51.7	50.3	47.8	45.6
H	46.3	44.2	43.5	49.9	46.5	40.5	51.4	48.9	45.9	38.2	40.2	36.7

B pH and buffer conditions

	1	2	3	4	5	6	7	8	9	10	11	12
A	water	water	4 M urea	100 mM citric acid pH 4.1	100 mM citric acid pH 4.6	100 mM citric acid pH 5.1	100 mM acetic acid pH 4.2	100 mM acetic acid pH 4.7	100 mM acetic acid pH 5.2	100 mM succinic acid pH 4.4	100 mM succinic acid pH 4.9	100 mM succinic acid pH 5.4
B	100 mM malic acid pH 4.3	100 mM malic acid pH 4.8	100 mM malic acid pH 5.3	100 mM tartaric acid pH 4.3	100 mM tartaric acid pH 4.8	100 mM tartaric acid pH 5.3	100 mM propionic acid pH 4.3	100 mM propionic acid pH 4.8	100 mM propionic acid pH 5.3	100 mM malonic acid pH 5.2	100 mM malonic acid pH 5.7	100 mM malonic acid pH 6.2
C	100 mM citric acid pH 5.5	100 mM citric acid pH 6.0	100 mM citric acid pH 6.5	100 mM succinic acid pH 5.6	100 mM succinic acid pH 6.1	100 mM succinic acid pH 6.6	100 mM MES pH 5.6	100 mM MES pH 6.1	100 mM MES pH 6.6	100 mM maleic acid pH 5.7	100 mM maleic acid pH 6.2	100 mM maleic acid pH 6.7
D	100 mM sodium cacodylate pH 5.7	100 mM sodium cacodylate pH 6.2	100 mM sodium cacodylate pH 6.7	100 mM ADA pH 6.1	100 mM ADA pH 6.6	100 mM ADA pH 7.1	100 mM bisTRIS pH 6.1	100 mM bisTRIS pH 6.6	100 mM bisTRIS pH 7.1	100 mM ACES pH 6.3	100 mM ACES pH 6.8	100 mM ACES pH 7.3
E	100 mM phosphate pH 6.3	100 mM phosphate pH 6.8	100 mM phosphate pH 7.3	100 mM PIPES pH 6.3	100 mM PIPES pH 6.8	100 mM PIPES pH 7.3	100 mM imidazole pH 6.6	100 mM imidazole pH 7.1	100 mM imidazole pH 7.6	100 mM MOPS pH 6.6	100 mM MOPS pH 7.1	100 mM MOPS pH 7.6
F	100 mM bisTRIS propane pH 6.6	100 mM bisTRIS propane pH 7.1	100 mM bisTRIS propane pH 7.6	100 mM HEPES pH 7.0	100 mM HEPES pH 7.5	100 mM HEPES pH 8.0	100 mM tricine pH 7.5	100 mM tricine pH 8.0	100 mM tricine pH 8.5	100 mM EPPS pH 7.5	100 mM EPPS pH 8.0	100 mM EPPS pH 8.5
G	100 mM TRIS pH 7.7	100 mM TRIS pH 8.2	100 mM TRIS pH 8.7	100 mM bicine pH 7.7	100 mM bicine pH 8.2	100 mM bicine pH 8.7	100 mM TAPS pH 7.9	100 mM TAPS pH 8.4	100 mM TAPS pH 8.9	100 mM bisTRIS propane pH 8.5	100 mM bisTRIS propane pH 9.0	100 mM bisTRIS propane pH 9.5
H	100 mM boric acid pH 8.6	100 mM boric acid pH 9.1	100 mM boric acid pH 9.6	100 mM CHES pH 8.6	100 mM CHES pH 9.3	100 mM CHES pH 9.8	100 mM glycine pH 9.2	100 mM glycine pH 9.7	100 mM glycine pH 10.2	100 mM CAPS pH 9.9	100 mM CAPS pH 10.4	100 mM CAPS pH 10.9

Figure 36. cTXNPx melting points (Tm) at different pH conditions. cTXNPx stability at distinct pH and buffer conditions was assessed by thermal shift assay. cTXNPx from *L. amazonensis,* in presence of SYPRO orange, were incubated at 96 pH and buffer conditions from The Durham screen MD1-101, and melting points calculated by NAMI software from SYPRO orange fluorescence using RT-PCR machine. **A**- *L. amazonensis* cTXNPx melting temperatures. **B**- MD1-101 conditions. Blue squares- ideal conditions for protein stability. The colour in each box represent comparison the protein in water and with distinct conditions, blue colour represent conditions which stabilize the proteins and red colour conditions that decreases protein stability.

A cTXNPx *L. amazonensis*

	1	2	3	4	5	6	7	8	9	10	11	12
A	52.6	52.8	32.6	N/S	30.0	32.3	37.5	42.7	47.4	52.3	50.7 60.4	51.9
B	78.9 89.0	49.4 73.7	49.7 65.1	50.8 59.9	54.9	51.9	71.3	49.7 59.2	56.3	53.4	50.4	50.2
C	48.5	50.3	49.8	49.9	49.9	50.6	44.6	45.8	46.5	47.4	48.6	49.8
D	53.6	52.0	50.8	50.8	50.2	48.3 72.9	48.8 62.9	58.0	54.4	52.0	49.9	50.5
E	51.5	52.5	49.8	50.7	48.5	50.3	53.3	52.3	46.7	47.9	51.0	45.3
F	48.8	43.9	52.5	52.7	52.2	66.8	64.7	53.8	52.9	52.0	52.7	80.0
G	63.8 84.4	65.0	52.0	52.7	52.6	52.8	51.6	52.2	52.4	52.3	52.3	52.2
H	51.9	51.3	51.0	50.8	51.0	52.8	53.0	53.5	52.6	52.6	52.1	52.8

B Salt additives

	1	2	3	4	5	6	7	8	9	10	11	12
A	water	water	4 M urea	3.0 M Gu-HCl	1.0 M Gu-HCl	0.8 M Gu-HCl	0.6 M Gu-HCl	0.4 M Gu-HCl	0.2 M Gu-HCl	5 mM Gu-HCl	0.5 M Na_3 citrate	0.2 M Na_3 citrate
B	1.5 M Na_2 malonate	1.0 M Na_2 malonate	0.8 M Na_2 malonate	0.6 M Na_2 malonate	0.4 M Na_2 malonate	0.2 M Na_2 malonate	1.5 M $(NH_4)_2SO_4$	1.0 M $(NH4)_2SO_4$	0.8 M $(NH_4)_2SO_4$	0.6 M $(NH_4)_2SO_4$	0.4 M $(NH_4)_2SO_4$	0.2 M $(NH_4)_2SO_4$
C	1.5 M NaCl	1.0 M NaCl	0.8 M NaCl	0.6 M NaCl	0.4 M NaCl	0.2 M NaCl	1.5 M NH_4Cl	1.0 M NH_4Cl	0.8 M NH_4Cl	0.6 M NH_4Cl	0.4 M NH_4Cl	0.2 M NH_4Cl
D	1.0 M $MgSO_4$	0.8 M $MgSO_4$	0.6 M $MgSO_4$	0.4 M $MgSO_4$	0.2 M $MgSO_4$	1.0 M Na_2SO_4	0.8 M Na_2SO_4	0.6 M Na_2SO_4	0.4 M Na_2SO_4	0.2 M Na_2SO_4	0.5 M KCl	0.2 M KCl
E	0.5 M LiCl	0.2 M LiCl	0.5 M RbCl	0.2 M RbCl	0.5 M CsCl	0.2 M CsCl	0.4 M NaF	0.1 M NaF	1.5 M NaBr	0.4 M NaBr	0.1 M NaBr	0.4 M NaI
F	0.1 M NaI	0.4 M $MgCl_2$	5 mM $MgCl_2$	5 mM $CaCl_2$	5 mM $SrCl_2$	1 mM $ZnCl_2$	0.1 mM $ZnCl_2$	1 mM $NiCl_2$	0.1 mM $NiCl_2$	5 mM $MnCl_2$	0.5 mM $MnCl_2$	1 mM $CoCl_2$
G	0.1 mM $CoCl_2$	1 mM $CuSO_4$	0.1 mM $CuSO_4$	1 mM $CdSO_4$	5 mM EDTA pH 7.5	5 mM EGTA pH 7.5	2 mM magic triangle pH 7.0	2 mM $La(NO_3)_3$	2 mM $PrCl_3$	2 mM $NdCl_3$	2 mM $SmCl_3$	2 mM $EuCl_3$
H	2 mM $GdCl_3$	2 mM $DyCl_3$	2 mM $HoCl_3$	2 mM $YbCl_3$	2 mM $LuCl_3$	5 mM Na_2HPO_4	5 mM Na_3VO_4	5 mM Na_2WO_4	5 mM Na_2MoO_4	5 mM DTT	5 mM TCEP pH 7.0	5 mM β-mercapto ethanol

Figure 37. cTXNPx melting points (Tm) at different salt conditions. cTXNPx stability at distinct salt additives was assessed by thermal shift assay. cTXNPx from *L. amazonensis,* in presence of SYPRO orange, were incubated at 96 salt conditions from the Durham screen MD1-102, and melting points calculated by NAMI software from SYPRO orange fluorescence using RT-PCR machine. **A**- *L. amazonensis* cTXNPx melting temperatures. **B**- MD1-102 conditions. Blue squares- ideal conditions for protein stability. The colour in each box represent comparison the protein in water and with distinct conditions, blue colour represent conditions which stabilize the proteins and red colour conditions that decreases protein stability.

The dihydrochalcone (**18**), was used in the thermal shift assays to further demonstrate the importance of the chalcone α, β-unsaturated bond for antileishmanial activity. Compounds **11** and **18** were evaluated by TSA to determine their effect on protein stability in solution. This involved the dialysis of cTXNPX using 20 mM HEPES buffer, pH 6.9, 50 mM NaCl and 5 mM DTT, these conditions were chosen from the last TSA trails. Then, proteins were incubated with compound **11** or **18** at distinct ratios (4:1, 2:1, 1:1, 1:2, 1:4) and melting temperatures and ΔTm were calculated from the changes in SYPRO orange fluorescence (Figure 38). This data clearly revealed that, chalcone **11** is able to interact with the protein in solution and change its melting temperature curves, as observed by a decrease in fluorescence signal, in a dose dependent manner (Figure 38A). On the other hand, chalcone **18,** without the double bound, caused no significant changes to the protein melting curves with even at higher concentrations (180 µM) of compound **18** no decrease in the fluorescent signal of SYPRO orange being seen (Figure 38B).

Compound **11** is capable of interacting with cTXNPx in solution and decreases the protein stability and protein melting temperature, as shown in Figure 38A. This observed effect suggests chalcone **11** binds primarily to the unfolded protein causing destabilisation[156; 157]. This interaction is dependent on the presence of a Michael acceptor as compound **18** did not interfere with the protein melting point (Figure 38C). Further experiments will be performed to better understand the influence of the enone group on antileishmanial activity.

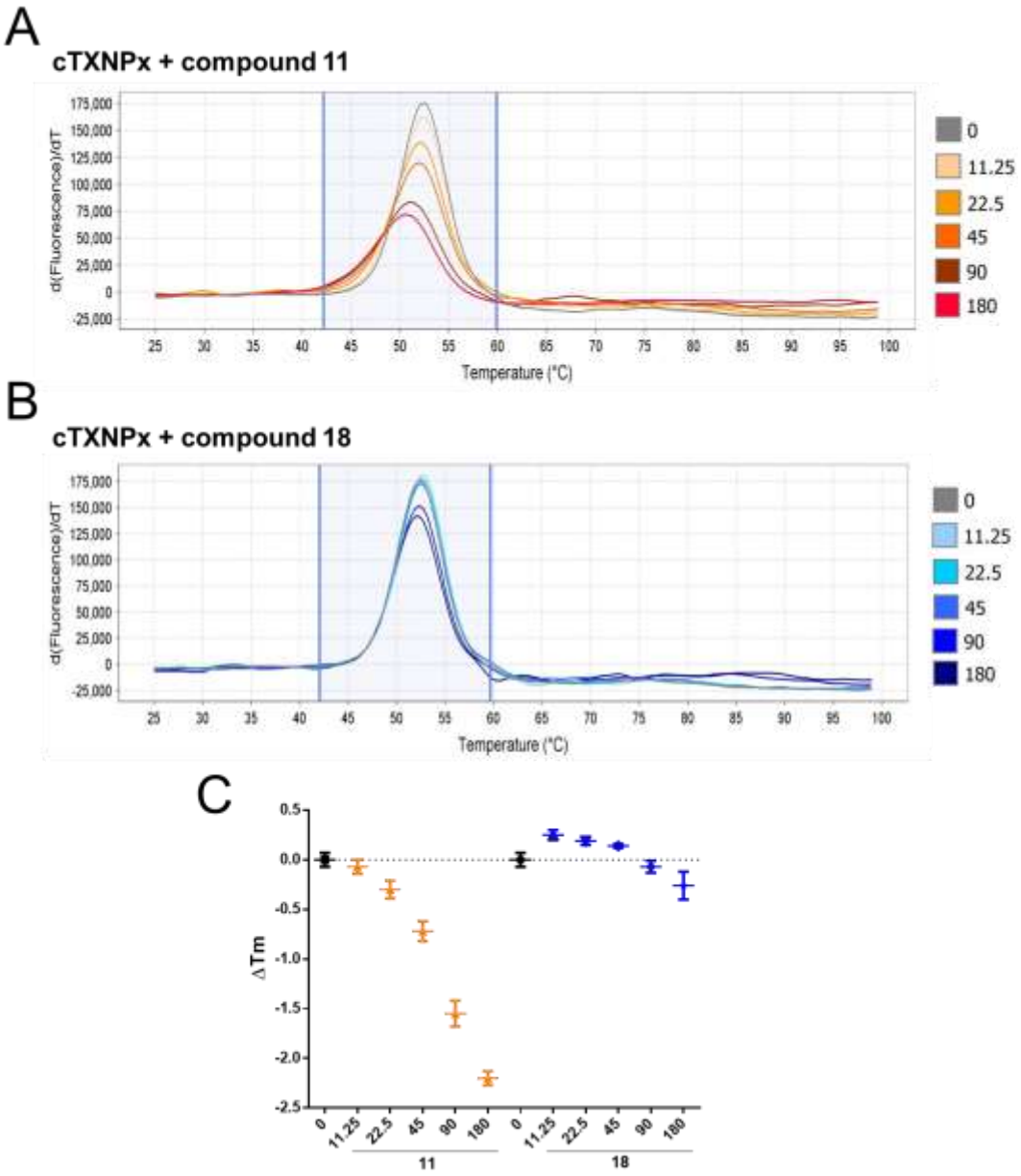

Figure 38. Effect of compound **11** and **18** on cTXNPx stability. cTXNPx (1mg /mL or 45uM) from *L. amazonensis* was incubated with **11** or **18** at different concentration in presence of SYPRO orange. Then protein stability was assessed by TSA. Melting point curves and ΔTm were calculated by Protein Thermal Shift Software v1.3 using SYPRO orange fluorescence signal from RT-PCR machine. **A**- Melting curves of *L. amazonensis* cTXNPx in the presence of **11**. **B-** Melting curves of *L. amazonensis* cTXNPx in the presence of **18. C-** *L. amazonensis* cTXNPx ΔTm after incubation with **11** or **18**.

4.10 Importance of enone group for chalcone activity

The results from TSA regarding protein stability identified the potential importance of the α, β-unsaturated ketone group for the interaction with recombinant protein. To better understand this relation between the enone group and chalcone activity against cTXNPx we proposed to compare the activity of compound **11** and **18** against the parasite.

4.10.1 Enone group influence on chalcone activity against *Leishmania*

First, an investigation was set up to evaluate whether the lack of a Michael acceptor on compound **18** will alter its activity in *Leishmania* promastigotes in comparison with compound **11**. Promastigotes of different species, *L. amazonensis, L. braziliensis* and *L. infantum*, were incubated with several concentrations of **11** or **18** at, for 72 h at 26 ºC. Then cell viability was evaluated fluorimetrically by alamarBlue method (Figure 39).

The results from this study exposed the essentiality of the double bond to kill the parasite (Figure 39A, B and C). As observed before, compound **11** has an excellent activity against all tested species, with IC_{50} values of 0.64, 1.96 and 0.76 µM for *L. amazonensis, L. braziliensis* and *L. infantum*, respectively. Consistent with the hypothesised mode of action, the absence of enone group on compound **18** deeply reduced its capacity to kill parasite, showing IC_{50} of 67.13, 252.00 and 26.28 µM for *L. amazonensis, L. braziliensis* and *L. infantum*. In comparison to compound **11**, the chalcone without enone group was 104 times less active against *L. amazonensis* promastigotes and 131 and 35 times for *L. braziliensis* and *L. infantum* parasites (Figure 39D).

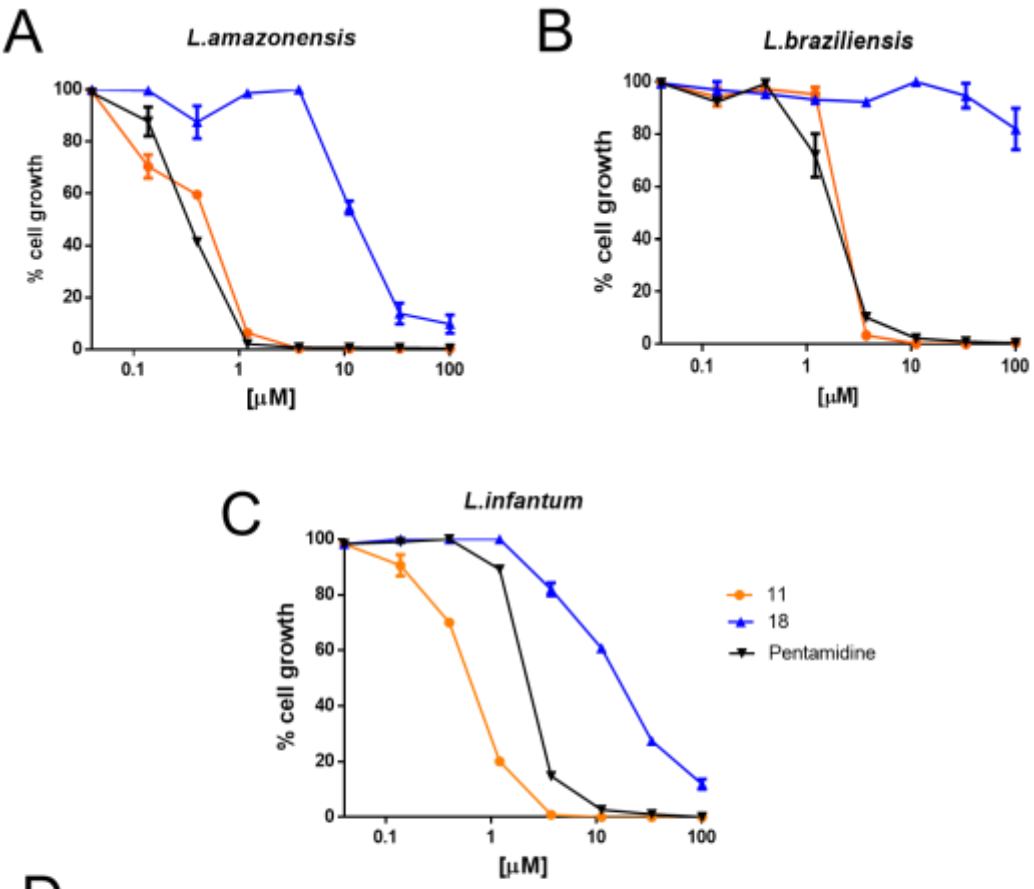

D

Treatments	IC_{50} [µM] Promastigotes		
	L.amazonensis	*L.braziliensis*	*L.infantum*
11	0.64 ± 0.08	1.96 ± 0.12	0.76 ± 0.08
18	67.13 ± 0.07	252 ± 0.09	26.18 ± 0.07
Pentamidine	0.54 ± 0.09	1.11 ± 0.09	1.52 ± 0.09
Ratio 18/11	104	131	35

Figure 39. Inhibition of *Leishmania* promastigote growth by compounds **11** and **18**. Promastigotes of distinct *Leishmania* species were incubated with molecules **11** or **18** at different concentrations. Then, parasite viability was assessed by the alamarBlue method after 72 h of incubation. Pentamidine was used as a positive control. **A**- *L. amazonensis*. **B**- *L. braziliensis*. **C**- *L. infantum*. **D**- Calculated IC_{50} values for each treatment. Means ± SD (n=3).

4.10.2 Influence of enone group on parasite selectivity

Having established that the enone group was essential for chalcone activity in the extracellular parasite form, the next step was to study if this effect was observed in the intracellular parasite stages.

For that, bone marrow derived macrophages (BMDM) were infected with *L. amazonensis* promastigotes in a 10:1 ratio. After 24h of infection, promastigotes had differentiated into amastigotes and macrophages were treated for 48 h with compound **11** or **18** at different concentrations, at 37 ºC. To measure the anti-amastigote activity, cells were stained with GIEMSA stain and the number of amastigotes in 200 macrophages were counted under a light microscope.

Similar to the promastigote assay, chalcone **11** reduced the number of intracellular amastigotes in a concentration-dependent manner (Figure 40A and C), with the IC_{50} value for compound **11** being 0.32 µM. This is pleasantly surprising as it is lower than the IC_{50} value of compound **11** against the promastigote form (0.6 µM). Furthermore, when infected macrophage cells were incubated with dihydrochalcone **18**, an IC_{50} value of 19.57 µM was obtained (Figure 40C). Hence, the absence of the enone group reduced the activity of compound **18** ~60 fold, compared to chalcone **11**. This drop in activity was consistent with that observed in the promastigote assays (Figure 39).

Toxicity to macrophages was also evaluated by incubation of BMDM with compound **11** or **18** for 48 h at 37 ºC. After this time, culture supernatants were collected and the presence of intracellular enzyme lactate dehydrogenase – LDH

was used as a parameter to appraise cell viability in comparison to Triton-X100, as a positive control (Figure 40B). Consistent with the other assays, the cytotoxicity of the chalcone is reduced 8 times when the double bond is removed with the CC_{50} for compounds **11** and **18** being 7.37 µM and 64.18 µM, respectively (Figure 40C).

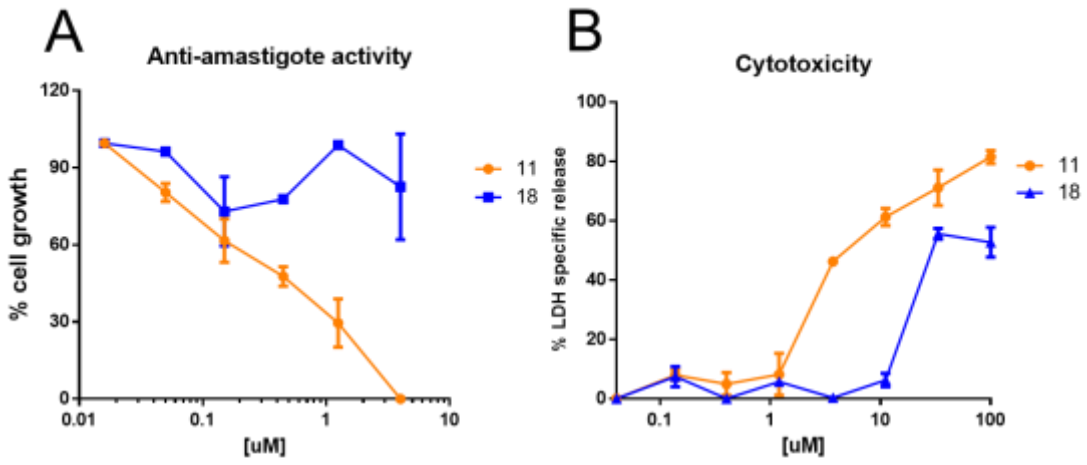

C

Treatments	IC_{50} [µM] amastigotes	CC_{50} [µM]	Selectivity index
	L.amazonensis	Macrophages	
11	0.32 ± 0.06	7.37 ± 0.06	23.03
18	19.57 ± 0.36	64.18 ± 0.07	3.28
Ratio 18/11	61.00	8.7	

Figure 40. Loss of parasite selectivity due to lack of enone group. BMDM ($1x10^5$/well) infected with *L. amazonensis* promastigotes (10:1) were treated, after 24 h of infection, with molecules **11** or **18** at different concentrations for 48h. Then cells were stained with GIEMSA and number of intracellular amastigotes in 200 macrophages were counted using light microscope. **A**- % of amastigote growth in macrophages after treatment. Cytotoxicity to macrophages was assessed by the quantification of lactate dehydrogenase (LDH) in the supernatant after 48 h of treatment with compound **11** and **18**. **B**- LDH specific release induced by the treatment. **C**- Calculated IC_{50}, CC_{50} and the selectivity index to the parasite. Means ± SD (n=3).

With IC_{50} and CC_{50} values in hand, the selectivity index of a drug to the parasite can be calculated. This is an important parameter to select promising compounds for development as antileishmanials[158]. Figure 40C enables us to confirm that the double bond is essential for chalcone selectivity because, despite the lower toxicity, compound **18** was only 3 times more active against parasite than host cell. On the other hand, compound **11** showed a selectivity index of 23, a value which is in accordance with DNDi guidelines[158].

In view of the decrease in anti-parasitic activity caused by the lack of the α,β-unsaturation, the interaction between compound **18** and recombinant LmTXNPx *in vitro* was evaluated. In this experiment, cTXNPx recombinant protein was incubated with compound **18** in a 1:1 ratio for 30 minutes. Then, the protein molecular weight was evaluated by mass spectrometry, as described in section 3.9.5 for protein and chalcone **11** interaction. Preliminary results show the Michael acceptor on chalcone structure to be essential for its interaction with the target. Figure 41 shows the protein mass spectra in presence of compound **18**. Contrary to that observed for chalcone **11**, Figure 34, no peak corresponding to protein + ligand was observed with the major peak seen having a mass corresponding to intact protein, [M-2H-Met requires 24136 Da]. This result supports the proposed mechanism of action of chalcone **11** in *Leishmania* parasites. Whilst, in this experiment cTXNPx from *L. major* was employed the close homology with the other orthologues suggest that similar results would be obtained with cTXNPx from *L. amazonensis.* Experiments to verify this are in progress but could be completed in the time frame of this thesis.

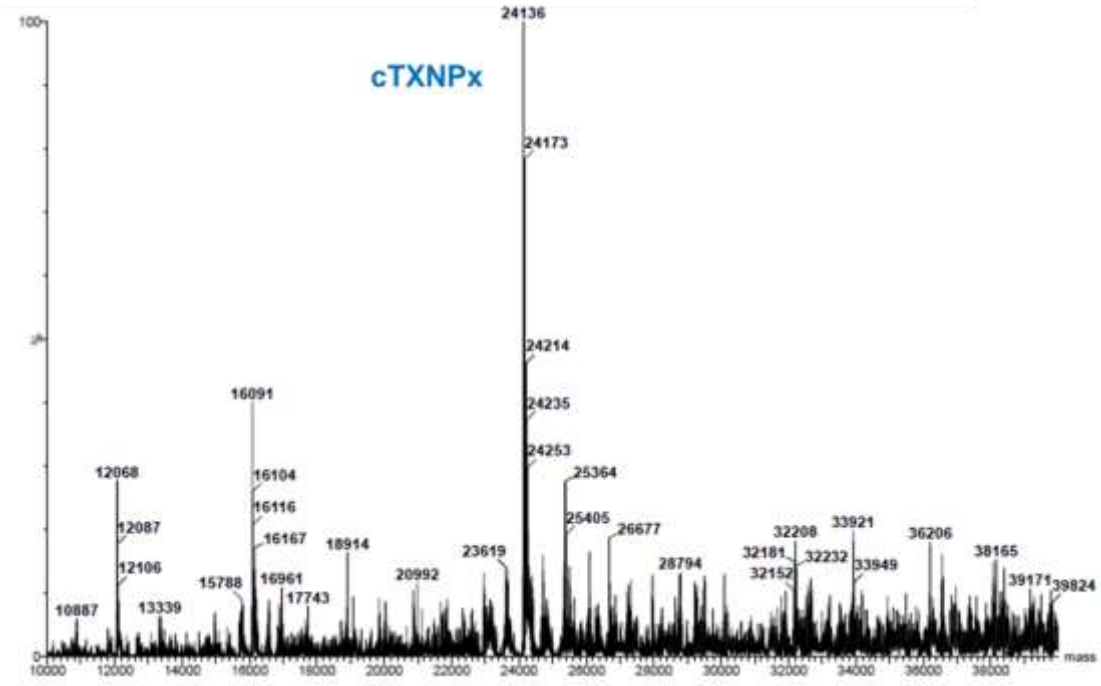

Figure 41. Influence of the enone group on interaction between chalcone and cTXNPx by mass spectrometry. cTXNPx of *L. major* (0.6 mg/mL) was incubated with compound 18 (1:1) for 30 minutes and their molecular weight analysed by Mass Spectrometry. cTXNPx of *L. major* molecular weight [M-2H-Met requires 24136 Da].

4.10.3 Inhibition of cTXNPx in the parasite causes ROS accumulation

The cTXNPx enzyme is known to be involved in maintaining parasite redox balance in both *Leishmania* stages[104]. It is 2-Cys peroxiredoxin, a terminal peroxidase in the TR-TXN-TXNPx pathway that primarily detoxify H_2O_2, a wide range of organic hydroxyl peroxides and, also in some parasites peroxynitrite ($OONO^-$)[104]. We hypothesised that, in this context, an enzyme inhibitor as a chalcone will disrupt the mechanism through which *Leishmania* deals with reactive oxygen species and consequently leads to an accumulation of ROS on parasites.

To confirm this assumption, ROS accumulation in promastigote parasite form was assessed. For this, *L. amazonensis* promastigotes were incubated with **11** or **18**, in the concentration of 0.35, 0.7 and 1.4 µM, for 48 h at 26ºC. Parasites were washed, counted and their concentration adjusted to 2 x 10^6/mL. To measure ROS production, cells were then incubated with the dye, H_2DCFDA, which has previously been used to monitor oxidative damage[159], for 30 min and its fluorescence quantified by fluorimetry (Figure 42A).

This experiment showed that, as observed before, compound **11** was able to decrease number of parasites in comparison to untreated promastigotes, (Figure 42A- dotted orange line). Interestingly, parasite killing was accompanied by ROS accumulation in these parasites (Figure 42A- orange line). Even at lower concentration of 0.35 µM, compound **11** induced an increase of ROS at promastigotes and this effect becomes larger as concentration of **11** increases.

In contrast, the lack of double bond in compound **18**, and consequently cTXNPx non-inhibition, resulted in a lower parasite killing (Figure 42B- dotted blue line) without ROS accumulation (Figure 42B-blue line). Significantly, this data revealed that compound **18** was not capable of inducing ROS formation in the parasites even in higher concentrations.

Next step was evaluating whether this outcome could be also noticed on amastigotes forms and/or macrophages. Thus, BMDM were infected or not with promastigotes of *L. amazonensis* for 4 h and incubated at 37ºC. This incubation was undertaken for 72 h, to achieve a high amount of amastigotes per macrophages and hence increase the sensitivity of the study. Subsequently, cells were incubated with compound **11** or **18** (0.07, 0.7 and 7.0 µM) for 1 h

followed by addition of H_2DCFDA (20 µM). Fluorescence of oxidative dye was used to evaluate ROS production by those macrophages. Compound **11** was able to induce ROS accumulation on macrophages containing intracellular amastigotes in comparison with untreated cells (Figure 42C). Compound **18** was, as observed with promastigotes, unable to induce ROS production on infected macrophages. Comparing to untreated cells, incubation with **18** decreased ROS amount produced by infected cells.

Chalcones are known by their anti-oxidative properties[160], and the results were in accordance with this statement. In uninfected cells, treatment with **11** and **18** did not induce ROS production, even in higher concentrations in comparison to untreated cells, (Figure 42D). These data prove the ROS production observed in infected macrophages can be attributed only to intracellular amastigotes.

Together, these results demonstrate that the chalcone interaction with cTXNPx *in vitro*, is mediated by the α,β-unsaturated ketone. Reaction of chalcone with the protein leads to enzyme inhibition and/or destabilization in both parasite stages, culminating in ROS accumulation and ultimately parasite death, corroborating the hypothesis for the mechanism of action.

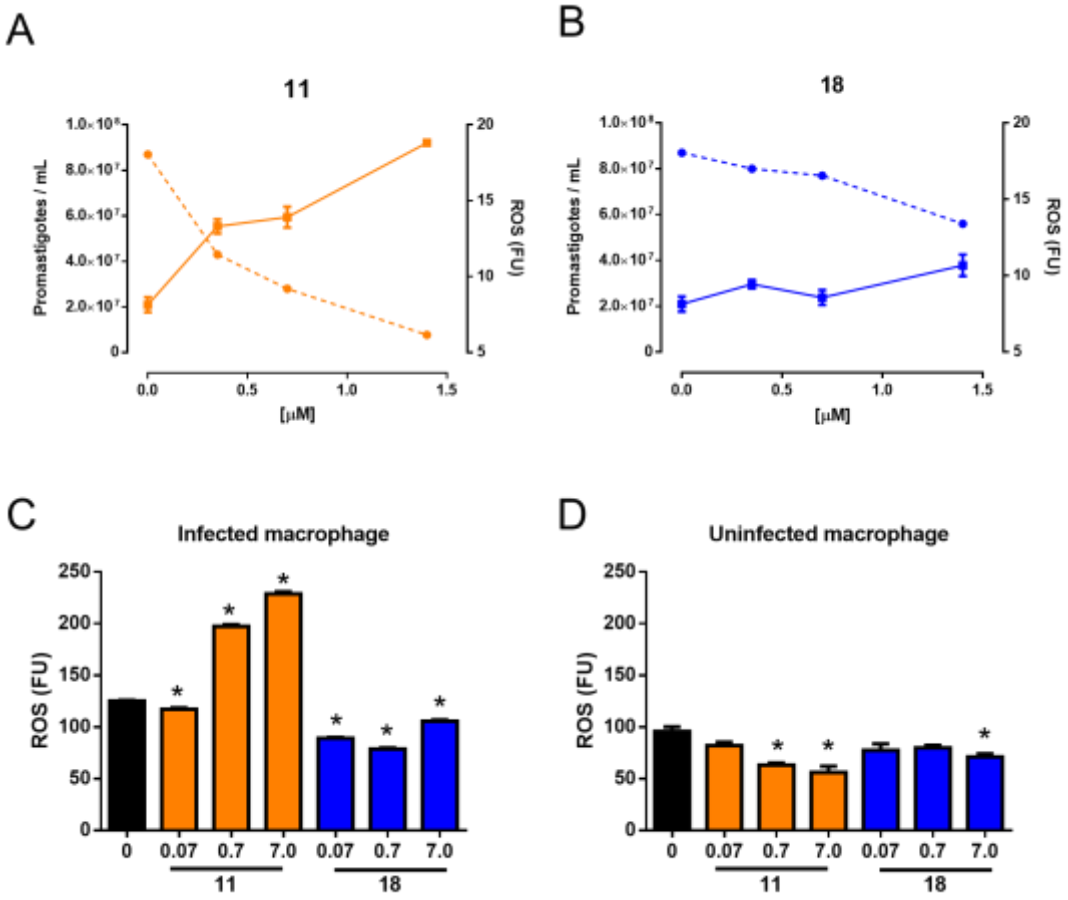

Figure 42. Influence of **11** and **18** on ROS production. *L. amazonensis* promastigotes (1 x 10^6/mL) were incubated with compound **11** or **18** at different concentrations (0.35, 0.7 and 1.4 µM) for 48h at 26ºC. Then harvested and adjusted to 2 x 10^6 cells/mL in PBS. Cells were transferred to black 96 well plates and ROS production assessed by fluorimetry with H_2DCFDA (20 µM), for 30 min at RT. **A**- Effect of **11** at ROS production. **B**- Effect of **18** at ROS production. Number of promastigotes, left, and ROS production, right. BMDM (1x10^5/well) infected or not with *L. amazonensis* promastigotes (10:1) for 72h on 96 well-plate, then cells were incubated with **11** or **18** (0.07, 0.7 and 7.0 µM) for 1h at 37ºC and ROS production measured as described for promastigotes. **C**- ROS production on infected macrophages. **D**- ROS production on uninfected macrophages. Means ± SD (n=3). ** p<0.01

4.11 Binding model between cTXNPx and chalcone *in silico*

All of these results indicated how chalcone could interact with the cTXNPx and importance of enone group for this it. In order to provide a molecular description, we decided to employ *in silico* analysis to explore it.

4.11.1 Molecular modelling

Firstly, a comparative molecular modelling of cTXNPx from *L. amazonensis* (LaTXNPx) was undertaken using the reported crystal structure of cTXNPx from *L. major*[145] as a starting point. The amino acid sequence of LaTXNPx was retrieved from UniProtKB database (access code Q4VKK8) (UniProt, 2012). The accuracy of the model depends on sequence similarity between template and target sequences, where higher identity gives better results. Within SWISS-MODEL server, the comparative modelling was carried out using the 3D structure of tryparedoxin peroxidase I from *L. major* (LmTXNPx) (PDB code 3TUE, 3.0 Á resolution) since it has 88% of identity with LaTXNPx.

The LaTXNPx model was obtained as a decamer (Figure 43), similar to the available template from *L. major*[101]. Contrasting with the available enzyme modelling, the C-terminal tail (residues His169–Lys198), which is missing in template (LmTXNPx), is present in the LaTXNPx model as a loop, revealing the complete active site structure of the protein.

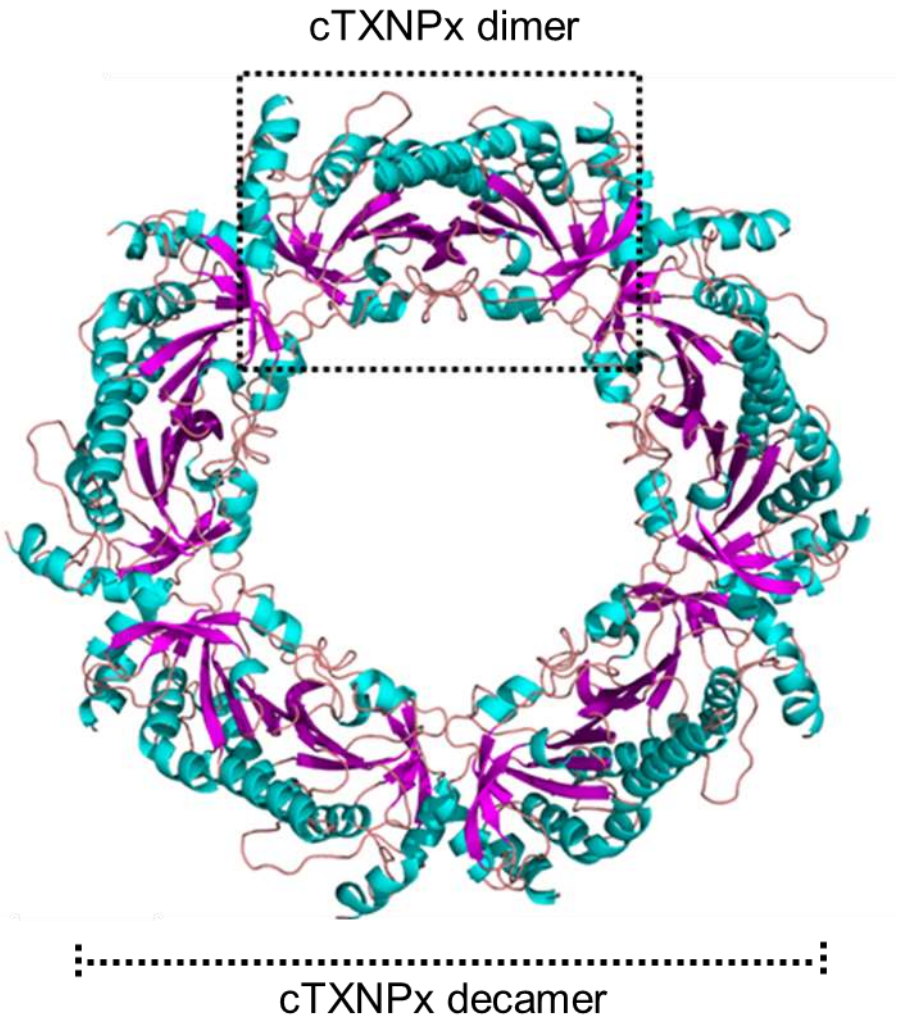

Figure 43. Ribbon diagram of the model *L. amazonensis* cTXNPx. Decameric form of cTXNPx from *L. amazonensis* generated using SWISS-MODEL. β-sheets are represented by violet colour and α-helices coloured in cyan. Dotted rectangle showed the dimeric form of cTXNPx.

To validate the three-dimensional model obtained by SWISS-MODEL we generated a Ramachandran plot to assess stereochemical quality of the structure. According to this Ramachandran plot (Figure 44), the LaTXNPx model showed 91.7% residues in allowed regions (Red regions), 7.7% of residues in additional allowed regions (Yellow regions) and 0.6% are in generously allowed regions (pale yellow regions), demonstrating an excellent structural fit.

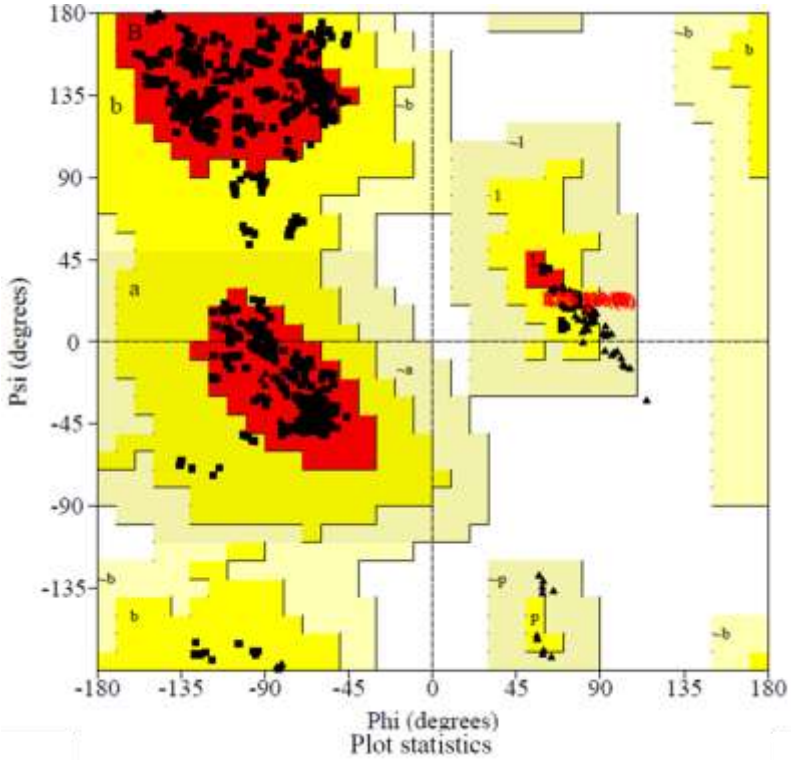

Figure 44. Ramachandran plot of *L. amazonensis* cTXNPx. The stereochemistry quality of the model of cTXNPx in a decameric form was assessed by Ramachandran plot on SAVES server (http://servicesn.mbi.ucla.edu/SAVES/).

Additionally, incorrect folding in the proposed model was evaluated using the Verify 3D tool that compared the 3D model structure to the protein amino acid sequence (2D) (Figure 45). This showed that the model had a compatible 1D–3D scores >0.2; thus this model could be considered appropriate for all docking studies.

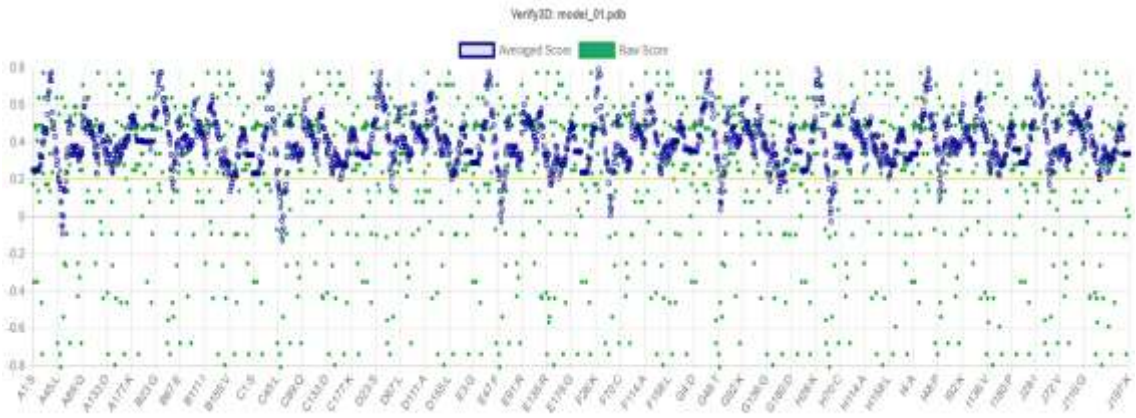

Figure 45. Validation of 3D model of *L. amazonensis* cTXNPx. The three-dimensional structure of the model proposed for cTXNPx were validated by the scores between 1D and 3D structures by Verify3D tool on SAVES.

4.11.2 Molecular docking

With a validated 3D model in hand, the next step was to examine the mode of interaction between LaTXNPx and chalcone. Docking studies with the dimer (CD chains) (Figure 46A) of LaTXNPx were performed using AutoDock 4.2 software running on a Windows-based PC[147]. Analyses of the binding mode and interactions of compound **11** within LaTXNPx showed an extended conformation in the fifty runs obtained. The geometry of the ligand is a crucial factor in the understanding of its mode of interaction with biomolecules. In this respect, the chalcone **11** shows restricted rotation due to the presence of the conjugated enone and aromatic sp2 hybridized carbons (Figure 46B).

Our docking studies showed compound **11** is oriented between Cys52 and Cys173 (Figure 46B) residues that form a disulfide bond, which prevent enzyme inactivation. The B ring of NAT22 with the nitro substituent is located near the catalytic cysteine, described as crucial for catalysis process[161], enabling

hydrogen bonds with Cys52, Val51, and Arg128 (chain D). Further, a hydrogen bond between methoxy substituent at the para position of ring A and Gln123 (3.3 Å) was observed. Hydrophobic interactions with residues Pro50, Val172 from chain D and Pro186 from chain C were also observed (Figure 46C).

In contrast to **11**, docking studies showed compound **18** is pointed out of enzyme catalytic site (Figure 46B). This feature is in agreement to *in vitro* experiments, which show a lack of antileishmanial activity on chalcone without double bond. Furthermore, compound **18** performed hydrogen bond interaction only with Arg128 residue and low energy interactions (i.e. hydrophobic interactions) with Thr49D, Pro188C e Pro50D (Figure 46C). Finally, compound **18** lies in the opposite side of the active site, which probably compromised its inhibitory profile.

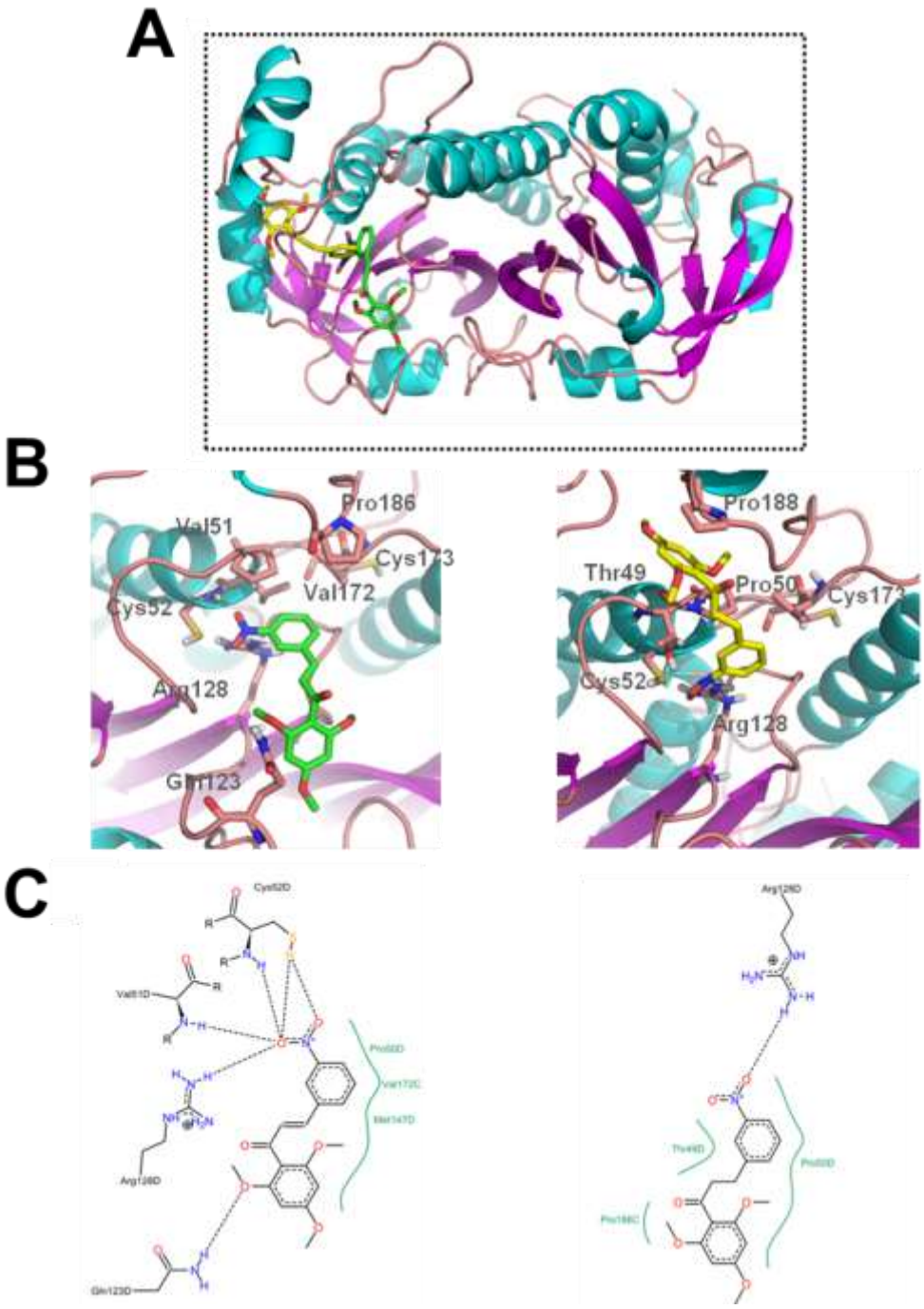

Figure 46. Binding mode of **11** and **18** on LacTXNPx. The docking studies between cTXNPx and compounds **11** or **18** were conducted using AutoDock 4.2 software. **A-** Functional Dimer selected for molecular docking studies. **B**- Binding model of compound **11** (coloured in green) or **18** (coloured in yellow) within active site of LaTXNPx. **C**- 2D interaction diagrams of **11** or **18** generated by PoseView.

Overall, these preliminary docking results support the capacity of chalcone **11** to bind into the active site of cTXNPx, interacting with important amino acid residues for protein function and leading to enzyme inhibition. Nevertheless, these results did not explain all presented data that evidenced a strong interaction between protein and chalcone. In particular, the model chosen for dynamic docking was not able to predict chalcone adduct formation, probably due to presence of C-terminal tail loop (residues His169–Lys198) which form a dynamic tail and confers flexibility to active site. In the proposed modelling, cTXNPx protein structure is in a reduced state and according to Fiorillo et al.[101], C loop, under reducing conditions, assumes a fully folded conformation that covers the active site hampering chalcone access to cysteine residue (Cys52). Further covalent docking studies are required to confirm our hypothesis of a covalent Michael adduct between chalcone α, β-unsaturated ketone and cysteine 52 of cTXNPx. However, this work could not be completed within the time frame of this thesis.

4.12 cTXNPx influence for parasite survival

Aiming to investigate the essentiality of the enzyme cytosolic tryparedoxin peroxidase to parasite physiology, we decided to generate promastigotes knockout of the cTXNPx gene using CRISPR-Cas9 system.

Due to availability of a well described CRISPR-Cas9 system giving a straightforward way to mutate genes in *L. mexicana*, we choose this platform to

explore this questions[148]. The first requirement was to find the genes within the genome that encode the enzyme.

Using the website http://tritrypdb.org to survey the parasite genome revealed that *Leishmania* cTXNPx is encoded by a two gene copies, in accordance with findings in the literature[102]. Both gene were found encoded in *L. mexicana* chromosome 15 (http://tritrypdb.org; LmxM.15.1040 and LmxM.15.1160, Figure 47A - blue rectangles). A BLAT alignment was performed with the sequences encoded in LmxM.15.1040 and LmxM.15.1160 and revealed a high identity with cytosolic tryparedoxin peroxidase from *L. amazonensis*, 99.5% and 100% of identity for LmxM.15.1040 and LmxM.15.1160, respectively (Figure 47B). Between the genes, two others ones can be found, LmxM.15.1050 and LmxM.15.1150, these genes encode a developmentally regulated protein, without a direct relationship with the genes for the enzyme (Figure 47B).

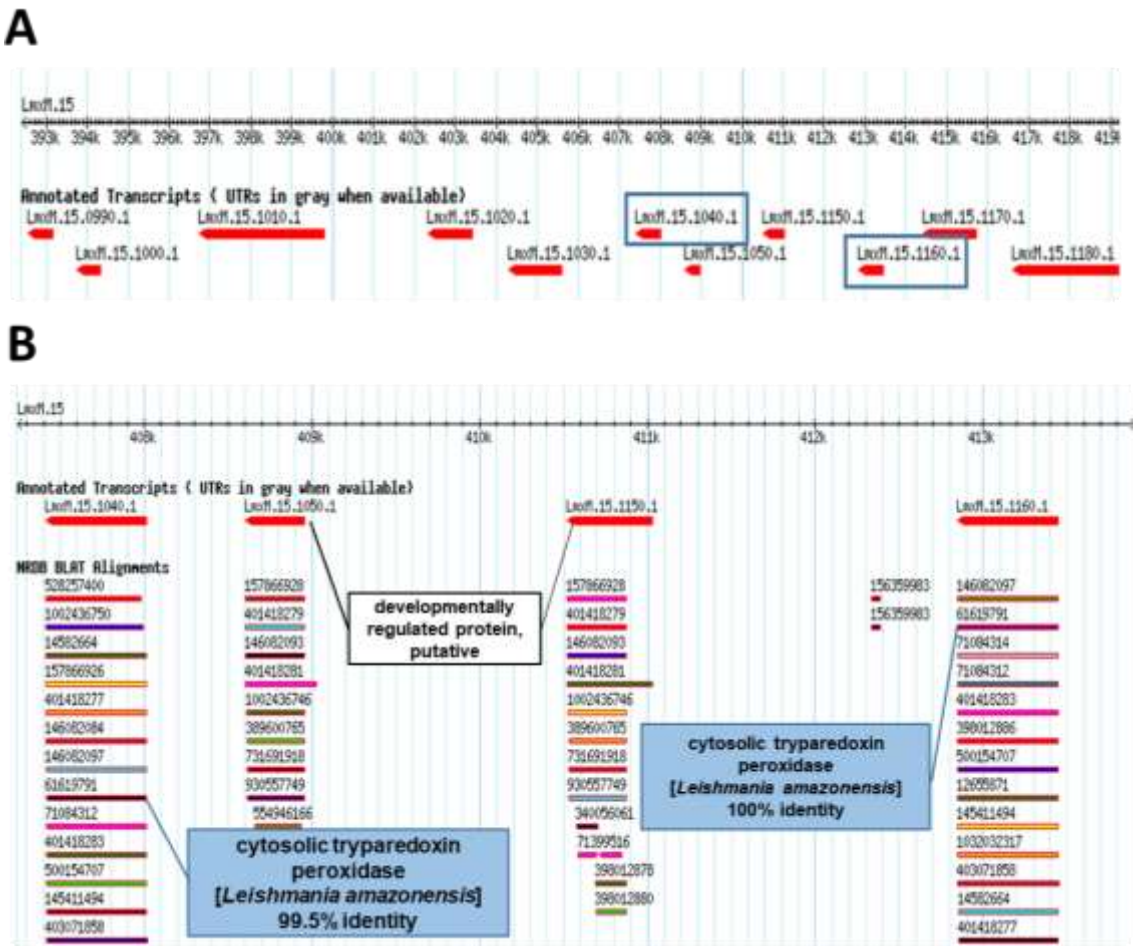

Figure 47. Localization of the genes encoding cTXNPx in the *L. mexicana* genome. **A**- Blue rectangles showing the encoding gene copies, LmxM.15.1040 and LmxM.15.1160, at chromosome 15. **B-** cTXNPx gene BLAT alignment between *L. mexicana* and *L. amazonensis.*

The next step was to generate oligonucleotides needed for gene editing by CRISPR-Cas9 system. According to Beneke et al[148], a single guide RNA 5' and 3' specific for desired gene to guide CRISPR-Cas9 to UTR gene region was required. In addition, primers to amplify the repair DNA cassette containing a puromycin antibiotic resistance gene, were needed. All of these oligonucleotides were created from each gene ID using the LeishEdit online platform and purchased from Sigma-Aldrich. Table 10 contains the sequences obtained from this online tool.

Table 10. Primers for CRISPR-Cas9 approach generated from LeishEdit online platform.

Gene ID	Primers	Oligonucleotide sequence
	5' sgRNA	gaaattaatacgactcactataggGCTGACCGGTGGCTGCGAGGgttttagagctagaaatagc
	3' sgRNA	gaaattaatacgactcactataggACTGATCCCGGTGCGCAGGAgttttagagctagaaatagc
LmxM.		
15.1040	Upstream forward	TCATTGTTTTCTCTCTCCCTCCCCGCGCCCgtataatgcagacctgctgc
	Downstream reverse	ATGAAAGGAGTCCGTGGGTGCCGACCAGTGccaatttgagagacctgtgc
	5' sgRNA	gaaattaatacgactcactataggGCTGACCGGTGGCTGCGAGGgttttagagctagaaatagc
	3' sgRNA	gaaattaatacgactcactataggTCTGTGAGTGTCACAGGAGCgttttagagctagaaatagc
LmxM.		
15.1160	Upstream forward	TCATTGTTTTCTCTCTCCCTCCCCGCGCCCgtataatgcagacctgctgc
	Downstream reverse	CCGGTGCCAATGGCGGGCGGGGTCACACCGccaatttgagagacctgtgc
	G00	AAAAGCACCGACTCGGTGCCACTTTTTCAAGTTGATAACGGACTAGCCTTATTTTAACTTGCTATTTCTAGCTCTAAAAC

Donor DNA and sgRNAs were successfully amplified by PCR reaction using GoTaq polymerase and analysed on 2% agarose gel. Using the donor DNA cassette, pT Puro, and forward and reverse primers specific for each gene copy, generated the desired product of approximately 1.2 Kbp for both genes (Figure 48). Similar results can be found at Figure 49 for the sgRNAs, in this case 5' and 3' sgRNAs were amplified by PCR reaction with a general primer G00 and the product was 120bp, as expected.

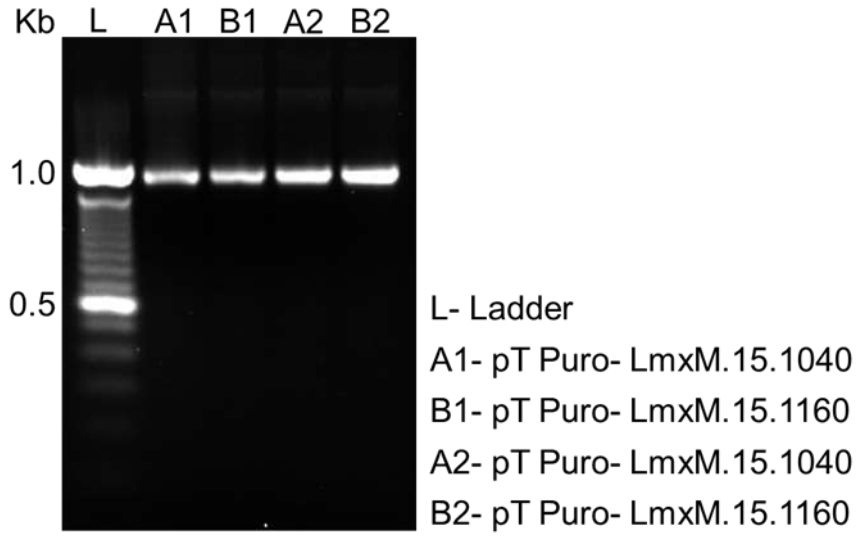

Figure 48. Amplification of donor DNA. 2% agarose gel showing desired DNA cassette amplified by PCR reaction with upstream forward and downstream reverse primers for each gene, at ~1200 Kb.

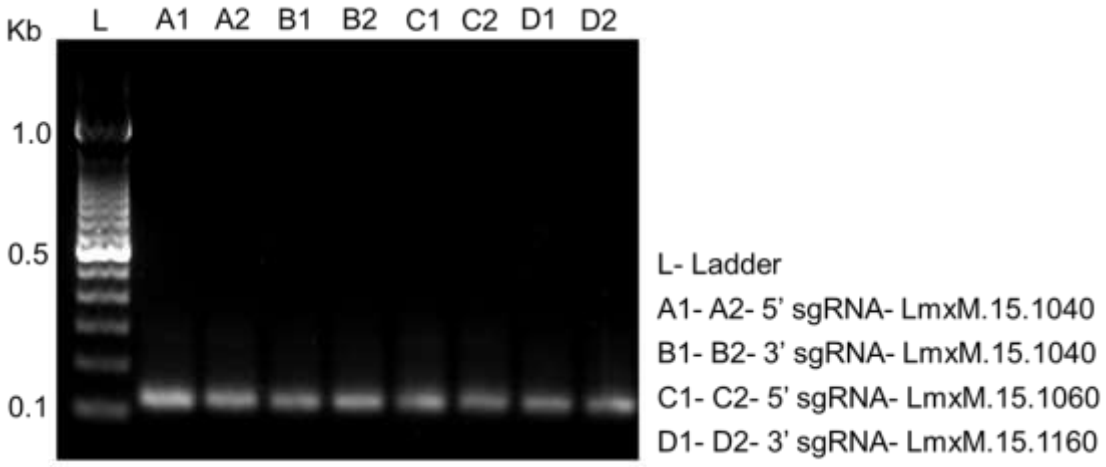

Figure 49. sgRNAs amplification. 5' and 3' sgRNAs specific for each gene were amplified by PCR reaction with G00 primer and PCR products containing oligonucleotides required for transfection were analysed by 2 % agarose gel.

After obtaining the cassettes/amplified fragments required to mutate the genes, the last step was to transfect promastigotes of *L. mexicana* with the cassettes. As the Cas9 enzyme is absent in trypanosomatids, we used

promastigotes of *L. mexicana* expressing Cas9 and T7 RNA polymerase, kindly donated by Eva Gluenz (Oxford University).

Transfection for each gene copy (LmxM.15.1040 and LmxM.15.1160) and one of both gene copies were performed using 5' and 3' sgRNAs and donor DNA. After transfection, using one pulse with program X-001 in an Amaxa Nucleofector IIb (Lonza), the cells were left to recover overnight at 26ºC in M199 media supplemented with 20% HIFCS. Then, transfected promastigotes were selected by addition of Puromycin (20 µg/mL) and phenotypes changes evaluate by light microscopy one week after transfection. Representative images of each transfection one week after antibiotic selection are shown in Figure 50. The expression of Cas9 and T7 RNAp (parental *L. mexicana*) did not cause phenotypic changes to the parasite and promastigotes had an elongated shape and a long flagellum. (Figure 50A).

In contrast, following transfection with the generated oligonucleotides some phenotypic changes could be observed in parasites lacking LmxM.15.1040 and LmxM.15.1160 (Figure 50B-D). The transfection process did not kill the parasites immediately, and the pictures in Figure 50 were taken one week after antibiotic selection. At this point the promastigotes, without either or both gene copies, assumed a rounded morphology with a short flagellum, lacked motility and stopped dividing (Figure 50B-D). Cells were viable for much longer, dying 10 days after transfection. To confirm the success of cassette integration by CRISPR-Cas9, further experiments employing PCR reactions with primers for each gene or for of PCR amplicons spanning the resistance cassette should have been carried out[148]. Unfortunately, due to the non-viability of the mutated *L.*

mexicana promastigotes, no further assays could be performed to better explore the influence of the enzyme on parasite physiology.

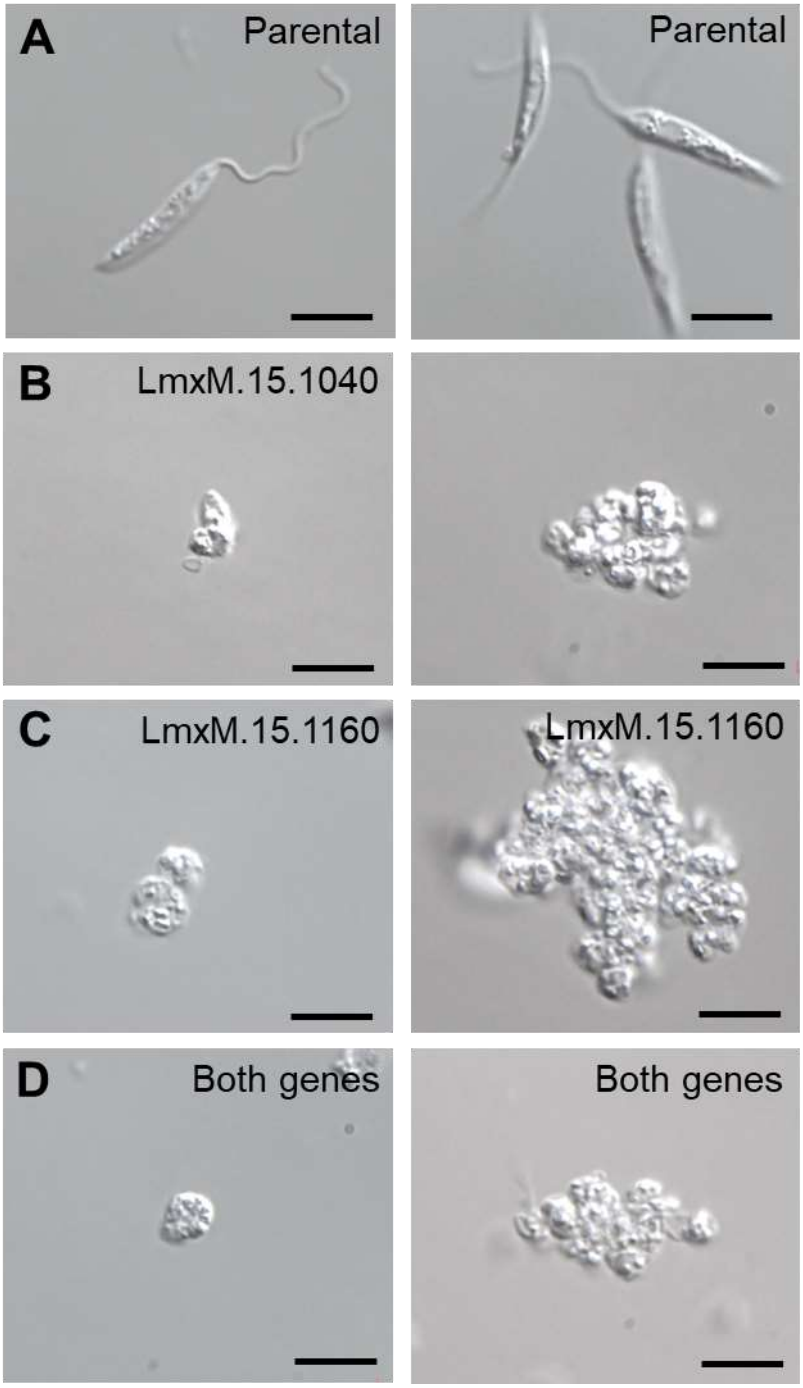

Figure 50. Importance of cTXNPx for *Leishmania* survival. Micrographs showing wild type parasites and parasites after transfection to mutate cTXNPx gene copies LmxM.15.1040, LmxM.15.1160 or both copies. The DIC images were taken seven days after transfection using Nikon Eclipse Ti at 1000 x magnification. Scale bar 5 µm

These preliminary results indicate that the enzyme is essential for promastigote survival with both genes being indispensable for parasite growth and morphology. Reports describing the importance of TXNPx for *Trypanosoma brucei*[103] and *Trypanosoma cruzi*[162] survival and infectivity can be found, but at this time, this is the first published data exploring the essentiality of cTXNPx to *Leishmania* survival. Whilst this work strongly supporting tryparedoxin peroxidase as a potential antileishmanial target, these data alone are not enough to validate cTXNPx as a drug target. However, further experiments employing other methodologies, such as DiCre gene deletion[54] or new rounds of CRISPR-Cas9 are required. Time precluded this study during the thesis period and this a matter for future work.

5. DISCUSSION

Conventional chemotherapy employed in leishmaniasis treatment consisting largely of antimonials, which has remained the same since 1945. Several second line treatments have been adopted since then, and new compounds and alternative therapies explored. However, despite efforts to understand the Biochemistry and Cellular Biology of the parasite, medicinal products authorized for human use are still quite restricted, possessing one or more of the following disadvantages: administration by invasive intramuscular or intravenous route, severe toxic side effects, low or variable efficacy, incompatible price with affected population, and the appearance of resistant strains to these drugs. All these related problems hamper patient adherence, treatment effectiveness and increase treatment costs due to the necessity for specialized staff and hospitalization.

The current scenario clearly points to the urgent demand for new treatments or innovative approaches to control this neglected disease which affects more than one million people worldwide per year[2]. This necessity encouraged research groups and pharmaceutical companies to look for new compounds against the parasite or new specific targets for the rational development of new drugs. To achieve this objective two main approaches have been employed to discover new hit antileishmanial compounds, they are phenotypic screening and target based screening, both have their strengths and weaknesses [54].

Our research group have been working on this issue over the last decades and during that time the efficacy a natural chalcone[46], DMC (**9**), and a synthetic nitrochalcone, CH8 (**10**)[48; 163], were attested to treat both clinical manifestations of leishmaniasis, CL and VL, by distinct routes[50; 51; 52; 164]. These chalcones were discovered through phenotypic screening against *Leishmania* parasites and as mentioned above this methodology is efficient in identifying active compounds but it does not allow identification of their molecular targets [56]. Consequently, until this project, the mechanism of action of these potent chalcones remained unknown.

Encouraged by our promising studies using chalcones to treat leishmaniasis in an animal model, and the need to elucidate the molecular basis of chalcone antileishmanial activity, we employed a chemical-proteomic approach, activity based protein profiling (ABPP), to investigate the molecular targets of the chalcones.

In this work we synthesized a trifunctional probe containing rhodamine for target visualization, biotin for affinity enrichments and azide for bio-orthogonal cycloaddition reaction[139]. We also synthesized a chalcone analogue, based on chalcone NAT22 (**19**), containing an alkyne group to react with the trifunctional probe. Results in this thesis clearly demonstrated the usefulness of this approach for target deconvolution of the chalcone analogue NAT22. Trifunctional tags are not restricted to our context, and compounds like this have been used to elucidate several cellular mechanisms including: protein post-translational modifications, such as cholesterylation[165] and N-myristoylation[166], and protein target profile for compounds such as artemisinin[167] and aspirin[134]. The results described in this

thesis enhance the knowledge and application of ABPP methodology and open doors for other research groups apply this technique to identify molecular targets of drugs, not only for leishmaniasis but for several relevant pathologies.

Extensive efforts have been made to identify specific targets for active molecules against *Leishmania* [56]. The knowledge of how a particular molecule acts to kill the parasite is exceptionally important as it will allow the design of combination therapies with drugs that act synergistically on different targets; consequently reducing therapeutic dose, related toxic effects and retarding resistance mechanisms[65; 168]. In addition, an understanding of specific targets allows rational structure-activity-relationship studies and the development of new potent and selective inhibitors with decreased off-target effects [168]. Examples of successful drug combinations were reported by Trinconi *et al*. with tamoxifen, used for treatment of breast cancer, and antileishmanial drugs with distinct molecular targets, such as amphotericin B [169] and miltefosine [170].

The first chalcone target described for *Leishmania* was the enzyme fumarate reductase that catalyses the reduction of fumarate to succinate, which is important to anaerobic energy metabolism, and it is absent in human cells [171]. Enzyme inhibition by licochalcone A was assessed using *L. donovani* parasites permeabilized with digitonin and enriched mitochondrion fractions[171]. This approach was efficient, but it could generate bias since alterations of parasite membranes will interfere with parasite physiology and isolated organelles do not match those found in live parasites. Some groups have also tried to describe chalcone molecular targets by enzymatic assays, such as inhibition of recombinant trypanothione reductase[172] or using molecular modelling and

docking [173]. However, both methodologies do not take into account the effect of inhibition of these targets on live parasites *in vitro* in both developmental stages[54; 174].

Contrasting to published works that explores one or two approaches to describe and characterize a target[171; 172; 173]. In this thesis, we employed a set of complementary tools and techniques, including chemical biology methods, phenotypic screening for promastigotes and amastigotes, protein expression, biophysical analysis, bioinformatics tools and gene edition to identify the cytosolic tryparedoxin peroxidase as the target for chalcone. Chalcone is the first covalent inhibitor of cTXNPx described for *Leishmania*.

The knowledge acquired in this work opens new perspectives for leishmaniasis treatment. Tryparedoxin peroxidase belong to a ubiquitous 2-Cys family of antioxidant enzymes responsible for protecting trypanosomatids against the deleterious effects of hydroperoxide and peroxynitrite [175]. The tryparedoxin peroxidase family is well conserved among trypanosomatids parasites, and this fact endorses the importance of these enzymes for parasite viability [175]. In all trypanosomatids two isoforms can be found, mitochondrial and cytosolic, sharing approximately 50% similarity at the protein level and with a conserved tertiary structure [102]. Our results showed chalcone NAT22 is likely to kill *Leishmania* by a strong interaction to cytosolic tryparedoxin peroxidase (cTXNPx), but not with the mitochondrial enzyme isoform.

The selective interaction with cTXNPx observed in our results can be explained by the differences in the enzyme active site. The capacity of 2-Cys proteins to reduce oxidative species is related to their structural conformation;

tryparedoxin peroxidase are homodimers that form two identical reaction centres containing two cysteine residues, one from each monomer, oriented close to the other. In cTXNPx, the active site is formed by the interaction between Cys52 of one subunit and Cys173 of other monomer[108]. In contrast, mTXNPx diverges in its second active Cys173 residue, with the motif Val–Cys–Pro being replaced by Ile–Pro–Cys[175]. This motif change may result in an alteration in its physical chemical properties, which could disfavour the interaction with chalcone.

A general anti-oxidant mechanism proposed for TXNPx, where the Cys of one monomer is oxidized by a peroxide species to cysteine sulfenic acid (Cys-SOH), reducing the peroxide substrate. Next, oxidized cysteine residue suffers attack by the inverted cysteine from the partner monomer, forming disulfite bond, which is then resolved by tryparedoxin [175]. By molecular modelling and docking we showed chalcone NAT22, and possibly CH8, accessing the active site on the cTXNPx dimeric form and fit between cysteine 52 and 173; this interaction appears to block the disulfite bond formation, thus inhibiting the enzyme activity.

In addition, our results provide evidence that the interaction between a chalcone and cTXNPx occurs through a covalent bond, and this binding was resistant to all the severe conditions applied during experimentation such as high temperature and reducing and alkylating agents. This is in accordance with reports that describe chalcone's ability to undergo Michael addition to sulfhydryl on cysteine residues resulting in covalent adducts between the protein and compound [37; 176]. This mechanism was confirmed by our studies of a chalcone lacking the enone group (**18**), where the data indicated that without α,β-

unsaturation the chalcone could not interact with the protein *in vitro*, *in situ* and *in silico,* and consequently no enzyme inhibition could be observed.

The parasites face high amounts of ROS during their life cycle and TXNPx is related to the survival and virulence of trypanosomatids [177]. Overexpression of TXNPx in *L. donovani* and *L. amazonensis* improves the protection against oxidative stress from macrophages, increasing parasite infectivity [100; 104]. Here we demonstrated that cTXNPx inhibition by chalcone interferes with the ability of *Leishmania* to detoxify oxidative species culminating in ROS accumulation and parasite killing.

Based on our findings, we propose a mechanism of action for the chalcone (**11**) (Figure 51). Chalcone NAT22 (**11**) is able to permeate through macrophage cell membrane, cross phagolysosome membrane and reach the intracellular amastigotes. There, the compound (**11**) is able to interact with cTXNPx, forming a covalent bond with cysteine residues (Cys 54 or Cys 173) in the active site. The mechanism of interaction seems to be based on Michael addition between the enone group on chalcone structure and sulfhydryl residues on cysteine. After the chalcone's irreversible interaction, cTXNPx becomes unable to return to its reduced state and consequently is incapable of detoxifying reactive oxygen species. High levels of ROS, specially H_2O_2 and $ONOO^-$, in the parasite cytoplasm will trigger cell death apoptosis-like due to the oxidation of lipids, proteins and nucleic acids [93; 178; 179]. Many indications of apoptosis-like cell death, such as mitochondrial damage [46], DNA fragmentation and morphological changes [180], were observed after chalcone treatment.

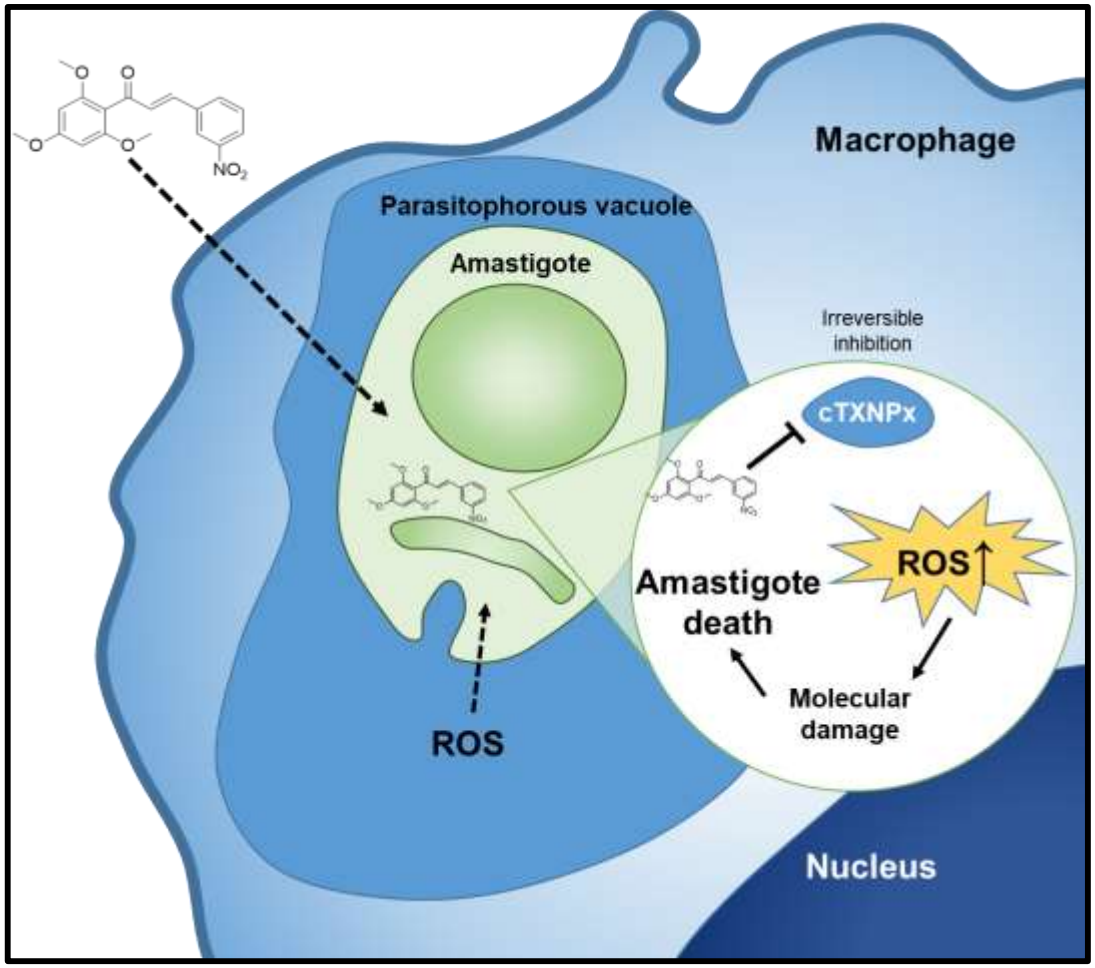

Figure 51 Antileishmanial mechanism of action of chalcone. Chalcone NAT22 (**11**) permeates host cell and amastigotes membranes, reaching parasite cytoplasm. Once inside, chalcone interacts covalently with cTXNPx in its dimeric form, this irreversible interaction results on enzyme inhibition. Without a functional cTXNPx parasite is unable to detoxify ROS, which accumulate in cytoplasm. High levels of ROS cause oxidation of proteins, lipids and nucleic acids, which should initiate parasite cell death mechanisms, thus controlling the infection.

The proposed mechanism is also supported by reports that describe the mechanism of inhibition of thioredoxin reductases by chalcones[181] and others Michael acceptors, such as curcumins and cinnamaldehydes[182; 183]. These enzymes belong to oxidoreductases family, which are found in human cells and play important roles in oxidative balance and tumorigenesis. Their inhibition by these compounds is attributed to an active Michael acceptor pharmacophore that

causes a covalent modification in one of the cysteines present in their structures [181; 182; 183], as proposed for cTXNPx inhibition by chalcone.

In summary, ABPP approach has enabled us to identify the cytosolic tryparedoxin peroxidase as a molecular target and describe the main mechanism of action for chalcone NAT22 (**11**) a potent compound against *Leishmania*. Therefore, our results do not exclude other possible mechanisms occasioned by weak interactions of chalcone (**11**) and parasite targets, which cannot be identified by ABPP approach.

6. CONCLUSION AND FUTURE WORK

The research in this thesis has identified, using a chemical biology approach, a potential drug target for chalcones in *Leishmania*, namely the cytosolic tryparedoxin peroxidase (cTXNPx). Results from several approaches allowed a detailed description of the mechanism of action of this potent class long of studied antileishmanial compounds. Additionally, we have described the chalcones as the first covalent inhibitors for cTXNPx, an underexplored drug target. Overall this work opens new treatment perspectives for this Neglected Tropical Disease which afflicts millions of people worldwide and has a high economic and social impact on society.

As a future work, the discovery of a molecular target for chalcone NAT22 (**11**) will contribute to the understanding of how similar chalcones, without a clear mechanism of action, are able to kill the parasite *in vitro* and *in vivo*. Furthermore, confirmation of the enzyme cTXNPx as a good pharmacological target will enable the implementation of a new screening platform for hit compounds with antileishmanial activity.

TXNPx has been reported as a parasite mechanism of resistance to conventional drugs, elevated levels of TXNPx expression were found in *Leishmania* isolates resistant to drugs including arsenite[105], amphotericin B[26; 106] and antimonials[97; 107]. As an irreversible inhibitor for cTXNPx, chalcones may be used in association with these drugs to circumvent this resistance mechanism.

The discovery of the first covalent inhibitor for cTXNPx will also allow the rational design of combination therapies that act at different targets. For this

propose, studies on the association of chalcone and antimonials, miltefosine and amphotericin B are in progress now. With these experiments, we will verify a synergistic antileishmanial effect between chalcone and each compounds and its effect to overcoming/preventing resistance.

This research raised new and relevant questions regarding chalcones and trypanosomatid chemotherapy. Chalcone NAT22 (**11**) has an excellent activity against parasite, although its bioavailability is not ideal for use as an oral treatment. The next step, based on studies of structure-activity-relationships, is be synthesize rational chalcone analogues specific for cTXNPx presenting a better solubility in water, the biggest issue regarding chalcones [37; 184].

The second question is about the specificity of cTXNPx for chalcones. Herein we demonstrated that chalcone NAT22 (**11**) and possibly CH8 (**10**) inhibit cTXNPx by covalent binding, but we need to know whether the enzyme target can be inhibited by others chalcones. Insights into this may classify cTXNPx as a general target for chalcones.

The third question is related to the capacity of chalcone to interact and inhibit cTXNPx from other *Leishmania* species; in this work we showed inhibition of cTXNPX from *L. amazonensis* and *L. major.* New experiments employing recombinant proteins and molecular modelling will provide evidence of chalcone's appropriateness to treat leishmaniasis caused by all species, worldwide.

Lastly, since the target is conserved in the trypanosomatids, what about chalcone activity against TXNPx from *T. cruzi* and *T. brucei*? Studies of

chalcones NAT22 and CH8 activity against *Trypanosoma* parasites will provide an overview of all the possibilities related to TXNPx inhibition by chalcones.

7. REFERENCES

1 MITRA, A. K.; MAWSON, A. R. Neglected Tropical Diseases: Epidemiology and Global Burden. **Tropical medicine and infectious disease,** v. 2, n. 3, p. 36, 2017.

2 ALVAR, J.; VÉLEZ, I. D.; BERN, C.; HERRERO, M.; DESJEUX, P.; CANO, J.; JANNIN, J.; DE BOER, M. Leishmaniasis worldwide and global estimates of its incidence. **PLoS ONE,** v. 7, n. 5, p. e35671-e35671, 2012.

3 WHO. Weekly Epidemiological Record. 2017. Acesso em: 22/08/2018.

4 DNDI. **Towards a new generation of treatments for leishmaniasis -**. 2018

5 BURZA, S.; CROFT, S. L.; BOELAERT, M. Leishmaniasis. **Lancet,** v. 392, n. 10151, p. 951-970, Sep 15 2018.

6 TORRES-GUERRERO, E.; QUINTANILLA-CEDILLO, M. R.; RUIZ-ESMENJAUD, J.; ARENAS, R. Leishmaniasis: a review. **F1000Research,** v. 6, p. 750-750, 2017.

7 LEITE DE SOUSA-GOMES, M.; ROMERO, G. A. S.; WERNECK, G. L. Visceral leishmaniasis and HIV/AIDS in Brazil: Are we aware enough? **PLoS Negl Trop Dis,** v. 11, n. 9, p. e0005772, Sep 2017.

8 SCORZA, B. M.; CARVALHO, E. M.; WILSON, M. E. Cutaneous Manifestations of Human and Murine Leishmaniasis. **International journal of molecular sciences,** v. 18, n. 6, p. 1296, 2017.

9 AMATO, V. S.; TUON, F. F.; BACHA, H. A.; NETO, V. A.; NICODEMO, A. C. Mucosal leishmaniasis: Current scenario and prospects for treatment. **Acta Tropica,** v. 105, n. 1, p. 1-9, 2008/01/01/ 2008.

10 BRASIL. **Ministério da Saúde. Secretaria de Vigilância em Saúde. Manual de Vigilância da Leishmaniose Tegumentar Americana. Serie A. Normas e Manuais Técnicos. 2 ed. atual. Brasília: Editora do Ministério da Saúde; 2007. 180 p**. 2010. 1-180 ISBN 9788533412705.

11 PUROHIT, H. M.; SHAH, A. N.; AMIN, B. K.; SHEVKANI, M. R. Diffuse cutaneous leishmaniasis - A rare cutaneous presentation in an HIV-positive patient. **Indian journal of sexually transmitted diseases and AIDS,** v. 33, n. 1, p. 62-64, Jan-Jun 2012.

12 VERNAL, S.; DE PAULA, N. A.; GOMES, C. M.; ROSELINO, A. M. Disseminated Leishmaniasis by Leishmania viannia Subgenus: A Series of 18 Cases in Southeastern Brazil. **Open forum infectious diseases,** v. 3, n. 1, p. ofv184-ofv184, 2016.

13 BEZERRA, J. M. T.; DE ARAÚJO, V. E. M.; BARBOSA, D. S.; MARTINS-MELO, F. R.; WERNECK, G. L.; CARNEIRO, M. Burden of leishmaniasis in Brazil and federated units, 1990-2016: Findings from Global Burden of Disease Study 2016. **PLoS neglected tropical diseases,** v. 12, n. 9, p. e0006697-e0006697, 2018.

14 GHORBANI, M.; FARHOUDI, R. Leishmaniasis in humans: drug or vaccine therapy? **Drug design, development and therapy,** v. 12, p. 25-40, 2017.

15 ADADE, C. M.; SOUTO-PADRÓN, T. Contributions of Ultrastructural Studies to the Cell Biology of Trypanos- matids : Targets for Anti-Parasitic Drugs. **The Open Parasitology Journal,** v. 4, p. 178-187, 2010.

16 TEIXEIRA, D. E.; BENCHIMOL, M.; RODRIGUES, J. C. F.; CREPALDI, P. H.; PIMENTA, P. F. P.; DE SOUZA, W. The Cell Biology of Leishmania: How to Teach Using Animations. **PLoS Pathogens,** v. 9, n. 10, p. e1003594-e1003594, 2013.

17 SACKS, D.; NOBEN-TRAUTH, N. The immunology of susceptibility and resistance to Leishmania major in mice. **Nat Rev Immunol,** v. 2, n. 11, p. 845-58, Nov 2002.

18 SÉGUIN, O.; DESCOTEAUX, A. Leishmania, the phagosome, and host responses: The journey of a parasite. **Cellular Immunology,** v. 309, p. 1-6, 2016/11/01/ 2016.

19 MORADIN, N.; DESCOTEAUX, A. Leishmania promastigotes: building a safe niche within macrophages. **Frontiers in Cellular and Infection Microbiology,** v. 2, p. 121-121, 2012.

20 HALDAR, A. K.; SEN, P.; ROY, S. Use of Antimony in the Treatment of Leishmaniasis: Current Status and Future Directions. **Molecular Biology International,** v. 2011, p. 23, 2011.

21 WHO, W. E. C. O. T. C. O. T. L. W. H. O. Control of the leishmaniases: report of a meeting of the WHO Expert Commitee on the Control of Leishmaniases, Geneva, 22-26 March 2010. v. 22-26 March 2010, 2010.

22 ULIANA, S. R. B.; TRINCONI, C. T.; COELHO, A. C. Chemotherapy of leishmaniasis: present challenges. **Parasitology,** v. 145, n. 4, p. 464-480, Apr 2018.

23 MASMOUDI, A.; HARIZ, W.; MARREKCHI, S.; AMOURI, M.; TURKI, H. Old World cutaneous leishmaniasis: Diagnosis and treatment. **Journal of Dermatological Case Reports,** v. 7, n. 2, p. 31-41, 2013.

24 BAIOCCO, P.; COLOTTI, G.; FRANCESCHINI, S.; ILARI, A. Molecular basis of antimony treatment in leishmaniasis. **J Med Chem,** v. 52, n. 8, p. 2603-12, Apr 23 2009.

25 ODDS, F. C.; BROWN, A. J. P.; GOW, N. A. R. Antifungal agents: mechanisms of action. **Trends in Microbiology,** v. 11, n. 6, p. 272-279, 2003/06/01/ 2003.

26 PURKAIT, B.; KUMAR, A.; NANDI, N.; SARDAR, A. H.; DAS, S.; KUMAR, S.; PANDEY, K.; RAVIDAS, V.; KUMAR, M.; DE, T.; SINGH, D.; DAS, P. Mechanism of Amphotericin B Resistance in Clinical Isolates of Leishmania donovani. **Antimicrobial Agents and Chemotherapy,** v. 56, n. 2, p. 1031-1041, 2012.

27 SUNDAR, S.; CHAKRAVARTY, J. An update on pharmacotherapy for leishmaniasis. **Expert Opinion on Pharmacotherapy,** v. 16, n. 9, p. 1347-1368, 2015.

28 YANG, G.; CHOI, G.; NO, J. H. Antileishmanial Mechanism of Diamidines Involves Targeting Kinetoplasts. **Antimicrobial agents and chemotherapy,** v. 60, n. 11, p. 6828-6836, 2016.

29 CHAKRAVARTY, J.; SUNDAR, S. Drug resistance in leishmaniasis. **Journal of global infectious diseases,** v. 2, n. 2, p. 167-176, May-Aug 2010.

30 MONGE-MAILLO, B.; LOPEZ-VELEZ, R. Miltefosine for visceral and cutaneous leishmaniasis: drug characteristics and evidence-based treatment recommendations. **Clin Infect Dis,** v. 60, n. 9, p. 1398-404, May 1 2015.

31 RAKOTOMANGA, M.; BLANC, S.; GAUDIN, K.; CHAMINADE, P.; LOISEAU, P. M. Miltefosine affects lipid metabolism in Leishmania donovani promastigotes. **Antimicrob Agents Chemother,** v. 51, n. 4, p. 1425-30, Apr 2007.

32 PARIS, C.; LOISEAU, P. M.; BORIES, C.; BRÉARD, J. Miltefosine induces apoptosis-like death in Leishmania donovani promastigotes. **Antimicrobial agents and chemotherapy,** v. 48, n. 3, p. 852-859, 2004.

33 PINTO-MARTINEZ, A. K.; RODRIGUEZ-DURÁN, J.; SERRANO-MARTIN, X.; HERNANDEZ-RODRIGUEZ, V.; BENAIM, G. Mechanism of action of miltefosine on Leishmania donovani involves the impairment of acidocalcisome function and the activation of the sphingosine-dependent plasma membrane Ca2+channel. **Antimicrobial Agents and Chemotherapy,** v. 62, n. 1, p. 1-10, 2018.

34 DE MENEZES, J. P. B.; GUEDES, C. E. S.; PETERSEN, A. L. D. O. A.; FRAGA, D. B. M.; VERAS, P. S. T. Advances in Development of New Treatment for Leishmaniasis. **BioMed Research International,** v. 2015, p. 1-11, 2015.

35 DNDI, D. F. N. D. I.-. Target product profile. 2018. Disponível em: < https://www.dndi.org/diseases-projects/leishmaniasis/leish-target-product-profile/ >.

36 SUNDAR, S.; SINGH, B. Emerging therapeutic targets for treatment of leishmaniasis. **Expert Opinion on Therapeutic Targets,** v. 22, n. 6, p. 467-486, 2018/06/03 2018.

37 ZHUANG, C.; ZHANG, W.; SHENG, C.; ZHANG, W.; XING, C.; MIAO, Z. **Chalcone: A Privileged Structure in Medicinal Chemistry**: American Chemical Society. 117**:** 7762-7810 p. 2017.

38 DE MELLO, M. V. P.; ABRAHIM-VIEIRA, B. D. A.; DOMINGOS, T. F. S.; DE JESUS, J. B.; DE SOUSA, A. C. C.; RODRIGUES, C. R.; SOUZA, A. M. T. D. A comprehensive review of chalcone derivatives as antileishmanial agents. **European Journal of Medicinal Chemistry,** v. 150, p. 920-929, 2018/04/25/ 2018.

39 MAHAPATRA, D. K.; BHARTI, S. K.; ASATI, V. Chalcone Derivatives: Anti-inflammatory Potential and Molecular Targets Perspectives. **Curr Top Med Chem,** v. 17, n. 28, p. 3146-3169, Nov 20 2017.

40 KARTHIKEYAN, C.; MOORTHY, N. S.; RAMASAMY, S.; VANAM, U.; MANIVANNAN, E.; KARUNAGARAN, D.; TRIVEDI, P. Advances in chalcones with anticancer activities. **Recent Pat Anticancer Drug Discov,** v. 10, n. 1, p. 97-115, 2015.

41 MAHAPATRA, D. K.; BHARTI, S. K.; ASATI, V. Chalcone scaffolds as anti-infective agents: structural and molecular target perspectives. **Eur J Med Chem,** v. 101, p. 496-524, Aug 28 2015.

42 COLE, A. L.; HOSSAIN, S.; COLE, A. M.; PHANSTIEL, O. T. Synthesis and bioevaluation of substituted chalcones, coumaranones and other flavonoids as anti-HIV agents. **Bioorg Med Chem,** v. 24, n. 12, p. 2768-76, Jun 15 2016.

43 KUMAR, D.; KUMAR, M.; KUMAR, A.; SINGH, S. K. Chalcone and curcumin derivatives: a way ahead for malarial treatment. **Mini Rev Med Chem,** v. 13, n. 14, p. 2116-33, Dec 2013.

44 CHEN, M.; CHRISTENSEN, S. B.; THEANDER, T. G.; KHARAZMI, A. Antileishmanial activity of licochalcone A in mice infected with Leishmania major

and in hamsters infected with Leishmania donovani. **Antimicrobial Agents and Chemotherapy,** v. 38, n. 6, p. 1339-1344, 1994.

45 TAJUDDEEN, N.; ISAH, M. B.; SULEIMAN, M. A.; VAN HEERDEN, F. R.; IBRAHIM, M. A. The chemotherapeutic potential of chalcones against leishmaniases: a review. **International Journal of Antimicrobial Agents**, 2017.

46 TORRES-SANTOS, E. C.; MOREIRA, D. L.; KAPLAN, M. A. C.; MEIRELLES, M. N.; ROSSI-BERGMANN, B. Selective effect of 2',6'-dihydroxy-4'-methoxychalcone isolated from Piper aduncum on Leishmania amazonensis. **Antimicrobial Agents and Chemotherapy,** v. 43, n. 5, p. 1234-1241, 1999.

47 TORRES-SANTOS, E. C.; SAMPAIO-SANTOS, M. I.; BUCKNER, F. S.; YOKOYAMA, K.; GELB, M.; URBINA, J. A.; ROSSI-BERGMANN, B. Altered sterol profile induced in Leishmania amazonensis by a natural dihydroxymethoxylated chalcone. **The Journal of antimicrobial chemotherapy,** v. 63, n. 3, p. 469-72, 1999.

48 BOECK, P.; BANDEIRA FALCÃO, C. A.; LEAL, P. C.; YUNES, R. A.; FILHO, V. C.; TORRES-SANTOS, E. C.; ROSSI-BERGMANN, B. Synthesis of chalcone analogues with increased antileishmanial activity. **Bioorganic & medicinal chemistry,** v. 14, n. 5, p. 1538-45, 2006.

49 PACIENZA-LIMA, W. **Ação da chalcoma natural DMC e seu análogo sintético CH8 sobre Leishmania amazonensis e outros Tripanossomatídeos com ênfase no metabolismo de lipideos**. 2007. 115-115 Research (MSc). Biophysics Institute Carlos Chagas Filho, Federal University of Rio de Janeiro

50 SOUSA-BATISTA, A. J.; ESCRIVANI-OLIVEIRA, D.; FALCAO, C. A. B.; PHILIPPON, C.; ROSSI-BERGMANN, B. Broad spectrum and safety of oral treatment with a promising nitrosylated chalcone in murine leishmaniasis. **Antimicrob Agents Chemother**, Jul 16 2018.

51 SOUSA-BATISTA, A. D. J.; PACIENZA-LIMA, W.; ARRUDA-COSTA, N.; FALCÃO, C. A. B.; RÉ, M. I.; ROSSI-BERGMANN, B. Depot Subcutaneous Injection with Chalcone CH8-Loaded Poly(Lactic-Co-Glycolic Acid) Microspheres as a Single-Dose Treatment of Cutaneous Leishmaniasis. **Antimicrobial agents and chemotherapy,** v. 62, n. 3, p. AAC.01822-17, 2018.

52 SOUSA-BATISTA, A. J.; ARRUDA-COSTA, N.; ROSSI-BERGMANN, B.; RÉ, M. I. Improved drug loading via spray drying of a chalcone implant for local treatment of cutaneous leishmaniasis. **Drug Development and Industrial Pharmacy,** v. 0, n. 0, p. 1-28, 2018.

53 REBELLO, N. D. A. C. C. **Ação da furosemida e da chalcona NAT22 nas leishmanioses: Mecanismo antiparasitário e nanoestruturação.** . 2016. 115 Research (PhD). Biophysics Institute Carlos Chagas Filho, Fedreal University of Rio de Janeiro, www.minerva.ufrj.br.

54 JONES, N. G.; CATTA-PRETA, C. M. C.; LIMA, A. P. C. A.; MOTTRAM, J. C. Genetically Validated Drug Targets in Leishmania: Current Knowledge and Future Prospects. **ACS infectious diseases,** v. 4, n. 4, p. 467-477, 2018.

55 SWINNEY, D. C.; ANTHONY, J. How were new medicines discovered? **Nature Reviews Drug Discovery,** v. 10, p. 507, 06/24/online 2011.

56 ZULFIQAR, B.; SHELPER, T. B.; AVERY, V. M. Leishmaniasis drug discovery: recent progress and challenges in assay development. **Drug Discov Today,** v. 22, n. 10, p. 1516-1531, Oct 2017.

57 PINTO-MARTINEZ, A. K.; RODRIGUEZ-DURAN, J.; SERRANO-MARTIN, X.; HERNANDEZ-RODRIGUEZ, V.; BENAIM, G. Mechanism of Action of Miltefosine on Leishmania donovani Involves the Impairment of Acidocalcisome Function and the Activation of the Sphingosine-Dependent Plasma Membrane Ca(2+) Channel. **Antimicrob Agents Chemother,** v. 62, n. 1, Jan 2018.

58 VERMEERSCH, M.; DA LUZ, R. I.; TOTÉ, K.; TIMMERMANS, J.-P.; COS, P.; MAES, L. In vitro susceptibilities of Leishmania donovani promastigote and amastigote stages to antileishmanial reference drugs: practical relevance of stage-specific differences. **Antimicrobial agents and chemotherapy,** v. 53, n. 9, p. 3855-3859, 2009.

59 ORTIZ, D.; GUIGUEMDE, W. A.; HAMMILL, J. T.; CARRILLO, A. K.; CHEN, Y.; CONNELLY, M.; STALHEIM, K.; ELYA, C.; JOHNSON, A.; MIN, J.; SHELAT, A.; SMITHSON, D. C.; YANG, L.; ZHU, F.; GUY, R. K.; LANDFEAR, S. M. Discovery of novel, orally bioavailable, antileishmanial compounds using phenotypic screening. **PLoS neglected tropical diseases,** v. 11, n. 12, p. e0006157-e0006157, 2017.

60 DE RYCKER, M.; HALLYBURTON, I.; THOMAS, J.; CAMPBELL, L.; WYLLIE, S.; JOSHI, D.; CAMERON, S.; GILBERT, I. H.; WYATT, P. G.; FREARSON, J. A.; FAIRLAMB, A. H.; GRAY, D. W. Comparison of a high-throughput high-content intracellular Leishmania donovani assay with an axenic amastigote assay. **Antimicrob Agents Chemother,** v. 57, n. 7, p. 2913-22, Jul 2013.

61 PEÑA, I.; PILAR MANZANO, M.; CANTIZANI, J.; KESSLER, A.; ALONSO-PADILLA, J.; BARDERA, A. I.; ALVAREZ, E.; COLMENAREJO, G.; COTILLO, I.; ROQUERO, I.; DE DIOS-ANTON, F.; BARROSO, V.; RODRIGUEZ, A.; GRAY, D. W.; NAVARRO, M.; KUMAR, V.; SHERSTNEV, A.; DREWRY, D. H.; BROWN, J. R.; FIANDOR, J. M.; JULIO MARTIN, J. New compound sets identified from high throughput phenotypic screening against three kinetoplastid parasites: an open resource. **Scientific reports,** v. 5, p. 8771-8771, 2015.

62 ZULFIQAR, B.; JONES, A. J.; SYKES, M. L.; SHELPER, T. B.; DAVIS, R. A.; AVERY, V. M. Screening a Natural Product-Based Library against Kinetoplastid Parasites. **Molecules (Basel, Switzerland),** v. 22, n. 10, p. 1715, 2017.

63 GILBERT, I. H. Drug Discovery for Neglected Diseases: Molecular Target-Based and Phenotypic Approaches. **Chemistry, Medicinal,** v. 56, n. (20), p. pp 7719-7726, 2013.

64 CHARLTON, R. L.; ROSSI-BERGMANN, B.; DENNY, P. W.; STEEL, P. G. Repurposing as a strategy for the discovery of new anti-leishmanials: the-state-of-the-art. **Parasitology,** v. 145, n. 2, p. 219-236, 2018.

65 SWINNEY, D. C. Chapter 18 - Molecular Mechanism of Action (MMoA) in Drug Discovery. In: MACOR, J. E. (Ed.). **Annual Reports in Medicinal Chemistry**: Academic Press, v.46, 2011. p.301-317. ISBN 0065-7743.

66 DE MACEDO-SILVA, S. T.; DE SOUZA, W.; RODRIGUES, J. C. Sterol Biosynthesis Pathway as an Alternative for the Anti-Protozoan Parasite Chemotherapy. **Curr Med Chem,** v. 22, n. 18, p. 2186-98, 2015.

67 CHAWLA, B.; MADHUBALA, R. Drug targets in Leishmania. **Journal of parasitic diseases : official organ of the Indian Society for Parasitology,** v. 34, n. 1, p. 1-13, 2010.

68 MINA, J. G.; MOSELY, J. A.; ALI, H. Z.; DENNY, P. W.; STEEL, P. G. Exploring Leishmania major inositol phosphorylceramide synthase (LmjIPCS): insights into the ceramide binding domain. **Org Biomol Chem,** v. 9, n. 6, p. 1823-30, Mar 21 2011.

69 MINA, J. G.; MOSELY, J. A.; ALI, H. Z.; SHAMS-ELDIN, H.; SCHWARZ, R. T.; STEEL, P. G.; DENNY, P. W. A plate-based assay system for analyses and screening of the Leishmania major inositol phosphorylceramide synthase. **Int J Biochem Cell Biol,** v. 42, n. 9, p. 1553-61, Sep 2010.

70 NORCLIFFE, J. L.; MINA, J. G.; ALVAREZ, E.; CANTIZANI, J.; DE DIOS-ANTON, F.; COLMENAREJO, G. Identifying inhibitors of the Leishmania inositol phosphorylceramide synthase with antiprotozoal activity using a yeast-based assay and ultra-high throughput screening platform. v. 8, n. 1, p. 3938, Mar 2 2018.

71 SHARMA, M.; CHAUHAN, P. M. S. Dihydrofolate reductase as a therapeutic target for infectious diseases: opportunities and challenges. **Future Medicinal Chemistry,** v. 4, n. 10, p. 1335-1365, 2012/06/01 2012.

72 PEZ, D.; LEAL, I.; ZUCCOTTO, F.; BOUSSARD, C.; BRUN, R.; CROFT, S. L.; YARDLEY, V.; RUIZ PEREZ, L. M.; GONZALEZ PACANOWSKA, D.;

GILBERT, I. H. 2,4-Diaminopyrimidines as inhibitors of Leishmanial and Trypanosomal dihydrofolate reductase. **Bioorg Med Chem,** v. 11, n. 22, p. 4693-711, Nov 3 2003.

73 KHABNADIDEH, S.; PEZ, D.; MUSSO, A.; BRUN, R.; PÉREZ, L. M. R.; GONZÁLEZ-PACANOWSKA, D.; GILBERT, I. H. Design, synthesis and evaluation of 2,4-diaminoquinazolines as inhibitors of trypanosomal and leishmanial dihydrofolate reductase. **Bioorganic & Medicinal Chemistry,** v. 13, n. 7, p. 2637-2649, 2005/04/01/ 2005.

74 HERRMANN, F. C.; SIVAKUMAR, N.; JOSE, J.; COSTI, M. P.; POZZI, C.; SCHMIDT, T. J. In Silico Identification and In Vitro Evaluation of Natural Inhibitors of Leishmania major Pteridine Reductase I. **Molecules,** v. 22, n. 12, Dec 6 2017.

75 DOERIG, C.; MEIJER, L.; MOTTRAM, J. C. Protein kinases as drug targets in parasitic protozoa. **Trends Parasitol,** v. 18, n. 8, p. 366-71, Aug 2002.

76 HASSAN, P.; FERGUSSON, D.; GRANT, K. M.; MOTTRAM, J. C. The CRK3 protein kinase is essential for cell cycle progression of Leishmania mexicana. **Mol Biochem Parasitol,** v. 113, n. 2, p. 189-98, Apr 6 2001.

77 WYLLIE, S.; THOMAS, M.; PATTERSON, S.; CROUCH, S.; DE RYCKER, M.; LOWE, R.; GRESHAM, S.; URBANIAK, M. D.; OTTO, T. D.; STOJANOVSKI, L.; SIMEONS, F. R. C.; MANTHRI, S.; MACLEAN, L. M.; ZUCCOTTO, F.; HOMEYER, N.; PFLAUMER, H.; BOESCHE, M.; SASTRY, L.; CONNOLLY, P.; ALBRECHT, S.; BERRIMAN, M.; DREWES, G.; GRAY, D. W.; GHIDELLI-DISSE, S.; DIXON, S.; FIANDOR, J. M.; WYATT, P. G.; FERGUSON, M. A. J.; FAIRLAMB, A. H.; MILES, T. J.; READ, K. D.; GILBERT, I. H. Cyclin-dependent kinase 12 is a drug target for visceral leishmaniasis. **Nature,** v. 560, n. 7717, p. 192-197, 2018/08/01 2018.

78 DACHER, M.; MORALES, M. A.; PESCHER, P.; LECLERCQ, O.; RACHIDI, N.; PRINA, E.; CAYLA, M.; DESCOTEAUX, A.; SPATH, G. F. Probing druggability and biological function of essential proteins in Leishmania combining facilitated null mutant and plasmid shuffle analyses. **Mol Microbiol,** v. 93, n. 1, p. 146-66, Jul 2014.

79 OJO, K. K.; ARAKAKI, T. L.; NAPULI, A. J.; INAMPUDI, K. K.; KEYLOUN, K. R.; ZHANG, L.; HOL, W. G.; VERLINDE, C. L.; MERRITT, E. A.; VAN VOORHIS, W. C. Structure determination of glycogen synthase kinase-3 from Leishmania major and comparative inhibitor structure-activity relationships with Trypanosoma brucei GSK-3. **Mol Biochem Parasitol,** v. 176, n. 2, p. 98-108, Apr 2011.

80 DAS, P.; ALAM, M. N.; PAIK, D.; KARMAKAR, K.; DE, T.; CHAKRABORTI, T. Protease inhibitors in potential drug development for Leishmaniasis. **Indian J Biochem Biophys,** v. 50, n. 5, p. 363-76, Oct 2013.

81 OLIVIER, M.; HASSANI, K. Protease inhibitors as prophylaxis against leishmaniasis: new hope from the major surface protease gp63. **Future Med Chem,** v. 2, n. 4, p. 539-42, Apr 2010.

82 SCHAD, C.; BAUM, U.; FRANK, B.; DIETZEL, U.; MATTERN, F.; GOMES, C.; PONTE-SUCRE, A.; MOLL, H.; SCHURIGT, U.; SCHIRMEISTER, T. Development of a New Antileishmanial Aziridine-2,3-Dicarboxylate-Based Inhibitor with High Selectivity for Parasite Cysteine Proteases. **Antimicrobial agents and chemotherapy,** v. 60, n. 2, p. 797-805, 2016.

83 MCLUSKEY, K.; PATERSON, N. G.; BLAND, N. D.; ISAACS, N. W.; MOTTRAM, J. C. Crystal structure of Leishmania major oligopeptidase B gives insight into the enzymatic properties of a trypanosomatid virulence factor. **The Journal of biological chemistry,** v. 285, n. 50, p. 39249-39259, 2010.

84 KHARE, S.; NAGLE, A. S.; BIGGART, A.; LAI, Y. H.; LIANG, F.; DAVIS, L. C.; BARNES, S. W.; MATHISON, C. J. N.; MYBURGH, E.; GAO, M.-Y.; GILLESPIE, J. R.; LIU, X.; TAN, J. L.; STINSON, M.; RIVERA, I. C.; BALLARD, J.; YEH, V.; GROESSL, T.; FEDERE, G.; KOH, H. X. Y.; VENABLE, J. D.; BURSULAYA, B.; SHAPIRO, M.; MISHRA, P. K.; SPRAGGON, G.; BROCK, A.; MOTTRAM, J. C.; BUCKNER, F. S.; RAO, S. P. S.; WEN, B. G.; WALKER, J. R.; TUNTLAND, T.; MOLTENI, V.; GLYNNE, R. J.; SUPEK, F. Proteasome inhibition for treatment of leishmaniasis, Chagas disease and sleeping sickness. **Nature,** v. 537, p. 229, 08/08/online 2016.

85 ILARI, A.; FIORILLO, A.; GENOVESE, I.; COLOTTI, G. Polyamine-trypanothione pathway: an update. **Future Med Chem,** v. 9, n. 1, p. 61-77, Jan 2017.

86 D'ANTONIO, E. L.; ULLMAN, B.; ROBERTS, S. C.; DIXIT, U. G.; WILSON, M. E.; HAI, Y.; CHRISTIANSON, D. W. Crystal structure of arginase from Leishmania mexicana and implications for the inhibition of polyamine biosynthesis in parasitic infections. **Arch Biochem Biophys,** v. 535, n. 2, p. 163-76, Jul 15 2013.

87 KAUR, K.; EMMETT, K.; MCCANN, P. P.; SJOERDSMA, A.; ULLMAN, B. Effects of DL-alpha-difluoromethylornithine on Leishmania donovani promastigotes. **J Protozool,** v. 33, n. 4, p. 518-21, Nov 1986.

88 BONNET, B.; SOULLEZ, D.; GIRAULT, S.; MAES, L.; LANDRY, V.; DAVIOUD-CHARVET, E.; SERGHERAERT, C. Trypanothione reductase inhibition/trypanocidal activity relationships in a 1,4-bis(3-aminopropyl)piperazine series. **Bioorg Med Chem,** v. 8, n. 1, p. 95-103, Jan 2000.

89 CHIBALE, K.; VISSER, M.; YARDLEY, V.; CROFT, S. L.; FAIRLAMB, A. H. Synthesis and evaluation of 9,9-dimethylxanthene tricyclics against

trypanothione reductase, Trypanosoma brucei, Trypanosoma cruzi and Leishmania donovani. **Bioorg Med Chem Lett,** v. 10, n. 11, p. 1147-50, Jun 5 2000.

90 SACCOLITI, F.; ANGIULLI, G.; PUPO, G.; PESCATORI, L.; MADIA, V. N.; MESSORE, A.; COLOTTI, G.; FIORILLO, A.; SCIPIONE, L.; GRAMICCIA, M.; DI MUCCIO, T.; DI SANTO, R.; COSTI, R.; ILARI, A. Inhibition of Leishmania infantum trypanothione reductase by diaryl sulfide derivatives. **Journal of enzyme inhibition and medicinal chemistry,** v. 32, n. 1, p. 304-310, 2017.

91 IYER, J. P.; KAPRAKKADEN, A.; CHOUDHARY, M. L.; SHAHA, C. Crucial role of cytosolic tryparedoxin peroxidase in Leishmania donovani survival, drug response and virulence. **Mol Microbiol,** v. 68, n. 2, p. 372-91, Apr 2008.

92 PROLO, C.; ÁLVAREZ, M. N.; RADI, R. **Peroxynitrite, a potent macrophage-derived oxidizing cytotoxin to combat invading pathogens**. 40**:** 215-225 p. 2014.

93 TURRENS, J. F. Oxidative stress and antioxidant defenses: a target for the treatment of diseases caused by parasitic protozoa. **Mol Aspects Med,** v. 25, n. 1-2, p. 211-20, Feb-Apr 2004.

94 SMITH, K. A.; WAYPA, G. B.; SCHUMACKER, P. T. Redox signaling during hypoxia in mammalian cells. **Redox biology,** v. 13, p. 228-234, 2017.

95 KRAUTH-SIEGEL, R. L.; COMINI, M. A. Redox control in trypanosomatids, parasitic protozoa with trypanothione-based thiol metabolism. **Biochimica et Biophysica Acta (BBA) - General Subjects,** v. 1780, n. 11, p. 1236-1248, 2008/11/01/ 2008.

96 VAN ASSCHE, T.; DESCHACHT, M.; DA LUZ, R. A. I.; MAES, L.; COS, P. Leishmania–macrophage interactions: Insights into the redox biology. **Free Radical Biology and Medicine,** v. 51, n. 2, p. 337-351, 2011/07/15/ 2011.

97 WYLLIE, S.; CUNNINGHAM, M. L.; FAIRLAMB, A. H. Dual action of antimonial drugs on thiol redox metabolism in the human pathogen Leishmania donovani. **J Biol Chem,** v. 279, n. 38, p. 39925-32, Sep 17 2004.

98 BOND, C. S.; ZHANG, Y.; BERRIMAN, M.; CUNNINGHAM, M. L.; FAIRLAMB, A. H.; HUNTER, W. N. Crystal structure of Trypanosoma cruzi trypanothione reductase in complex with trypanothione, and the structure-based discovery of new natural product inhibitors. **Structure,** v. 7, n. 1, p. 81-9, Jan 15 1999.

99 BARR, S. D.; GEDAMU, L. Cloning and characterization of three differentially expressed peroxidoxin genes from Leishmania chagasi. Evidence for an enzymatic detoxification of hydroxyl radicals. **J Biol Chem,** v. 276, n. 36, p. 34279-87, Sep 7 2001.

100 DAS, S.; GIRI, S.; SUNDAR, S.; SHAHA, C. Functional involvement of Leishmania donovani tryparedoxin peroxidases during infection and drug treatment. **Antimicrobial Agents and Chemotherapy,** v. 62, n. 1, 2018.

101 FIORILLO, A.; COLOTTI, G.; BOFFI, A.; BAIOCCO, P.; ILARI, A. The Crystal Structures of the Tryparedoxin-Tryparedoxin Peroxidase Couple Unveil the Structural Determinants of Leishmania Detoxification Pathway. **PLoS Neglected Tropical Diseases,** v. 6, n. 8, 2012.

102 CASTRO, H.; SOUSA, C.; SANTOS, M.; CORDEIRO-DA-SILVA, A.; FLOHE, L.; TOMAS, A. M. Complementary antioxidant defense by cytoplasmic and mitochondrial peroxiredoxins in Leishmania infantum. **Free Radic Biol Med,** v. 33, n. 11, p. 1552-62, Dec 1 2002.

103 WILKINSON, S. R.; HORN, D.; PRATHALINGAM, S. R.; KELLY, J. M. RNA interference identifies two hydroperoxide metabolizing enzymes that are essential to the bloodstream form of the african trypanosome. **J Biol Chem,** v. 278, n. 34, p. 31640-6, Aug 22 2003.

104 HENARD, C. A.; CARLSEN, E. D.; HAY, C.; KIMA, P. E.; SOONG, L. Leishmania amazonensis Amastigotes Highly Express a Tryparedoxin Peroxidase Isoform That Increases Parasite Resistance to Macrophage Antimicrobial Defenses and Fosters Parasite Virulence. **PLOS Neglected Tropical Diseases,** v. 8, n. 7, p. e3000, 2014.

105 LIN, Y.-C.; HSU, J.-Y.; CHIANG, S.-C.; LEE, S. T. Distinct overexpression of cytosolic and mitochondrial tryparedoxin peroxidases results in preferential detoxification of different oxidants in arsenite-resistant Leishmania amazonensis with and without DNA amplification. **Molecular and Biochemical Parasitology,** v. 142, n. 1, p. 66-75, 2005/07/01/ 2005.

106 BROTHERTON, M.-C.; BOURASSA, S.; LÉGARÉ, D.; POIRIER, G. G.; DROIT, A.; OUELLETTE, M. Quantitative proteomic analysis of amphotericin B resistance in Leishmania infantum. **International Journal for Parasitology: Drugs and Drug Resistance,** v. 4, n. 2, p. 126-132, 2014/08/01/ 2014.

107 ANDRADE, J. M.; MURTA, S. M. Functional analysis of cytosolic tryparedoxin peroxidase in antimony-resistant and -susceptible Leishmania braziliensis and Leishmania infantum lines. **Parasit Vectors,** v. 7, p. 406, Aug 29 2014.

108 BRINDISI, M.; BROGI, S.; RELITTI, N.; VALLONE, A.; BUTINI, S.; GEMMA, S.; NOVELLINO, E.; COLOTTI, G.; ANGIULLI, G.; DI CHIARO, F.; FIORILLO, A.; ILARI, A.; CAMPIANI, G. Structure-based discovery of the first non-covalent inhibitors of Leishmania major tryparedoxin peroxidase by high throughput docking. **Scientific Reports,** v. 5, p. 1-10, 2015.

109 MEIER, A.; ERLER, H.; BEITZ, E. Targeting Channels and Transporters in Protozoan Parasite Infections. **Front Chem,** v. 6, p. 88, 2018.

110 SINGH, N.; KUMAR, M.; SINGH, R. K. Leishmaniasis: current status of available drugs and new potential drug targets. **Asian Pac J Trop Med,** v. 5, n. 6, p. 485-97, Jun 2012.

111 AMBIT, A.; FASEL, N.; COOMBS, G. H.; MOTTRAM, J. C. An essential role for the Leishmania major metacaspase in cell cycle progression. **Cell Death Differ,** v. 15, n. 1, p. 113-22, Jan 2008.

112 REGUERA, R. M.; ESCUDERO-MARTÍNEZ, J. M.; DOMÍNGUEZ-ASENJO, B.; GUTIÉRREZ-CORBO, C.; BALAÑA-FOUCE, R. Chapter 17 DNA Topoisomerases as Promising Targets for Leishmania Chemotherapy. In: (Ed.). **Drug Discovery for Leishmaniasis**: The Royal Society of Chemistry, 2018. p.348-370. ISBN 978-1-78262-889-7.

113 VERLINDE, C. L.; HANNAERT, V.; BLONSKI, C.; WILLSON, M.; PERIE, J. J.; FOTHERGILL-GILMORE, L. A.; OPPERDOES, F. R.; GELB, M. H.; HOL, W. G.; MICHELS, P. A. Glycolysis as a target for the design of new anti-trypanosome drugs. **Drug Resist Updat,** v. 4, n. 1, p. 50-65, Feb 2001.

114 KAPIL, S.; SINGH, P. K.; SILAKARI, O. An update on small molecule strategies targeting leishmaniasis. **Eur J Med Chem,** v. 157, p. 339-367, Sep 5 2018.

115 LEE, J.; BOGYO, M. Target deconvolution techniques in modern phenotypic profiling. **Curr Opin Chem Biol,** v. 17, n. 1, p. 118-26, Feb 2013.

116 KUBOTA, K.; FUNABASHI, M.; OGURA, Y. Target deconvolution from phenotype-based drug discovery by using chemical proteomics approaches. **Biochimica et Biophysica Acta (BBA) - Proteins and Proteomics,** v. 1867, n. 1, p. 22-27, 2019/01/01/ 2019.

117 VAN DORST, B.; MEHTA, J.; ROUAH-MARTIN, E.; SOMERS, V.; DE COEN, W.; BLUST, R.; ROBBENS, J. cDNA phage display as a novel tool to screen for cellular targets of chemical compounds. **Toxicol In Vitro,** v. 24, n. 5, p. 1435-40, Aug 2010.

118 MCPHERSON, M.; YANG, Y.; HAMMOND, P. W.; KREIDER, B. L. Drug receptor identification from multiple tissues using cellular-derived mRNA display libraries. **Chem Biol,** v. 9, n. 6, p. 691-8, Jun 2002.

119 WADA, A.; HARA, S.; OSADA, H. Ribosome Display and Photo-Cross-Linking Techniques for In Vitro Identification of Target Proteins of Bioactive Small Molecules. **Analytical Chemistry,** v. 86, n. 14, p. 6768-6773, 2014/07/15 2014.

120 BECKER, F.; MURTHI, K.; SMITH, C.; COME, J.; COSTA-ROLDAN, N.; KAUFMANN, C.; HANKE, U.; DEGENHART, C.; BAUMANN, S.; WALLNER, W.; HUBER, A.; DEDIER, S.; DILL, S.; KINSMAN, D.; HEDIGER, M.; BOCKOVICH, N.; MEIER-EWERT, S.; KLUGE, A. F.; KLEY, N. A three-hybrid approach to scanning the proteome for targets of small molecule kinase inhibitors. **Chem Biol,** v. 11, n. 2, p. 211-23, Feb 2004.

121 ZHU, H.; BILGIN, M.; BANGHAM, R.; HALL, D.; CASAMAYOR, A.; BERTONE, P.; LAN, N.; JANSEN, R.; BIDLINGMAIER, S.; HOUFEK, T.; MITCHELL, T.; MILLER, P.; DEAN, R. A.; GERSTEIN, M.; SNYDER, M. Global analysis of protein activities using proteome chips. **Science,** v. 293, n. 5537, p. 2101-5, Sep 14 2001.

122 KIM, B.; JO, J.; HAN, J.; PARK, C.; LEE, H. In silico re-identification of properties of drug target proteins. **BMC bioinformatics,** v. 18, n. Suppl 7, p. 248-248, 2017.

123 KEISER, M. J.; SETOLA, V.; IRWIN, J. J.; LAGGNER, C.; ABBAS, A. I.; HUFEISEN, S. J.; JENSEN, N. H.; KUIJER, M. B.; MATOS, R. C.; TRAN, T. B.; WHALEY, R.; GLENNON, R. A.; HERT, J.; THOMAS, K. L.; EDWARDS, D. D.; SHOICHET, B. K.; ROTH, B. L. Predicting new molecular targets for known drugs. **Nature,** v. 462, n. 7270, p. 175-81, Nov 12 2009.

124 SMITH, E.; COLLINS, I. Photoaffinity labeling in target- and binding-site identification. **Future Medicinal Chemistry,** v. 7, n. 2, p. 159-183, 2015/02/01 2015.

125 MARTINEZ MOLINA, D.; NORDLUND, P. The Cellular Thermal Shift Assay: A Novel Biophysical Assay for In Situ Drug Target Engagement and Mechanistic Biomarker Studies. **Annu Rev Pharmacol Toxicol,** v. 56, p. 141-61, 2016.

126 HUANG, F.; ZHANG, B.; ZHOU, S.; ZHAO, X.; BIAN, C.; WEI, Y. Chemical proteomics: terra incognita for novel drug target profiling. **Chinese journal of cancer,** v. 31, n. 11, p. 507-518, 2012.

127 CRAVATT, B. F.; WRIGHT, A. T.; KOZARICH, J. W. Activity-based protein profiling: from enzyme chemistry to proteomic chemistry. **Annu Rev Biochem,** v. 77, p. 383-414, 2008.

128 MARTELL, J.; WEERAPANA, E. Applications of copper-catalyzed click chemistry in activity-based protein profiling. **Molecules,** v. 19, n. 2, p. 1378-93, Jan 27 2014.

129 WANG, S.; TIAN, Y.; WANG, M.; WANG, M.; SUN, G.-B.; SUN, X.-B. Advanced Activity-Based Protein Profiling Application Strategies for Drug Development. **Frontiers in Pharmacology,** v. 9, n. 353, 2018-April-09 2018.

130 WANG, J.; ZHANG, J.; ZHANG, C.-J.; WONG, Y. K.; LIM, T. K.; HUA, Z.-C.; LIU, B.; TANNENBAUM, S. R.; SHEN, H.-M.; LIN, Q. In situ Proteomic Profiling of Curcumin Targets in HCT116 Colon Cancer Cell Line. **Scientific reports,** v. 6, p. 22146-22146, 2016.

131 WANG, J.; ZHANG, C.-J.; CHIA, W. N.; LOH, C. C. Y.; LI, Z.; LEE, Y. M.; HE, Y.; YUAN, L.-X.; LIM, T. K.; LIU, M.; LIEW, C. X.; LEE, Y. Q.; ZHANG, J.; LU, N.; LIM, C. T.; HUA, Z.-C.; LIU, B.; SHEN, H.-M.; TAN, K. S. W.; LIN, Q. Haem-activated promiscuous targeting of artemisinin in Plasmodium falciparum. **Nature communications,** v. 6, p. 10111-10111, 2015.

132 STAUB, I.; SIEBER, S. A. Beta-lactams as selective chemical probes for the in vivo labeling of bacterial enzymes involved in cell wall biosynthesis, antibiotic resistance, and virulence. **J Am Chem Soc,** v. 130, n. 40, p. 13400-9, Oct 8 2008.

133 YANG, P.-Y.; LIU, K.; ZHANG, C.; CHEN, G. Y. J.; SHEN, Y.; NGAI, M. H.; LEAR, M. J.; YAO, S. Q. Chemical Modification and Organelle-Specific Localization of Orlistat-Like Natural-Product-Based Probes. **Chemistry – An Asian Journal,** v. 6, n. 10, p. 2762-2775, 2011/10/04 2011.

134 BATEMAN, L. A.; ZARO, B. W.; MILLER, S. M.; PRATT, M. R. An alkyne-aspirin chemical reporter for the detection of aspirin-dependent protein modification in living cells. **J Am Chem Soc,** v. 135, n. 39, p. 14568-73, Oct 2 2013.

135 BACHOVCHIN, D. A.; BROWN, S. J.; ROSEN, H.; CRAVATT, B. F. Identification of selective inhibitors of uncharacterized enzymes by high-throughput screening with fluorescent activity-based probes. **Nat Biotechnol,** v. 27, n. 4, p. 387-94, Apr 2009.

136 YOUSSEF, D. T. A.; RAMADAN, M. A.; KHALIFA, A. A. Acetophenones, a chalcone, a chromone and flavonoids from Pancratium maritimum. **Phytochemistry,** v. 49, n. 8, p. 2579-2583, 1998/12/20/ 1998.

137 WANG, X.; LIU, Y.; MARTIN, R. Ni-Catalyzed Divergent Cyclization/Carboxylation of Unactivated Primary and Secondary Alkyl Halides with CO2. **Journal of the American Chemical Society,** v. 137, n. 20, p. 6476-6479, 2015/05/27 2015.

138 JUNKER, A.; BALASUBRAMANIAN, R.; CIANCETTA, A.; ULIASSI, E.; KISELEV, E.; MARTIRIGGIANO, C.; TRUJILLO, K.; MTCHEDLIDZE, G.; BIRDWELL, L.; BROWN, K. A.; HARDEN, T. K.; JACOBSON, K. A. Structure-Based Design of 3-(4-Aryl-1H-1,2,3-triazol-1-yl)-Biphenyl Derivatives as P2Y14 Receptor Antagonists. **Journal of Medicinal Chemistry,** v. 59, n. 13, p. 6149-6168, 2016/07/14 2016.

139 ADAM, G. C.; SORENSEN, E. J.; CRAVATT, B. F. Trifunctional Chemical Probes for the Consolidated Detection and Identification of Enzyme Activities from Complex Proteomes. **Molecular & Cellular Proteomics,** v. 1, n. 10, p. 828-835, 2002.

140 NRC. **Guide for the Care and Use of Laboratory Animals**. 8th edition. Washington (DC): National Academies Press (US), 2011. ISBN 978-0-309-15400-0.

141 MARIM, F. M.; SILVEIRA, T. N.; LIMA, D. S.; ZAMBONI, D. S. A Method for Generation of Bone Marrow-Derived Macrophages from Cryopreserved Mouse Bone Marrow Cells. **PLoS ONE,** v. 5, n. 12, p. 1-8, 2010.

142 STENGER, S.; VAN ZANDBERGEN, G. Measuring the killing of intracellular pathogens: Leishmania. **Curr Protoc Immunol,** v. Chapter 14, p. Unit14 23, Apr 2011.

143 BERROW, N. S.; ALDERTON, D.; SAINSBURY, S.; NETTLESHIP, J.; ASSENBERG, R.; RAHMAN, N.; STUART, D. I.; OWENS, R. J. A versatile ligation-independent cloning method suitable for high-throughput expression screening applications. **Nucleic Acids Res,** v. 35, n. 6, p. e45, 2007.

144 GRØFTEHAUGE, M. K.; HAJIZADEH, N. R.; SWANN, M. J.; POHL, E. Protein-ligand interactions investigated by thermal shift assays (TSA) and dual polarization interferometry (DPI). **Acta crystallographica. Section D, Biological crystallography,** v. 71, n. Pt 1, p. 36-44, 2015.

145 FIORILLO, A.; COLOTTI, G.; BOFFI, A.; BAIOCCO, P.; ILARI, A. The crystal structures of the tryparedoxin-tryparedoxin peroxidase couple unveil the structural determinants of Leishmania detoxification pathway. **PLoS Negl Trop Dis,** v. 6, n. 8, p. e1781, 2012.

146 WATERHOUSE, A.; BERTONI, M.; BIENERT, S.; STUDER, G.; TAURIELLO, G.; GUMIENNY, R.; HEER, F. T.; DE BEER, T. A. P.; REMPFER, C.; BORDOLI, L.; LEPORE, R.; SCHWEDE, T. SWISS-MODEL: homology modelling of protein structures and complexes. **Nucleic Acids Res,** v. 46, n. W1, p. W296-w303, Jul 2 2018.

147 MORRIS, G. M.; HUEY, R.; LINDSTROM, W.; SANNER, M. F.; BELEW, R. K.; GOODSELL, D. S.; OLSON, A. J. AutoDock4 and AutoDockTools4: Automated docking with selective receptor flexibility. **J Comput Chem,** v. 30, n. 16, p. 2785-91, Dec 2009.

148 BENEKE, T.; MADDEN, R.; MAKIN, L.; VALLI, J.; SUNTER, J.; GLUENZ, E. A CRISPR Cas9 high-throughput genome editing toolkit for kinetoplastids. **Royal Society Open Science,** v. 4, n. 5, p. 170095, 05/03

02/03/received

03/29/accepted 2017.

149 LI, L.; ZHANG, Z. Development and Applications of the Copper-Catalyzed Azide-Alkyne Cycloaddition (CuAAC) as a Bioorthogonal Reaction. **Molecules,** v. 21, n. 10, Oct 24 2016.

150 HONG, V.; PRESOLSKI, S. I.; MA, C.; FINN, M. G. Analysis and optimization of copper-catalyzed azide-alkyne cycloaddition for bioconjugation. **Angewandte Chemie (International ed. in English),** v. 48, n. 52, p. 9879-9883, 2009.

151 WRIGHT, M. H.; SIEBER, S. A. Chemical proteomics approaches for identifying the cellular targets of natural products. **Natural product reports,** v. 33, n. 5, p. 681-708, 2016.

152 GALLAGHER, S. R. One-dimensional SDS gel electrophoresis of proteins. **Curr Protoc Mol Biol,** v. Chapter 10, p. Unit 10 2A, Jan 2012.

153 TEIXEIRA, P. C.; VELASQUEZ, L. G.; LEPIQUE, A. P.; DE REZENDE, E.; BONATTO, J. M.; BARCINSKI, M. A.; CUNHA-NETO, E.; STOLF, B. S. Regulation of Leishmania (L.) amazonensis protein expression by host T cell dependent responses: differential expression of oligopeptidase B, tryparedoxin peroxidase and HSP70 isoforms in amastigotes isolated from BALB/c and BALB/c nude mice. **PLoS Negl Trop Dis,** v. 9, n. 2, p. e0003411, Feb 2015.

154 VIJAYAKUMAR, S.; DAS, P. Recent progress in drug targets and inhibitors towards combating leishmaniasis. **Acta Trop,** v. 181, p. 95-104, May 2018.

155 HOSEINI, S. S.; SAUER, M. G. Molecular cloning using polymerase chain reaction, an educational guide for cellular engineering. **Journal of biological engineering,** v. 9, p. 2-2, 2015.

156 KABIR, A.; HONDA, R. P.; KAMATARI, Y. O.; ENDO, S.; FUKUOKA, M.; KUWATA, K. Effects of ligand binding on the stability of aldo-keto reductases: Implications for stabilizer or destabilizer chaperones. **Protein Sci,** v. 25, n. 12, p. 2132-2141, Dec 2016.

157 CIMMPERMAN, P.; BARANAUSKIENĖ, L.; JACHIMOVIČIŪTĖ, S.; JACHNO, J.; TORRESAN, J.; MICHAILOVIENĖ, V.; MATULIENĖ, J.; SEREIKAITĖ, J.; BUMELIS, V.; MATULIS, D. A Quantitative Model of Thermal Stabilization and Destabilization of Proteins by Ligands. **Biophysical Journal,** v. 95, n. 7, p. 3222-3231, 2008/10/01/ 2008.

158 DON, R. O. B.; IOSET, J.-R. Screening strategies to identify new chemical diversity for drug development to treat kinetoplastid infections. **Parasitology,** v. 141, n. 01, p. 140-146, 2014.

159 FONSECA-SILVA, F.; INACIO, J. D.; CANTO-CAVALHEIRO, M. M.; ALMEIDA-AMARAL, E. E. Reactive oxygen species production and mitochondrial dysfunction contribute to quercetin induced death in Leishmania amazonensis. **PLoS One,** v. 6, n. 2, p. e14666, Feb 8 2011.

160 WANG, J.; HUANG, L.; CHENG, C.; LI, G.; XIE, J.; SHEN, M.; CHEN, Q.; LI, W.; HE, W.; QIU, P.; WU, J. Design, synthesis and biological evaluation of chalcone analogues with novel dual antioxidant mechanisms as potential anti-ischemic stroke agents. **Acta Pharmaceutica Sinica B**, 2019/01/07/ 2019.

161 BRINDISI, M.; BROGI, S.; RELITTI, N.; VALLONE, A.; BUTINI, S.; GEMMA, S.; NOVELLINO, E.; COLOTTI, G.; ANGIULLI, G.; DI CHIARO, F.; FIORILLO, A.; ILARI, A.; CAMPIANI, G. Structure-based discovery of the first non-covalent inhibitors of Leishmania major tryparedoxin peroxidase by high throughput docking. **Sci Rep,** v. 5, p. 9705, May 7 2015.

162 PIACENZA, L.; PELUFFO, G.; ALVAREZ, M. N.; MARTÍNEZ, A.; RADI, R. Trypanosoma cruzi Antioxidant Enzymes As Virulence Factors in Chagas Disease. **Antioxidants & Redox Signaling,** v. 19, n. 7, p. 723-734, 2013/09/01 2012.

163 FALCÃO, C. A. B. **Avaliação de sistemas de liberação controlada para uma nova droga ativa no tratamento de leishmaniose cutânea priorizando vias não invasivas**. 2010. 159-159 Research (PhD). Biophysics Institute Carlos Chagas Filho, Federal University of Rio de Janeiro

164 SOUSA-BATISTA, A. D. J.; PHILIPON, C. I. M. S.; ALBERNAZ, M. D. S.; PINTO, S. R.; ROSSI-BERGMANN, B.; SANTOS-OLIVEIRA, R. New Chalcone Compound as a Promising Antileishmanial Drug for an Old Neglected Disease: Biological Evaluation using Radiolabeled Biodistribution. **Journal of Global Antimicrobial Resistance**, 2017.

165 HEAL, W. P.; JOVANOVIC, B.; BESSIN, S.; WRIGHT, M. H.; MAGEE, A. I.; TATE, E. W. Bioorthogonal chemical tagging of protein cholesterylation in living cells. **Chem Commun (Camb),** v. 47, n. 14, p. 4081-3, Apr 14 2011.

166 WRIGHT, M. H.; PAAPE, D.; STORCK, E. M.; SERWA, R. A.; SMITH, D. F.; TATE, E. W. Global analysis of protein N-myristoylation and exploration of N-myristoyltransferase as a drug target in the neglected human pathogen Leishmania donovani. **Chem Biol,** v. 22, n. 3, p. 342-54, Mar 19 2015.

167 ISMAIL, H. M.; BARTON, V.; PHANCHANA, M.; CHAROENSUTTHIVARAKUL, S.; WONG, M. H. L.; HEMINGWAY, J.; BIAGINI, G. A.; O'NEILL, P. M.; WARD, S. A. Artemisinin activity-based probes identify multiple molecular targets within the asexual stage of the malaria parasites Plasmodium falciparum 3D7. **Proceedings of the National Academy of Sciences,** v. 113, n. 8, p. 2080, 2016.

168 WYATT, P. G.; GILBERT, I. H.; READ, K. D.; FAIRLAMB, A. H. Target validation: linking target and chemical properties to desired product profile. **Current topics in medicinal chemistry,** v. 11, n. 10, p. 1275-1283, 2011.

169 TRINCONI, C. T.; REIMÃO, J. Q.; YOKOYAMA-YASUNAKA, J. K. U.; MIGUEL, D. C.; ULIANA, S. R. B. Combination Therapy with Tamoxifen and Amphotericin B in Experimental Cutaneous Leishmaniasis. **Antimicrobial Agents and Chemotherapy,** v. 58, n. 5, p. 2608, 2014.

170 TRINCONI, C. T.; REIMAO, J. Q.; COELHO, A. C.; ULIANA, S. R. Efficacy of tamoxifen and miltefosine combined therapy for cutaneous leishmaniasis in the murine model of infection with Leishmania amazonensis. **J Antimicrob Chemother,** v. 71, n. 5, p. 1314-22, May 2016.

171 CHEN, M.; ZHAI, L.; CHRISTENSEN, S. B.; THEANDER, T. G.; KHARAZMI, A. Inhibition of fumarate reductase in Leishmania major and L. donovani by chalcones. **Antimicrobial agents and chemotherapy,** v. 45, n. 7, p. 2023-2029, 2001.

172 ORTALLI, M.; ILARI, A.; COLOTTI, G.; DE IONNA, I.; BATTISTA, T.; BISI, A.; GOBBI, S.; RAMPA, A.; DI MARTINO, R. M. C.; GENTILOMI, G. A.; VARANI, S.; BELLUTI, F. Identification of chalcone-based antileishmanial agents targeting trypanothione reductase. **Eur J Med Chem,** v. 152, p. 527-541, May 25 2018.

173 GOMES, M. N.; ALCANTARA, L. M.; NEVES, B. J.; MELO-FILHO, C. C.; FREITAS-JUNIOR, L. H.; MORAES, C. B.; MA, R.; FRANZBLAU, S. G.; MURATOV, E.; ANDRADE, C. H. Computer-aided discovery of two novel chalcone-like compounds active and selective against Leishmania infantum. **Bioorg Med Chem Lett,** v. 27, n. 11, p. 2459-2464, Jun 1 2017.

174 LAMOTTE, S.; AULNER, N.; SPÄTH, G. F.; PRINA, E. Discovery of novel hit compounds with broad activity against visceral and cutaneous Leishmania species by comparative phenotypic screening. **Scientific Reports,** v. 9, n. 1, p. 438, 2019/01/24 2019.

175 CASTRO, H.; TOMAS, A. M. Peroxidases of trypanosomatids. **Antioxid Redox Signal,** v. 10, n. 9, p. 1593-606, Sep 2008.

176 SRINIVASAN, B.; JOHNSON, T. E.; LAD, R.; XING, C. Structure-activity relationship studies of chalcone leading to 3-hydroxy-4,3',4',5'-tetramethoxychalcone and its analogues as potent nuclear factor kappaB inhibitors and their anticancer activities. **J Med Chem,** v. 52, n. 22, p. 7228-35, Nov 26 2009.

177 OSORIO-MÉNDEZ, J. F.; CEVALLOS, A. M. Discovery and Genetic Validation of Chemotherapeutic Targets for Chagas' Disease. **Frontiers in cellular and infection microbiology,** v. 8, p. 439-439, 2019.

178 DAS, M.; MUKHERJEE, S. B.; SHAHA, C. Hydrogen peroxide induces apoptosis-like death in Leishmania donovani promastigotes. **Journal of Cell Science,** v. 114, n. 13, p. 2461, 2001.

179 SEN, N.; DAS, B. B.; GANGULY, A.; MUKHERJEE, T.; TRIPATHI, G.; BANDYOPADHYAY, S.; RAKSHIT, S.; SEN, T.; MAJUMDER, H. K. Camptothecin induced mitochondrial dysfunction leading to programmed cell death in unicellular hemoflagellate Leishmania donovani. **Cell Death Differ,** v. 11, n. 8, p. 924-36, Aug 2004.

180 ESCRIVANI-OLIVEIRA, D. **Encapsulação da chalcona CH8 em nanocápsulas de núcleo lipídico (LNCs): Efeito sobre a Leishmania amazonensis, macrófagos infectados e na infecção murina**. 2015. 126-126

181 GAN, F.-F.; KAMINSKA, K. K.; YANG, H.; LIEW, C.-Y.; LEOW, P.-C.; SO, C.-L.; TU, L. N. L.; ROY, A.; YAP, C.-W.; KANG, T.-S.; CHUI, W.-K.; CHEW, E.-H. Identification of Michael acceptor-centric pharmacophores with substituents that yield strong thioredoxin reductase inhibitory character correlated to antiproliferative activity. **Antioxidants & redox signaling,** v. 19, n. 11, p. 1149-1165, 2013.

182 FANG, J.; LU, J.; HOLMGREN, A. Thioredoxin reductase is irreversibly modified by curcumin: a novel molecular mechanism for its anticancer activity. **J Biol Chem,** v. 280, n. 26, p. 25284-90, Jul 1 2005.

183 CHEW, E. H.; NAGLE, A. A.; ZHANG, Y.; SCARMAGNANI, S.; PALANIAPPAN, P.; BRADSHAW, T. D.; HOLMGREN, A.; WESTWELL, A. D. Cinnamaldehydes inhibit thioredoxin reductase and induce Nrf2: potential candidates for cancer therapy and chemoprevention. **Free Radic Biol Med,** v. 48, n. 1, p. 98-111, Jan 1 2010.

184 HUNTER, W. N. Structure-based ligand design and the promise held for antiprotozoan drug discovery. **The Journal of biological chemistry,** v. 284, n. 18, p. 11749-11753, 2009.

8. APPENDIX

Project development

Activities	UFRJ	DU
Analogues and probe synthesis		
ABPP tool validation		
Target isolation (promastigote lysate preparation and SDS-PAGE)		
Target identification (mass spectrometry)		
Target confirmation (2D-electrophoresis and western blot)		
Target specificity		
Recombinant protein expression		
Protein and chalcone interaction (mass spectrometry)		
Protein and chalcone interaction (TSA)		
In silico studies (modelling and docking)		
cTXNPx knockout parasites		

UFRJ- Federal University of Rio de Janeiro
DU- Durham Univesirty

NMR spectra

Compound 18

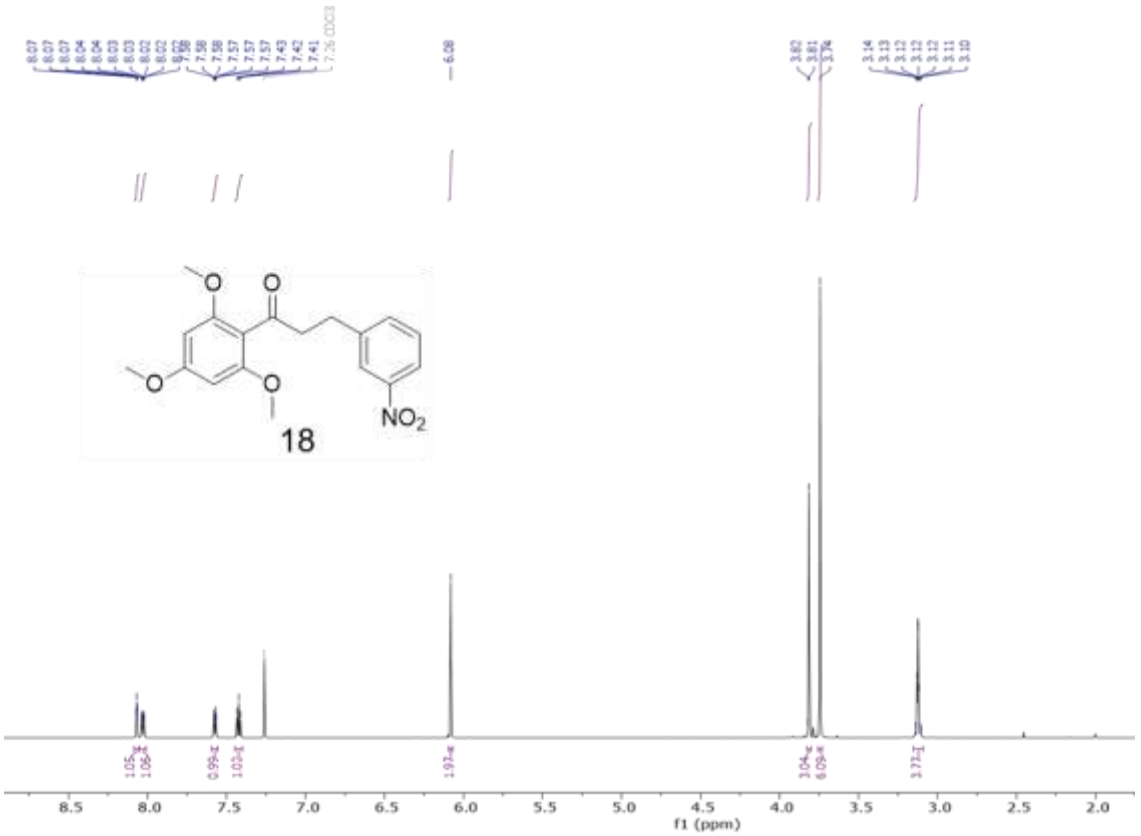

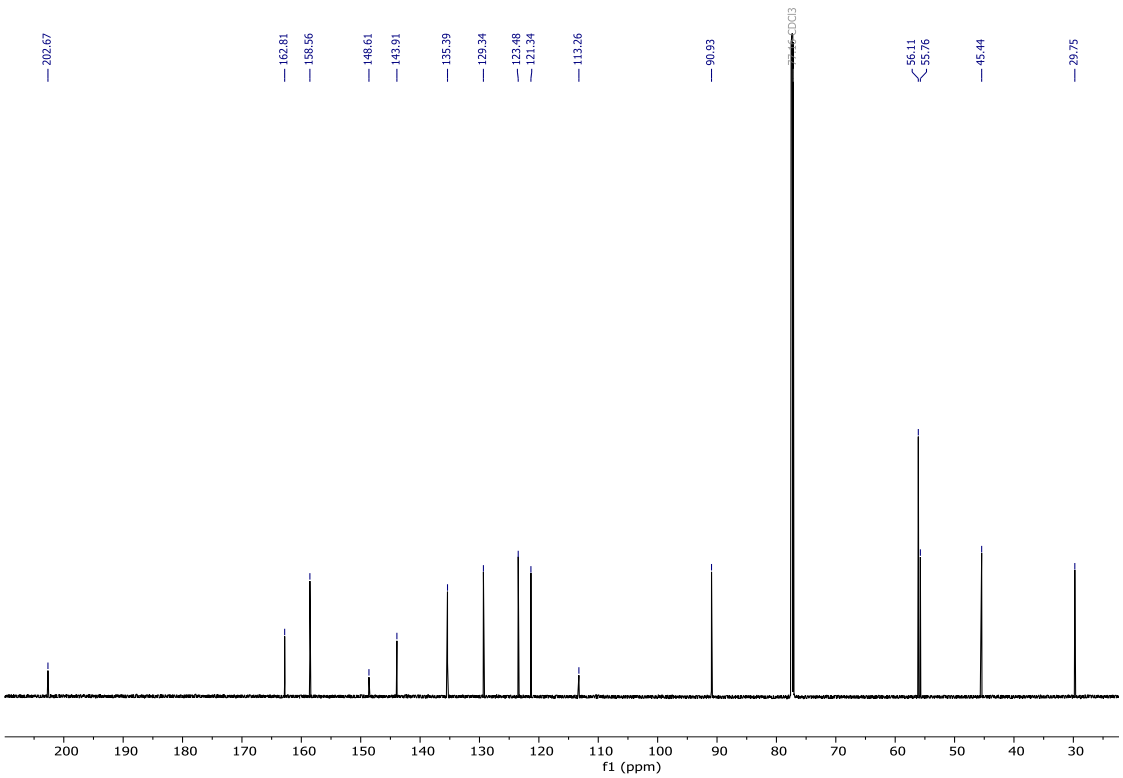

Mass spectra

Compound 18

Single Mass Analysis
Tolerance = 3.0 mDa / DBE: min = -1.5, max = 50.0
Element prediction: Off
Number of isotope peaks used for i-FIT = 3

Monoisotopic Mass, Even Electron Ions
401 formula(e) evaluated with 2 results within limits (up to 500 best isotopic matches for each mass)
Elements Used:
C: 0-100 H: 0-100 N: 0-6 O: 0-18

18-Sep-2017
RC1180 HPLC2 529 (4.453) Cm (514:530)

1: TOF MS ES+
1.11e+004

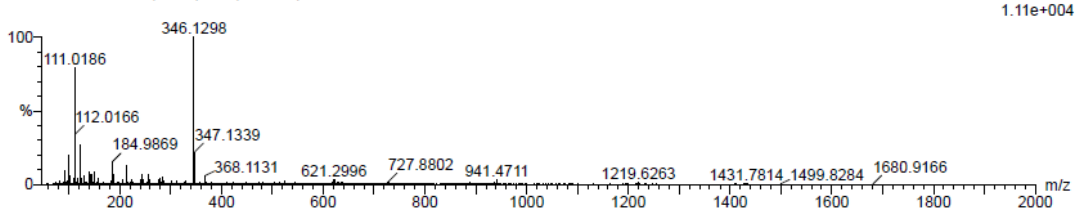

Minimum:				-1.5			
Maximum:		3.0	5.0	50.0			
Mass	Calc. Mass	mDa	PPM	DBE	i-FIT	i-FIT (Norm)	Formula
346.1298	346.1291	0.7	2.0	9.5	317.6	0.1	C18 H20 N O6
	346.1304	-0.6	-1.7	14.5	320.4	2.9	C19 H16 N5 O2

NMR spectra

Compound 19b

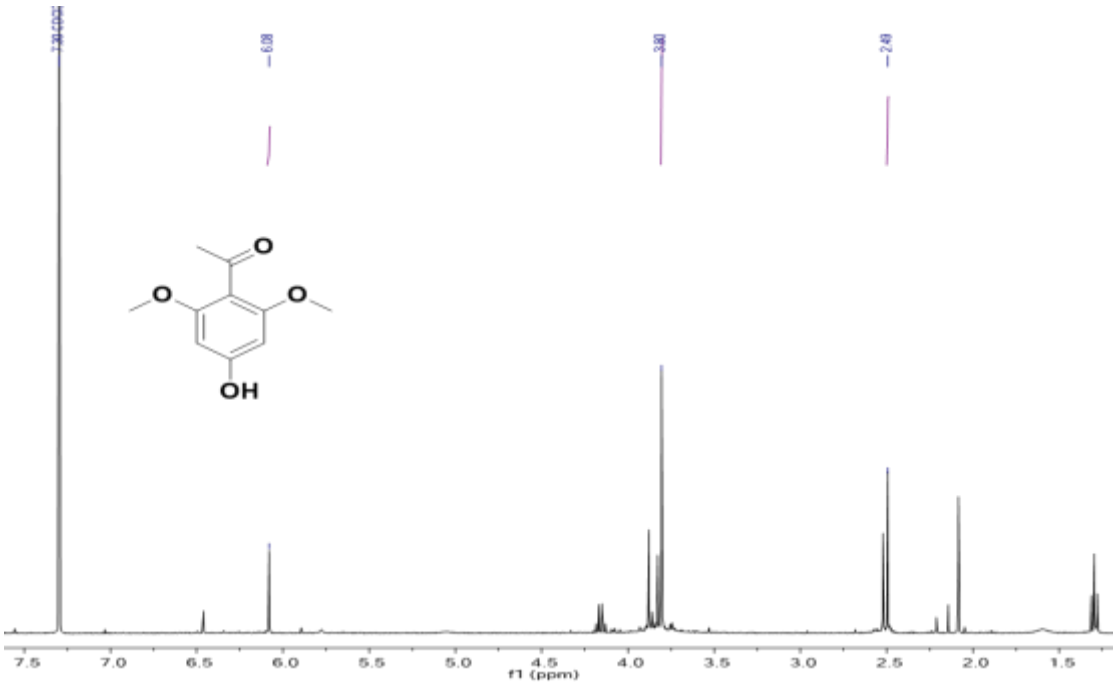

Compound 19c

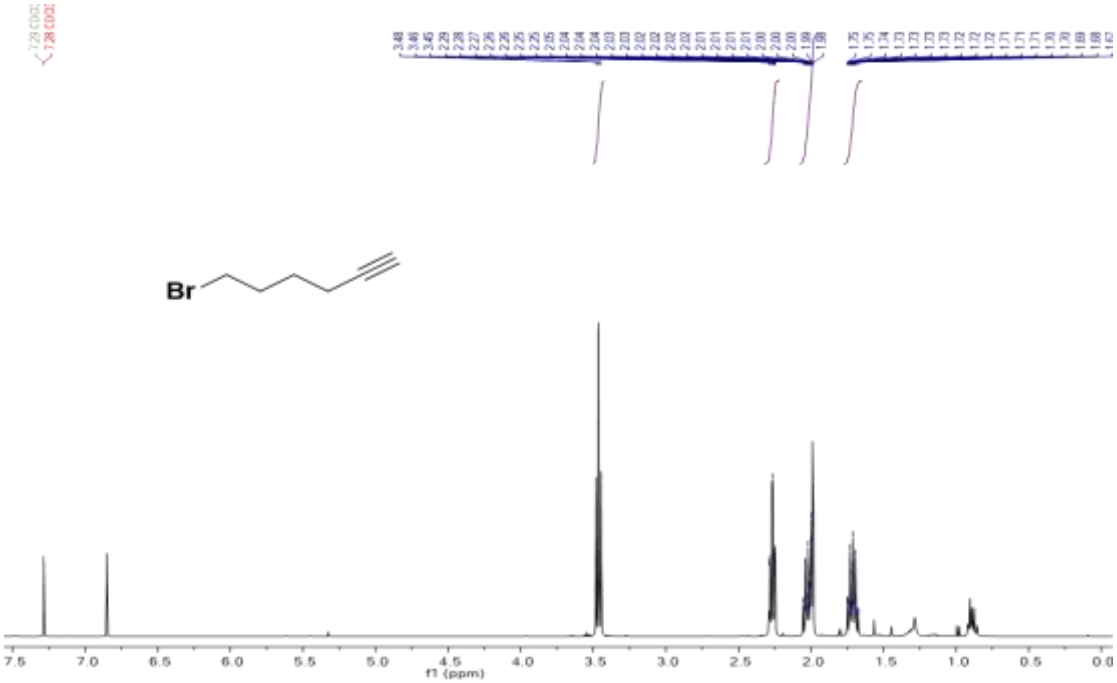

Compound 19d

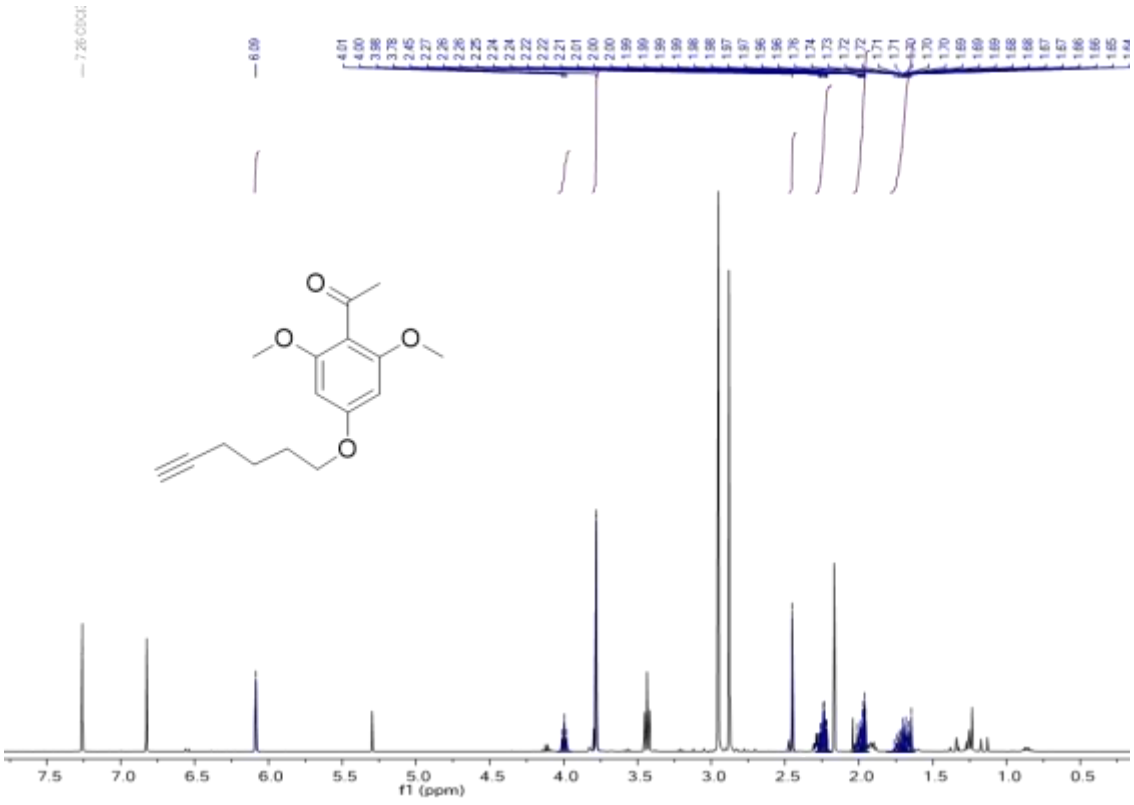

Compound 19

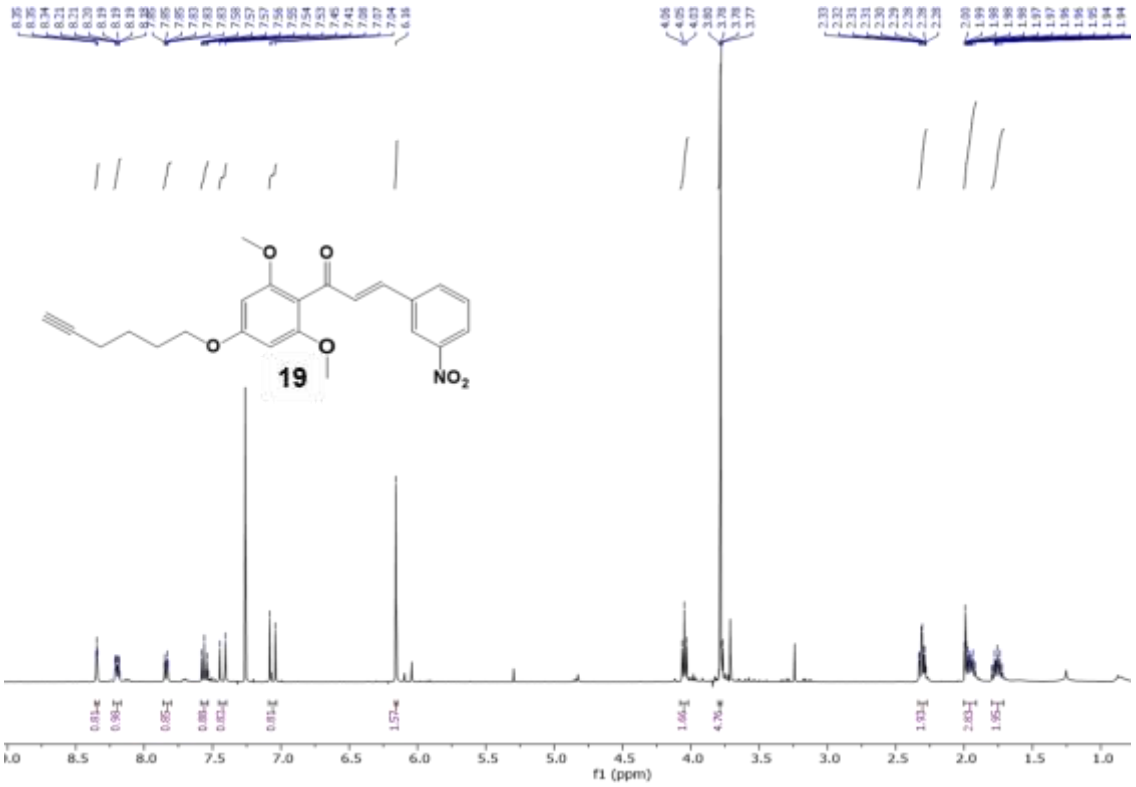

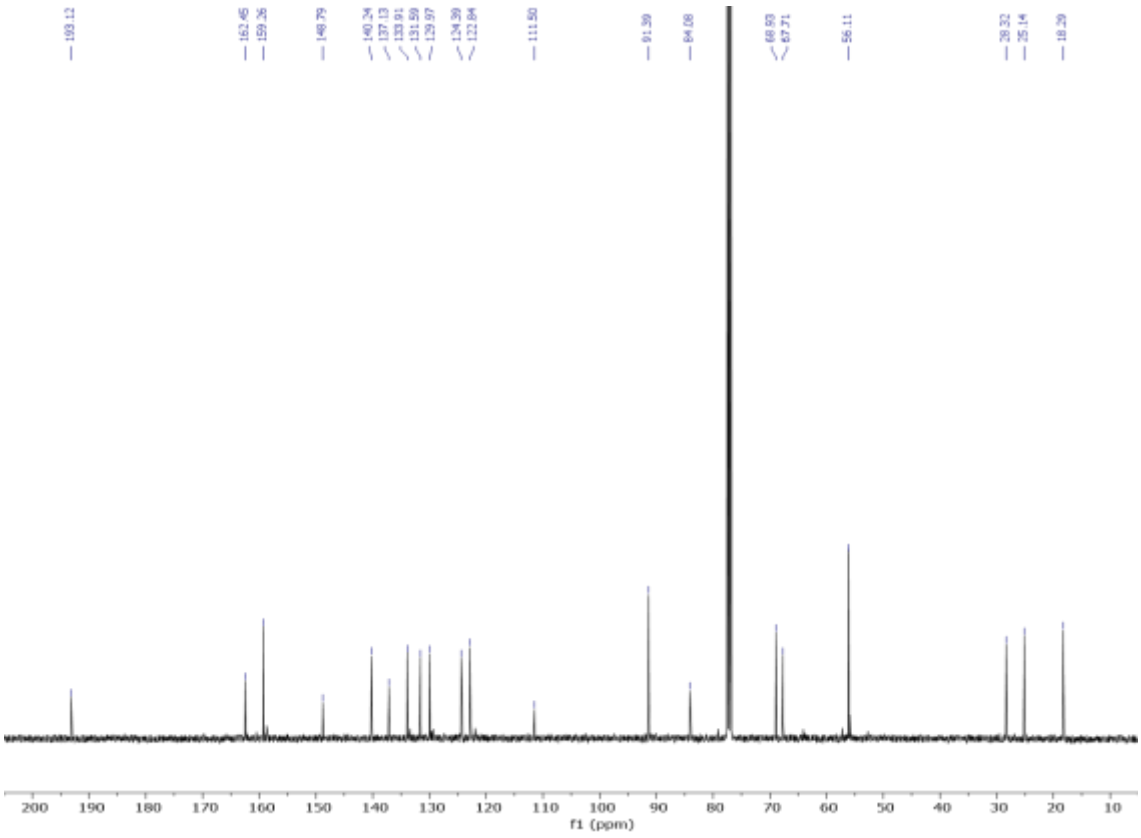

Mass spectra

Compound 19

Single Mass Analysis
Tolerance = 5.0 mDa / DBE: min = -1.5, max = 50.0
Element prediction: Off
Number of isotope peaks used for i-FIT = 3

Monoisotopic Mass, Even Electron Ions
381 formula(e) evaluated with 5 results within limits (up to 50 closest results for each mass)
Elements Used:
C: 0-40 H: 0-80 N: 0-8 O: 0-8

Douglas Oliveira
1: TOF MS ES+

LCT Premier

DEO37 423 (3.384) Cm (421:444)

2.40e+005

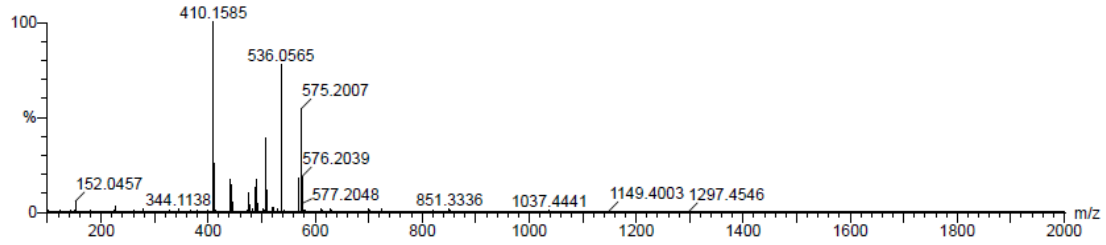

Minimum:				-1.5			
Maximum:		5.0	5.0	50.0			
Mass	Calc. Mass	mDa	PPM	DBE	i-FIT	i-FIT (Norm)	Formula
410.1585	410.1577	0.8	2.0	13.5	725.7	6.2	C19 H20 N7 O4
	410.1604	-1.9	-4.6	12.5	719.6	0.0	C23 H24 N O6
	410.1563	2.2	5.4	8.5	726.4	6.8	C18 H24 N3 O8
	410.1617	-3.2	-7.8	17.5	724.7	5.1	C24 H20 N5 O2
	410.1545	4.0	9.8	21.5	728.3	8.7	C30 H20 N O

Mass spectra

Compound 20a

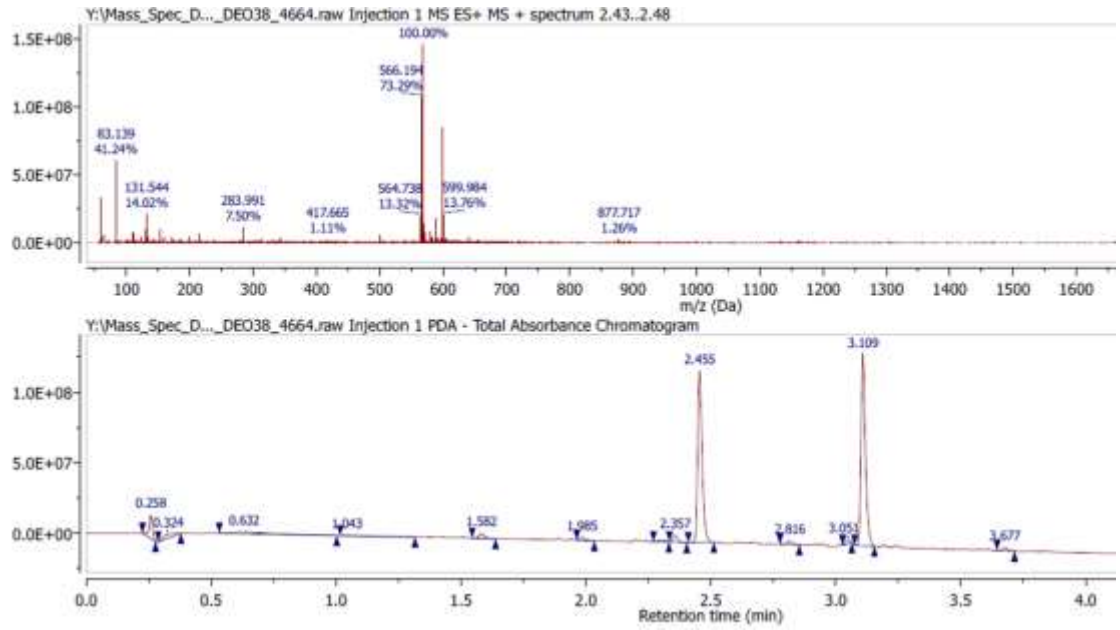

Compound 20b

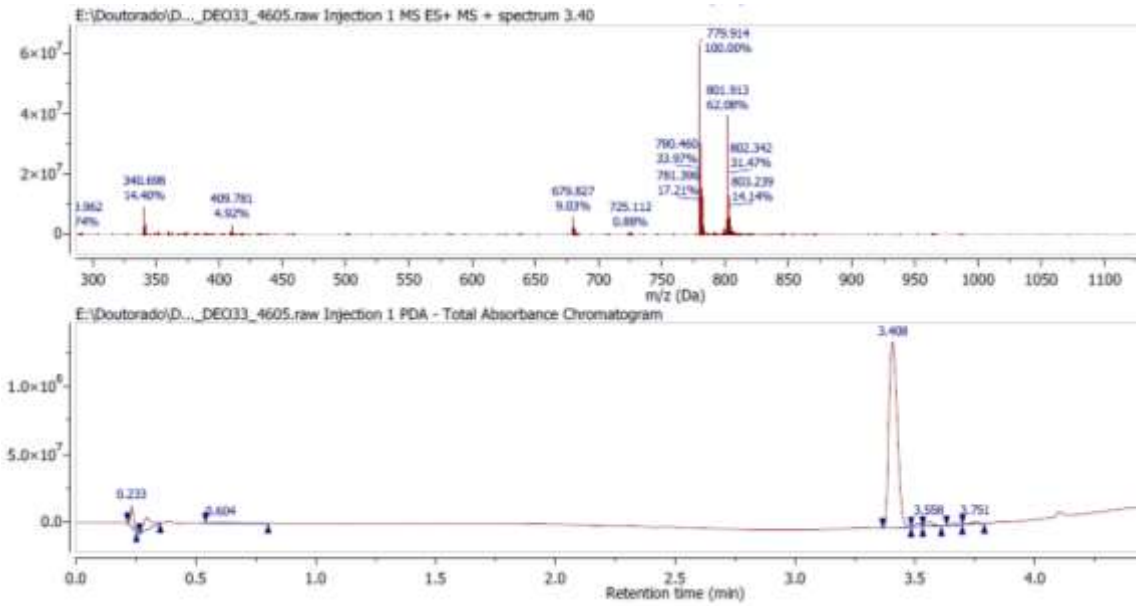

Compound 20

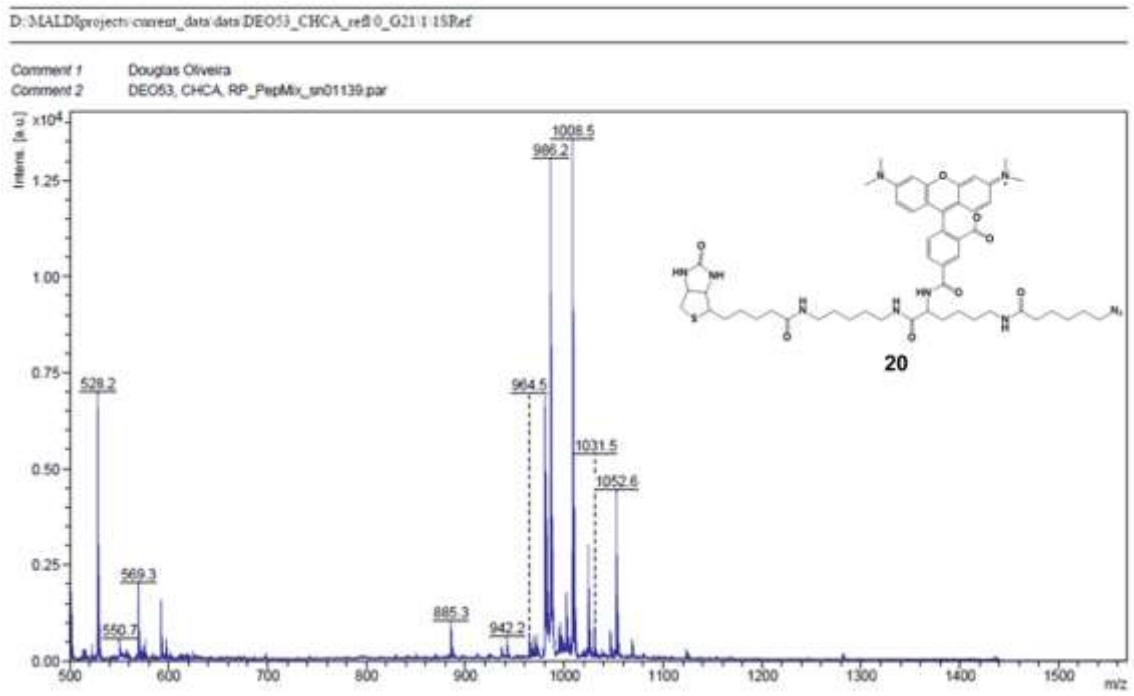
D:\MALDI\projects\current_data\data DEO53_CHCA_refl 0_G21 1 1SRef
Comment 1 Douglas Oliveira
Comment 2 DEO53, CHCA, RP_PepMix_sn01139.par
Intens. [a.u.] x10^4
1008.5
986.2
528.2
964.5
1031.5
1052.6
569.3
885.3
550.7
942.2
20
m/z

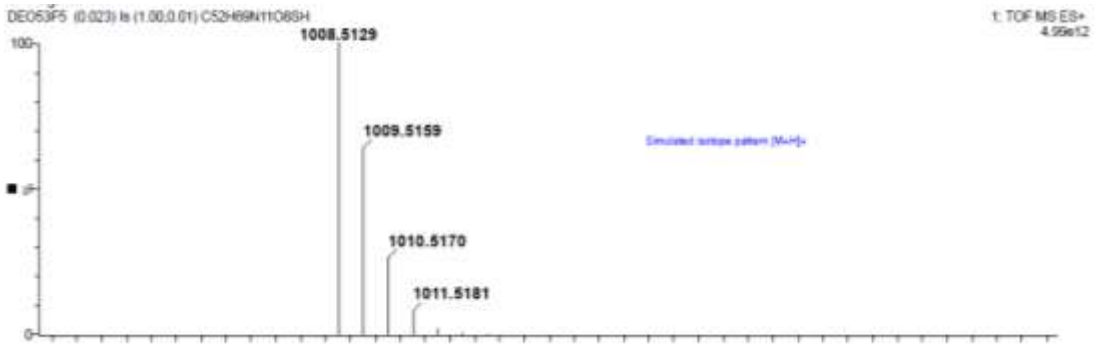
DEO53F5 (0.023) Is (1.00,0.01) C52H69N11O8SH
1: TOF MS ES+
4.99e12
1008.5129
1009.5159
1010.5170
1011.5181